STATIC AND DYNAMIC ANALYSIS OF PERIODIC LATTICE STRUCTURES WITH APPLICATIONS TO ACOUSTIC CLOAKS OF THE PENTAMODE TYPE

by

ADAM JULIUS NAGY

A dissertation submitted to the

Graduate School—New Brunswick

Rutgers, The State University of New Jersey

In partial fulfillment of the requirements

For the degree of

Doctor of Philosophy

Graduate Program in Mechanical and Aerospace Engineering

Written under the direction of

Dr. Andrew N. Norris

And approved by

_____

_____

_____

_____

New Brunswick, New Jersey

MAY, 2015

ABSTRACT OF THE DISSERTATION

Static and dynamic analysis of periodic lattice structures with applications to acoustic cloaks of the pentamode type

by Adam Julius Nagy

Dissertation Director: Dr. Andrew N. Norris

As a first step towards producing pentamode acoustic cloaks, so named for the type of elasticity required, periodic lattice structured materials are designed that mimic the acoustic properties of water. This material is termed Metal Water and is analyzed in detail. The requirements considered are matching of density and wave speed, this produces a type of metamaterial that couples acoustic wave energy from a background fluid into an elastic medium without reflection. General elastodynamic, scattering, and acoustic cloaking theories are reviewed. In application to scattering, a new method is developed for cylindrically layered elastic media, which combines impedance and matricant propagator matrices in a stable integration scheme. A variety of techniques are used to estimate and improve the homogenized material properties associated with Metal Water. Dispersion curves are found by the application of Bloch-Floquet theory where a new approach that utilizes Euler-Bernoulli beams is developed. Results are compared against finite element methods capable of more accurately determining homogenized properties. Several designs are proposed in two and three dimensions with detailed studies including dispersion curve analysis as well as statically determined properties.

Keywords: acoustic, cloaking, passive, matricant, metamaterial, Stroh, pentamode, homogenization

Acknowledgements

I am sincerely indebted to my advisor, Dr. Andrew Norris for his extraordinary guidance, expertise and patience. He is an excellent mentor and has made my experience in the graduate program tremendously rewarding. To Dr. Nachiket Gokhale and Dr. Jeffrey Cipolla of Weidlinger Associates. To my research group, special thanks to Alexey Titovich, Feruza Amirkulova and Xiaoshi Su. And especially to my family, who have always supported my endeavors. Lastly, this work was completed with support from the National Science Foundation and the Office of Naval Research.

Dedication

Special dedication to my parents.

Table of Contents

List of Tables

List of Figures

Chapter 1

Introduction

Cloaking devices cause an object to be invisible to incoming waves, energy is diverted and passes through the region without scattering. Interest in the subject started with developments in the electromagnetic (EM) spectrum and have given life to the study of acoustic cloaks. It was found in electromagnetism that strong anisotropic parameters are required for EM cloaking [9, 10]. This is an obvious consequence as the device is required to steer wave energy around an object in a rather short distance. Materials with such characteristics do not occur naturally in nature and so metamaterials, meaning man-made materials with extraordinary properties, must be created. Further studies in EM metamaterials have shown unprecedented control of wave propagation for devices such as: concentrators [11], beam splitters [12], and of course cloaks [13, 14]. By the technique of transformation optics, material parameters can be derived to achieve the desired effect. The method consists of applying a form-invariant coordinate transform to the EM equations, which deforms space in a specified manner based on a mapping function [12]. Similarly, transformation acoustics applies a form-invariant coordinate transform to the Helmholtz equation.

The first theorized acoustic cloaks were of the inertial type where material properties are described by an anisotropic density tensor and a scalar bulk modulus. In order to achieve anisotropic mass properties, Milton et al. [15] conceptually described how a system of spring-loaded masses could create the needed mass anisotropy, building on the work of Willis [16] who demonstrated that, for a composite material in which density varied, the effective density operator took the form of a second-order tensor. One of the first proposed inertial cloaks came about by relating the electromagnetic equation to the acoustic and matching associated parameters [13]. In order to produce

anisotropic inertia a simple layering of fluids is sufficient [17, 18, 19]. Norris [20] later showed the effective material properties of an acoustic cloak are not uniquely defined and have special relations to the transformation mapping. This result meant that an infinite number of mappings which define the material properties of the cloak can be used in designing the device. One issue with the mapping function, which transforms a point into a finite region, are singularities in the required material properties [21]. In application to inertial cloaks the transformation requires a singularity in density meaning infinite mass is required. One way of resolving this issue is by relaxing the transformation and instead map a small area to a larger one, such that the cloak could be considered near perfect. This would help remove singularities in density but still require a device with large mass.

Another approach is to consider cloaks made from an elastic medium, this relieves the requirement of large mass and instead large anisotropy in elasticity is required [15]. In this case materials that are described by pentamode elasticity are needed. Pentamode materials are special as compression and shear waves are not coupled, this is a consequence of the ideally infinite ratio between the bulk and shear moduli. The Poisson's ratio in such a material is approximately one half [22]. Fluid like behavior occurs as the eigenvalues of the elasticity tensor are all zero except for one, meaning that only one mode of deformation opposes applied stress. Transformation mappings have been studied for pentamode cloaks [23], where properties including constant density, constant radial stiffness, constant tangential stiffness and others including a mapping that considers minimizing elastic anisotropy have been studied. Other studies have considered the producibility of such a material [24] and whether shear rigidity would play an important role in the cloak [25].

In developing acoustic cloaks of the pentamode type an important first step is developing an elastic based material that has the same acoustic response as water. To do this micro-structured materials termed Metal Water are proposed and analyzed. The designed material will be impedance matched to the exterior fluid which will couple the two mediums as to not produce reflections when an acoustic wave is incident upon the device. Metal Water can be thought as being the very first layer, coupling wave energy

from an acoustic medium to an elastic. In order to develop Metal Water static homogenization theory and dispersion curve analysis is utilized. The results described here are two and three dimensional structures capable of mimicking the acoustic properties of water.

1.1 Outline of the Thesis

The thesis begins with a study of elastodynamics in chapter 2 where acoustic and elastic waves are reviewed. Material symmetries are then discussed as it becomes important to understand what components of the elasticity tensor should be considered when designing structures with certain reflection planes. The chapter ends with a review of the Christoffel equation which computes the group velocities for longitudinal and shear waves in elastic media. In chapter 3 the global matrix method for scattering from a layered elastic medium is developed, where the medium can be at most described by elasticity with transverse isotropy. This method requires rather large matrices to be inverted, especially in the application to acoustic cloaking theory where material properties of the cloak vary as a function of the radius. This is resolved by the integration method reviewed and developed in chapter 4 where the Stroh formalism is used in conjunction with the matricant and impedance matrices offering a stable solution scheme. The method is able to quickly solve for a large number of layers with general anisotropy. This is an important tool as it is used in chapter 5 where acoustic cloaking theory is reviewed and examples are considered. It is shown that pentamode elasticity is required for devices created using transformation acoustics theory. This special type of elasticity only allows for longitudinal waves to propagate as shear wave speeds are zero in such a medium. However, it is found that the cloaking medium can tolerate some level of shear wave presence, shown by example. This is an important result as it means elastic structures can be developed and used with this theory. Static homogenization methods are reviewed in chapter 6 where elasticity components of periodic media can be found by both analytical and finite element means. In chapter 7, Bloch-Floquet analysis is extensively reviewed using several different methods with new results in the application of Euler-Bernoulli beams. This offers dispersion curve analysis in which group velocities

can be found and static elastic moduli can be backed out and compared against other methods. Lastly, in chapters 8 and 9 Metal Water designs are considered and analyzed in two and three dimensions. The thesis ends with chapter 10 where the summary of results, original contributions and future work to be considered are discussed.

Chapter 2

Brief review of elastodynamics

The method of producing metamaterial devices used in this thesis consists of creating periodic lattice type structures with desired elastic and density properties. These structures are developed later in chapters 8 and 9 where the goal is to produce a material with water like behavior, in an acoustic sense. In order to reach this goal we start with a review of elastodynamics. Sections 2.1 and 2.2 go over the general equations of motion for acoustic and elastic media. This will be helpful in chapters 3 and 4 where scattering solutions of elastic cylindrical media are sought. Then in section 2.2.1 we review what elements of the elasticity tensor must be considered due to material symmetries as well as determining group velocities of longitudinal and shear waves from the density and elastic moduli properties of the material. This is helpful in the understanding of how a solid medium can be used to approximate an acoustic one by taking shear wave speeds to zero. It can also be used to check the numeric results of homogenization methods, reviewed in chapters 6 and 7, that seek to find elastic properties of lattice structures based on the analysis of a unit cell.

2.1 Acoustic theory

Before entering the realm of elastic materials we briefly describe waves in acoustic media. The pressure of an incident wave is defined by

$$P_{inc} = P_0 e^{i(\mathbf{k}\cdot\mathbf{x}-\omega t)}, \tag{2.1}$$

where P_0 is the amplitude, $\mathbf{k}$ is the wave vector and ω is the angular frequency. The wave vector has the property

$$k = |\mathbf{k}| = \sqrt{k_x^2 + k_y^2 + k_z^2} = 2\pi/\lambda, \tag{2.2}$$

where λ is the wavelength. Considering two dimensional problems in the $x-z$ plane, such that the y component of $\mathbf{k}\cdot\mathbf{x}$ vanishes, we have

$$P_{inc} = P_0 e^{i(k_x x + k_z z - \omega t)}. \tag{2.3}$$

Next we wish to convert to cylindrical coordinates, (r,θ,z), and represent the incident wave as a series involving Bessel functions for later use in a detailed solution with acoustic-elastic structure interaction, discussed in chapters 3 and 4. In cylindrical coordinates $k_x = k\cos\alpha$ and $k_z = k\sin\alpha$, where α is the angle between the wave vector, $\mathbf{k}$, and the x axis. Finally we will make use of the identity

$$e^{iz\cos\theta} = \sum_{n=-\infty}^{\infty} i^n J_n(z) e^{in\theta} = \sum_{n=0}^{\infty} \epsilon_n i^n J_n(z)\cos n\theta, \tag{2.4}$$

where $J_n(z)$ is the Bessel function of the first kind, $\epsilon_n = 1$ for $n = 0$ and $\epsilon_n = 2$ for $n > 0$ [26]. The incident pressure wave, equation (2.3), is rewritten using equation (2.4) with

$$P_{inc} = P_0 e^{i(k_z z - \omega t)} \sum_{n=0}^{\infty} \epsilon_n i^n J_n(k_x r)\cos n\theta. \tag{2.5}$$

The scattered field has a different form as the incident wave will not usually fit the boundary conditions of the outer surface of a cylinder and therefore an additional scattered wave must be present [27]. The scattered wave must radiate outward by the Sommerfeld radiation condition, which states that the energy radiated from sources must scatter to infinity and energy from infinity does not radiate back to the field. Therefore the scattered field is represented by Hankel functions of the first kind as compared with Hankel functions of the second kind which would represent a wave traveling inward toward the field. The scattered pressure is then

$$P_{sca} = P_0 e^{i(k_z z - \omega t)} \sum_{n=0}^{\infty} \epsilon_n i^n H_n^{(1)}(k_x r)\cos n\theta, \quad r > a, \tag{2.6}$$

where a is the outer radius of the cylinder. Understanding the incident and scattered pressure fields in an acoustic medium will come into use later. Next elastodynamic theory is reviewed.

2.2 Elastic theory

We begin discussion of elastodynamic theory with the conservation of linear momentum, given by

$$\nabla \cdot \boldsymbol{\sigma} + \rho \mathbf{b} = \rho \frac{\partial \mathbf{v}}{\partial t}, \tag{2.7}$$

where $\boldsymbol{\sigma}$ is the symmetric Cauchy stress tensor, ρ is the density, $\mathbf{b}$ is the body force per unit volume, $\mathbf{v} = \partial \mathbf{u}/\partial t$ is the velocity field and $\mathbf{u}$ is the displacement field in the body. The constitutive relation between stress and strain is $\sigma = \mathbf{C} : \varepsilon$, or in component form $\sigma_{ij} = C_{ijkl}\varepsilon_{kl}$, where $\mathbf{C}$ is the fourth order elasticity tensor having $3^4 = 81$ components. The strain-displacement relation is given by $\varepsilon = \frac{1}{2}(\nabla \mathbf{u} + (\nabla \mathbf{u})^T)$, or in component form

$$\varepsilon_{ij} = \frac{1}{2}\left(\frac{\partial u_i}{\partial x_j} + \frac{\partial u_j}{\partial x_i}\right). \tag{2.8}$$

Later on it will be convenient to have the stain-displacement relation in cylindrical coordinates for which

$$\begin{aligned} &\varepsilon_{rr} = \frac{\partial u_r}{\partial r}, \quad \varepsilon_{r\theta} = \frac{1}{2}\left(\frac{1}{r}\frac{\partial u_r}{\partial \theta} + \frac{\partial u_\theta}{\partial r} - \frac{u_\theta}{r}\right), \quad \varepsilon_{rz} = \frac{1}{2}\left(\frac{\partial u_r}{\partial z} + \frac{\partial u_z}{\partial r}\right), \\ &\varepsilon_{\theta z} = \frac{1}{2}\left(\frac{\partial u_\theta}{\partial z} + \frac{1}{r}\frac{\partial u_z}{\partial \theta}\right), \quad \varepsilon_{\theta\theta} = \frac{1}{r}\left(\frac{\partial u_\theta}{\partial \theta} + u_r\right), \quad \varepsilon_{zz} = \frac{\partial u_z}{\partial z}. \end{aligned} \tag{2.9}$$

Due to the symmetry of the Cauchy stress and strain tensors it is easily found that $C_{ijkl} = C_{jikl}$, $C_{ijkl} = C_{ijlk}$, which are known as the minor symmetries, reducing the number of independent components from 81 to 36. We may further reduce the number of components of the elasticity tensor by defining the strain energy density function written as $\omega(\varepsilon) = \frac{1}{2}\varepsilon : \mathbf{C} : \varepsilon = \frac{1}{2}C_{ijkl}\varepsilon_{ij}\varepsilon_{kl}$, which should remain invariant when components ij are interchanged with kl [28]. This leads to the symmetry $C_{ijkl} = C_{klij}$, the major symmetries, reducing the independent components to 21. All symmetries of the elasticity tensor have been found so far without consideration of material symmetries, equation (2.7) can then be rewritten as

$$\nabla \cdot (\mathbf{C} : \nabla \mathbf{u}) + \rho \mathbf{b} = \rho \frac{\partial^2 \mathbf{u}}{\partial t^2}. \tag{2.10}$$

The above equation can be taken from the time domain to the frequency domain using the Fourier transform, defined as

$$\hat{f}(\omega) = \mathcal{F}[f(t)] = \int_{-\infty}^{\infty} f(t) e^{i\omega t} \mathrm{d}t. \tag{2.11}$$

Dropping the body force term and taking the Fourier transform of equation (2.10),

$$\int_{-\infty}^{\infty} \nabla \cdot \boldsymbol{\sigma} e^{i\omega t} \mathrm{d}t = \rho \int_{-\infty}^{\infty} \frac{\partial^2 \mathbf{u}}{\partial t^2} e^{i\omega t} \mathrm{d}t. \tag{2.12}$$

Integrating the term on the right by parts twice gives

$$\int_{-\infty}^{\infty} \frac{\partial^2 \mathbf{u}}{\partial t^2} e^{i\omega t} \mathrm{d}t = (\frac{\partial \mathbf{u}}{\partial t} - i\omega \mathbf{u}) e^{i\omega t} \Big|_{-\infty}^{\infty} - \int_{-\infty}^{\infty} \omega^2 \mathbf{u} e^{i\omega t} \mathrm{d}t. \tag{2.13}$$

Inspection of the above reveals that if the imaginary part of the frequency is greater or equal to zero, which we will assume, only the last term survives. We have now found the wave equation for elastodynamics, for which we can drop the hats by taking the inverse Fourier transform, with the convention $f(t) = \mathcal{F}^{-1}(\hat{f}(\omega))$. Equation (2.10) becomes

$$\nabla \cdot (\mathbf{C} : \nabla \mathbf{u}) + \omega^2 \rho \mathbf{u} = \mathbf{0}. \tag{2.14}$$

If the medium in question were a metamaterial with anisotropic density defined by the density tensor $\boldsymbol{\rho}$ we find [29]

$$\nabla \cdot \boldsymbol{\sigma} = -\omega^2 \boldsymbol{\rho} \cdot \mathbf{u}, \tag{2.15}$$

where such a medium may be developed by the simple layering of fluids [19]. In the next section we further reduce the number of independent components of the elasticity tensor by considering material symmetries.

2.2.1 Material symmetries

Classes of anisotropic materials and the associated elasticity components are reviewed in this section through the use of material planes of symmetry. Orthogonal transformations of the stress, strain and elasticity tensors are accomplished by using the rotation tensor, $\mathbf{A}$, with the properties $\mathbf{A}^T \cdot \mathbf{A} = \mathbf{I}$, where $\mathbf{A}^T = \mathbf{A}^{-1}$. The components of $\mathbf{A}$ for an in plane rotation in matrix form are

$$A_x(\theta) = \begin{bmatrix} 1 & 0 & 0 \\ 0 & \cos\theta & -\sin\theta \\ 0 & \sin\theta & \cos\theta \end{bmatrix}, \quad A_y(\theta) = \begin{bmatrix} \cos\theta & 0 & \sin\theta \\ 0 & 1 & 0 \\ -\sin\theta & 0 & \cos\theta \end{bmatrix}, \quad A_z(\theta) = \begin{bmatrix} \cos\theta & -\sin\theta & 0 \\ \sin\theta & \cos\theta & 0 \\ 0 & 0 & 1 \end{bmatrix}, \tag{2.16}$$

where $A_k(\theta)$ describes the rotation θ about the k axis, for $k \in \{x, y, z\}$. Multiplying all three matrices, $[\mathbf{A}] = A_x(\phi)A_y(\theta)A_z(\psi)$ the components are

$$[\mathbf{A}] = \begin{bmatrix} \cos\theta\cos\phi & \sin\psi\sin\theta\cos\phi - \cos\psi\sin\theta & \cos\psi\sin\theta\cos\phi + \sin\psi\sin\phi \\ \cos\theta\sin\phi & \sin\psi\sin\theta\sin\phi + \cos\psi\cos\phi & \cos\psi\sin\theta\sin\phi - \sin\psi\cos\phi \\ -\sin\theta & \sin\psi\cos\theta & \cos\psi\cos\theta \end{bmatrix}, \tag{2.17}$$

where ϕ, θ, and ψ are known as the Euler angles measured about the x, y, and z axes respectively. Instead of using Euler angles it is sometimes easier to write the rotation matrix in terms of three orthogonal unit vectors, these will make the basis coordinates in the rotated system for which

$$[\mathbf{A}] = \begin{bmatrix} \hat{u}_x & \hat{v}_x & \hat{w}_x \\ \hat{u}_y & \hat{v}_y & \hat{w}_y \\ \hat{u}_z & \hat{v}_z & \hat{w}_z \end{bmatrix} = \begin{bmatrix} \hat{\mathbf{u}} & \hat{\mathbf{v}} & \hat{\mathbf{w}} \end{bmatrix}. \tag{2.18}$$

This is referred to as the direction cosines matrix where $\hat{\mathbf{u}}$, $\hat{\mathbf{v}}$, $\hat{\mathbf{w}}$ are orthogonal unit vectors. Three laws regarding (2.18) are 1: the sum of the squares of the elements in any row or column is one, 2: the sum of the products of corresponding elements in any two rows or columns is zero, and 3: the determinant is one [30]. Next the rotation matrices for the elasticity components utilizing Voigt notation are developed where due to symmetry of the stress and strain tensors we define the components

$$\begin{array}{lccccccc} ij & = 11 & 22 & 33 & 23, 32 & 13, 31 & 12, 21 & \\ \Downarrow & \Downarrow & \Downarrow & \Downarrow & \Downarrow & \Downarrow & \Downarrow & , \\ \alpha & = 1 & 2 & 3 & 4 & 5 & 6 & \end{array} \tag{2.19}$$

such that the components of the stress and strain tensors may be rewritten in vector form as

$$[\sigma]_{(6\text{x}1)} = \begin{bmatrix} \sigma_{11} \\ \sigma_{22} \\ \sigma_{33} \\ \sigma_{23} \\ \sigma_{31} \\ \sigma_{12} \end{bmatrix} = \begin{bmatrix} \sigma_1 \\ \sigma_2 \\ \sigma_3 \\ \sigma_4 \\ \sigma_5 \\ \sigma_6 \end{bmatrix}, \quad [\varepsilon]_{(6\text{x}1)} = \begin{bmatrix} \varepsilon_{11} \\ \varepsilon_{22} \\ \varepsilon_{33} \\ 2\varepsilon_{23} \\ 2\varepsilon_{31} \\ 2\varepsilon_{12} \end{bmatrix} = \begin{bmatrix} \varepsilon_1 \\ \varepsilon_2 \\ \varepsilon_3 \\ \varepsilon_4 \\ \varepsilon_5 \\ \varepsilon_6 \end{bmatrix}, \tag{2.20}$$

where the stress strain relationship is

$$\begin{bmatrix}\sigma_1\\ \sigma_2\\ \sigma_3\\ \sigma_4\\ \sigma_5\\ \sigma_6\end{bmatrix} = \begin{bmatrix}C_{11} & C_{12} & C_{13} & C_{14} & C_{15} & C_{16}\\ C_{12} & C_{22} & C_{23} & C_{24} & C_{25} & C_{26}\\ C_{13} & C_{23} & C_{33} & C_{34} & C_{35} & C_{36}\\ C_{14} & C_{24} & C_{34} & C_{44} & C_{45} & C_{46}\\ C_{15} & C_{25} & C_{35} & C_{45} & C_{55} & C_{56}\\ C_{16} & C_{26} & C_{36} & C_{46} & C_{56} & C_{66}\end{bmatrix} \begin{bmatrix}\varepsilon_1\\ \varepsilon_2\\ \varepsilon_3\\ \varepsilon_4\\ \varepsilon_5\\ \varepsilon_6\end{bmatrix}, \tag{2.21}$$

note that the elasticity matrix is fully anisotropic with 21 independent components as explained in the beginning of section 2.2. The problem now becomes finding the six by six rotation matrix. For a given rotation tensor $\mathbf{A}$, the rotated stress tensor is given by $\hat{\sigma} = \mathbf{A}\sigma\mathbf{A}^T$ or in component form $\hat{\sigma}_{ib} = A_{ij}\sigma_{jm}A_{bm}$. Undergoing a similar derivation as done in [31] we find the components of the six by six rotation matrix, $[\mathbf{A}_\sigma]_{(6\text{x}6)}$, such that $[\hat{\sigma}]_{(6\text{x}1)} = [\mathbf{A}_\sigma]_{(6\text{x}6)}[\sigma]_{(6\text{x}1)}$. To find the first column of components of $[\mathbf{A}_\sigma]$ we have

$$[\hat{\sigma}]_{3\text{x}3} = \begin{bmatrix}A_{11} & A_{12} & A_{13}\\ A_{21} & A_{22} & A_{23}\\ A_{31} & A_{32} & A_{33}\end{bmatrix} \begin{bmatrix}\sigma_{11} & 0 & 0\\ 0 & 0 & 0\\ 0 & 0 & 0\end{bmatrix} \begin{bmatrix}A_{11} & A_{21} & A_{31}\\ A_{12} & A_{22} & A_{32}\\ A_{13} & A_{23} & A_{33}\end{bmatrix}, \tag{2.22}$$

expressed in components $\hat{\sigma}_{ib} = A_{i1}A_{b1}\sigma_{11}$. Utilizing (2.20), the first column of $\mathbf{A}_\sigma$ is, $[\mathbf{A}_\sigma](:,1) = \{A_{11}^2, A_{21}^2, A_{31}^2, A_{21}A_{31}, A_{31}A_{11}, A_{11}A_{21}\}^T$, we continue this process such that,

$$[\mathbf{A}_\sigma](:,2) = \{A_{12}^2, A_{22}^2, A_{32}^2, A_{22}A_{32}, A_{32}A_{12}, A_{12}A_{22}\}^T, \tag{2.23}$$

$$[\mathbf{A}_\sigma](:,3) = \{A_{13}^2, A_{23}^2, A_{33}^2, A_{23}A_{33}, A_{33}A_{13}, A_{13}A_{23}\}^T. \tag{2.24}$$

Now for the off diagonal components, consider $\sigma_{23} = \sigma_{32}$ such that

$$[\hat{\sigma}]_{3\text{x}3} = \begin{bmatrix}A_{11} & A_{12} & A_{13}\\ A_{21} & A_{22} & A_{23}\\ A_{31} & A_{32} & A_{33}\end{bmatrix} \begin{bmatrix}0 & 0 & 0\\ 0 & 0 & \sigma_{23}\\ 0 & \sigma_{32} & 0\end{bmatrix} \begin{bmatrix}A_{11} & A_{21} & A_{31}\\ A_{12} & A_{22} & A_{32}\\ A_{13} & A_{23} & A_{33}\end{bmatrix}, \tag{2.25}$$

in components $\hat{\sigma}_{ib} = A_{i2}A_{b3}\sigma_{23} + A_{i3}A_{b2}\sigma_{32}$. Then the fourth and subsequent columns of $[\mathbf{A}_\sigma]$ are found similarly

$$[\mathbf{A}_\sigma](:,4) = \{2A_{12}A_{13}, 2A_{22}A_{23}, 2A_{32}A_{33}, A_{22}A_{33} + A_{23}A_{32}, A_{32}A_{13} + A_{33}A_{12}, A_{12}A_{23} + A_{13}A_{22}\}^T, \tag{2.26}$$

$$[\mathbf{A}_\sigma](:,5) = \{2A_{13}A_{11}, 2A_{23}A_{21}, 2A_{33}A_{31}, A_{23}A_{31} + A_{21}A_{33}, A_{33}A_{11} + A_{31}A_{13}, A_{13}A_{21} + A_{11}A_{23}\}^T, \tag{2.27}$$

$$[\mathbf{A}_\sigma](:,6) = \{2A_{11}A_{12}, 2A_{21}A_{22}, 2A_{31}A_{32}, A_{21}A_{32} + A_{22}A_{31}, A_{31}A_{12} + A_{32}A_{11}, A_{11}A_{22} + A_{12}A_{21}\}^T. \tag{2.28}$$

Finally the components of $\mathbf{A}_\sigma$ are

$$[\mathbf{A}_\sigma] = \begin{bmatrix} A_{11}^2 & A_{12}^2 & A_{13}^2 & 2A_{12}A_{13} & 2A_{13}A_{11} & 2A_{11}A_{12} \\ A_{21}^2 & A_{22}^2 & A_{23}^2 & 2A_{22}A_{23} & 2A_{23}A_{21} & 2A_{21}A_{22} \\ A_{31}^2 & A_{32}^2 & A_{33}^2 & 2A_{32}A_{33} & 2A_{33}A_{31} & 2A_{31}A_{32} \\ A_{21}A_{31} & A_{22}A_{32} & A_{23}A_{33} & A_{22}A_{33} + A_{23}A_{32} & A_{23}A_{31} + A_{21}A_{33} & A_{32}A_{21} + A_{22}A_{31} \\ A_{31}A_{11} & A_{32}A_{12} & A_{33}A_{13} & A_{32}A_{13} + A_{33}A_{12} & A_{33}A_{11} + A_{31}A_{13} & A_{31}A_{12} + A_{32}A_{11} \\ A_{11}A_{21} & A_{12}A_{22} & A_{13}A_{23} & A_{12}A_{23} + A_{13}A_{22} & A_{13}A_{21} + A_{11}A_{23} & A_{11}A_{22} + A_{12}A_{21} \end{bmatrix}. \tag{2.29}$$

In the same fashion we find $\mathbf{A}_\varepsilon$ where, $\hat{\varepsilon} = \mathbf{A}\varepsilon\mathbf{A}^T$ and $[\hat{\varepsilon}]_{(6\times1)} = [\mathbf{A}_\varepsilon]_{(6\times6)}[\varepsilon]_{(6\times1)}$

$$[\mathbf{A}_\varepsilon] = \begin{bmatrix} A_{11}^2 & A_{12}^2 & A_{13}^2 & A_{12}A_{13} & A_{13}A_{11} & A_{11}A_{12} \\ A_{21}^2 & A_{22}^2 & A_{23}^2 & A_{22}A_{23} & A_{23}A_{21} & A_{21}A_{22} \\ A_{31}^2 & A_{32}^2 & A_{33}^2 & A_{32}A_{33} & A_{33}A_{31} & A_{31}A_{32} \\ 2A_{21}A_{31} & 2A_{22}A_{32} & 2A_{23}A_{33} & A_{22}A_{33} + A_{23}A_{32} & A_{23}A_{31} + A_{21}A_{33} & A_{32}A_{21} + A_{22}A_{31} \\ 2A_{31}A_{11} & 2A_{32}A_{12} & 2A_{33}A_{13} & A_{32}A_{13} + A_{33}A_{12} & A_{33}A_{11} + A_{31}A_{13} & A_{31}A_{12} + A_{32}A_{11} \\ 2A_{11}A_{21} & 2A_{12}A_{22} & 2A_{13}A_{23} & A_{12}A_{23} + A_{13}A_{22} & A_{13}A_{21} + A_{11}A_{23} & A_{11}A_{22} + A_{12}A_{21} \end{bmatrix}. \tag{2.30}$$

Lastly a rotation matrix for the elasticity is found where the elastic equation in Voigt notation is $\sigma_I = C_{IJ}\varepsilon_J$ where I, J take on values 1 through 6. In the rotated coordinates

$$\hat{\sigma}_I = \hat{C}_{IJ}\hat{\varepsilon}_J = [\mathbf{A}_\sigma]_{IM}\sigma_M = [\mathbf{A}_\sigma]_{IM}C_{MK}\varepsilon_K = [\mathbf{A}_\sigma]_{IM}C_{MK}[\mathbf{A}_\varepsilon]^{-1}_{KJ}\hat{\varepsilon}_J, \tag{2.31}$$

which gives

$$0 = ([\mathbf{A}_\sigma]_{IM}C_{MK}[\mathbf{A}_\varepsilon]^{-1}_{KJ} - \hat{C}_{IJ})\hat{\varepsilon}_J \;\; \rightarrow \;\; \hat{C}_{IJ} = [\mathbf{A}_\sigma]_{IM}C_{MK}[\mathbf{A}_\varepsilon]^{-1}_{KJ}. \tag{2.32}$$

In a lengthy derivation it can be shown that $[\mathbf{A}_\sigma]_{KJ} = [\mathbf{A}_\varepsilon]^{-1}_{JK}$, meaning the rotated elasticity components take on the form [31]

$$\hat{C}_{IJ} = [\mathbf{A}_\sigma]_{IM}C_{MK}[\mathbf{A}_\sigma]_{JK} \Leftrightarrow \hat{\mathbf{C}} \;\; = \mathbf{A}_\sigma\mathbf{C}\mathbf{A}_\sigma^T. \tag{2.33}$$

Material planes of symmetry

An orthotropic material has three orthogonal symmetry planes, starting with one plane of symmetry we will show how the number of independent elements of the elasticity matrix is reduced with each additional plane of symmetry. Starting by taking equation (2.18) with the transformed system such that, $\hat{\mathbf{u}}_x = \mathbf{u}_x$, $\hat{\mathbf{v}}_y = \mathbf{v}_y$, $\hat{\mathbf{w}}_z = -\mathbf{w}_z$, or in matrix form

$$[\mathbf{A}] = \begin{bmatrix} 1 & 0 & 0 \\ 0 & 1 & 0 \\ 0 & 0 & -1 \end{bmatrix}. \tag{2.34}$$

Inserting into equation (2.29) we have

$$[\mathbf{A}_\sigma] = \begin{bmatrix} 1 & 0 & 0 & 0 & 0 & 0 \\ 0 & 1 & 0 & 0 & 0 & 0 \\ 0 & 0 & 1 & 0 & 0 & 0 \\ 0 & 0 & 0 & -1 & 0 & 0 \\ 0 & 0 & 0 & 0 & -1 & 0 \\ 0 & 0 & 0 & 0 & 0 & 1 \end{bmatrix}, \tag{2.35}$$

plugging this into equation (2.33) and requiring that the transformed elasticity matrix is equivalent to the original, such that a material plane of symmetry exists, we obtain, $C_{14} = -C_{14}$, $C_{15} = -C_{15}$, $C_{24} = -C_{24}$, $C_{25} = -C_{25}$, $C_{34} = -C_{34}$, $C_{35} = -C_{35}$, $C_{46} = -C_{46}$, $C_{56} = -C_{56}$, which imply these terms must be zero, reducing the number of independent terms from 21 to 13. This material is defined as monoclinic as there is a single symmetry plane through the origin and it's elasticity components are

$$[\mathbf{C}]_{\text{Mono}} = \begin{bmatrix} C_{11} & C_{12} & C_{13} & 0 & 0 & C_{16} \\ C_{12} & C_{22} & C_{23} & 0 & 0 & C_{26} \\ C_{13} & C_{23} & C_{33} & 0 & 0 & C_{36} \\ 0 & 0 & 0 & C_{44} & C_{45} & 0 \\ 0 & 0 & 0 & C_{45} & C_{55} & 0 \\ C_{16} & C_{26} & C_{36} & 0 & 0 & C_{66} \end{bmatrix}. \tag{2.36}$$

We add an additional plane of symmetry with $\hat{\mathbf{u}}_x = \mathbf{u}_x$, $\hat{\mathbf{v}}_y = -\mathbf{v}_y$, $\hat{\mathbf{w}}_z = \mathbf{w}_z$, or in matrix form

$$[\mathbf{A}] = \begin{bmatrix} 1 & 0 & 0 \\ 0 & -1 & 0 \\ 0 & 0 & 1 \end{bmatrix}, \tag{2.37}$$

this means the components of the elasticity transformation matrix are

$$[\mathbf{A}_\sigma] = \begin{bmatrix} 1 & 0 & 0 & 0 & 0 & 0 \\ 0 & 1 & 0 & 0 & 0 & 0 \\ 0 & 0 & 1 & 0 & 0 & 0 \\ 0 & 0 & 0 & -1 & 0 & 0 \\ 0 & 0 & 0 & 0 & 1 & 0 \\ 0 & 0 & 0 & 0 & 0 & -1 \end{bmatrix}. \tag{2.38}$$

Continuing in the same fashion yields: $C_{16} = C_{26} = C_{36} = C_{45} = 0$, reducing the number of independent components to nine. By inspection if we were to consider a rotation such that $\hat{\mathbf{u}}_x = -\mathbf{u}_x$, $\hat{\mathbf{v}}_y = \mathbf{v}_y$, $\hat{\mathbf{w}}_z = \mathbf{w}_z$, we would find no further elements that vanish, this is due to the form of equation (2.29), which means reflections about two orthogonal symmetry planes are not independent of the third plane. The elasticity components of an orthotropic material are then

$$[\mathbf{C}]_{\text{Ortho}} = \begin{bmatrix} C_{11} & C_{12} & C_{13} & 0 & 0 & 0 \\ C_{12} & C_{22} & C_{23} & 0 & 0 & 0 \\ C_{13} & C_{23} & C_{33} & 0 & 0 & 0 \\ 0 & 0 & 0 & C_{44} & 0 & 0 \\ 0 & 0 & 0 & 0 & C_{55} & 0 \\ 0 & 0 & 0 & 0 & 0 & C_{66} \end{bmatrix}. \tag{2.39}$$

This is an important result as later on when developing materials with three orthogonal planes of symmetry in three dimensions or two planes in two dimensions these will be the elasticity components to consider. Transverse isotropy is considered next, which is described as having a transverse plane in which material properties are the same in all directions. Taking equation (2.16) where we wish to consider any rotation about the

x_3 axis as invariant yields

$$[\mathbf{A}_\sigma] = \begin{bmatrix} \cos^2\theta & \sin^2\theta & 0 & 0 & 0 & -2\cos\theta\sin\theta \\ \sin^2\theta & \cos^2\theta & 0 & 0 & 0 & 2\cos\theta\sin\theta \\ 0 & 0 & 1 & 0 & 0 & 0 \\ 0 & 0 & 0 & \cos\theta & \sin\theta & 0 \\ 0 & 0 & 0 & -\sin\theta & \cos\theta & 0 \\ \cos\theta\sin\theta & -\cos\theta\sin\theta & 0 & 0 & 0 & \cos^2\theta - \sin^2\theta \end{bmatrix}, \tag{2.40}$$

where θ is taken about the x_3 axis. Using equation (2.33) we find the elasticity matrix takes the form

$$[\mathbf{C}]_{\mathrm{TI}} = \begin{bmatrix} C_{11} & C_{12} & C_{13} & 0 & 0 & 0 \\ C_{12} & C_{11} & C_{13} & 0 & 0 & 0 \\ C_{13} & C_{13} & C_{33} & 0 & 0 & 0 \\ 0 & 0 & 0 & C_{44} & 0 & 0 \\ 0 & 0 & 0 & 0 & C_{44} & 0 \\ 0 & 0 & 0 & 0 & 0 & (C_{11} - C_{12})/2 \end{bmatrix}. \tag{2.41}$$

The components of the transformed elasticity matrix are computed using the software package Maple. With a bit of algebra the above is attained where we have reduced the number of independent components to five. Using equation (2.40) and asking Maple to solve the system such that $[\mathbf{C}] = [\hat{\mathbf{C}}]$, for any θ yields

$$[\mathbf{C}]_{\mathrm{TI}} = \begin{bmatrix} C_{22} & C_{22} - 2C_{66} & C_{23} & 0 & 0 & 0 \\ C_{22} - 2C_{66} & C_{22} & C_{23} & 0 & 0 & 0 \\ C_{23} & C_{23} & C_{33} & 0 & 0 & 0 \\ 0 & 0 & 0 & C_{55} & 0 & 0 \\ 0 & 0 & 0 & 0 & C_{55} & 0 \\ 0 & 0 & 0 & 0 & 0 & C_{66} \end{bmatrix}. \tag{2.42}$$

The above system has five independent components, this is seen if we introduce $C_{12} = C_{22} - 2C_{66}$ or $C_{66} = \frac{C_{22}-C_{12}}{2}$, and we transform this into equation (2.41) by redefining the names of the independent components. This review was done as it is important to understand what elasticity components should be considered when developing structured materials with unique planes of symmetry. For more information on

different types of symmetries such as: trigonal, tetragonal, cubic, isotropic and so on, reference [31] is an excellent source.

2.2.2 Group velocities

Next we develop an understanding of how anisotropic material properties of the constitutive elasticity tensor affect the group velocities of longitudinal and shear waves. A plane harmonic wave traveling along the direction of the wave vector $\mathbf{k}$ with amplitude vector $\mathbf{u}_0$ takes the form

$$\mathbf{u} = \mathbf{u}_0 e^{i(\mathbf{k}\cdot\mathbf{x}-\omega t)}, \tag{2.43}$$

where the wave vector can be expressed as $\mathbf{k} = \frac{\omega}{c}\mathbf{n}$, where c is the group velocity. It is interesting to take a moment and describe how $\mathbf{u}_0$ and $\mathbf{n}$ are related. For instance if $\mathbf{u}_0 \times \mathbf{n} = 0$, the wave is a linearly polarized longitudinal wave. If $\mathbf{u}_0 \cdot \mathbf{n} = 0$, the wave is a linearly polarized transverse wave [32]. The first term of the equation of motion in Cartesian coordinates is obtained by a substitution of equation (2.43) into equation (2.14),

$$\begin{aligned}
\nabla\mathbf{u} &= \frac{\partial}{\partial x_i} u_{0_j} e^{i(\frac{\omega}{c}n_k x_k - \omega t)} \mathbf{e}_i\mathbf{e}_j = \frac{i\omega}{c} n_i u_{0_j} e^{i(\frac{\omega}{c}n_k x_k - \omega t)} \mathbf{e}_i\mathbf{e}_j = \frac{i\omega}{c}\mathbf{n}\mathbf{u}, \\
\nabla\cdot(\mathbf{C}:\nabla\mathbf{u}) &= \frac{\partial}{\partial x_m}\cdot(\frac{i\omega}{c} C_{ijkl} n_k u_{0_l} e^{i(\frac{\omega}{c}n_z x_z - \omega t)} \mathbf{e}_i\mathbf{e}_j) \\
&= \frac{\partial}{\partial x_i}(\frac{i\omega}{c} C_{ijkl} n_k u_{0_l} e^{i(\frac{\omega}{c}n_z x_z - \omega t)})\mathbf{e}_j \\
&= -\frac{\omega^2}{c^2} C_{ijkl} n_k u_{0_l} n_i e^{i(\frac{\omega}{c}n_z x_z - \omega t)} \mathbf{e}_j = -\frac{\omega^2}{c^2}\mathbf{n}\cdot\mathbf{C}\cdot\mathbf{n}\cdot\mathbf{u},
\end{aligned} \tag{2.44}$$

where the last relation comes from the symmetries of the elasticity tensor. Plugging the above into equation (2.14) we find

$$(\mathbf{n}\cdot\mathbf{C}\cdot\mathbf{n} - \rho c^2\mathbf{I})\cdot\mathbf{u} = \mathbf{0}, \tag{2.45}$$

where $\mathbf{n}\cdot\mathbf{C}\cdot\mathbf{n}$ is known as the acoustic tensor and $\mathbf{I}$ is the diagonal identity tensor. The above equation has nontrivial solutions so long as

$$\det(\mathbf{n}\cdot\mathbf{C}\cdot\mathbf{n} - \rho c^2\mathbf{I}) = 0, \tag{2.46}$$

for which in three dimensions there will be three solutions for the group velocity, one longitudinal and two transverse speeds. Following the steps of [32] we find relations for

the group velocities for the most general anisotropic material. The acoustic tensor is defined as $\mathbf{\Gamma}(\mathbf{n}) = \mathbf{n}\cdot\mathbf{C}\cdot\mathbf{n}$ or in components $\Gamma_{jk} = C_{ijkl}n_i n_l$. Then for fully anisotropic media

$$\begin{aligned}
\Gamma_{11} &= C_{11}n_1^2 + C_{66}n_2^2 + C_{55}n_3^2 + 2C_{16}n_1n_2 + 2C_{15}n_1n_3 + 2C_{56}n_2n_3,\\
\Gamma_{12} &= C_{16}n_1^2 + C_{26}n_2^2 + C_{45}n_3^2 + n_1n_2(C_{12}+C_{66}) + n_1n_3(C_{14}+C_{56}) + n_2n_3(C_{46}+C_{25}),\\
\Gamma_{13} &= C_{15}n_1^2 + C_{64}n_2^2 + C_{53}n_3^2 + n_1n_2(C_{14}+C_{65}) + n_1n_3(C_{13}+C_{55}) + n_2n_3(C_{63}+C_{54}),\\
\Gamma_{22} &= C_{66}n_1^2 + C_{22}n_2^2 + C_{44}n_3^2 + 2C_{26}n_1n_2 + 2C_{46}n_1n_3 + 2C_{24}n_2n_3,\\
\Gamma_{23} &= C_{65}n_1^2 + C_{24}n_2^2 + C_{34}n_3^2 + n_1n_2(C_{46}+C_{25}) + n_1n_3(C_{36}+C_{45}) + n_2n_3(C_{23}+C_{44}),\\
\Gamma_{33} &= C_{55}n_1^2 + C_{44}n_2^2 + C_{33}n_3^2 + 2C_{45}n_1n_2 + 2C_{35}n_1n_3 + 2C_{34}n_2n_3,
\end{aligned} \tag{2.47}$$

note $\mathbf{\Gamma} = \mathbf{\Gamma}^T$. Solutions of equation (2.46) for general anisotropy are much too long to reproduce here and so we leave with an equation to be solved

$$\begin{aligned}
0 = (\Gamma_{11}-\rho c^2)(\Gamma_{22}-\rho c^2)(\Gamma_{33}-\rho c^2) + \Gamma_{12}\Gamma_{23}\Gamma_{13} + \Gamma_{13}\Gamma_{12}\Gamma_{23}\\
+ \Gamma_{23}^2(\rho c^2+\Gamma_{11}) + \Gamma_{12}^2(\rho c^2+\Gamma_{33}) + \Gamma_{13}^2(\rho c^2+\Gamma_{22}).
\end{aligned} \tag{2.48}$$

This equation can be used to check the results we find later on where material group velocities are found from dispersion curves for various metamaterials with proposed substructure.

Transverse isotropy

Plugging the constitutive relations of equation (2.41) into equation (2.47) the components of the acoustic tensor are

$$\begin{aligned}
\Gamma_{11} &= C_{11}n_1^2 + \frac{C_{11}-C_{12}}{2}n_2^2 + C_{44}n_3^2,\\
\Gamma_{12} &= (C_{11} + \frac{C_{12}}{2})n_1n_2,\\
\Gamma_{13} &= (C_{13}+C_{44})n_1n_3,\\
\Gamma_{22} &= \frac{C_{11}-C_{12}}{2}n_1^2 + C_{11}n_2^2 + C_{44}n_3^2,\\
\Gamma_{23} &= (C_{13}+C_{44})n_2n_3,\\
\Gamma_{33} &= C_{44}n_1^2 + C_{44}n_2^2 + C_{33}n_3^2.
\end{aligned} \tag{2.49}$$

Recalling our derivation of transversely isotropic media, we took rotations about the x_3 axis and let any rotation θ about this axis to be symmetric such that material

properties in the $x_1 - x_2$ plane are isotropic. Following the reasoning in [31], we start by considering propagation in the $x_1 - x_2$ plane, such that $n_3 = 0$. Since this plane is isotropic we consider propagation in any direction and to simplify the analysis we let $[\mathbf{n}] = [1, 0, 0]^T$, inserting into equation (2.45) we have

$$\begin{bmatrix} C_{11} - \rho c^2 & 0 & 0 \\ 0 & \frac{C_{11}-C_{12}}{2} - \rho c^2 & 0 \\ 0 & 0 & C_{44} \end{bmatrix} \begin{bmatrix} u_1 \\ u_2 \\ u_3 \end{bmatrix} = \begin{bmatrix} 0 \\ 0 \\ 0 \end{bmatrix}. \tag{2.50}$$

The longitudinal velocity also known as the P wave velocity is found by allowing $[\mathbf{u}] = [1, 0, 0]^T$, plugging into equation (2.50) immediately yields $C_{11} - \rho c_P^2 = 0$, or

$$c_P = \pm\sqrt{\frac{C_{11}}{\rho}}. \tag{2.51}$$

Following the same procedure the in plane shear wave velocity is found by letting $[\mathbf{u}] = [0, 1, 0]^T$,

$$c_{SH} = \pm\sqrt{\frac{C_{11} - C_{12}}{2\rho}}. \tag{2.52}$$

Finally the out of plane shear wave velocity is then found by taking $[\mathbf{u}] = [0, 0, 1]^T$,

$$c_{SV} = \pm\sqrt{\frac{C_{44}}{\rho}}. \tag{2.53}$$

Cubic material

By making use of the work in [33], the fourth order elasticity tensor for a cubic material can be expressed in terms of three moduli. In terms of the compliance tensor, $\mathbf{S}$, where $\mathbf{C} = \mathbf{S}^{-1}$, the elasticity of the material is defined by

$$\mathbf{S}^{\pm 1} = (3\kappa)^{\mp 1}\mathbf{J} + (2\mu_1)^{\mp 1}(\mathbf{I} - \mathbf{D}) + (2\mu_2)^{\mp 1}(\mathbf{D} - \mathbf{J}), \tag{2.54}$$

where $\mathbf{I}$ is the fourth order identity tensor with components $I_{ijkl} = \frac{1}{2}(\delta_{ik}\delta_{jl} + \delta_{il}\delta_{jk})$, $J_{ijkl} = \frac{1}{3}\delta_{ij}\delta_{kl}$, and

$$D_{ijkl} = \delta_{i1}\delta_{j1}\delta_{k1}\delta_{l1} + \delta_{i2}\delta_{j2}\delta_{k2}\delta_{l2} + \delta_{i3}\delta_{j3}\delta_{k3}\delta_{l3}, \tag{2.55}$$

where δ_{ij} is Kronecker's delta [34]. The acoustic tensor in component form is then

$$\begin{aligned} \Gamma_{jk} =& \kappa n_j n_k + 2\mu_1 \left[\frac{1}{2}(n_k n_j + n_i n_i \delta_{jk}) - (n_1^2\delta_{j1}\delta_{k1} + n_2^2\delta_{j2}\delta_{k2} + n_3^2\delta_{j3}\delta_{k3})\right] \\ &+ 2\mu_2 \left[n_1^2\delta_{j1}\delta_{k1} + n_2^2\delta_{j2}\delta_{k2} + n_3^2\delta_{j3}\delta_{k3} - \frac{1}{3}n_j n_k\right], \end{aligned} \tag{2.56}$$

where the individual components written out are

$$\begin{aligned}
\Gamma_{11} &= \kappa n_1^2 + \mu_1(n_2^2 + n_3^2) + \frac{4}{3}\mu_2 n_1^2, \\
\Gamma_{22} &= \kappa n_2^2 + \mu_1(n_1^2 + n_3^2) + \frac{4}{3}\mu_2 n_2^2, \\
\Gamma_{33} &= \kappa n_3^2 + \mu_1(n_1^2 + n_2^2) + \frac{4}{3}\mu_2 n_3^2, \\
\Gamma_{12} &= n_1 n_2(\kappa + \mu_1 - \frac{2}{3}\mu_2), \\
\Gamma_{13} &= n_1 n_3(\kappa + \mu_1 - \frac{2}{3}\mu_2), \\
\Gamma_{23} &= n_2 n_3(\kappa + \mu_1 - \frac{2}{3}\mu_2).
\end{aligned} \tag{2.57}$$

Solving for the Christoffel equation, $\det(\mathbf{\Gamma}(\mathbf{n}) - \rho c^2)$, the eigenvalues of $\mathbf{\Gamma}$ are equal to ρc^2 for which there will be two shear speeds and one longitudinal. Three unique directions are chosen that will come into use later. We find

$$\begin{aligned}
\rho c^2 \begin{bmatrix} 1 \\ 0 \\ 0 \end{bmatrix} &= \left\{ \kappa + \frac{4}{3}\mu_2, \mu_1, \mu_1 \right\}, \\
\rho c^2 \begin{bmatrix} 1/\sqrt{2} \\ 1/\sqrt{2} \\ 0 \end{bmatrix} &= \left\{ \frac{1}{3}(3\kappa + 3\mu_1 + \mu_2), \mu_1, \mu_2 \right\}, \\
\rho c^2 \begin{bmatrix} 1/\sqrt{3} \\ 1/\sqrt{3} \\ 1/\sqrt{3} \end{bmatrix} &= \left\{ \frac{1}{3}(3\kappa + 4\mu_1), \frac{1}{3}(\mu_1 + 2\mu_2), \frac{1}{3}(\mu_1 + 2\mu_2) \right\},
\end{aligned} \tag{2.58}$$

where in brackets is the unit direction $\mathbf{n}$ in consideration. This analysis was completed here as these directions have a specific meaning when it comes to dispersion curves with cubic symmetries discussed towards the end of chapter 9. This review of material symmetries and group velocities was done due to it's importance when designing lattice structured metamaterials which will be discussed later in the thesis. Next attention is turned to acoustic scattering solutions from cylindrical elastic media.

Chapter 3

Elastic scattering solutions

A goal of this thesis is to produce elastic based metamaterials with application to acoustic cloaking. The problem is defined by reducing acoustic scattering of a cylindrical elastic scatterer to zero. To understand this phenomenon we start by deriving scattering solutions of a general multi-layered elastic cylinder in an acoustic background medium. Cloaking theory is reviewed in chapter 5 where the elastic moduli and density properties are found to be functions of the radius of the cloak. We approximate continuous properties by the discrete layering of materials. The approximation is valid if the layer thickness is small compared to the global dimensions of the cloak. Scattering solutions are developed for isotropic cylinders and fluid filled cylinders in sections 3.1 and 3.2, respectively. Potential functions are used to solve for isotropic or at most transversely isotropic cylinders. The problem, shown in figure 3.1, is of an incident wave interacting with a cylindrical layering of fluids and solids in a background external fluid. As similarly done in [35] and [36] we begin with scalar and vector potentials

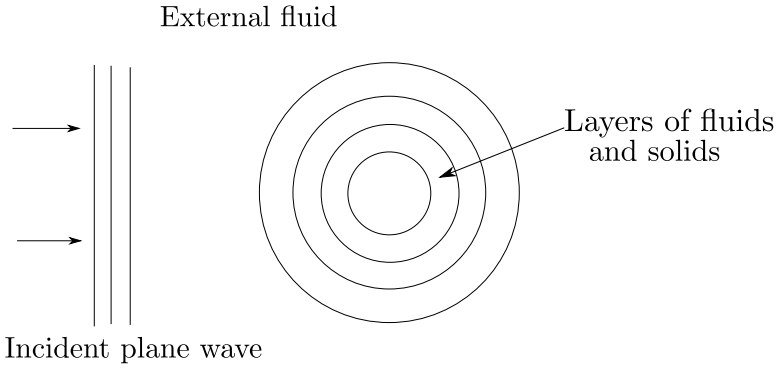

Figure 3.1: Problem setup of an incident wave in an external fluid interacting with cylindrical layers of fluids and solids.

that solve the equilibrium equations in cylindrical coordinates and generalize the equations in matrix form to solve for the scattering coefficients. This leads to the global matrix method solution, reviewed in section 3.3.

3.1 Isotropic cylinders

The displacement in the cylindrical solid is written in terms of the scalar potential, φ, and vector potential, $\psi\mathbf{e}_z$, with

$$\mathbf{u} = (\nabla\varphi + \nabla \times \psi\mathbf{e}_z)e^{-i\omega t}, \tag{3.1}$$

where φ represents longitudinal motion and $\psi\mathbf{e}_z$ represents transverse, we omit the time dependence $e^{i\omega t}$ henceforth. The potentials are

$$\varphi = \frac{1}{k_L}\sum_{n=0}^{\infty} A_n^0 R_{0n}^l z_n^l(k_L r)\cos n\theta, \quad \psi = \frac{1}{k_T}\sum_{n=0}^{\infty} n A_n^0 T_{0n}^l z_n^l(k_T r)\sin n\theta, \tag{3.2}$$

where $l = 1,\ 3$, and $A_n^0 = \epsilon_n i^n$ [36]. For $l = 1$: $z_n^1(k_L r) = J_n(k_L r)$, which is the Bessel function of the first kind representing incident waves, and for $l = 3$: $z_n^3(k_L r) = H_n(k_L r)$, which is the Hankel function of the first kind representing scattered waves. k_L and k_T are the longitudinal and transverse wave numbers, respectively. R_{on}^l are the unknown longitudinal scattering coefficients and T_{0n}^l are the unknown transverse scattering coefficients. In cylindrical coordinates the gradient and curl operators take the form

$$\begin{aligned} \nabla\varphi &= \frac{\partial\varphi}{\partial r}\mathbf{e}_r + \frac{1}{r}\frac{\partial\varphi}{\partial\theta}\mathbf{e}_\theta, \\ \nabla \times \psi\mathbf{e}_z &= \frac{1}{r}\frac{\partial\psi}{\partial\theta}\mathbf{e}_r - \frac{\partial\psi}{\partial r}\mathbf{e}_\theta. \end{aligned} \tag{3.3}$$

Using Equations (3.1) and (3.2) the displacement components are found with

$$\begin{aligned} u_r &= \sum_{n=0}^{\infty} A_n^0 \cos n\theta\big[R_{0n}^l z_n^{l'}(k_L r) + \frac{n^2}{k_T r}T_{0n}^l z_n^l(k_T r)\big], \\ u_\theta &= \sum_{n=0}^{\infty}(n^{-1}A_n^0\frac{\partial}{\partial\theta}\cos n\theta)\big[\frac{n}{k_L r}R_{0n}^l z_n^l(k_L r) + nT_{0n}^l z_n^{l'}(k_T r)\big]. \end{aligned} \tag{3.4}$$

In order to simplify the solution equation (3.4) is rewritten in matrix form. We define the vectors $\mathbf{P}_{0n}$ and $\mathbf{B}_{0n}$ as

$$\mathbf{P}_{0n} = A_n^0 \cos n\theta\mathbf{e}_r, \quad \mathbf{B}_{0n} = \eta_n A_n^0\frac{\partial}{\partial\theta}\cos n\theta\mathbf{e}_\theta, \tag{3.5}$$

where $\eta_n = n^{-1}$. The unknown scattering coefficients are written in vector form as

$$\mathbf{w}_{0n}^{l} = \begin{pmatrix} R_{0n}^{l} \\ T_{0n}^{l} \end{pmatrix}. \tag{3.6}$$

Defining the 2×2 matrix

$$\mathbf{U}_{n}^{l} = \begin{pmatrix} z_n^{l'}(k_L r) & (\eta_n^2 k_T r)^{-1} z_n^{l}(k_T r) \\ (\eta_n k_L r)^{-1} z_n^{l}(k_L r) & \eta_n^{-1} z_n^{l'}(k_T r) \end{pmatrix}, \tag{3.7}$$

the displacement is then written as

$$\mathbf{u} = \begin{pmatrix} \mathbf{P}_{0n} & \mathbf{B}_{0n} \end{pmatrix}_{2\times 2} \begin{pmatrix} \mathbf{U}_n^1 & \mathbf{U}_n^3 \end{pmatrix}_{2\times 4} \begin{pmatrix} \mathbf{w}_{0n}^1 \\ \mathbf{w}_{0n}^3 \end{pmatrix}_{4\times 1}, \tag{3.8}$$

where $\mathbf{u} = \begin{bmatrix} u_r & u_\theta \end{bmatrix}^T$. The strains are found by combining the displacement components of equation (3.4) into the strain definition of equation (2.9), this yields

$$\begin{aligned}
\varepsilon_{rr} &= \sum_{n=0}^{\infty} A_n^0 \cos n\theta \big[R_{0n}^{l} k_L z_n^{l''}(k_L r) + T_{0n}^{l} (\frac{n^2}{r} z_n^{l'}(k_T r) - \frac{n^2}{k_T r^2} z_n^{l}(k_T r)) \big], \\
\varepsilon_{\theta\theta} &= \frac{1}{r} \sum_{n=0}^{\infty} A_n^0 \cos n\theta \Big[R_{0n}^{l} \big[z_n^{l'}(k_L r) - \frac{n^2}{k_L r} z_n^{l}(k_L r) \big] + \\
&\quad T_{0n}^{l} \big[\frac{n^2}{k_T r} z_n^{l}(k_T r) - n^2 z_n^{l'}(k_T r) \big] \Big], \\
\varepsilon_{r\theta} &= \frac{1}{2} \sum_{n=0}^{\infty} (n^{-1} A_n^0 \frac{\partial}{\partial \theta} \cos n\theta) \Big[R_{0n} \big[\frac{2n}{r} z_n^{l'}(k_L r) - \frac{2n}{k_L r^2} z_n^{l}(k_L r) \big] + \\
&\quad T_{0n} \big[(\frac{2n^3}{k_T r^2} - n k_T) z_n^{l}(k_T r) - \frac{2n}{r} z_n^{l'}(k_T r) \big] \Big].
\end{aligned} \tag{3.9}$$

The stress strain constitutive relations for an isotropic medium are

$$\begin{bmatrix} \sigma_{rr} \\ \sigma_{\theta\theta} \\ \sigma_{zz} \\ \sigma_{\theta z} \\ \sigma_{rz} \\ \sigma_{r\theta} \end{bmatrix} = \begin{bmatrix} 2\mu+\lambda & \lambda & \lambda & 0 & 0 & 0 \\ \lambda & 2\mu+\lambda & \lambda & 0 & 0 & 0 \\ \lambda & \lambda & 2\mu+\lambda & 0 & 0 & 0 \\ 0 & 0 & 0 & \mu & 0 & 0 \\ 0 & 0 & 0 & 0 & \mu & 0 \\ 0 & 0 & 0 & 0 & 0 & \mu \end{bmatrix} \begin{bmatrix} \varepsilon_{rr} \\ \varepsilon_{\theta\theta} \\ \varepsilon_{zz} \\ 2\varepsilon_{\theta z} \\ 2\varepsilon_{rz} \\ 2\varepsilon_{r\theta} \end{bmatrix}. \tag{3.10}$$

We can write the above relations using the longitudinal and transverse wavenumbers where

$$k_T = \frac{\omega}{c_T} = \frac{\omega}{\sqrt{\mu/\rho}}, \quad k_L = \frac{\omega}{c_L} = \frac{\omega}{\sqrt{(\lambda+2\mu)/\rho}}, \tag{3.11}$$

and c_T, c_L are the transverse and longitudinal group velocities as found from the Christoffel equation from the previous chapter. The stress strain relation is then

$$\begin{bmatrix}\sigma_{rr}\\ \sigma_{\theta\theta}\\ \sigma_{zz}\\ \sigma_{\theta z}\\ \sigma_{rz}\\ \sigma_{r\theta}\end{bmatrix} = \mu \begin{bmatrix} (k_T/k_L)^2 & (k_T/k_L)^2-2 & (k_T/k_L)^2-2 & 0 & 0 & 0\\ (k_T/k_L)^2-2 & (k_T/k_L)^2 & (k_T/k_L)^2-2 & 0 & 0 & 0\\ (k_T/k_L)^2-2 & (k_T/k_L)^2-2 & (k_T/k_L)^2 & 0 & 0 & 0\\ 0 & 0 & 0 & 1 & 0 & 0\\ 0 & 0 & 0 & 0 & 1 & 0\\ 0 & 0 & 0 & 0 & 0 & 1 \end{bmatrix} \begin{bmatrix}\varepsilon_{rr}\\ \varepsilon_{\theta\theta}\\ \varepsilon_{zz}\\ 2\varepsilon_{\theta z}\\ 2\varepsilon_{rz}\\ 2\varepsilon_{r\theta}\end{bmatrix}. \tag{3.12}$$

A substitution of the strain relations from equations (3.9) into the constitutive relations of equation (3.12) yields the stresses σ_{rr} and $\sigma_{r\theta}$,

$$\begin{aligned}\sigma_{rr} &= \mu\sum_{n=0}^{\infty} A_n^0 \cos n\theta \Big[R_{0n}^l \big[2k_L z_n^{l''}(k_L r) + (2k_L - \frac{k_T^2}{k_L}) z_n^l(k_L r)\big] + \\ &\quad T_{0n}^l \big[\frac{2n^2}{r} z_n^{l'}(k_T r) - \frac{2n^2}{k_T r^2} z_n^l(k_T r)\big]\Big], \\ \sigma_{r\theta} &= \mu\sum_{n=0}^{\infty} (n^{-1} A_n^0 \frac{\partial}{\partial\theta}\cos n\theta) \Big[R_{0n}\big[\frac{2n}{r} z_n^{l'}(k_L r) - \frac{2n}{k_L r^2} z_n^l(k_L r)\big] + \\ &\quad T_{0n}\big[n[\frac{2n^2}{k_T r^2} - k_T] z_n^l(k_T r) - 2\frac{n}{r} z_n^{l'}(k_T r)\big]\Big].\end{aligned} \tag{3.13}$$

These equations are converted to the matrix form with

$$\mathbf{t} = \begin{pmatrix}\mathbf{P}_{0n} & \mathbf{B}_{0n}\end{pmatrix}_{2\times 2} \begin{pmatrix}\mathbf{T}_n^1 & \mathbf{T}_n^3\end{pmatrix}_{2\times 4} \begin{pmatrix}\mathbf{w}_{0n}^1\\ \mathbf{w}_{0n}^3\end{pmatrix}_{4\times 1}, \tag{3.14}$$

where $\mathbf{t} = \begin{bmatrix}\sigma_{rr} & \sigma_{r\theta}\end{bmatrix}^T$ and

$$\mathbf{T}_n^l = \mu\times \begin{pmatrix} k_L(2z_n^{l''}(k_L r) - (\frac{k_T^2}{k_L^2}-2) z_n^l(k_L r)) & 2(\eta_n^2 r)^{-1}(z_n^{l'}(k_T r) - \frac{z_n^l(k_T r)}{k_T r}) \\ 2(\eta_n r)^{-1}(z_n^{l'}(k_L r) - \frac{z_n^l(k_L r)}{k_L r}) & (\eta_n r)^{-1}((2n^2 - (k_T r)^2)\frac{z_n^l(k_T r)}{k_T r} - 2z_n^{l'}(k_T r)) \end{pmatrix}. \tag{3.15}$$

The global matrix method can be developed using this formulation of displacement and stress vectors for cylindrical layers of isotropic materials. It will be continuity of radial displacement u_r and traction components σ_{rr} and $\sigma_{r\theta}$ that will allow for this. Next these vectors are found for layers of acoustic fluids.

3.2 Acoustic fluids

We review section 2.1 from the previous chapter in order to solve for either fluid filled cylindrical layers or the background fluid in matrix form. The pressure in an acoustic fluid is given by

$$P = \sum_{n=0}^{\infty} (A_n^0 \cos n\theta) R_{0n}^l \kappa k z_n^l(kr), \tag{3.16}$$

where $\kappa = \rho c^2$, is the bulk modulus, $k = \omega/c$, is the wave number, and in cylindrical coordinates it is convenient to note $\sigma_{rr} = -P$. Next we take advantage of the momentum balance equation in order to find the displacement field in the fluid. The momentum balance equation gives

$$\rho \frac{\partial \mathbf{v}}{\partial t} + \nabla P = -\rho\omega^2 \mathbf{u} + \nabla P = 0, \tag{3.17}$$

where the gradient of P in cylindrical coordinates is

$$\nabla P = \frac{\partial P}{\partial r}\mathbf{e}_r + \frac{1}{r}\frac{\partial P}{\partial \theta}\mathbf{e}_\theta. \tag{3.18}$$

Using equation (3.16) and looking at the radial component of the gradient we find

$$\frac{\partial P}{\partial r} = \sum_{n=0}^{\infty} A_n^0 \cos n\theta R_{0n}^l \kappa k^2 z_n^{l'}(kr) = \rho\omega^2 \sum_{n=0}^{\infty} A_n^0 \cos n\theta R_{0n}^l z_n^{l'}(kr), \tag{3.19}$$

comparing with equation (3.17) the radial displacement is

$$u_r = \sum_{n=0}^{\infty} A_n^0 \cos n\theta R_{0n}^l z_n^{l'}(kr). \tag{3.20}$$

Undergoing the same analysis the angular component of the displacement is found by analyzing the second term of equation (3.18), where

$$\frac{1}{r}\frac{\partial P}{\partial \theta} = \frac{1}{r}\sum_{n=0}^{\infty} (n^{-1} A_n^0 \frac{\partial}{\partial \theta} \cos n\theta) R_{0n}^l \kappa k z_n^l(kr), \tag{3.21}$$

this implies

$$u_\theta = \sum_{n=0}^{\infty} (n^{-1} A_n^0 \frac{\partial}{\partial \theta} \cos n\theta) R_{0n}^l \frac{n^{-1}}{rk} z_n^l(kr). \tag{3.22}$$

Comparing to the previous analysis for elastic cylinders there is no need to change how the displacements are defined in equation (3.8). To change from solid to fluid displacement or traction we take shear moduli terms as zero and replace k_L by k.

3.3 Global matrix method

The previous sections worked to form the stress and displacements components of fluid or elastic cylinders in matrix form. Next we construct these elements into a global matrix system to solve for the scattering problem of a plane wave incident upon a system of concentrically layered fluid or elastic cylinders.

3.3.1 Acoustic scattering from a solid elastic cylinder

Starting with the simplest case of a plane wave incident upon a single elastic cylinder we use continuity of displacement and traction to create a global matrix to solve this scattering problem. The system is defined by

$$\begin{aligned} &\text{solid, } \rho_1,\ \lambda_1,\ \mu_1, && 0 \le r < a, \\ &\text{fluid, } \rho_0,\ \kappa_0 = \rho_0 c_0^2, && a \le r < \infty. \end{aligned} \tag{3.23}$$

In the outer fluid the displacement is given by

$$\mathbf{u}(r) = \begin{pmatrix} \mathbf{P}_{0n} & \mathbf{B}_{0n} \end{pmatrix} \begin{pmatrix} a_n^1(k_0 r) & a_n^3(k_0 r) \\ c_n^1(k_0 r) & c_n^3(k_0 r) \end{pmatrix} \begin{pmatrix} R_{0n}^{1,0} \\ R_{0n}^{3,0} \end{pmatrix}. \tag{3.24}$$

Boundary conditions for this problem require continuity of radial displacement, u_r, and traction components σ_{rr}, $\sigma_{r\theta}$. Equation (3.24) has the radial displacement component as

$$u_r = A_n^0 \cos n\theta \begin{pmatrix} a_n^1(k_0 r) & a_n^3(k_0 r) \end{pmatrix} \begin{pmatrix} R_{0n}^{1,0} \\ R_{0n}^{3,0} \end{pmatrix}, \tag{3.25}$$

where

$$a_n^1(k_0 r) = J_n^{'}(k_0 r), \quad a_n^3(k_0 r) = H_n^{(1)'}(k_0 r). \tag{3.26}$$

The stresses σ_{rr} and $\sigma_{r\theta}$ in the outer fluid are

$$\sigma_{rr} = A_n^0 \cos n\theta \begin{pmatrix} \bar{\alpha}_n^1(r, k_0, \kappa_0) & \bar{\alpha}_n^3(r, k_0, \kappa_0) \end{pmatrix} \begin{pmatrix} R_{0n}^{1,0} \\ R_{0n}^{3,0} \end{pmatrix}, \ \ \sigma_{r\theta} = 0, \tag{3.27}$$

where

$$\bar{\alpha}_n^1(r, k_0, \kappa_0) = -\kappa_0 k_0 J_n(k_0 r), \quad \bar{\alpha}_n^3(k_0 r) = -\kappa_0 k_0 H_n^{(1)}(k_0 r). \tag{3.28}$$

In this example the radius of the solid goes to zero, this means the scalar potentials must take the form

$$\begin{aligned}\varphi &= \frac{1}{k_L}\sum_{n=0}^{\infty} A_n^0 \cos n\theta R_{0n}^1 J_n(k_L r),\\ \psi &= \frac{1}{k_T}\sum_{n=0}^{\infty} n A_n^0 \sin n\theta T_{0n}^1 J_n(k_T r).\end{aligned} \tag{3.29}$$

The displacement in the solid is given by

$$u_r = A_n^0 \cos n\theta \begin{pmatrix} a_n^1(k_L r) & b_n^1(k_T r)\end{pmatrix}\begin{pmatrix} R_{0n}^{1,1} \\ T_{0n}^{1,1}\end{pmatrix}, \tag{3.30}$$

where

$$a_n^1(k_L r) = J_n^{'}(k_L r),\;\; b_n^1(k_T r) \;\; = \frac{n^2}{k_T r} J_n(k_T r). \tag{3.31}$$

The stresses are then given by

$$\begin{aligned}\sigma_{rr} &= A_n^0 \cos n\theta \begin{pmatrix} \alpha_n^1(k_L r) & \beta_n^1(k_T r)\end{pmatrix}\begin{pmatrix} R_{0n}^{1,1} \\ T_{0n}^{1,1}\end{pmatrix},\\ \sigma_{r\theta} &= -A_n^0 \sin n\theta \begin{pmatrix} \gamma_n^1(k_L r) & \delta_n^1(k_T r)\end{pmatrix}\begin{pmatrix} R_{0n}^{1,1} \\ T_{0n}^{1,1}\end{pmatrix},\end{aligned} \tag{3.32}$$

where

$$\begin{aligned}\alpha_n^1(k_L r) &= \mu_1 k_L (2J_n^{''}(k_L r) - (\frac{k_T^2}{k_L^2} - 2) J_n(k_L r)),\\ \beta_n^1(k_T r) &= \mu_1 \frac{2n^2}{r}(J_n^{'}(k_T r) - \frac{J_n(k_T r)}{k_T r}),\end{aligned} \tag{3.33}$$

and

$$\begin{aligned}\gamma_n^1(k_L r) &= \mu_1 \frac{2n}{r}(J_n^{'}(k_L r) - \frac{J_n(k_L r)}{k_L r}),\\ \delta_n^1(k_T r) &= \mu_1 \frac{n}{r}((2n^2 - (k_T r)^2)\frac{J_n^{(}k_T r)}{k_T r} - 2J_n^{'}(k_T r)).\end{aligned} \tag{3.34}$$

The system that results when boundary conditions for displacements and stresses are applied is given by

$$\begin{pmatrix} a_n^3(k_0 a) & a_n^1(k_L a) & b_n^1(k_T a) \\ \bar{\alpha}_n^3(a, k_0, \kappa_0) & \alpha_n^1(k_L a) & \beta_n^1(k_T a) \\ 0 & \gamma_n^1(k_L a) & \delta_n^1(k_T a)\end{pmatrix}\begin{pmatrix} -R_{0n}^{3,0} \\ R_{0n}^{1,1} \\ T_{0n}^{1,1}\end{pmatrix} = R_{0n}^{1,0}\begin{pmatrix} a_n^1(k_0 a) \\ \bar{\alpha}_n^1(a, k_0, \kappa_0) \\ 0\end{pmatrix}. \tag{3.35}$$

This is the global matrix to be solved for the simplest case of one elastic cylinder in an acoustic background medium.

3.3.2 Acoustic scattering from a fluid filled elastic cylinder

The system properties for this problem are

$$\begin{aligned} &\text{fluid, } \rho_{in},\ \kappa_{in} = \rho_{in}c_{in}^2, && 0 \le r < b, \\ &\text{solid, } \rho_1,\ \lambda_1,\ \mu_1, && b \le r < a, \\ &\text{fluid, } \rho_0,\ \kappa_0 = \rho_0 c_0^2, && a \le r < \infty. \end{aligned} \tag{3.36}$$

We must keep in mind that the solid layer does not contain $r = 0$ which means both Bessel functions, $J_n(X)$ and $Y_n(X)$, are present there. In the outer fluid the displacement is given by

$$\mathbf{u}(r) = \begin{pmatrix} \mathbf{P}_{0n} & \mathbf{B}_{0n} \end{pmatrix} \begin{pmatrix} a_n^1(k_0 r) & a_n^3(k_0 r) \\ c_n^1(k_0 r) & c_n^3(k_0 r) \end{pmatrix} \begin{pmatrix} R_{0n}^{1,0} \\ R_{0n}^{3,0} \end{pmatrix}. \tag{3.37}$$

We will only be interested in continuity of u_r and tractions σ_{rr} and $\sigma_{r\theta}$. Equation (3.37) states that

$$u_r = A_n^0 \cos n\theta \begin{pmatrix} a_n^1(k_0 r) & a_n^3(k_0 r) \end{pmatrix} \begin{pmatrix} R_{0n}^{1,0} \\ R_{0n}^{3,0} \end{pmatrix}, \tag{3.38}$$

where

$$a_n^1(k_0 r) = J_n^{'}(k_0 r), \quad a_n^3(k_0 r) = H_n^{(1)'}(k_0 r). \tag{3.39}$$

Next the stresses, σ_{rr} and $\sigma_{r\theta}$ are given by

$$\sigma_{rr} = A_n^0 \cos n\theta \begin{pmatrix} \bar{\alpha}_n^1(r, k_0, \kappa_0) & \bar{\alpha}_n^3(r, k_0, \kappa_0) \end{pmatrix} \begin{pmatrix} R_{0n}^{1,0} \\ R_{0n}^{3,0} \end{pmatrix}, \ \ \sigma_{r\theta} = 0, \tag{3.40}$$

where

$$\bar{\alpha}_n^1(r, k_0, \kappa_0) = -\kappa_0 k_0 J_n(k_0 r), \quad \bar{\alpha}_n^3(k_0 r) = -\kappa_0 k_0 H_n^{(1)}(k_0 r). \tag{3.41}$$

In the solid, so long as the radius does not go to zero, that is the solid is a shell, then Bessel functions $J_n(X)$ and $Y_n(X)$ solutions are possible. For this situation the scalar potentials are given by

$$\begin{aligned} \varphi &= \frac{1}{k_L} \sum_{n=0}^{\infty} A_n^0 \cos n\theta (R_{0n}^1 J_n(k_L r) + R_{0n}^2 Y_n(k_L r)), \\ \psi &= \frac{1}{k_T} \sum_{n=0}^{\infty} n A_n^0 \sin n\theta (T_{0n}^1 J_n(k_T r) + T_{0n}^2 Y_n(k_T r)). \end{aligned} \tag{3.42}$$

The radial displacement in the solid is given by

$$u_r = A_n^0 \cos n\theta \begin{pmatrix} a_n^1(k_L r) & b_n^1(k_T r) & a_n^2(k_L r) & b_n^2(k_T r) \end{pmatrix} \begin{pmatrix} R_{0n}^{1,1} \\ T_{0n}^{1,1} \\ R_{0n}^{2,1} \\ T_{0n}^{2,1} \end{pmatrix}, \tag{3.43}$$

where

$$\begin{aligned} a_n^1(k_L r) = J_n^{'}(k_L r), \;\; b_n^1(k_T r) &= \frac{n^2}{k_T r} J_n(k_T r), \\ a_n^2(k_L r) = Y_n^{'}(k_L r), \;\; b_n^2(k_T r) &= \frac{n^2}{k_T r} Y_n(k_T r). \end{aligned} \tag{3.44}$$

The stresses are then

$$\begin{aligned} \sigma_{rr} &= A_n^0 \cos n\theta \begin{pmatrix} \alpha_n^1(k_L r) & \beta_n^1(k_T r) & \alpha_n^2(k_L r) & \beta_n^2(k_T r) \end{pmatrix} \begin{pmatrix} R_{0n}^{1,1} \\ T_{0n}^{1,1} \\ R_{0n}^{2,1} \\ T_{0n}^{2,1} \end{pmatrix}, \\ \sigma_{r\theta} &= -A_n^0 \sin n\theta \begin{pmatrix} \gamma_n^1(k_L r) & \delta_n^1(k_T r) & \gamma_n^2(k_L r) & \delta_n^2(k_T r) \end{pmatrix} \begin{pmatrix} R_{0n}^{1,1} \\ T_{0n}^{1,1} \\ R_{0n}^{2,1} \\ T_{0n}^{2,1} \end{pmatrix}, \end{aligned} \tag{3.45}$$

where

$$\begin{aligned} \alpha_n^1(k_L r) &= \mu_1 k_L (2J_n^{''}(k_L r) - (\frac{k_T^2}{k_L^2} - 2) J_n(k_L r)), \\ \beta_n^1(k_T r) &= \mu_1 \frac{2n^2}{r} (J_n^{'}(k_T r) - \frac{J_n(k_T r)}{k_T r}), \\ \alpha_n^2(k_L r) &= \mu_1 k_L (2Y_n^{''}(k_L r) - (\frac{k_T^2}{k_L^2} - 2) Y_n^{(}k_L r)), \\ \beta_n^2(k_T r) &= \mu_1 \frac{2n^2}{r} (Y_n^{'}(k_T r) - \frac{Y_n(k_T r)}{k_T r}), \end{aligned} \tag{3.46}$$

and

$$\begin{aligned} \gamma_n^1(k_L r) &= \mu_1 \frac{2n}{r} (J_n^{'}(k_L r) - \frac{J_n(k_L r)}{k_L r}), \\ \delta_n^1(k_T r) &= \mu_1 \frac{n}{r} ((2n^2 - (k_T r)^2) \frac{J_n^{(}k_T r)}{k_T r} - 2J_n^{'}(k_T r)), \\ \gamma_n^2(k_L r) &= \mu_1 \frac{2n}{r} (Y_n^{'}(k_L r) - \frac{Y_n(k_L r)}{k_L r}), \\ \delta_n^2(k_T r) &= \mu_1 \frac{n}{r} ((2n^2 - (k_T r)^2) \frac{Y_n^{(}k_T r)}{k_T r} - 2Y_n^{'}(k_T r)). \end{aligned} \tag{3.47}$$

In the inner fluid the displacement is given by

$$u_r = A_n^0 \cos n\theta \left(a_n^1(k_{in}r)\right)\left(R_{0n}^{1,in}\right), \tag{3.48}$$

where

$$a_n^1(k_{in}r) = J_n^{'}(k_{in}r). \tag{3.49}$$

The stresses are

$$\sigma_{rr} = A_n^0 \cos n\theta \left(\bar{\alpha}_n^1(r, k_{in}, \kappa_{in})\right)\left(R_{0n}^{1,in}\right), \;\; \sigma_{r\theta} = 0, \tag{3.50}$$

where

$$\bar{\alpha}_n^1(r, k_{in}, \kappa_{in}) = -\kappa_{in}k_{in}J_n(k_0 r). \tag{3.51}$$

There are six unknown coefficients in this problem, which are

$$R_{0n}^{3,0},\; R_{0n}^{1,1},\; T_{0n}^{1,1},\; R_{0n}^{2,1},\; T_{0n}^{2,1},\; R_{0n}^{1,in}, \tag{3.52}$$

note that we are taking $R_{0n}^{1,0}$ as a known amplitude of incoming waves. The six boundary conditions needed to solve this system are continuity of traction components $\sigma_{r\theta}$, σ_{rr}, and displacement u_r at each boundary. At $n = 0$ the system has a singularity which is resolved by multiplying the $\sigma_{r\theta}$ equations by $\frac{r}{n}$. The final six by six system to be solved is

$$\begin{pmatrix} a_n^3(k_0a) & a_n^1(k_La) & b_n^1(k_Ta) & a_n^2(k_La) & b_n^2(k_Ta) & 0 \\ \bar{\alpha}_n^3(a,k_0,\kappa_0) & \alpha_n^1(k_La) & \beta_n^1(k_Ta) & \alpha_n^2(k_La) & \beta_n^2(k_Ta) & 0 \\ 0 & \frac{a}{n}\gamma_n^1(k_La) & \frac{a}{n}\delta_n^1(k_Ta) & \frac{a}{n}\gamma_n^2(k_La) & \frac{a}{n}\delta_n^2(k_Ta) & 0 \\ 0 & a_n^1(k_Lb) & b_n^1(k_Tb) & a_n^2(k_Lb) & b_n^2(k_Tb) & a_n^1(k_{in}b) \\ 0 & \alpha_n^1(k_Lb) & \beta_n^1(k_Tb) & \alpha_n^2(k_Lb) & \beta_n^2(k_Tb) & \bar{\alpha}_n^1(b,k_{in},\kappa_{in}) \\ 0 & \frac{b}{n}\gamma_n^1(k_Lb) & \frac{b}{n}\delta_n^1(k_Tb) & \frac{b}{n}\gamma_n^2(k_Lb) & \frac{b}{n}\delta_n^2(k_Tb) & 0 \end{pmatrix} \times \begin{pmatrix} -R_{0n}^{3,0} \\ R_{0n}^{1,1} \\ T_{0n}^{1,1} \\ R_{0n}^{2,1} \\ T_{0n}^{2,1} \\ -R_{0n}^{1,in} \end{pmatrix} = R_{0n}^{1,0} \begin{pmatrix} a_n^1(k_0a) \\ \bar{\alpha}_n^1(a,k_0,\kappa_0) \\ 0 \\ 0 \\ 0 \\ 0 \end{pmatrix}. \tag{3.53}$$

Clearly as more layers are added to the system the matrix to be solved grows quickly, which is a general pitfall of the global matrix method especially for larger systems.

3.3.3 Acoustic scattering from a cladded rod

In the example studied here we see how replacing the inner fluid of the previous problem with an elastic medium grows the matrix to be solved. The system setup is

$$\begin{aligned} &\text{solid, } \rho_2,\ \lambda_2,\ \mu_2, && 0 \le r < b, \\ &\text{solid, } \rho_1,\ \lambda_1,\ \mu_1, && b \le r < a, \\ &\text{fluid, } \rho_0,\ \kappa_0 = \rho_0 c_0^2, && a \le r < \infty. \end{aligned} \tag{3.54}$$

Again in the background outer fluid the displacement is given by

$$\mathbf{u}(r) = \begin{pmatrix} \mathbf{P}_{0n} & \mathbf{B}_{0n} \end{pmatrix} \begin{pmatrix} a_n^1(k_0 r) & a_n^3(k_0 r) \\ c_n^1(k_0 r) & c_n^3(k_0 r) \end{pmatrix} \begin{pmatrix} R_{0n}^{1,0} \\ R_{0n}^{3,0} \end{pmatrix}. \tag{3.55}$$

For fluid-solid interfaces we are only interested in continuity of displacement u_r and traction components σ_{rr} and $\sigma_{r\theta}$. The radial displacement for the background medium is

$$u_r = A_n^0 \cos n\theta \begin{pmatrix} a_n^1(k_0 r) & a_n^3(k_0 r) \end{pmatrix} \begin{pmatrix} R_{0n}^{1,0} \\ R_{0n}^{3,0} \end{pmatrix}, \tag{3.56}$$

where

$$a_n^1(k_0 r) = J_n^{'}(k_0 r), \quad a_n^3(k_0 r) = H_n^{(1)'}(k_0 r). \tag{3.57}$$

Next the stresses, σ_{rr}, and $\sigma_{r\theta}$ are

$$\sigma_{rr} = A_n^0 \cos n\theta \begin{pmatrix} \bar{\alpha}_n^1(r, k_0, \kappa_0) & \bar{\alpha}_n^3(r, k_0, \kappa_0) \end{pmatrix} \begin{pmatrix} R_{0n}^{1,0} \\ R_{0n}^{3,0} \end{pmatrix}, \ \ \sigma_{r\theta} = 0, \tag{3.58}$$

where

$$\bar{\alpha}_n^1(r, k_0, \kappa_0) = -\kappa_0 k_0 J_n(k_0 r), \quad \bar{\alpha}_n^3(k_0 r) = -\kappa_0 k_0 H_n^{(1)}(k_0 r). \tag{3.59}$$

Solid annulus $(b < r < a)$

Since we have two elastic media in contact, we will now be concerned about the continuity of u_θ displacements between solid-solid interfaces. As in the previous section for

$b < r < a$ where the radius of the solid doesn't go to zero the scalar potentials must take the form

$$\begin{aligned}\varphi &= \frac{1}{k_L}\sum_{n=0}^{\infty} A_n^0 \cos n\theta (R_{0n}^{1,1} J_n(k_{L1}r) + R_{0n}^{2,1} Y_n(k_{L1}r)),\\ \psi &= \frac{1}{k_T}\sum_{n=0}^{\infty} n A_n^0 \sin n\theta (T_{0n}^{1,1} J_n(k_{T1}r) + T_{0n}^{2,1} Y_n(k_{T1}r)).\end{aligned} \tag{3.60}$$

The displacement components in the solid are given by

$$\begin{aligned}u_r &= A_n^0 \cos n\theta \begin{pmatrix} a_n^1(k_{L1}r) & b_n^1(k_{T1}r) & a_n^2(k_{L1}r) & b_n^2(k_{T1}r)\end{pmatrix} \begin{pmatrix} R_{0n}^{1,1}\\ T_{0n}^{1,1}\\ R_{0n}^{2,1}\\ T_{0n}^{2,1}\end{pmatrix},\\ u_\theta &= -A_n^0 \sin n\theta \begin{pmatrix} c_n^1(k_{L1}r) & d_n^1(k_{T1}r) & c_n^2(k_{L1}r) & d_n^2(k_{T1}r)\end{pmatrix} \begin{pmatrix} R_{0n}^{1,1}\\ T_{0n}^{1,1}\\ R_{0n}^{2,1}\\ T_{0n}^{2,1}\end{pmatrix},\end{aligned} \tag{3.61}$$

where

$$\begin{aligned} a_n^1(k_{L1}r) &= J_n^{'}(k_{L1}r), & b_n^1(k_{T1}r) &= \frac{n^2}{k_{T1}r} J_n(k_{T1}r),\\ a_n^2(k_{L1}r) &= Y_n^{'}(k_{L1}r), & b_n^2(k_{T1}r) &= \frac{n^2}{k_{T1}r} Y_n(k_{T1}r),\\ c_n^1(k_{L1}r) &= \frac{n}{k_{L1}r} J_n(k_{L1}r), & d_n^1(k_{T1}r) &= n J_n^{'}(k_{T1}r),\\ c_n^2(k_{L1}r) &= \frac{n}{k_{L1}r} Y_n(k_{L1}r), & d_n^2(k_{T1}r) &= n Y_n^{'}(k_{T1}r).\end{aligned} \tag{3.62}$$

The stresses are then

$$\begin{aligned}\sigma_{rr} &= A_n^0 \cos n\theta \begin{pmatrix} \alpha_n^1(k_{L1}r) & \beta_n^1(k_{T1}r) & \alpha_n^2(k_{L1}r) & \beta_n^2(k_{T1}r)\end{pmatrix} \begin{pmatrix} R_{0n}^{1,1}\\ T_{0n}^{1,1}\\ R_{0n}^{2,1}\\ T_{0n}^{2,1}\end{pmatrix},\\ \sigma_{r\theta} &= -A_n^0 \sin n\theta \begin{pmatrix} \gamma_n^1(k_{L1}r) & \delta_n^1(k_{T1}r) & \gamma_n^2(k_{L1}r) & \delta_n^2(k_{T1}r)\end{pmatrix} \begin{pmatrix} R_{0n}^{1,1}\\ T_{0n}^{1,1}\\ R_{0n}^{2,1}\\ T_{0n}^{2,1}\end{pmatrix},\end{aligned} \tag{3.63}$$

where

$$\begin{aligned}
\alpha_n^1(k_{L1}r) &= \mu_1 k_{L1}(2J_n^{''}(k_{L1}r) - (\frac{k_{T1}^2}{k_{L1}^2} - 2)J_n(k_{L1}r)),\\
\alpha_n^2(k_{L1}r) &= \mu_1 k_{L1}(2Y_n^{''}(k_{L1}r) - (\frac{k_{T1}^2}{k_{L1}^2} - 2)Y_n(k_{L1}r)),\\
\beta_n^1(k_{T1}r) &= \mu_1 \frac{2n^2}{r}(J_n^{'}(k_{T1}r) - \frac{J_n(k_{T1}r)}{k_{T1}r}),\\
\beta_n^2(k_{T1}r) &= \mu_1 \frac{2n^2}{r}(Y_n^{'}(k_{T1}r) - \frac{Y_n(k_{T1}r)}{k_{T1}r}),
\end{aligned} \tag{3.64}$$

and

$$\begin{aligned}
\gamma_n^1(k_{L1}r) &= \mu_1 \frac{2n}{r}(J_n^{'}(k_{L1}r) - \frac{J_n(k_{L1}r)}{k_{L1}r}),\\
\gamma_n^2(k_{L1}r) &= \mu_1 \frac{2n}{r}(Y_n^{'}(k_{L1}r) - \frac{Y_n(k_{L1}r)}{k_{L1}r}),\\
\delta_n^1(k_{T1}r) &= \mu_1 \frac{n}{r}((2n^2 - (k_{T1}r)^2)\frac{J_n(k_{T1}r)}{k_{T1}r} - 2J_n^{'}(k_{T1}r)),\\
\delta_n^2(k_{T1}r) &= \mu_1 \frac{n}{r}((2n^2 - (k_{T1}r)^2)\frac{Y_n(k_{T1}r)}{k_{T1}r} - 2Y_n^{'}(k_{T1}r)).
\end{aligned} \tag{3.65}$$

Solid core $(r < b)$

Since the radius of the solid is allowed to go to zero the scalar potentials must take the form

$$\begin{aligned}
\varphi &= \frac{1}{k_L}\sum_{n=0}^{\infty} A_n^0 \cos n\theta R_{0n}^{1,2} J_n(k_{L2}r),\\
\psi &= \frac{1}{k_T}\sum_{n=0}^{\infty} nA_n^0 \sin n\theta T_{0n}^{1,2} J_n(k_{T2}r).
\end{aligned} \tag{3.66}$$

The displacement components are

$$\begin{aligned}
u_r &= A_n^0 \cos n\theta \begin{pmatrix} a_n^1(k_{L2}r) & b_n^1(k_{T2}r) \end{pmatrix} \begin{pmatrix} R_{0n}^{1,2} \\ T_{0n}^{1,2} \end{pmatrix},\\
u_\theta &= -A_n^0 \sin n\theta \begin{pmatrix} c_n^1(k_{L2}r) & d_n^1(k_{T2}r) \end{pmatrix} \begin{pmatrix} R_{0n}^{1,2} \\ T_{0n}^{1,2} \end{pmatrix},
\end{aligned} \tag{3.67}$$

where

$$\begin{aligned}
a_n^1(k_{L2}r) &= J_n^{'}(k_{L2}r), & b_n^1(k_{T2}r) &= \frac{n^2}{k_{T2}r}J_n(k_{T2}r),\\
c_n^1(k_{L2}r) &= \frac{n}{k_{L2}r}J_n(k_{L2}r), & d_n^1(k_{T2}r) &= nJ_n^{'}(k_{T2}r).
\end{aligned} \tag{3.68}$$

The stresses are then

$$\begin{aligned}\sigma_{rr} &= A_n^0 \cos n\theta \begin{pmatrix} \alpha_n^1(k_{L2}r) & \beta_n^1(k_{T2}r) \end{pmatrix} \begin{pmatrix} R_{0n}^{1,2} \\ T_{0n}^{1,2} \end{pmatrix}, \\ \sigma_{r\theta} &= -A_n^0 \sin n\theta \begin{pmatrix} \gamma_n^1(k_{L2}r) & \delta_n^1(k_{T2}r) \end{pmatrix} \begin{pmatrix} R_{0n}^{1,2} \\ T_{0n}^{1,2} \end{pmatrix}, \end{aligned} \tag{3.69}$$

where

$$\begin{aligned}\alpha_n^1(k_{L2}r) &= \mu_1 k_{L2}(2J_n^{''}(k_L r) - (\frac{k_{T2}^2}{k_{L2}^2} - 2)J_n(k_{L2}r)), \\ \beta_n^1(k_{T2}r) &= \mu_1 \frac{2n^2}{r}(J_n^{'}(k_{T2}r) - \frac{J_n(k_{T2}r)}{k_{T2}r}), \end{aligned} \tag{3.70}$$

and

$$\begin{aligned}\gamma_n^1(k_{L2}r) &= \mu_1 \frac{2n}{r}(J_n^{'}(k_{L2}r) - \frac{J_n(k_{L2}r)}{k_{L2}r}), \\ \delta_n^1(k_{T2}r) &= \mu_1 \frac{n}{r}((2n^2 - (k_{T2}r)^2)\frac{J_n(k_{T2}r)}{k_{T2}r} - 2J_n^{'}(k_{T2}r)). \end{aligned} \tag{3.71}$$

Here the system has seven unknown coefficients which are found by equating the displacement and traction at the boundaries. For fluid-elastic boundaries we require continuity of displacement u_r and traction components σ_{rr} and $\sigma_{r\theta}$. For elastic-elastic boundaries the additional continuity of angular displacement, u_θ, is needed. The system to be solved is

$$\begin{pmatrix} a_n^3(k_0a) & a_n^1(k_{L1}a) & b_n^1(k_{T1}a) & a_n^2(k_{L1}a) & b_n^2(k_{T1}a) & 0 & 0 \\ \bar{\alpha}_n^3(a,k_0,\kappa_0) & \alpha_n^1(k_{L1}a) & \beta_n^1(k_{T1}a) & \alpha_n^2(k_{L1}a) & \beta_n^2(k_{T1}a) & 0 & 0 \\ 0 & \gamma_n^1(k_{L1}a) & \delta_n^1(k_{T1}a) & \gamma_n^2(k_{L1}a) & \delta_n^2(k_{T1}a) & 0 & 0 \\ 0 & a_n^1(k_{L1}b) & b_n^1(k_{T1}b) & a_n^2(k_{L1}b) & b_n^2(k_{T1}b) & a_n^1(k_{L2}b) & b_n^1(k_{T2}b) \\ 0 & c_n^1(k_{L1}b) & d_n^1(k_{T1}b) & c_n^2(k_{L1}b) & d_n^2(k_{T1}b) & c_n^1(k_{L2}b) & d_n^1(k_{T2}b) \\ 0 & \alpha_n^1(k_{L1}b) & \beta_n^1(k_{T1}b) & \alpha_n^2(k_{L1}b) & \beta_n^2(k_{T1}b) & \alpha_n^1(k_{L2}b) & \beta_n^1(k_{T2}b) \\ 0 & \gamma_n^1(k_{L1}b) & \delta_n^1(k_{T1}b) & \gamma_n^2(k_{L1}b) & \delta_n^2(k_{T1}b) & \gamma_n^1(k_{L2}b) & \delta_n^1(k_{T2}b) \end{pmatrix} \tag{3.72}$$

$$\times \begin{pmatrix} -R_{0n}^{3,0} \\ R_{0n}^{1,1} \\ T_{0n}^{1,1} \\ R_{0n}^{2,1} \\ T_{0n}^{2,1} \\ -R_{0n}^{1,2} \\ -T_{0n}^{1,2} \end{pmatrix} = R_{0n}^{1,0} \begin{pmatrix} a_n^1(k_0a) \\ \bar{\alpha}_n^1(a,k_0,\kappa_0) \\ 0 \\ 0 \\ 0 \\ 0 \\ 0 \end{pmatrix}.$$

The global matrix method for solving scattering from concentrically placed elastic or fluid filled cylinders can be generalized to any finite number of cylinders. However, this method can be numerically challenging depending on the number of cylinders to be considered. This is the case when considering the efficiency of acoustic cloaks as many layers are needed to approximate properties that continuously change as a function of

the radius. The next section reviews changing the elastic material from isotropic to transversely isotropic media.

3.4 Elastic scattering solutions for transversely isotropic cylinders

As done before we use potential functions to describe the displacement field however here we require an additional function due to the added complexity of transversely isotropic media. Using scalar potentials to describe the displacement as first used by Buchwald [37] and later used by [38] and [39] we define

$$\mathbf{u} = \nabla\varphi + \nabla \times (\chi \mathbf{e_z}) + \big(\frac{\partial \psi}{\partial z} - \frac{\partial \varphi}{\partial z}\big)\mathbf{e_z}. \tag{3.73}$$

The components of $\mathbf{u}$ are then

$$u_r = \frac{\partial \varphi}{\partial r} + \frac{1}{r}\frac{\partial \chi}{\partial \theta}, \quad u_\theta = \frac{1}{r}\frac{\partial \varphi}{\partial \theta} - \frac{\partial \chi}{\partial r}, \quad u_z = \frac{\partial \psi}{\partial z}. \tag{3.74}$$

For this problem the cylinder is located along the z axis. Oblique incidence is also considered such that the incoming plane wave may have a wave vector component with non-zero k_z, the general solution of the equilibrium equations are then in the form $\{\varphi, \chi, \psi\} = \{\bar{\varphi}, \bar{\chi}, \bar{\psi}\} e^{\mathrm{i}(n\theta + k_z z - \omega t)}$ where

$$\begin{aligned} \bar{\varphi} &= R^l_{on}\,\frac{1}{k_1} z^l_n(k_1 r) + \frac{1}{k_2} S^l_{on}\, z^l_n(k_2 r), \\ \bar{\psi} &= \frac{\kappa_1}{k_1}\, R^l_{on}\, z^l_n(k_1 r) + S^l_{on}\frac{\kappa_2}{k_2}\, z^l_n(k_2 r), \end{aligned} \qquad \bar{\chi} = -\,T^l_{on}\,\frac{1}{k_3} z^l_n(k_3 r), \tag{3.75}$$

and R^l_{on}, S^l_{on}, T^l_{on} are unknown coefficients. As before $z^l_n(x)$ are cylindrical functions where $z^1_n(x) = J_n(x)$ for solutions that are regular at $r = 0$, $z^2_n(x) = Y_n(x)$ for real valued irregular solutions at $r = 0$, $z^3_n(x) = H^{(1)}_n(x)$ for outgoing (radiating) solutions and $z^4_n(x) = H^{(2)}_n(x)$ for ingoing solutions. Again $J_n(x)$ is the Bessel function of the first kind, $Y_n(x)$ is the Bessel function of the second kind, $H^{(1,2)}_n(x)$ is the Hankel functions of the first and second kind. The displacement field can be represented as a linear combination of any two of the four types of cylindrical functions $f^l_n(x)$, $(l = \overline{1,4})$. The wavenumbers k_1, k_2, k_3, and non-dimensional numbers κ_1, κ_2 are given by [40]

$$\begin{aligned} k^2_{1,\,2} &= \frac{a \mp \sqrt{a^2 - b}}{2\, c_{11}\, c_{44}}, \quad k^2_3 = \frac{\rho\,\omega^2 - c_{44} k^2_z}{c_{66}}, \quad \kappa_i = \frac{c_{66}\, k^2_3 - c_{11}\, k^2_i}{\big(c_{13} + c_{44}\big) k_z}, \quad (i = 1, 2), \\ a &= \big(c_{11} + c_{44}\big)\rho\,\omega^2 + \big(c^2_{13} + 2c_{13}c_{44} - c_{11}\, c_{33}\big) k^2_z, \\ b &= 4 c_{11}\, c_{44}\,\big(\rho\omega^2 - c_{33}\, k^2_z\big)\big(\rho\omega^2 - \, c_{44}\, k^2_z\big). \end{aligned} \tag{3.76}$$

For isotropic materials the wavenumbers k_i and κ_i reduce to $k_1^2 = \omega^2\rho/(\lambda+2\mu) - k_z^2$, $k_2^2 = k_3^2 = \omega^2\rho/\mu - k_z^2$, $\kappa_1 = 1$, and $\kappa_2 = -k_2^2/k_z^2$. Using equations (3.73), (3.74), (3.75) and the constitutive relation for transversely isotropic materials, equation (2.41), the displacement and traction vectors are obtained in matrix form as

$$\mathbf{u} = \begin{bmatrix} u_r \\ u_\theta \\ u_z \end{bmatrix} = \left[\sum_l \mathbf{X}^l(r)\mathbf{w}^l\right] e^{i(n\theta + k_z z - \omega t)}, \quad \mathbf{t} = \begin{bmatrix} \sigma_{rr} \\ \sigma_{r\theta} \\ \sigma_{rz} \end{bmatrix} = \left[\sum_l \mathbf{Y}^l(r)\mathbf{w}^l\right] e^{i(n\theta + k_z z - \omega t)}, \quad (3.77)$$

where $\mathbf{w}^l = \begin{pmatrix} R_{on}^l & S_{on}^l & T_{on}^l \end{pmatrix}^T$ is the unknown coefficient vector, the summation on l is over any two of the possible $l = \overline{1,4}$, and

$$\mathbf{X}^l(r) = \begin{bmatrix} f_n^{l\prime}(k_1 r) & f_n^{l\prime}(k_2 r) & -\frac{\mathrm{i}n}{k_3 r} f_n^l(k_3 r) \\ \frac{\mathrm{i}n}{k_1 r} f_n^l(k_1 r) & \frac{\mathrm{i}n}{k_2 r} f_n^l(k_2 r) & f_n^{l\,\prime}(k_3 r) \\ \frac{\mathrm{i}\kappa_1}{k_1} f_n^l(k_1 r) & \frac{\mathrm{i}\kappa_2}{k_2} f_n^l(k_2 r) & 0 \end{bmatrix}, \quad (3.78)$$

$$\mathbf{Y}^l(r) = -\mathrm{i}\mathbf{z}^l(r)\mathbf{X}^l(r), \quad (3.79)$$

and $\mathbf{z}^l$, $l = \overline{1,4}$, follows from [40]:

$$\begin{aligned} \mathbf{z}^l(r) = &\begin{pmatrix} 2c_{66} & \mathrm{i}n2c_{66} & \mathrm{i}k_z r c_{44} \\ -\mathrm{i}n2c_{66} & 2c_{66} & 0 \\ -\mathrm{i}k_z r c_{44} & 0 & Z_z \end{pmatrix} \\ &+ c_0 \begin{pmatrix} \xi_3(y_1 - y_2) & \mathrm{i}n(y_1 - y_2) & \mathrm{i}\xi_3(\xi_1 - \xi_2) \\ -\mathrm{i}n(y_1 - y_2) & \xi_2 y_1 - \xi_1 y_2 & n(\xi_1 - \xi_2) \\ -\mathrm{i}\xi_3(\xi_1 - \xi_2) & n(\xi_1 - \xi_2) & 0 \end{pmatrix}, \end{aligned} \quad (3.80)$$

$$\begin{aligned} Z_z &= c_{44}\left(\frac{n^2(\xi_1 y_1 - \xi_2 y_2) - \xi_1\xi_2\xi_3(y_1 - y_2)}{\xi_3(\xi_2 y_1 - \xi_1 y_2) - n^2(y_1 - y_2)}\right), \quad y_i = \kappa_i r \quad (i = 1,2), \\ c_0 &= \frac{c_{66}k_3^2 r^2}{\xi_3(\xi_2 y_1 - \xi_1 y_2) - n^2(y_1 - y_2)}, \quad \xi_j = k_j r \frac{f_n^{l\,\prime}(k_j r)}{f_n^l(k_j r)} \quad (j = 1,2,3). \end{aligned} \quad (3.81)$$

Note that $\mathbf{z}^l(r)$ acts as an impedance relating the stresses and displacements via equations (3.79) and (3.77). An explicit derivation can be found in [40] where it should be noted that $\mathbf{z}^1(r)$ ($l \equiv 1$) is the exact form of the conditional impedance of a solid cylinder, that is a cylinder with material at $r = 0$. Lastly we can follow the steps of section 3.3 in order to build a global matrix solution for cylinders involving transverse isotropy. Although as noted before this method can become challenging for systems

with large numbers of layers, for that reason an integration scheme using Stroh formalism is reviewed in the next chapter which can quickly solve these larger systems.

Chapter 4

Stable solution method for layered structures

This chapter reviews the work in [41] which focuses on producing a stable method to solve for elastic scattering using the matricant propagator approach. As compared to the global matrix method of the previous chapter this method offers a less numerically challenging solution for systems with large numbers of elastic layers, which also has the advantage for solving for layers with complete general anisotropy. In section 4.1 we review the Stroh formalism which here focuses on transforming the equilibrium equations in cylindrical coordinates to a linear system of ordinary differential equations dependent on the radial coordinate. The outcome of this approach is a scattering solution using the impedance matrix which satisfies the Ricatti differential equation, however it is found to be inherently unstable. A stable solution method is found by combining the impedance matrix and matricant for radially inhomogeneous cylindrically anisotropic structures. The impedance and matricant matrices are defined in section 4.2. In section 4.3 the instability of the problem is shown and an approach for a stable solution technique is found using several different expansions, which are compared in section 4.3.6. Lastly a scattering example is done in section 4.4. It will be the method developed here that is used in the next chapter which focuses on developing acoustic cloaks of the pentamode type.

4.1 Stroh formalism for cylindrically anisotropic media

Here we review the Stroh formalism of the equations of elasticity in cylindrical coordinates in order to develop the matricant. The equations of motion in cylindrical

coordinates are

$$\begin{aligned}\rho\ddot{u}_r &= \sigma_{rr,r} + r^{-1}\sigma_{r\theta,\theta} + r^{-1}(\sigma_{rr} - \sigma_{\theta\theta}) + \sigma_{rz,z},\\ \rho\ddot{u}_\theta &= \sigma_{r\theta,r} + r^{-1}\sigma_{\theta\theta,\theta} + 2r^{-1}\sigma_{r\theta} + \sigma_{\theta z,z},\\ \rho\ddot{u}_z &= \sigma_{rz,r} + r^{-1}\sigma_{\theta z,\theta} + r^{-1}\sigma_{rz} + \sigma_{zz,z},\end{aligned} \tag{4.1}$$

where the conventional notation is used with commas referring to partial derivative with respect to the given coordinate. These three equations are rewritten in matrix form using three traction vectors defined by

$$\mathbf{t}_r = \begin{bmatrix}\sigma_{rr}\\ \sigma_{r\theta}\\ \sigma_{rz}\end{bmatrix}, \quad \mathbf{t}_\theta = \begin{bmatrix}\sigma_{r\theta}\\ \sigma_{\theta\theta}\\ \sigma_{\theta z}\end{bmatrix}, \quad \mathbf{t}_z = \begin{bmatrix}\sigma_{rz}\\ \sigma_{\theta z}\\ \sigma_{zz}\end{bmatrix}. \tag{4.2}$$

Rewriting equation (4.1) in matrix form using equation (4.2) gives

$$(r\mathbf{t}_r)_{,r} + \mathbf{t}_{\theta,\theta} + \mathbf{K}\mathbf{t}_\theta + r\mathbf{t}_{z,z} = r\rho\ddot{\mathbf{u}}, \tag{4.3}$$

where

$$\mathbf{K} = \begin{bmatrix}0 & -1 & 0\\ 1 & 0 & 0\\ 0 & 0 & 0\end{bmatrix}. \tag{4.4}$$

Using the stress-strain relationship, $\sigma_{ij} = C_{ijkl}\varepsilon_{kl}$, and considering a fully anisotropic medium we wish to write the equations of motion, equation (4.3), in displacement form. Using the strain-displacement equation (2.9) and Voigt notation of the constitutive relations from equation (2.21) the three traction vectors in terms of displacement are

$$\begin{aligned}\mathbf{t}_r &= \mathbf{Q}\mathbf{u}_{,r} + r^{-1}\mathbf{R}(\mathbf{u}_{,\theta} + \mathbf{K}\mathbf{u}) + \mathbf{P}\mathbf{u}_{,z},\\ \mathbf{t}_\theta &= \mathbf{R}^T\mathbf{u}_{,r} + r^{-1}\mathbf{T}(\mathbf{u}_{,\theta} + \mathbf{K}\mathbf{u}) + \mathbf{S}\mathbf{u}_{,z},\\ \mathbf{t}_z &= \mathbf{P}^T\mathbf{u}_{,r} + r^{-1}\mathbf{S}^T(\mathbf{u}_{,\theta} + \mathbf{K}\mathbf{u}) + \mathbf{M}\mathbf{u}_{,z},\end{aligned} \tag{4.5}$$

where the displacement vector has the form $\mathbf{u} = \begin{bmatrix}u_r & u_\theta & u_z\end{bmatrix}^T$. In a more condensed matrix form the traction vectors are [42, 43]

$$\begin{pmatrix}\mathbf{t}_r\\ \mathbf{t}_\theta\\ \mathbf{t}_z\end{pmatrix} = \begin{pmatrix}\hat{\mathbf{Q}} & \mathbf{R} & \mathbf{P}\\ \mathbf{R}^T & \hat{\mathbf{T}} & \mathbf{S}\\ \mathbf{P}^T & \mathbf{S}^T & \hat{\mathbf{M}}\end{pmatrix}\begin{pmatrix}\mathbf{u}_{,r}\\ r^{-1}(\mathbf{u}_{,\theta} + \mathbf{K}\mathbf{u})\\ \mathbf{u}_{,z}\end{pmatrix}, \tag{4.6}$$

where

$$\hat{\mathbf{Q}} = \begin{pmatrix} C_{11} & C_{16} & C_{15} \\ C_{16} & C_{66} & C_{56} \\ C_{15} & C_{56} & C_{55} \end{pmatrix}, \ \hat{\mathbf{T}} = \begin{pmatrix} C_{66} & C_{26} & C_{46} \\ C_{26} & C_{22} & C_{24} \\ C_{46} & C_{24} & C_{44} \end{pmatrix}, \ \hat{\mathbf{M}} = \begin{pmatrix} C_{55} & C_{45} & C_{35} \\ C_{45} & C_{44} & C_{34} \\ C_{35} & C_{34} & C_{33} \end{pmatrix},$$
$$\mathbf{R} = \begin{pmatrix} C_{16} & C_{12} & C_{14} \\ C_{66} & C_{26} & C_{46} \\ C_{56} & C_{25} & C_{45} \end{pmatrix}, \ \mathbf{P} = \begin{pmatrix} C_{15} & C_{14} & C_{13} \\ C_{56} & C_{46} & C_{36} \\ C_{55} & C_{45} & C_{35} \end{pmatrix}, \ \mathbf{S} = \begin{pmatrix} C_{56} & C_{46} & C_{36} \\ C_{25} & C_{24} & C_{23} \\ C_{45} & C_{44} & C_{34} \end{pmatrix}. \tag{4.7}$$

We consider solutions in the form of time-harmonic cylindrical waves where the displacement and radial traction vectors are

$$\mathbf{u} = \mathbf{U}^{(n)}(r)\mathrm{e}^{\mathrm{i}(n\theta + k_z z - \omega t)}, \quad \mathrm{i}r\mathbf{t}_r = \mathbf{V}^{(n)}(r)\mathrm{e}^{\mathrm{i}(n\theta + k_z z - \omega t)}, \tag{4.8}$$

where ω is the frequency, k_z is the axial wave number, and $n = 0,\ 1,\ 2,\ \ldots$ is the circumferential number. Plugging equation (4.8) into equations (4.3) and (4.6) yields a differential equation for the state vector, $\boldsymbol{\eta}^{(n)}$, which is comprised of the displacement and radial traction vectors.

$$\frac{\mathrm{d}}{\mathrm{d}\,r}\boldsymbol{\eta}^{(n)}(r) = \frac{\mathrm{i}}{r}\mathbf{G}(r)\boldsymbol{\eta}^{(n)}(r) \quad \text{with} \quad \boldsymbol{\eta}^{(n)}(r) = \begin{pmatrix} \mathbf{U}^{(n)}(r) \\ \mathbf{V}^{(n)}(r) \end{pmatrix}. \tag{4.9}$$

The six by six matrix that relates the derivative of the state vector to itself is known as the system matrix, which has the form

$$\mathrm{i}\mathbf{G} = \begin{pmatrix} \mathbf{g}^{\{1\}} & \mathrm{i}\mathbf{g}^{\{2\}} \\ \mathrm{i}\mathbf{g}^{\{3\}} & -\mathbf{g}^{\{1\}+} \end{pmatrix}, \tag{4.10}$$

where all terms depend on the radial coordinate, r, and superscript $^+$ indicates Hermitian transpose [42] . The three by three matrices in equation (4.10) are

$$\begin{aligned} &\mathbf{g}^{\{1\}} = -\hat{\mathbf{Q}}^{-1}\tilde{\mathbf{R}} - \mathrm{i}k_z r\hat{\mathbf{Q}}^{-1}\mathbf{P}, \quad \mathbf{g}^{\{2\}} = \mathbf{g}^{\{2\}T} = -\hat{\mathbf{Q}}^{-1}, \\ &\mathbf{g}^{\{3\}} = \mathbf{g}^{\{3\}+} = \tilde{\mathbf{T}} - \tilde{\mathbf{R}}^{+}\hat{\mathbf{Q}}^{-1}\tilde{\mathbf{R}} + \mathrm{i}k_z r\big[\mathbf{P}^T\hat{\mathbf{Q}}^{-1}\tilde{\mathbf{R}} - \tilde{\mathbf{S}} - (\mathbf{P}^T\hat{\mathbf{Q}}^{-1}\tilde{\mathbf{R}} - \tilde{\mathbf{S}})^{+}\big] \\ &\qquad\qquad + r^2\big[k_z^2(\hat{\mathbf{M}} - \mathbf{P}^T\hat{\mathbf{Q}}^{-1}\mathbf{P}) - \rho\omega^2\mathbf{I}\big], \end{aligned} \tag{4.11}$$

where $\mathbf{I}$ is the three by three identity matrix and

$$\tilde{\mathbf{R}} = \mathbf{R}\boldsymbol{\kappa}, \ \ \tilde{\mathbf{S}} = \boldsymbol{\kappa}\mathbf{S}, \ \ \tilde{\mathbf{T}} = \tilde{\mathbf{T}}^{+} = \boldsymbol{\kappa}^{+}\hat{\mathbf{T}}\boldsymbol{\kappa}, \quad \text{with} \ \ \boldsymbol{\kappa} = \mathbf{K} + in\mathbf{I} \ \big(= -\boldsymbol{\kappa}^{+}\big). \tag{4.12}$$

The system matrix, $\mathbf{G}$, has the important symmetry which follows from the form of equation (4.10),

$$\mathbf{G} = \mathbf{T}\mathbf{G}^{+}\mathbf{T}, \text{ with } \mathbf{T} = \begin{pmatrix} \mathbf{0} & \mathbf{I} \\ \mathbf{I} & \mathbf{0} \end{pmatrix}. \tag{4.13}$$

The problem is now reduced to finding a solution to equation (4.9) subject to appropriate boundary conditions. Next we introduce the matricant and impedance matrices based on solutions of equation (4.9).

4.2 Impedance and matricant matrices

In this section we develop the conditional impedance matrix which relates $\mathbf{U}(r)$ and $\mathbf{V}(r)$ from equation (4.8) associated with displacement and traction, respectively. The dimension of each vector is taken as general $m = 3,\ 2,\ 1$, where $m = 3$ is the general case, $m = 2$ if $z-$dependence is not considered, i.e. $k_z = 0$ perpendicular incidence, and $m = 1$ for pure out-of-plane shear horizontal (SH) motion. The $m \times m$ conditional impedance matrix $\mathbf{z}$ is defined such that

$$\mathbf{V}(r) = -\mathrm{i}\mathbf{z}(r)\mathbf{U}(r). \tag{4.14}$$

In section 4.1 we found the equations for linear elastodynamics can be cast as a system of $2m$ linear ordinary differential equations via equation (4.9) with

$$\frac{\mathrm{d}\,\boldsymbol{\eta}}{\mathrm{d}\,r} = \mathbf{Q}\boldsymbol{\eta} \quad \text{with } \boldsymbol{\eta}(r) = \begin{pmatrix} \mathbf{U} \\ \mathbf{V} \end{pmatrix}, \quad \mathbf{Q}(r) = \begin{pmatrix} \mathbf{Q}_1 & \mathbf{Q}_2 \\ \mathbf{Q}_3 & \mathbf{Q}_4 \end{pmatrix}, \tag{4.15}$$

where $\mathbf{Q} = \frac{i}{r}\mathbf{G}(r)$ from equation (4.9) [40]. Using the conditional impedance relation, equation (4.14), in equation (4.15) we find that $\mathbf{z}(r)$ satisfies a differential Riccati equation

$$\frac{\mathrm{d}\,\mathbf{z}}{\mathrm{d}\,r} + \mathbf{z}\mathbf{Q}_1 - \mathbf{Q}_4\mathbf{z} - i\mathbf{z}\mathbf{Q}_2\mathbf{z} - i\mathbf{Q}_3 = \mathbf{0}, \tag{4.16}$$

which can be solved for with an initial condition $\mathbf{z}(r_0)$ at a specified $r = r_0$. For transverse isotropy, equation (3.80) gives an explicit form of the conditional impedance matrix and can be used as the initial condition $\mathbf{z}(r_0)$. Our approach for solving the

conditional impedance matrix, $\mathbf{z}$, is to first solve for the $2m \times 2m$ matricant $\mathbf{M}(r, r_0)$ which is defined as the solution of the initial value problem

$$\frac{\mathrm{d}\,\mathbf{M}}{\mathrm{d}\,r}(r, r_0) = \mathbf{Q}(r)\mathbf{M}(r, r_0),\ \mathbf{M}(r_0, r_0) = \mathbf{I}_{(2m)},\ \mathbf{M} = \begin{pmatrix} \mathbf{M}_1 & \mathbf{M}_2 \\ \mathbf{M}_3 & \mathbf{M}_4 \end{pmatrix}. \tag{4.17}$$

Using the matricant the state vector $\boldsymbol{\eta}$ can be propagated with

$$\boldsymbol{\eta}(r) = \mathbf{M}(r, r_0)\boldsymbol{\eta}(r_0). \tag{4.18}$$

Using equation (4.14) and the matricant relations, equations (4.17) and (4.18), we find

$$\mathbf{U}\,(r) = (\mathbf{M}_1 - \mathrm{i}\mathbf{M}_2\mathbf{z}(r_0))\,\mathbf{U}\,(r_0)\,, \quad \mathbf{V}\,(r) = (\mathbf{M}_3 - \mathrm{i}\mathbf{M}_4\mathbf{z}(r_0))\,\mathbf{U}\,(r_0)\,. \tag{4.19}$$

Combining the above relations the conditional impedance can be expressed in terms of the matricant as

$$\mathbf{z}(r) = i\big(\mathbf{M}_3 - i\mathbf{M}_4\mathbf{z}(r_0)\big)\big(\mathbf{M}_1 - i\mathbf{M}_2\mathbf{z}(r_0)\big)^{-1}. \tag{4.20}$$

The propagator nature of the matricant is apparent from equation (4.18) and from the property $\mathbf{M}(r, r_1)\ \mathbf{M}(r_1, r_0) = \mathbf{M}(r, r_0)$, and in particular $\mathbf{M}(r, r_0) = \mathbf{M}(r_0, r)^{-1}$. Also, the symmetry from equation (4.13) implies $\mathbf{M}(r, r_0) = \mathbf{T}\mathbf{M}^{+}(r_0, r)\mathbf{T}$. Hence, $\mathbf{M}^{-1}(r, r_0) = \mathbf{T}\mathbf{M}^{+}(r, r_0)\mathbf{T}$, that is, $\mathbf{M}$ is $\mathbf{T}$-unitary [44].

Another approach for finding the conditional impedance uses the two point impedance matrix [41], which like the matricant relates vectors at two values of r but by the following way [40]

$$\begin{pmatrix} \mathbf{V}(r_0) \\ -\mathbf{V}(r) \end{pmatrix} = -\mathrm{i}\mathbf{Z}(r, r_0) \begin{pmatrix} \mathbf{U}(r_0) \\ \mathbf{U}(r) \end{pmatrix}, \quad \mathbf{Z} = \begin{pmatrix} \mathbf{Z}_1 & \mathbf{Z}_2 \\ \mathbf{Z}_3 & \mathbf{Z}_4 \end{pmatrix}. \tag{4.21}$$

The relations between the matricant of equation (4.17) and the impedance matrix of equation (4.21) evaluated at cylindrical surfaces r, r_0 are easily deduced

$$\begin{aligned} \mathbf{M}(r, r_0) &= \begin{pmatrix} -\mathbf{Z}_2^{-1}\mathbf{Z}_1 & \mathrm{i}\mathbf{Z}_2^{-1} \\ \mathrm{i}\mathbf{Z}_3 - \mathrm{i}\mathbf{Z}_4\mathbf{Z}_2^{-1}\mathbf{Z}_1 & -\mathbf{Z}_4\mathbf{Z}_2^{-1} \end{pmatrix}, \\ \mathbf{Z}(r, r_0) &= \begin{pmatrix} -\mathrm{i}\mathbf{M}_2^{-1}\mathbf{M}_1 & \mathrm{i}\mathbf{M}_2^{-1} \\ \mathrm{i}\mathbf{M}_4\mathbf{M}_2^{-1}\mathbf{M}_1 - \mathbf{M}_3 & -\mathrm{i}\mathbf{M}_4\mathbf{M}_2^{-1} \end{pmatrix}. \end{aligned} \tag{4.22}$$

Introducing equation (4.22) into equation (4.20), we can relate the conditional impedance $\mathbf{z}(r)$ to the two point impedance matrix $\mathbf{Z}(r, r_0)$ according to

$$\mathbf{z}(r) = \mathbf{Z}_3\big(\mathbf{Z}_1 - \mathbf{z}(r_0)\big)^{-1}\mathbf{Z}_2 - \mathbf{Z}_4. \tag{4.23}$$

We leave the development of the two point impedance matrix here however in [41] a recursive algorithm for layered piecewise uniform transversely isotropic cylinders is developed and a general global two point impedance is found relating surfaces r_0 to some r_k.

4.3 Stable solution technique for general anisotropy

In this section we develop a stable numerical scheme for solving the conditional impedance matrix defined by equation (4.14). We consider fully anisotropic media where the properties are radially dependent, i.e. density and elastic moduli are arbitrary functions of r: $\rho(r)$, $C_{ijkl}(r)$.

4.3.1 Stability issues

Due to the stiff nature of equation (4.17) direct numerical integration for the matricant, $\mathbf{M}(r, r_0)$, leads to exponentially growing instabilities, which become unavoidable at large values of n and/or kr. Additionally singularities and numeric instabilities form when equation (4.16) is integrated for the conditional impedance $\mathbf{z}(\mathbf{r})$, which is a well known issue for Riccati equations [45]. These occur at finite values of r associated with traction-free modes for a given frequency. We can avoid singularities caused by traction-free modes by inverting the equation and using the admittance $\mathbf{A} = \mathbf{z}^{-1}$ [46]. The admittance satisfies a similar Riccati differential equation, which follows from equation (4.16)

$$\frac{\mathrm{d}\,\mathbf{A}}{\mathrm{d}\,r} + \mathrm{i}\mathbf{A}\mathbf{Q}_3\mathbf{A} + \mathbf{A}\mathbf{Q}_4 - \mathbf{Q}_1\mathbf{A} + \mathrm{i}\mathbf{Q}_2 = 0. \tag{4.24}$$

Although singularities still occur except now corresponding to rigid modes. Switching back and forth between integrating the impedance and admittance seems to be a solution however the locations of the singularities are not known in advance and can

be clustered together causing issues with a switching scheme. The curves shown in Figure 4.1 exemplify the problem of singularities in the impedance where appearance of peaks indicate values of r beyond which an accurate numerical solution can not be obtained regardless of the step size in the integration scheme. The inability of such standard methods to obtain correct results was the motivation behind the proposed solution technique discussed next.

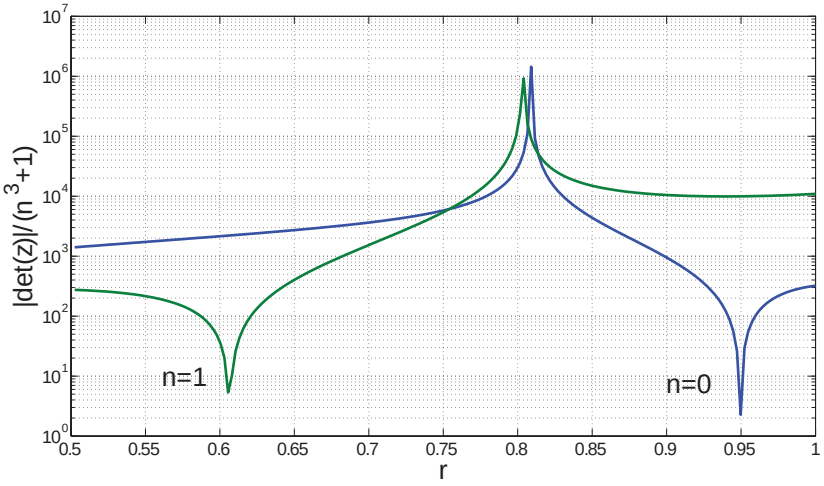

Figure 4.1: Solid, aluminium cylinder integrated with 200 evenly spaced steps, using the fourth order scheme of section 4.3.4, from $r = 0.5$ to $r = 1.0$, with $k_z = 0$ and $ka = 10$. Plotted is the determinant of the upper left 2×2 sub-matrix of the the 3×3 conditional impedance matrix normalized by $n^3 + 1$ vs. r. Where equation (3.80) was used for the initial impedance at $r = 0.5\ m$.

4.3.2 Möbius scheme

In order to accurately calculate the conditional impedance and matricant we follow an approach based on [45] which views the solution of the Riccati equation as a "Grassmanian flow" of m-dimensional subspaces on a larger vector space of dimension $2m$. The idea is to recast the equation for $\mathbf{z}$ in the form of a forward marching scheme of step size h based on equation (4.20)

$$\mathbf{z}(r+h) = \mathrm{i}\big(\mathbf{M}_3 - \mathrm{i}\mathbf{M}_4\mathbf{z}(r)\big)\big(\mathbf{M}_1 - \mathrm{i}\mathbf{M}_2\mathbf{z}(r)\big)^{-1}, \tag{4.25}$$

where $\mathbf{M} = \mathbf{M}(r+h, r)$. The key to the method is that $\mathbf{M}$ can always be calculated in a stable manner for sufficiently small step size h. This approach is one of a class

of methods called Möbius schemes, which by design are formulated on the natural geometrical setting of the larger vector space. Accordingly Möbius schemes are able to handle numerical instability and pass smoothly and accurately through singularities [45]. The method therefore combines both the matricant and the impedance, each of which is unstable when solved in a global sense separately.

4.3.3 Approximations for $\mathbf{M}(r+h, r)$

Using the Möbius scheme shifts the problem to finding approximations for $\mathbf{M}(r+h, r)$ accurate to some given order in step size h. We develop approximations in the form

$$\mathbf{M}(r+h, r) = \mathbf{I}_{(2m)} + h\mathbf{M}^{(1)}(r) + \frac{h^2}{2!}\mathbf{M}^{(2)}(r) + \frac{h^3}{3!}\mathbf{M}^{(3)}(r) + \ldots, \tag{4.26}$$

where the terms $\mathbf{M}^{(2)}(r)$ do not require explicit integration schemes for their evaluation. Considering the first case of $\mathbf{Q}$ being sufficiently smooth, then the identity

$$\mathbf{M}(r+h, r) = \mathbf{I}_{(2m)} + \int_0^h \mathbf{Q}(r+s)\mathbf{M}(r+s, r)\,\mathrm{d}\,s, \tag{4.27}$$

may be written in the form of a series in powers of h by using equation (4.26) for the left member and a Taylor series evaluated at r for $\mathbf{Q}$ in the integral,

$$\begin{aligned} h\mathbf{M}^{(1)} + \frac{h^2}{2!}\mathbf{M}^{(2)} + \frac{h^3}{3!}\mathbf{M}^{(3)} + \ldots = \int_0^h \Big(\big[\mathbf{Q} + s\mathbf{Q}' + \frac{s^2}{2!}\mathbf{Q}'' \\ + \frac{s^3}{3!}\mathbf{Q}''' + \ldots\big] \times \big[\mathbf{I}_{(2m)} + s\mathbf{M}^{(1)} + \frac{s^2}{2!}\mathbf{M}^{(2)} + \ldots\big] \Big)\,\mathrm{d}\,s. \end{aligned} \tag{4.28}$$

Comparing equal orders of h^k in equation (4.28) yields

$$\begin{aligned} \mathbf{M}^{(1)}(r) &= \mathbf{Q}(r), \\ \mathbf{M}^{(2)}(r) &= \mathbf{Q}'(r) + \mathbf{Q}(r)\mathbf{M}^{(1)}(r), \\ \mathbf{M}^{(3)}(r) &= \mathbf{Q}''(r) + 2\mathbf{Q}'(r)\mathbf{M}^{(1)}(r) + \mathbf{Q}(r)\mathbf{M}^{(2)}(r), \\ \mathbf{M}^{(4)}(r) &= \mathbf{Q}'''(r) + 3\mathbf{Q}''(r)\mathbf{M}^{(1)}(r) + 3\mathbf{Q}'(r)\mathbf{M}^{(2)}(r) + \mathbf{Q}(r)\mathbf{M}^{(3)}(r), \end{aligned} \tag{4.29}$$

and so on. Using equation (4.26) an approximation for the matricant can be found however the series used in equation (4.29) is restricted to profiles that are analytically smooth functions of r and is not suitable for piece-wise constant or piece-wise smooth

profiles and therefore derivatives of the profile are to be avoided. The approximation formed from equations (4.26) and (4.29) is only valid to $\mathrm{O}(h)$, and the iterative scheme of equation (4.25) shares the same accuracy.

An expansion accurate to second order can be obtained by using a Taylor series expansion evaluated at the midpoint [45]

$$\mathbf{Q}(r+s) \approx \mathbf{Q}(r+\frac{h}{2}) + (s-\frac{h}{2})\mathbf{Q}'(r+\frac{h}{2}) + (s-\frac{h}{2})^2\mathbf{Q}'' + \mathrm{O}(s^3). \tag{4.30}$$

Substitution into equation (4.27) using equation (4.26) then gives

$$\mathbf{M}^{(1)} = \mathbf{M}^{(2)} = \mathbf{Q}(r+\frac{h}{2}), \quad \mathbf{M}^{(3)} = \big(\mathbf{I}_{(2m)} + \frac{1}{2}\mathbf{Q}'(r+\frac{h}{2})\big)\mathbf{M}^{(1)}. \tag{4.31}$$

This leads to an expansion up to $\mathrm{O}(h^2)$ requiring only $\mathbf{Q}$ at a single position with no derivatives

$$\text{TS 2nd}: \quad \mathbf{M}(r+h,r) = \mathbf{I}_{(2m)} + h\mathbf{Q}(r+\frac{h}{2}) + \frac{h^2}{2}\mathbf{Q}^2(r+\frac{h}{2}) + \mathrm{O}(h^3). \tag{4.32}$$

The form of equation (4.32) suggests an alternative expression that is accurate to the same order

$$\text{EXP 2nd}(a): \quad \mathbf{M}(r+h,r) = \exp\big(h\mathbf{Q}(r+\frac{h}{2})\big) + \mathrm{O}(h^3). \tag{4.33}$$

The approximations of equations (4.32) and (4.33), together with equation (4.25) each yield a second order accurate Möbius scheme. Detailed comparisons are provided in section 4.3.6.

4.3.4 Lagrange interpolation expansions

In order to obtain higher order expressions without using derivatives of $\mathbf{Q}(r)$ we consider Lagrange polynomial expansions for $\mathbf{Q}$ in equation (4.27) . The Lagrange polynomial of order n approximates $\mathbf{Q}(r+s)$ with [47]

$$\mathbf{Q}(r+s) = \sum_{j=0}^{n} \mathbf{Q}(r+x_j h) L_j\big(\frac{s}{h}\big), \qquad L_j(x) = \prod_{l=0, l\neq j}^{n} \left(\frac{x-x_l}{x_j-x_l}\right), \tag{4.34}$$

where $x_j \in [0,1]$, and $j = 0, 1, \ldots, n$ are chosen points. Substituting into equation (4.28) and using the notation $\mathbf{Q}_{x_j} = \mathbf{Q}(r + x_j h)$ implies the sequence

$$\begin{aligned} \mathbf{M}^{(k)} &= \Big\{ \sum_{j=0}^{n} L_j^{(k)} \mathbf{Q}_{x_j} \Big\} \mathbf{M}^{(k-1)}, \quad \mathbf{M}^{(0)} \equiv \mathbf{I}, \\ L_j^{(k)} &= k \int_0^1 L_j(x) x^{k-1} \, \mathrm{d}x, \end{aligned} \qquad k = 1, 2, 3 \ldots. \tag{4.35}$$

Note that $\sum_{j=0}^{n} L_j^{(k)} = 1$. In the following subsections we derive expansions based on equation (4.34) for $n = 1$ and $n = 3$.

Two point approximation: Halves

We approximate $\mathbf{Q}$ with two points using equation (4.34) for $n = 1$. In this case the integrals $L_j^{(k)}$ can be simplified with the result that

$$\mathbf{M}^{(k)} = \Big\{ \sum_{j=0}^{1} L_j\big(\frac{k}{k+1}\big) \mathbf{Q}_{x_j} \Big\} \mathbf{M}^{(k-1)}, \quad \mathbf{M}^{(0)} \equiv \mathbf{I}, \quad k = 1, 2, 3 \ldots. \tag{4.36}$$

Taking equi-space points $x_0 = \frac{1}{4}$ and $x_1 = \frac{3}{4}$, yields

$$\text{LP 2nd}: \quad \mathbf{M}(r+h, r) = \mathbf{I}_{(2m)} + \frac{h}{2}\big(\mathbf{Q}_{\frac{1}{4}} + \mathbf{Q}_{\frac{3}{4}}\big) + \frac{h^2}{24}\big(\mathbf{Q}_{\frac{1}{4}} + 5\mathbf{Q}_{\frac{3}{4}}\big)\big(\mathbf{Q}_{\frac{1}{4}} + \mathbf{Q}_{\frac{3}{4}}\big) + \mathrm{O}(h^3). \tag{4.37}$$

This again gives a Möbius scheme of second order accuracy in h and it also suggests, by analogy with equation (4.33),

$$\text{EXP 2nd}(b): \quad \mathbf{M}(r+h, r) = \exp\big(\frac{h}{2}\mathbf{Q}_{\frac{3}{4}}\big) \exp\big(\frac{h}{2}\mathbf{Q}_{\frac{1}{4}}\big) + \mathrm{O}(h^3). \tag{4.38}$$

Note that the expansions given in equations (4.37) and (4.38) only agree with one another to first order, $\mathrm{O}(h)$.

Four point approximation: Fourths

Taking four evenly spaced points to approximate $\mathbf{Q}$, $x_j = \frac{1}{8} + \frac{j}{4}$, $j = 0, 1, 2, 3$, and using the symbolic algebra program Maple, yields

$$\text{LP 4th}: \quad \begin{aligned} \mathbf{M}^{(1)} =& \tfrac{13}{48}\mathbf{Q}_{\frac{1}{8}} + \tfrac{11}{48}\mathbf{Q}_{\frac{3}{8}} + \tfrac{11}{48}\mathbf{Q}_{\frac{5}{8}} + \tfrac{13}{48}\mathbf{Q}_{\frac{7}{8}}, \\ \mathbf{M}^{(2)} =& \big(\tfrac{23}{720}\mathbf{Q}_{\frac{1}{8}} + \tfrac{67}{240}\mathbf{Q}_{\frac{3}{8}} + \tfrac{43}{240}\mathbf{Q}_{\frac{5}{8}} + \tfrac{367}{720}\mathbf{Q}_{\frac{7}{8}}\big)\mathbf{M}^{(1)}, \\ \mathbf{M}^{(3)} =& \big(-\tfrac{1}{48}\mathbf{Q}_{\frac{1}{8}} + \tfrac{19}{80}\mathbf{Q}_{\frac{3}{8}} + \tfrac{7}{80}\mathbf{Q}_{\frac{5}{8}} + \tfrac{167}{240}\mathbf{Q}_{\frac{7}{8}}\big)\mathbf{M}^{(2)}, \\ \mathbf{M}^{(4)} =& \big(-\tfrac{23}{560}\mathbf{Q}_{\frac{1}{8}} + \tfrac{389}{1680}\mathbf{Q}_{\frac{3}{8}} - \tfrac{67}{1680}\mathbf{Q}_{\frac{5}{8}} + \tfrac{1427}{1680}\mathbf{Q}_{\frac{7}{8}}\big)\mathbf{M}^{(3)}. \end{aligned} \tag{4.39}$$

Substitution of these terms into equation (4.26) gives $\mathbf{M}(r+h, r)$ up to fourth order accuracy. Interestingly, when more points were taken to evaluate $\mathbf{Q}$ the numerical accuracy was not found to improve. This was tried with even spacings, using from five up to ten points. Again, by analogy with equation (4.38),

$$\text{EXP 2nd}(c): \quad \mathbf{M}(r+h, r) = \exp\left(\tfrac{h}{4}\mathbf{Q}_{\frac{7}{8}}\right)\exp\left(\tfrac{h}{4}\mathbf{Q}_{\frac{5}{8}}\right)\exp\left(\tfrac{h}{4}\mathbf{Q}_{\frac{3}{8}}\right)\exp\left(\tfrac{h}{4}\mathbf{Q}_{\frac{1}{8}}\right) + \mathrm{O}(h^3), \tag{4.40}$$

which, like equations (4.37) and (4.38), is consistent with the four-term Lagrange interpolation scheme.

4.3.5 Fourth order Magnus integrator scheme

The Magnus integrator, created by Wilhelm Magnus [48], and further developed in [49] with a convergence proof and recurrence relations, is a method to approximate a solution to equation (4.17) with

$$\mathbf{M}(r+h, r) = e^{\mathbf{\Omega}}\mathbf{M}(r, r-h). \tag{4.41}$$

Here we consider a fourth order Magnus integrator scheme similarly done in [50] for the Helmholtz equation. We use the following definitions to march a solution forward in r,

$$\text{MG 4th}: \quad \begin{aligned} &\mathbf{M}(r+h, r) = e^{\mathbf{\Omega}}\mathbf{M}(r, r-h), \\ &\mathbf{\Omega} = \frac{h}{2}(\mathbf{Q}_{(1)} + \mathbf{Q}_{(2)}) + \frac{\sqrt{3}h^2}{12}(\mathbf{Q}_{(2)}\mathbf{Q}_{(1)} - \mathbf{Q}_{(1)}\mathbf{Q}_{(2)}), \\ &\mathbf{Q}_{(1)} = \mathbf{Q}(r + h(\frac{1}{2} - \frac{\sqrt{3}}{6})), \quad \mathbf{Q}_{(2)} = \mathbf{Q}(r + h(\frac{1}{2} + \frac{\sqrt{3}}{6})). \end{aligned} \tag{4.42}$$

As a fourth order scheme the numerical precision of this method is very similar to that of the four point Lagrange polynomial approximation, equation (4.39), which is seen in the examples of the following section.

4.3.6 Numerical examples and convergence

In order to illustrate the convergence property of the different expansions proposed (exponential, Magnus, Taylor series, Lagrange polynomials), we consider a solid aluminium sample with properties $\rho = 2700\ kg/m^3$, $E = 70\ GPa$, $G = 26\ GPa$ and radius of $r = 1\ m$ and normalized these properties with respect to water for which $\rho = 1000\ kg/m^3$ and speed of sound in water $c = 1.470\ km/s$. The numerical values reported were computed by implementing the Möbius scheme, equation (4.25), and in the case of the Magnus integrator implementing equation (4.20), starting at $r = 0.5$ with initial condition given by the explicit solution, equation (3.80) from [40] and discussed in section 4.3. In all examples we take $k_z = 0$. Figure 4.2 plots the difference of the determinant of the upper left 2×2 sub-matrix of the exact conditional impedance from equation (3.80), and that calculated by iterating equation (4.25) until $r = 1$ is reached. The right hand side of Figure 4.2 refers to the type of approximation used: Taylor Series (TS), Lagrange Polynomial (LP), Exponential (EXP), Magnus (MG), and to the accuracy order. Thus, LP 1st was calculated using equation (4.29), TS 2nd by (4.31), EXP (a) by (4.33), EXP (b) by (4.38), EXP (c) by (4.40), LP 2nd by (4.37), LP 4th by (4.39), MG 4th by (4.42), and LP 3rd was calculated using a Lagrange Polynomial with points $\{x_0, x_1, x_2\} = \{\frac{1}{6}, \frac{1}{2}, \frac{5}{6}\}$. Interestingly, the three EXP methods (equations (4.33), (4.38) and (4.40)) gave similar results and were the best results for the fewest number of approximation points. Figure 4.3 plots the difference of the upper 2×2 sub-matrices at $r = 1.0$ vs. the number of steps used in the iteration from $r = 0.5$ to $r = 1.0$. As expected, the higher order schemes are more accurate and require fewer steps in the integration process to yield the same accuracy as a lower order scheme.

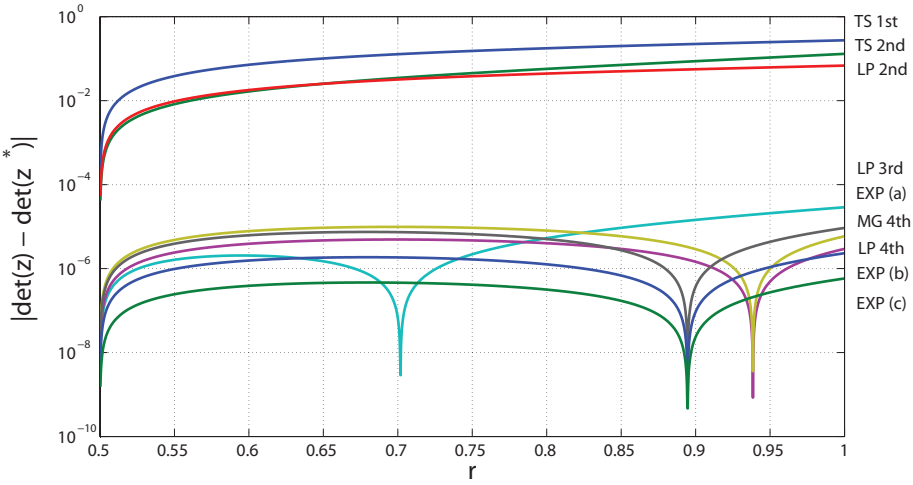

Figure 4.2: Solid, aluminium cylinder integrated with 2000 evenly spaced steps from $r = 0.5$ to $r = 1.0$, with $k_z = 0$, $n = 0$ and $ka = 5$. Plotted is the difference of the determinants of the upper left 2×2 sub-matrices of equation (3.80) and those calculated from section 4.3. As noted in section 4.3.6, the right hand side refers to the type and order accuracy, they are listed top to bottom as worst to best at $r = 1$

4.4 Scattering example

In this section we explore the use of the impedance matrix by considering acoustic scattering from a solid aluminum cylinder immersed in water. Perpendicular plane wave incidence, i.e. $k_z = 0$, in a uniform exterior fluid is considered with time harmonic dependence $e^{-\mathrm{i}\omega t}$. The total radial stress and displacement fields in the surrounding fluid are

$$\begin{aligned} \sigma_{rr} &= -Kk \sum_{n=-\infty}^{\infty} i^n \big(J_n(kr) + B_n H_n^{(1)}(kr)\big) e^{i(n\theta - \omega t)}, \\ u_r &= -\sum_{n=-\infty}^{\infty} i^n \big(J_n'(kr) + B_n H_n^{(1)\prime}(kr)\big) e^{i(n\theta - \omega t)}, \end{aligned} \tag{4.43}$$

where r is the radial coordinate, K is the bulk modulus, k is the wave number, $H_n^{(1)}$ is the Hankel function of the first kind, and the coefficients B_n are to be determined [27]. Unlike Chapter 3, here we take the summation over positive and negative values of n allowing for the use of the $e^{in\theta}$ term whereas before we dealt with summation over the positive range of n giving $\cos n\theta$ and $\sin n\theta$ terms. We consider an initial impedance $\mathbf{z}(r = b) = \mathbf{z}_1$ using equation (3.80) and then integrating via the proposed technique we find the impedance of the outer surface $\mathbf{z}(r = a) = \mathbf{z}_2$. Using the definition of the

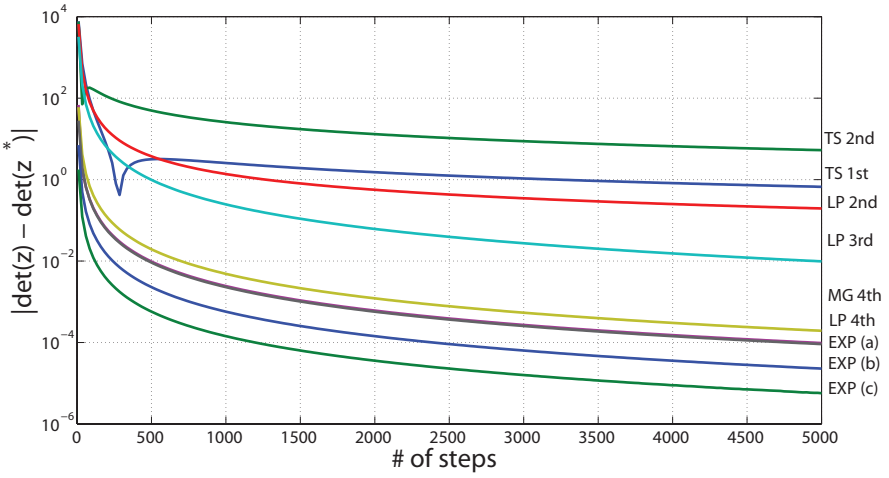

Figure 4.3: Solid, aluminium cylinder integrated from $r = 0.5$ to $r = 1.0$, with $k_z = 0$, $n = 0$ and $ka = 25$. Plotted is the difference of the determinants of the upper left 2 $\times$ 2 sub-matrices of equation (3.80) and those calculated from section 4.3 at $r = 1$ vs. number of steps.

conditional impedance matrix from equation (4.14) and writing this statement for $r = b$ and $r = a$ gives

$$\mathbf{V}(b) = -\mathrm{i}\mathbf{z}_1\mathbf{U}(b), \quad \mathbf{V}(a) = -\mathrm{i}\mathbf{z}_2\mathbf{U}(a). \tag{4.44}$$

The conditional impedance matrix, $\mathbf{z}_2 = \mathbf{z}(a)$, is found from the integration technique outlined in section 4.3 and can be checked directly for transversely isotropic materials using equation (3.80). Considering acoustic fluid in the exterior we write equation (4.44) for $r = a$ in detail for which the shear stress, $\sigma_{r\theta}$, must be zero with

$$ia\begin{pmatrix}\sigma_{rr}(a)\\ 0\end{pmatrix} = -i\mathbf{z}_2\begin{pmatrix}u_r(a)\\ u_\theta(a)\end{pmatrix} = -i\begin{pmatrix}p_1 & q_1\\ p_2 & q_2\end{pmatrix}\begin{pmatrix}u_r(a)\\ u_\theta(a)\end{pmatrix}. \tag{4.45}$$

Eliminating u_θ using the second row of equation (4.45) implies

$$ia\frac{\sigma_{rr}(a)}{u_r(a)} = \frac{i}{q_2}(q_1p_2 - q_2p_1) \equiv -iz_0. \tag{4.46}$$

Using equation (4.43) and equating it with equation (4.46) we find the scattering coefficient

$$B_n = -\frac{KkaJ_n(ka) + z_0J_n'(ka)}{KkaH_n^{(1)}(ka) + z_0H_n^{(1)'}(ka)}. \tag{4.47}$$

Numerical simulation for a solid aluminium cylinder was considered with properties normalized with respect to water and with the total pressure field illustrated in Figure

4.4. Figure 4.5 shows both the total scattering cross-section σ_{tot} and the back-scattering amplitude $f(\pi)$, where the far field form function, $f(\theta)$ is

$$f(\theta) = \frac{2}{\sqrt{k}} \sum_{n=0}^{\infty} \mathrm{i}^{2n-1} \epsilon_n B_n \cos n\theta, \tag{4.48}$$

where $\epsilon_0 = 1$ and $\epsilon_m = 2$ for $m > 0$. The total scattering cross section is then

$$\sigma_{tot} = \frac{4\pi}{ka} \mathrm{Imag}(f(0)). \tag{4.49}$$

Figure 4.5 closely matches the behavior of a similar analysis conducted in [51].

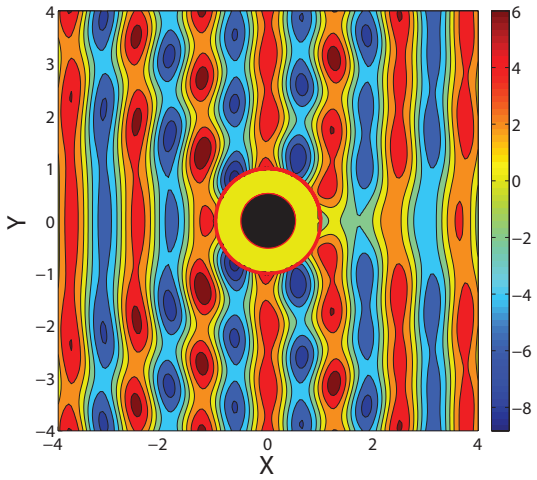

Figure 4.4: Plotted pressure field described by equation (4.43) for an aluminium cylinder, integrated from $r = 0.5$ to $r = 1.0$ (area between the two red circles drawn) using the fourth order scheme, equation (4.39), with 500 steps. The initial impedance at $r = 0.5$ was found using equation (3.80). $ka = 5$, $k_z = 0$, and $\sigma_{tot} = 2.468$.

The Riccati equation for the impedance matrix was formulated by seeking solutions of 3D elasticity in the form of time-harmonic cylindrical waves. As discussed in section 4.3.1 direct integration of the Riccati equation leads to exponentially growing instabilities associated with traction-free modes for the impedance and rigid modes for the admittance. We developed a new stable numerical scheme for cylindrically anisotropic structures that passes through these singularities by combining the impedance and matricant. This scheme evaluates the impedance matrix for continuous systems by integrating the Riccati equation over the thickness of each layer. Different expansion methods were considered and compared, it was noted that matrix exponential

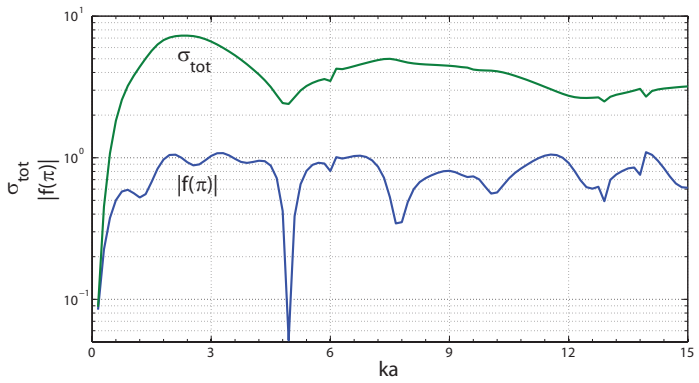

Figure 4.5: Total scattering cross section and backscattering amplitude plotted against non-dimensional frequency, ka. Aluminum cylinder with the same properties as listed in figure 4.4, integrated using the fourth order scheme from $r = 0.5$ to $r = 1.0$ using 500 steps. The initial impedance at $r = 0.5$ was found using equation (3.80).

approximations yielded the best results. An example of acoustic scattering from a solid aluminum cylinder immersed in water was considered using the impedance matrix and compared with the literature. Plots of the total pressure field, form function and total scattering cross section agree with previously published results. It will be this method that is used in the next chapter that focuses on scattering from different targets surrounded in many layers of elastic media characterized by the pentamode type of acoustic cloaks.

Chapter 5

Pentamode materials for transformation acoustics

Interest in cloaking objects from incident waves first started in the electromagnetic spectrum by using a transformation of coordinates in the wave equation called transformation optics [52, 53, 54]. Similar transformations can be done to the acoustic wave equation and devices such as cloaks and lenses can be developed with specific goals using transformation acoustics [55, 56, 57]. We consider passive, directionally independent, broadband cloaks. In chapters 8 and 9 the development of these devices is made by designing materials with periodic substructure. In general, acoustic cloaks fall into three categories inertial cloaks, pure pentamode cloaks, and a combination of the two [20]. Inertial cloaks achieve the desired phenomenon by having material properties described by an anisotropic density tensor and a scalar bulk modulus, which can be achieved by the simple layering of fluids [19]. These types of cloaks have been largely studied in the literature [58, 59, 60, 61]. Pentamode cloaks achieve the effect with an anisotropic elasticity tensor and a scalar density. The name pentamode refers to the five zero eigenvalues of the elasticity tensor, this means that there is only one mode of deformation that induces stress. The types of cloaks that are of interest here are the pure pentamode or the combination of the two where a material with pentamode elasticity is considered with possible anisotropic density.

5.1 Pentamode materials as fluids

It can be easily seen that pentamode elasticity is required for acoustic transformations as it means that shear waves will not be able to propagate. In this sense these materials can be thought of as anisotropic fluids. Considering periodic microstructure design which will have certain symmetries we look at two dimensional cylindrical elasticity

with the following relations

$$\begin{pmatrix} \sigma_{rr} \\ \sigma_{\theta\theta} \\ \sigma_{r\theta} \end{pmatrix} = \begin{pmatrix} C_{11} & C_{12} & 0 \\ C_{12} & C_{22} & 0 \\ 0 & 0 & C_{66} \end{pmatrix} \begin{pmatrix} \varepsilon_{rr} \\ \varepsilon_{\theta\theta} \\ 2\varepsilon_{r\theta} \end{pmatrix}. \tag{5.1}$$

If we use the Christoffel equation, $\det(\mathbf{\Gamma}(\mathbf{n}) - \rho c^2 \mathbf{I}) = 0$, from equation (2.46), to find the group velocities we find

$$\rho c^2 = \begin{cases} \{C_{11}, C_{66}\} \text{ for } \mathbf{n} = \begin{bmatrix} 1 & 0 \end{bmatrix}^T, \\ \{C_{22}, C_{66}\} \text{ for } \mathbf{n} = \begin{bmatrix} 0 & 1 \end{bmatrix}^T, \\ \{\lambda_+, \lambda_-\} \text{ for } \mathbf{n} = \frac{1}{\sqrt{2}} \begin{bmatrix} 1 & 1 \end{bmatrix}^T, \end{cases} \tag{5.2}$$

where

$$2\lambda_\pm = C_{11} + C_{22} \pm \sqrt{(C_{11} - C_{22})^2 + 4C_{12}^2}. \tag{5.3}$$

In order to find fluid like properties from the elastic medium we remove shear waves. This means the lower values for the wave speed, c, found in equation (5.2) must be zero as these represent the shear wave speeds. Setting these speeds to zero obtains the relations

$$C_{66} = 0, \quad C_{11}C_{22} = C_{12}^2. \tag{5.4}$$

Another method to find this behavior is to simply take the eigenvalues of the elasticity tensor and set all but one to zero. Looking at equation (5.1) the eigenvalues are λ_+, λ_-, and C_{66}, taking all but one to zero gives the same result, equation (5.4). In this sense the material will only propagate bulk waves and can be thought of as a type of anisotropic fluid.

5.2 Cloaking theory

If one were to consider a pentamode cloak with transversely isotropic symmetry (see [20]) having elastic components displayed in equation (2.41), then all shear moduli must be set to zero, which implies that $C_{44} = 0$ and $C_{12} = C_{11}$. The result of setting all but one eigenvalue to zero is $C_{11}C_{33} - C_{13}^2 = 0$. The material then has two independent

moduli for which we define $C_{11} = K_r(r)$ and $C_{33} = K_\perp(r)$, which are defined by a mapping function, $f(r)$, which maps in two dimensions a larger annulus to a much smaller one which ideally becomes a point, reference figure 5.1. Interestingly the mapping function has a large degree of freedom with boundary condition on the outer surface of the cloak, $f(b) = b$, and that for the cloak to become effective we take at the inner surface $f(a) = \delta \approx 0$. We note that setting δ equal to zero results in a perfect cloak mapping however as seen next this requires moduli to become singular. Instead by taking δ small but non-zero we can attain near perfect cloaking and avoid the singularities in the moduli. If we consider a pure pentamode cloak in two dimensions where the

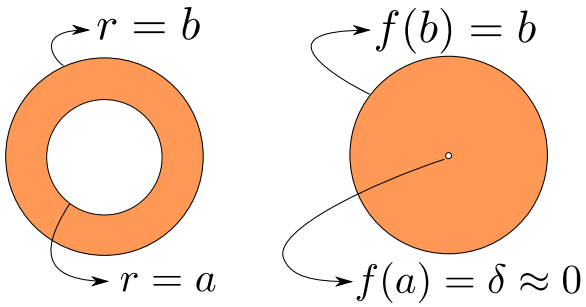

Figure 5.1: Mapping diagram shown where $f(r)$ maps the physical space (left) to the virtual space (right). The cloaking material is between radii $r = a$ (inner surface) and $r = b$ (outer surface).

density is isotropic we have

$$\rho(r) = \rho_0 f' \frac{f}{r}, \quad K_r(r) = K_0 \frac{1}{f'} \frac{f}{r}, \quad K_\perp(r) = K_0 f' \frac{r}{f}, \tag{5.5}$$

then the elasticity components are

$$\mathbf{C} = \begin{bmatrix} C_{11} & C_{13} & 0 \\ C_{13} & C_{33} & 0 \\ 0 & 0 & C_{66} \end{bmatrix} = \begin{bmatrix} K_r & \sqrt{K_r K_\perp} & 0 \\ \sqrt{K_r K_\perp} & K_\perp & 0 \\ 0 & 0 & 0 \end{bmatrix}, \tag{5.6}$$

where ρ_0 and K_0 are the background fluids density and bulk modulus. For three dimensional cylindrical structures the form for the elasticity components can be simplified. Letting $\mathbf{s}$ have components

$$\mathbf{s} = \begin{bmatrix} f/r & f' & 1 & 0 & 0 & 0 \end{bmatrix}, \tag{5.7}$$

the elasticity components are then [20]

$$\mathbf{C} = K_0 \frac{r}{f f'} \mathbf{s}^T \mathbf{s}. \tag{5.8}$$

The large degree of freedom in f is also seen in pure inertial cloaks and as shown in [19] instead of choosing a mapping and then finding material properties to suit such a transformation the inverse problem is possible where material characteristics can be considered to put further constraints on f. Such transformations have been studied for pentamode cloaks [23], where properties including constant density, constant radial stiffness, constant tangential stiffness and others including a mapping that considers minimizing elastic anisotropy have been studied.

Using the stable impedance Ricatti method of chapter 4 we can simulate a cloak using the elastic properties in equation (5.6) and change the properties as a function of r by discretizing between the radii $r = a$ and $r = b$. Doing this resulted in the example of figure 5.3. The total field without the cloak is in figure 5.2. The linear mapping function was used,

$$f(r) = \big((a-\delta)r - (b-\delta)a\big)/(a-b), \tag{5.9}$$

where we took $\delta = 0.01b$. The solution was found using the second order Taylor series, equation (4.32), with 2000 evenly spaced steps between $r = a$ and $r = b$.

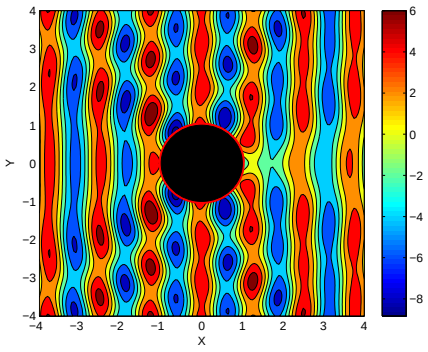

Figure 5.2: Total pressure field described by equation (4.43) for an aluminum cylinder of radius $r = 1\ m$. Impedance was found directly from (3.80). $ka = 5$, $k_z = 0$, and σ_{tot}= 2.468.

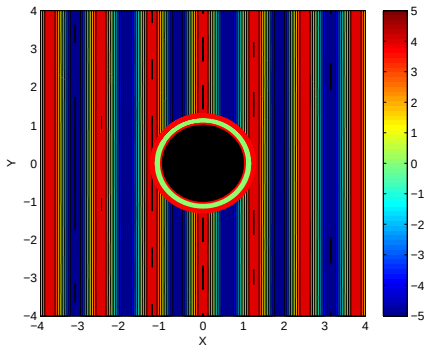

Figure 5.3: Total pressure field for aluminum cylinder surrounded by cloaking medium for $r = a = 1\ m$ to $r = b = 1.25\ m$. kb= 1, k_z=0, and $\sigma_{tot} = 0.0127$.

5.2.1 Effects of shear

Unfortunately the relation for the shear moduli, $C_{66} = 0$, must be relaxed in order for the material to maintain it's structure. Effects of shear in cloaking mediums has been studied [25]. Here we explore what adding a shear modulus to the elastic properties of equation (5.8) does to the efficiency of the cloak for two dimensional structures. We add a shear modulus μ to the elasticity components in the following manner

$$\mathbf{C} = \left(K\frac{r}{ff'} - \frac{2\mu}{3\mathbf{s}\mathbf{s}^T}\right)\mathbf{s}^T\mathbf{s} + \mu\begin{bmatrix} 2\mathbf{I}^{(3)} & \mathbf{0}^{(3)} \\ \mathbf{0}^{(3)} & \mathbf{I}^{(3)} \end{bmatrix}, \tag{5.10}$$

where $\mathbf{I}^{(3)}$ is a 3x3 identity matrix and $\mathbf{0}^{(3)}$ is a 3x3 matrix of zeros. This essentially adds an isotropic modulus where we have using lamé parameters the standard $\lambda = K - 2\mu/3$ relation. Additionally we consider a shear modulus that includes a small amount of damping. This is done by giving the shear modulus a small imaginary part by taking $\mu = \hat{\mu}e^{-i\psi}$, where we take $\psi = 0.05$. We start by considering a bubble of radius $r = 1$ m surrounded by water for which the total pressure field can be found in figure 5.6, for ka=5. The scattering cross section at this frequency is $\sigma_{tot}(ka = 5) = 6.57$. We apply several different cloaks between the radii $r = a = 1$ m and $r = b = 0.8$ m while varying the shear modulus. Examples of the total pressure field are given in the figures of 5.5, for which the frequency was kept constant at $ka = 5$ and $\delta = .01b$ for the transformation function.

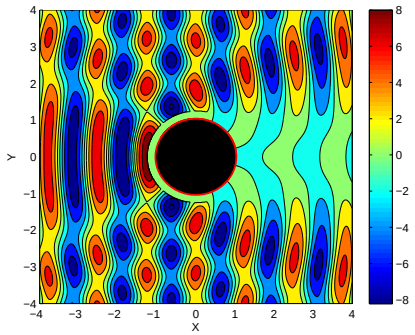

Figure 5.4: Total normalized pressure field for a traction free surface at $r = 1$ m. Parameters are ka= 5, k_z=0, and scattering cross section and backscatter are $\sigma_{tot} = 6.57$ and $f(\pi) = 0.89$.

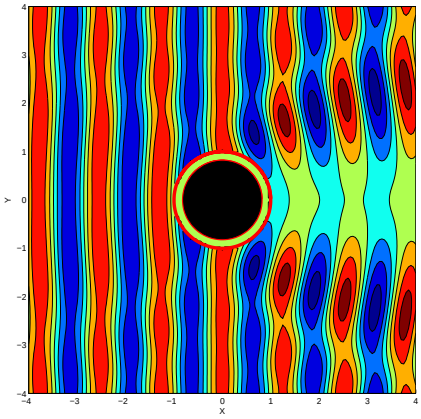

(a) $K/\mu = 5$, $\sigma_{tot} = 4.51$.

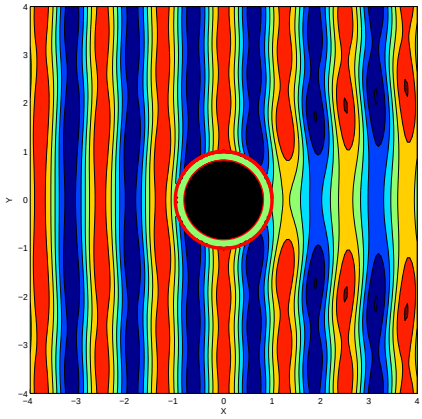

(b) $K/\mu = 10$, $\sigma_{tot} = 1.92$.

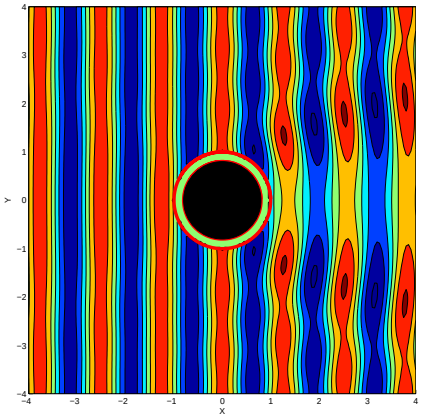

(c) $K/\mu = 15$, $\sigma_{tot} = 1.30$.

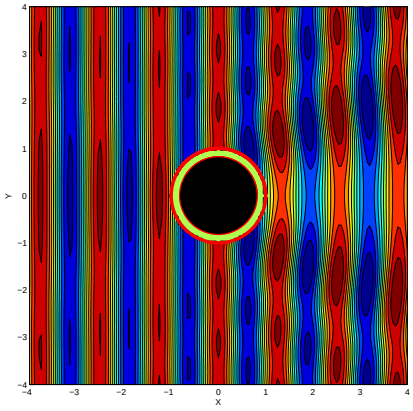

(d) $K/\mu = 25$, $\sigma_{tot} = 0.81$.

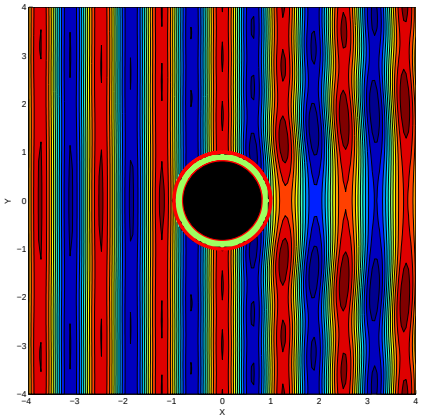

(e) $K/\mu = 50$, $\sigma_{tot} = 0.50$.

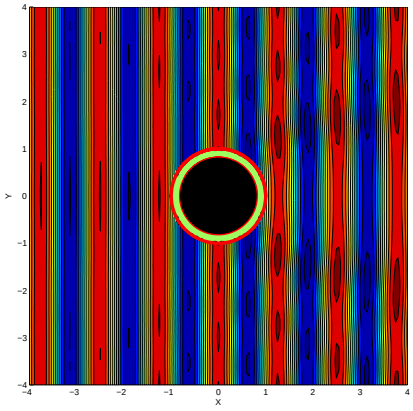

(f) $K/\mu = 100$, $\sigma_{tot} = 0.21$.

Figure 5.5: Total normalized pressure field for cloaks varying in shear modulus. All examples have ka=5, and $\delta = 0.01b$ for the mapping.

Varying the frequency and computing the back scatter and scattering cross section was also done. Figure 5.6 computes this for the case of a traction free surface without a cloaking medium.

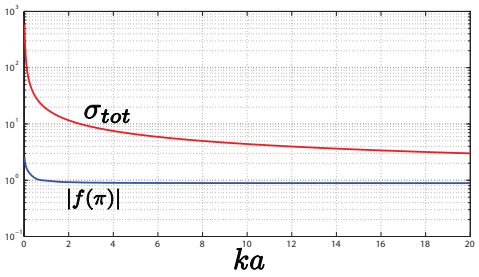

Figure 5.6: Scattering cross section, equation (4.49), and back scatter, equation (4.48), frequency behavior for a traction free surface at $r = 1\ m$ surrounded by water.

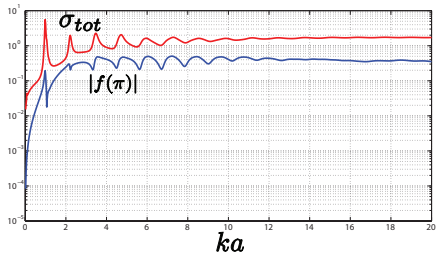

(a) $K/\mu = 22$, $\delta = 0.1b$.

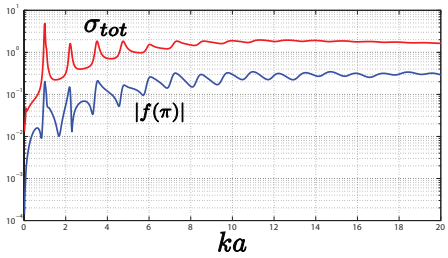

(b) $K/\mu = 22$, $\delta = 0.01b$.

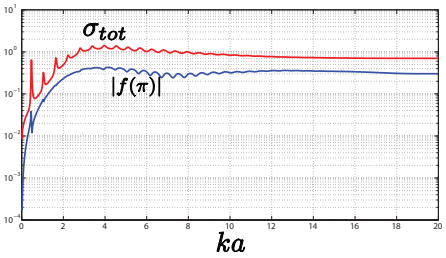

(c) $K/\mu = 100$, $\delta = 0.1b$.

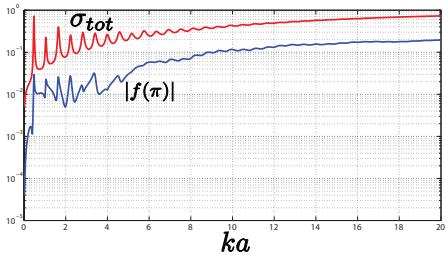

(d) $K/\mu = 100$, $\delta = 0.01b$.

Figure 5.7: Scattering cross section σ_{tot} and back scatter frequency behavior, with changing δ parameter between left and right. Cloak between radii $a = 1$ and $b = 0.8$.

In the figures of 5.7, two different levels of shear moduli as well as the parameter δ were studied. It is seen that at a shear modulus of roughly five percent of the bulk the δ parameter has little affect. At smaller shear modulus, roughly one percent of the bulk, the δ parameter has much more influence and it seems that this level for the shear modulus is tolerable. It is clear that when the ratio of κ/μ becomes large enough the cloaking medium becomes more effective. This is because the theory used

here requires pentamode elasticity and does not account for wave energy to be entered into shearing modes. We leave cloaking theory here with the result that by adding in some amount of shear modulus we can still have an effective device, especially when the shear modulus is roughly one percent or less compared to the bulk modulus. Next our attention is focused on producing periodic micro-structure designs that may be able to produce cloaking devices. This is done by first reviewing static and dynamic methods that account for a materials global elastic response based on the study of a repeating unit cell.

Chapter 6

Metallic foams and static homogenization

This chapter focuses on a static means of determining the effective elastic constants of foam structures. In the review of acoustic cloaking theory from the previous chapter it was found that pentamode elasticity is required for elastic based devices that are created with transformation acoustics. This class of material also satisfies the problem of relating the elastic equation of motion to the acoustic. In order to achieve pentamode elasticity we turn to metallic foams as they offer the ability to achieve the desired macroscopic properties based on a unit cell design. Metallic foams have been largely studied, most notably by Gibson and Ashby [62], and can offer exotic properties including negative Poisson's ratio [63]. More recently studies looking into the feasibility of creating pentamode materials [24] has occurred with focus on the creation of metamaterial devices. Foam structures are also known to have relatively small shear rigidity in comparison to the compression stiffness which is essential for approximating pentamode behavior. Furthermore, the regular structure of the foam allows the simultaneous variation of both the effective density and bulk modulus. We review static homogenization theory of cellular materials by both analytical and numerical methods for consistency and accuracy. Later on in chapter 8 these methods are used to design a material that can mimic the acoustic properties of water.

6.1 Analytical

As a step towards creating cloaking devices the first problem considered is that of mimicking the acoustic properties of water in two dimensions. This material falls into the category of pentamode elasticity, requiring isotropic behavior, matching of the bulk modulus, maintaining small shear modulus by comparison, and matching of the density

of water. The material is called Metal Water and is developed later in chapter 8. In two dimensions, foams that have the property of being isotropic fall under regular hexagonal geometry (honeycomb lattice). In this case we review the results of Kim and Al-Hassani [64] for which effective elastic constants can be determined based on strut geometry for such a structure. In the three dimensional case tetrahedral geometry (diamond lattice) is needed to achieve isotropy for which case we review the results of [65], which is done later in the beginning of chapter 9.

Effective moduli for honeycomb structures was found by Kim and Al-Hassani [64] by using figure 6.1 and applying loads on a rectangular boundary and then by strain energy formulation a displacement can be calculated caused by the applied load giving a constitutive relation between stress and strain, later on we do the same analysis on the three-dimensional structure to calculate an effective bulk modulus. From [64], the effective in-plane Young's modulus, E_i^*, Poisson's ratio, ν_{ij}^*, and shear modulus, G_{ij}^*, are given for plane strain as

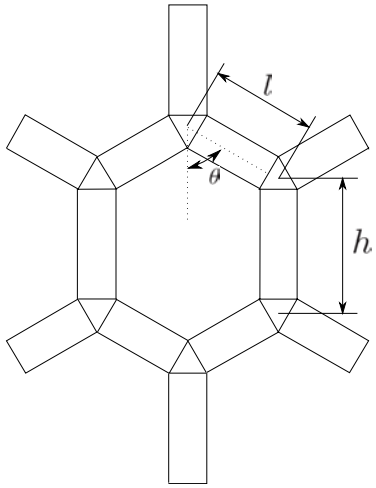

Figure 6.1: General cellular structure.

$$
\begin{aligned}
E_1^* &= \frac{l\sin\theta}{2b(h+l\cos\theta)(N_l'\cos^2\theta + M_l\sin^2\theta)},\\
E_2^* &= \frac{h+l\cos\theta}{2bl\sin\theta(N_l'\sin^2\theta + M_l\cos^2\theta + 2M_h)},\\
\nu_{12}^* &= \frac{l\sin\theta(N_l'-M_l)\cos\theta\sin\theta}{(h+l\cos\theta)(N_l'\cos^2\theta + M_l\sin^2\theta)},\\
\nu_{21}^* &= \frac{(h+l\cos\theta)(N_l'-M_l)\cos\theta\sin\theta}{l\sin\theta(N_l'\sin^2\theta + M_l\cos^2\theta + 2M_h)},\\
G_{12}^* &= \frac{(h+l\cos\theta)l\sin\theta}{2b((h^2N_l' + 2l^2N_h')\sin^2\theta + M_l(l+h\cos\theta)^2)},
\end{aligned}
\tag{6.1}
$$

where

$$
N_l' = N_l + 2(1+\nu)kM_l. \tag{6.2}
$$

M_a and N_a refer to axial and bending compliance where

$$
M_a = \int_0^{a/2} \frac{\mathrm{d}\,x}{EA}, \quad N_a = \int_0^{a/2} \frac{x^2\,\mathrm{d}\,x}{EI}. \tag{6.3}
$$

Here h and l are the strut lengths, b is the depth into the page such that $A = bt$ with member thickness t, $I = bt^3/12$, and θ describes the angle between vertical and the strut as shown in figure 6.1. The relation to the Voigt moduli for two dimensional elasticity are given by [66]:

$$
\boldsymbol{C} = \begin{pmatrix} C_{11} & C_{12} & C_{16} \\ C_{12} & C_{22} & C_{26} \\ C_{16} & C_{26} & C_{66} \end{pmatrix} = \begin{pmatrix} \frac{E_1^*}{1-\nu_{12}^*\nu_{21}^*} & \frac{\nu_{21}^*E_1^*}{1-\nu_{12}^*\nu_{21}^*} & 0 \\ \frac{\nu_{12}^*E_2^*}{1-\nu_{12}^*\nu_{21}^*} & \frac{E_2^*}{1-\nu_{12}^*\nu_{21}^*} & 0 \\ 0 & 0 & G_{12}^* \end{pmatrix}, \tag{6.4}
$$

and hence

$$
\begin{aligned}
C_{11} &= \frac{l\sin\theta}{4bM_hM_lN_l'\,(h+l\cos\theta)}\left(\frac{2M_h + M_l\cos^2\theta + N_l'\sin^2\theta}{\frac{1}{2M_h} + \frac{1}{M_l}\cos^2\theta + \frac{1}{N_l'}\sin^2\theta}\right),\\
C_{22} &= \frac{(h+l\cos\theta)}{4bM_hM_lN_l'\,l\sin\theta}\left(\frac{M_l\sin^2\theta + N_l'\cos^2\theta}{\frac{1}{2M_h} + \frac{1}{M_l}\cos^2\theta + \frac{1}{N_l'}\sin^2\theta}\right),\\
C_{12} &= \frac{\cos\theta\sin\theta}{4bM_hM_lN_l'}\left(\frac{N_l'-M_l}{\frac{1}{2M_h} + \frac{1}{M_l}\cos^2\theta + \frac{1}{N_l'}\sin^2\theta}\right),\\
C_{66} &= \frac{(h+l\cos\theta)l\sin\theta}{2b((h^2N_l' + 2l^2N_h')\sin^2\theta + M_l(l+h\cos\theta)^2)}.
\end{aligned}
\tag{6.5}
$$

Using an alternative method similar to Wang and Cuitino [67] these constants were

found as

$$
\begin{aligned}
C_{11} &= \frac{R_2 \sin\theta}{4M_1M_2N(R_1+R_2\cos\theta)}\left(\frac{2M_1+M_2\cos^2\theta+N\sin^2\theta}{\frac{1}{2M_1}+\frac{1}{M_2}\cos^2\theta+\frac{1}{N}\sin^2\theta}\right),\\
C_{22} &= \frac{(R_1+R_2\cos\theta)}{4M_1M_2NR_2\sin\theta}\left(\frac{M_2\sin^2\theta+N\cos^2\theta}{\frac{1}{2M_1}+\frac{1}{M_2}\cos^2\theta+\frac{1}{N}\sin^2\theta}\right),\\
C_{12} &= \frac{\cos\theta\sin\theta}{4M_1M_2N}\left(\frac{N-M_2}{\frac{1}{2M_1}+\frac{1}{M_2}\cos^2\theta+\frac{1}{N}\sin^2\theta}\right),\\
C_{66} &= \frac{(R_1+R_2\cos\theta)\,R_2\sin\theta}{2\left[\left(R_1^2N_2+R_2^2N_1\right)\sin^2\theta+M_2\left(R_2+R_1\cos\theta\right)^2\right]},
\end{aligned}
\tag{6.6}
$$

where

$$
N^{-1} = \frac{1}{N_2}+\frac{1}{N_2+\frac{R_2^2}{R_1^2}N_1}. \tag{6.7}
$$

These equations were derived using a unit cell as shown in figure 6.2, where it is

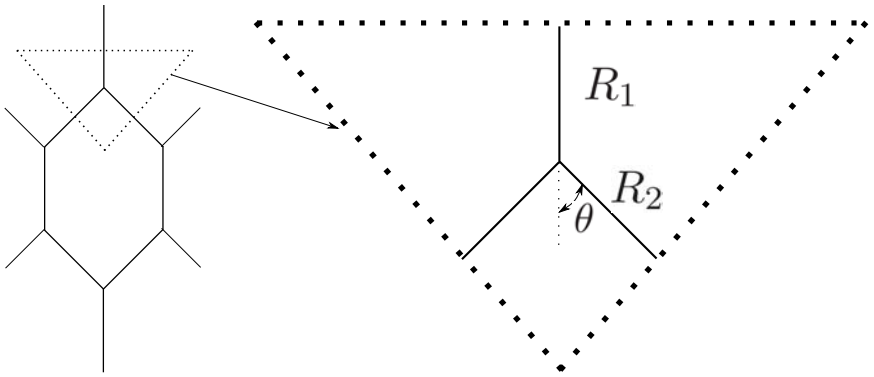

Figure 6.2: Structure and unit cell description.

easily seen that $R_1 = \frac{h}{2}$ and $R_2 = \frac{l}{2}$. Again M_i is the axial compliance and N_i the bending compliance. We see similarity between equations (6.5) and (6.6) however all of the moduli differ, for C_{11}, C_{22} and C_{12} the difference arises because of the more complicated form of N in equation (6.7) as compared with N_l', which is equivalent to N_2. The shear modulus C_{66} is different because of the disparity between the terms $2l^2N_h'$ and $R_2^2N_1$. We will make use of the Kim and Al-Hassani results, equation (6.5), for the remainder of the thesis.

Limit of thin members

In the limit of very thin members N_l and N_h become much larger than M_l and M_h, and taking the limit as the ratio $M_a/N_b \to 0$,

$$\mathbf{C} = C_0 \begin{pmatrix} \alpha & 1 & 0 \\ 1 & \frac{1}{\alpha} & 0 \\ 0 & 0 & 0 \end{pmatrix}, \quad C_0 = \frac{\cos\theta \sin\theta}{2b[M_l + 2M_h \cos^2\theta]}, \quad \alpha = \frac{l \sin^2\theta}{(h + l\cos\theta)\cos\theta}. \tag{6.8}$$

This is of pentamode form since $\mathbf{C}$ has only one non-zero eigenvalue. It is interesting to note that the ratio C_{11}/C_{22} depends on the geometrical parameter α, which will be important in cloak design. For the regular hex we have $\alpha = 1$. From this analysis we

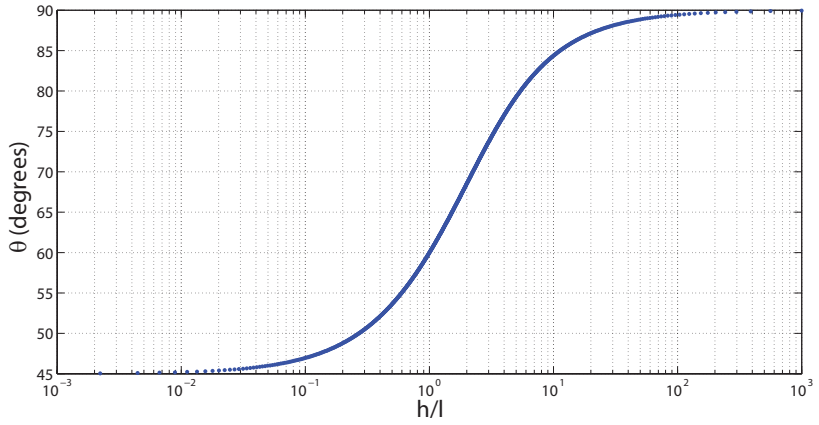

Figure 6.3: Values for θ and h/l to attain $\alpha = 1$ in equation (6.8).

see designs for which $h = l$ requires the angle $\theta = \pi/3$, meaning the structure has regular hexagonal shape. Utilizing equation (6.5) Ashby charts can be created that show an effective range of elastic properties as well as density properties based on parameters defining the strut geometry. With that it is possible to find and create materials that can accommodate acoustic cloaking depending on the versatility of the unit cell. This analysis is continued later in chapter 8 where we consider regular hexagonal foam structures, $\theta = \pi/3$, and use equation (6.5) to find the effective moduli in order to design the first Metal Water prototype. The next section reviews a finite element method that allows for a more precise method of producing desired moduli from the study of a single unit cell.

6.2 Finite element homogenization

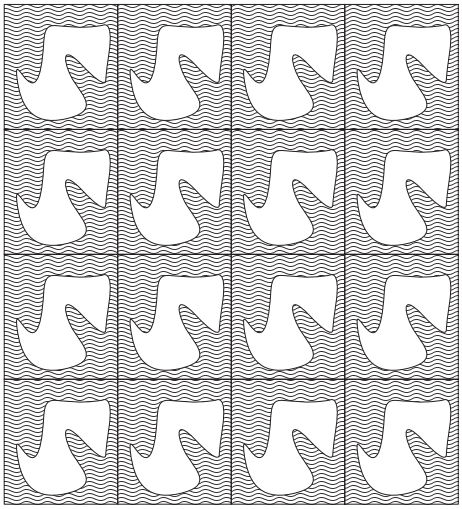

Figure 6.4: Example of a periodic elastic material for which elastic moduli can be calculated via static homogenization technique with finite elements.

The methods of section 6.1 rely on beam or foam mechanics theories to produce the effective elasticity of structured foam like materials. We next want to compare the results of the previous section to another approximation of the homogenized properties to do this we turn to finite elements. With this method general periodic structures can be analyzed such as the one shown in figure 6.4. Derivation of the macroscopic elastic moduli for structures with periodic unit cells was done by [68] and was further developed in [1] to include boundary conditions for unit cells with symmetric properties. A complete review of the theory and it's application is given in [69, 70, 71]. The homogenized elasticity is found from

$$C^H_{ijkl} = \frac{1}{|Y|} \int_{\mathbf{Y}} C_{ijkl} - C_{ijpq}\chi^{kl}_{p,q} \,\mathrm{d}\, Y, \tag{6.9}$$

where $\mathbf{Y}$ is an open rectangular parallel-piped describing the unit cell, $|Y|$ denotes the total area of the unit cell in two dimensions or the volume in three dimensions, and χ^{kl}_p is a periodic displacement solution of the governing equation which is [1]

$$\int_{\mathbf{Y}} v_{i,j} C_{ijpq}\chi^{kl}_{p,q} \,\mathrm{d}\, Y = \int_{\mathbf{Y}} v_{i,j} C_{ijkl} \,\mathrm{d}\, Y. \tag{6.10}$$

The governing equation (6.10) was derived in [68] and came about by performing a double-scale asymptotic expansion on the virtual displacement equation where v_i is an arbitrary test function. Next we go through the derivation of applying the finite element method as done in [1, 70]. We take equations (6.9) and (6.10) and go into further detail by writing out in component form the various cases for three dimensional geometries. In two dimensions, equation (6.10) would only need to be considered for the three cases of: a) $k = l = 1$, b) $k = l = 2$, and c) $k = 1$, $l = 2$. In three dimensions we will have to consider six cases which will include cases a) b) and c) as well as d) $k = 1$, $l = 3$, e) $k = 2$, $l = 3$, and f) $k = l = 3$. Assuming orthotropic anisotropy, the elastic constants to be concerned with include those listed in equation (2.39). For **case a)** $k = l = 1$ equation (6.10) yields

$$\begin{aligned}
&\int_Y \Big[\big(C_{1111}\chi^{11}_{1,1} + C_{1122}\chi^{11}_{2,2} + C_{1133}\chi^{11}_{3,3}\big)v_{1,1} + \big(C_{2211}\chi^{11}_{1,1} + C_{2222}\chi^{11}_{2,2} + C_{2233}\chi^{11}_{3,3}\big)v_{2,2} \\
&\quad + \big(C_{3311}\chi^{11}_{1,1} + C_{3322}\chi^{11}_{2,2} + C_{3333}\chi^{11}_{3,3}\big)v_{3,3} + C_{2323}\big(\chi^{11}_{2,3} + \chi^{11}_{3,2}\big)\big(v_{2,3} + v_{3,2}\big) \\
&\quad + C_{1313}\big(\chi^{11}_{1,3} + \chi^{11}_{3,1}\big)\big(v_{1,3} + v_{3,1}\big) + C_{1212}\big(\chi^{11}_{1,2} + \chi^{11}_{2,1}\big)\big(v_{1,2} + v_{2,1}\big)\Big]\mathrm{d}Y \\
&= \int_Y \Big[C_{1111}v_{1,1} + C_{2211}v_{2,2} + C_{3311}v_{3,3}\Big]\mathrm{d}Y,
\end{aligned} \tag{6.11}$$

and the homogenized properties are

$$\begin{aligned}
C^H_{1111} &= \frac{1}{|Y|}\int_Y C_{1111} - \big[C_{1111}\chi^{11}_{1,1} + C_{1122}\chi^{11}_{2,2} + C_{1133}\chi^{11}_{3,3}\big]\mathrm{d}Y, \\
C^H_{2211} &= \frac{1}{|Y|}\int_Y C_{2211} - \big[C_{2211}\chi^{11}_{1,1} + C_{2222}\chi^{11}_{2,2} + C_{2233}\chi^{11}_{3,3}\big]\mathrm{d}Y, \\
C^H_{3311} &= \frac{1}{|Y|}\int_Y C_{3311} - \big[C_{3311}\chi^{11}_{1,1} + C_{3322}\chi^{11}_{2,2} + C_{3333}\chi^{11}_{3,3}\big]\mathrm{d}Y.
\end{aligned} \tag{6.12}$$

For **case b)** $k = l = 2$ equation (6.10) yields

$$\begin{aligned}
&\int_Y \Big[\big(C_{1111}\chi^{22}_{1,1} + C_{1122}\chi^{22}_{2,2} + C_{1133}\chi^{22}_{3,3}\big)v_{1,1} + \big(C_{2211}\chi^{22}_{1,1} + C_{2222}\chi^{22}_{2,2} + C_{2233}\chi^{22}_{3,3}\big)v_{2,2} \\
&\quad + \big(C_{3311}\chi^{22}_{1,1} + C_{3322}\chi^{22}_{2,2} + C_{3333}\chi^{22}_{3,3}\big)v_{3,3} + C_{2323}\big(\chi^{22}_{2,3} + \chi^{22}_{3,2}\big)\big(v_{2,3} + v_{3,2}\big) \\
&\quad + C_{1313}\big(\chi^{22}_{1,3} + \chi^{22}_{3,1}\big)\big(v_{1,3} + v_{3,1}\big) + C_{1212}\big(\chi^{22}_{1,2} + \chi^{22}_{2,1}\big)\big(v_{1,2} + v_{2,1}\big)\Big]\mathrm{d}Y \\
&= \int_Y \Big[C_{1122}v_{1,1} + C_{2222}v_{2,2} + C_{3322}v_{3,3}\Big]\mathrm{d}Y,
\end{aligned} \tag{6.13}$$

and the homogenized properties are

$$\begin{aligned} C^H_{1122} &= \frac{1}{|Y|}\int_Y C_{1122} - \big[C_{1111}\chi^{22}_{1,1} + C_{1122}\chi^{22}_{2,2} + C_{1133}\chi^{22}_{3,3}\big]\mathrm{d}Y, \\ C^H_{2222} &= \frac{1}{|Y|}\int_Y C_{2222} - \big[C_{2211}\chi^{22}_{1,1} + C_{2222}\chi^{22}_{2,2} + C_{2233}\chi^{22}_{3,3}\big]\mathrm{d}Y, \\ C^H_{3322} &= \frac{1}{|Y|}\int_Y C_{3322} - \big[C_{3311}\chi^{22}_{1,1} + C_{3322}\chi^{22}_{2,2} + C_{3333}\chi^{22}_{3,3}\big]\mathrm{d}Y. \end{aligned} \tag{6.14}$$

For **case c)** $k = 1$**,** $l = 2$ equation (6.10) yields

$$\begin{aligned} &\int_Y \Big[\big(C_{1111}\chi^{12}_{1,1} + C_{1122}\chi^{12}_{2,2} + C_{1133}\chi^{12}_{3,3}\big)v_{1,1} + \big(C_{2211}\chi^{12}_{1,1} + C_{2222}\chi^{12}_{2,2} + C_{2233}\chi^{12}_{3,3}\big)v_{2,2} \\ &\quad + \big(C_{3311}\chi^{12}_{1,1} + C_{3322}\chi^{12}_{2,2} + C_{3333}\chi^{12}_{3,3}\big)v_{3,3} + C_{2323}\big(\chi^{12}_{2,3} + \chi^{12}_{3,2}\big)\big(v_{2,3} + v_{3,2}\big) \\ &\quad + C_{1313}\big(\chi^{12}_{1,3} + \chi^{12}_{3,1}\big)\big(v_{1,3} + v_{3,1}\big) + C_{1212}\big(\chi^{12}_{1,2} + \chi^{12}_{2,1}\big)\big(v_{1,2} + v_{2,1}\big)\Big]\mathrm{d}Y \\ &= \int_Y \Big[C_{1212}\big(v_{1,2} + v_{2,1}\big)\Big]\mathrm{d}Y, \end{aligned} \tag{6.15}$$

and the homogenized properties are

$$C^H_{1212} = \frac{1}{|Y|}\int_Y C_{1212}\big(1 - \chi^{12}_{1,2} - \chi^{12}_{2,1}\big)\mathrm{d}Y, \tag{6.16}$$

For **case d)** $k = 1$**,** $l = 3$ equation (6.10) yields

$$\begin{aligned} &\int_Y \Big[\big(C_{1111}\chi^{13}_{1,1} + C_{1122}\chi^{13}_{2,2} + C_{1133}\chi^{13}_{3,3}\big)v_{1,1} + \big(C_{2211}\chi^{13}_{1,1} + C_{2222}\chi^{13}_{2,2} + C_{2233}\chi^{13}_{3,3}\big)v_{2,2} \\ &\quad + \big(C_{3311}\chi^{13}_{1,1} + C_{3322}\chi^{13}_{2,2} + C_{3333}\chi^{13}_{3,3}\big)v_{3,3} + C_{2323}\big(\chi^{13}_{2,3} + \chi^{13}_{3,2}\big)\big(v_{2,3} + v_{3,2}\big) \\ &\quad + C_{1313}\big(\chi^{13}_{1,3} + \chi^{13}_{3,1}\big)\big(v_{1,3} + v_{3,1}\big) + C_{1212}\big(\chi^{13}_{1,2} + \chi^{13}_{2,1}\big)\big(v_{1,2} + v_{2,1}\big)\Big]\mathrm{d}Y \\ &= \int_Y \Big[C_{1313}\big(v_{1,3} + v_{3,1}\big)\Big]\mathrm{d}Y, \end{aligned} \tag{6.17}$$

and the homogenized properties are

$$C^H_{1313} = \frac{1}{|Y|}\int_Y C_{1313}\big(1 - \chi^{13}_{1,3} - \chi^{13}_{3,1}\big)\mathrm{d}Y, \tag{6.18}$$

For **case d)** $k = 2$**,** $l = 3$ equation (6.10) yields

$$\begin{aligned}
&\int_Y \Big[\big(C_{1111}\chi^{23}_{1,1} + C_{1122}\chi^{23}_{2,2} + C_{1133}\chi^{23}_{3,3}\big)v_{1,1} + \big(C_{2211}\chi^{23}_{1,1} + C_{2222}\chi^{23}_{2,2} + C_{2233}\chi^{23}_{3,3}\big)v_{2,2} \\
&\quad + \big(C_{3311}\chi^{23}_{1,1} + C_{3322}\chi^{23}_{2,2} + C_{3333}\chi^{23}_{3,3}\big)v_{3,3} + C_{2323}\big(\chi^{23}_{2,3} + \chi^{23}_{3,2}\big)\big(v_{2,3} + v_{3,2}\big) \\
&\quad + C_{1313}\big(\chi^{23}_{1,3} + \chi^{23}_{3,1}\big)\big(v_{1,3} + v_{3,1}\big) + C_{1212}\big(\chi^{23}_{1,2} + \chi^{23}_{2,1}\big)\big(v_{1,2} + v_{2,1}\big)\Big] \mathrm{d}Y \\
&= \int_Y \Big[C_{2323}\big(v_{2,3} + v_{3,2}\big)\Big] \mathrm{d}Y,
\end{aligned} \tag{6.19}$$

and the homogenized properties are

$$C^H_{2323} = \frac{1}{|Y|}\int_Y C_{2323}\big(1 - \chi^{23}_{2,3} - \chi^{23}_{3,2}\big)\mathrm{d}Y, \tag{6.20}$$

For **case f)** $k = l = 3$ equation (6.10) yields

$$\begin{aligned}
&\int_Y \Big[\big(C_{1111}\chi^{33}_{1,1} + C_{1122}\chi^{33}_{2,2} + C_{1133}\chi^{33}_{3,3}\big)v_{1,1} + \big(C_{2211}\chi^{33}_{1,1} + C_{2222}\chi^{33}_{2,2} + C_{2233}\chi^{33}_{3,3}\big)v_{2,2} \\
&\quad + \big(C_{3311}\chi^{33}_{1,1} + C_{3322}\chi^{33}_{2,2} + C_{3333}\chi^{33}_{3,3}\big)v_{3,3} + C_{2323}\big(\chi^{33}_{2,3} + \chi^{33}_{3,2}\big)\big(v_{2,3} + v_{3,2}\big) \\
&\quad + C_{1313}\big(\chi^{33}_{1,3} + \chi^{33}_{3,1}\big)\big(v_{1,3} + v_{3,1}\big) + C_{1212}\big(\chi^{33}_{1,2} + \chi^{33}_{2,1}\big)\big(v_{1,2} + v_{2,1}\big)\Big] \mathrm{d}Y \\
&= \int_Y \Big[C_{1133}v_{1,1} + C_{2233}v_{2,2} + C_{3333}v_{3,3}\Big] \mathrm{d}Y,
\end{aligned} \tag{6.21}$$

and the homogenized properties are

$$\begin{aligned}
C^H_{1133} &= \frac{1}{|Y|}\int_Y C_{1133} - \big[C_{1111}\chi^{33}_{1,1} + C_{1122}\chi^{33}_{2,2} + C_{1133}\chi^{33}_{3,3}\big]\mathrm{d}Y, \\
C^H_{2233} &= \frac{1}{|Y|}\int_Y C_{2233} - \big[C_{2211}\chi^{33}_{1,1} + C_{2222}\chi^{33}_{2,2} + C_{2233}\chi^{33}_{3,3}\big]\mathrm{d}Y, \\
C^H_{3333} &= \frac{1}{|Y|}\int_Y C_{3333} - \big[C_{3311}\chi^{33}_{1,1} + C_{3322}\chi^{33}_{2,2} + C_{3333}\chi^{33}_{3,3}\big]\mathrm{d}Y.
\end{aligned} \tag{6.22}$$

6.2.1 Vectorization of the equations

Case a) $k = l = 1$. Using Voigt notation and letting $\chi_1^{11} = \Phi_1$, $\chi_2^{11} = \Phi_2$, and $\chi_3^{11} = \Phi_3$, we find

$$\begin{aligned}
&\int_Y \Big[\big(C_{11}\Phi_{1,1} + C_{12}\Phi_{2,2} + C_{13}\Phi_{3,3}\big)v_{1,1} + \big(C_{21}\Phi_{1,1} + C_{22}\Phi_{2,2} + C_{23}\Phi_{3,3}\big)v_{2,2} \\
&\quad + \big(C_{31}\Phi_{1,1} + C_{32}\Phi_{2,2} + C_{33}\Phi_{3,3}\big)v_{3,3} + C_{44}\big(\Phi_{2,3} + \Phi_{3,2}\big)\big(v_{2,3} + v_{3,2}\big) \\
&\quad + C_{55}\big(\Phi_{1,3} + \Phi_{3,1}\big)\big(v_{1,3} + v_{3,1}\big) + C_{66}\big(\Phi_{1,2} + \Phi_{2,1}\big)\big(v_{1,2} + v_{2,1}\big)\Big]\mathrm{d}Y \\
&= \int_Y \Big[C_{11}v_{1,1} + C_{21}v_{2,2} + C_{31}v_{3,3}\Big]\mathrm{d}Y,
\end{aligned} \tag{6.23}$$

and the homogenized properties are

$$\begin{aligned}
C_{11}^H &= \frac{1}{|Y|}\int_Y C_{11} - \big[C_{11}\Phi_{1,1} + C_{12}\Phi_{2,2} + C_{13}\Phi_{3,3}\big]\mathrm{d}Y, \\
C_{21}^H &= \frac{1}{|Y|}\int_Y C_{21} - \big[C_{21}\Phi_{1,1} + C_{22}\Phi_{2,2} + C_{23}\Phi_{3,3}\big]\mathrm{d}Y, \\
C_{31}^H &= \frac{1}{|Y|}\int_Y C_{31} - \big[C_{31}\Phi_{1,1} + C_{32}\Phi_{2,2} + C_{33}\Phi_{3,3}\big]\mathrm{d}Y.
\end{aligned} \tag{6.24}$$

Equation (6.23) is rewritten in the form

$$\begin{aligned}
&\int_Y \Bigg\{ \begin{bmatrix} v_{1,1} & v_{2,2} & v_{3,3} & v_{2,3}+v_{3,2} & v_{1,3}+v_{3,1} & v_{1,2}+v_{2,1} \end{bmatrix} \\
&\quad \times \begin{bmatrix} C_{11} & C_{12} & C_{13} & 0 & 0 & 0 \\ C_{12} & C_{22} & C_{23} & 0 & 0 & 0 \\ C_{13} & C_{23} & C_{33} & 0 & 0 & 0 \\ 0 & 0 & 0 & C_{44} & 0 & 0 \\ 0 & 0 & 0 & 0 & C_{55} & 0 \\ 0 & 0 & 0 & 0 & 0 & C_{66} \end{bmatrix} \begin{bmatrix} \Phi_{1,1} \\ \Phi_{2,2} \\ \Phi_{3,3} \\ \Phi_{2,3}+\Phi_{3,2} \\ \Phi_{1,3}+\Phi_{3,1} \\ \Phi_{1,2}+\Phi_{2,1} \end{bmatrix} \Bigg\}\mathrm{d}Y \\
&= \int_Y \Bigg\{ \begin{bmatrix} v_{1,1} & v_{2,2} & v_{3,3} & v_{2,3}+v_{3,2} & v_{1,3}+v_{3,1} & v_{1,2}+v_{2,1} \end{bmatrix} \begin{bmatrix} C_{11} \\ C_{12} \\ C_{13} \\ 0 \\ 0 \\ 0 \end{bmatrix} \Bigg\}\mathrm{d}Y.
\end{aligned} \tag{6.25}$$

Next we define

$$\begin{aligned}\epsilon(v) &= \begin{bmatrix} v_{1,1} & v_{2,2} & v_{3,3} & v_{2,3}+v_{3,2} & v_{1,3}+v_{3,1} & v_{1,2}+v_{2,1}\end{bmatrix}^T, \\ \epsilon(\Phi) &= \begin{bmatrix} \Phi_{1,1} & \Phi_{2,2} & \Phi_{3,3} & \Phi_{2,3}+\Phi_{3,2} & \Phi_{1,3}+\Phi_{3,1} & \Phi_{1,2}+\Phi_{2,1}\end{bmatrix}^T,\end{aligned} \tag{6.26}$$

and again using orthotropic elasticity,

$$\mathbf{C} = \begin{bmatrix} C_{11} & C_{12} & C_{13} & 0 & 0 & 0 \\ C_{12} & C_{22} & C_{23} & 0 & 0 & 0 \\ C_{13} & C_{23} & C_{33} & 0 & 0 & 0 \\ 0 & 0 & 0 & C_{44} & 0 & 0 \\ 0 & 0 & 0 & 0 & C_{55} & 0 \\ 0 & 0 & 0 & 0 & 0 & C_{66} \end{bmatrix} = \begin{bmatrix} \mathbf{d}_1 & \mathbf{d}_2 & \mathbf{d}_3 & \mathbf{d}_4 & \mathbf{d}_5 & \mathbf{d}_6 \end{bmatrix} \tag{6.27}$$

Then equation (6.25) may be written as

$$\int_Y \epsilon(v)^T \mathbf{C} \epsilon(\Phi) \mathrm{d}Y = \int_Y \epsilon^T(v) \mathbf{d}_1 \mathrm{d}Y, \tag{6.28}$$

and the homogenized elastic properties are

$$\begin{aligned} C_{11}^H &= \frac{1}{|Y|}\int_Y \Big(C_{11} - \mathbf{d}_1^T \epsilon(\Phi) \Big) \mathrm{d}Y, \\ C_{21}^H &= \frac{1}{|Y|}\int_Y \Big(C_{21} - \mathbf{d}_2^T \epsilon(\Phi) \Big) \mathrm{d}Y, \\ C_{31}^H &= \frac{1}{|Y|}\int_Y \Big(C_{31} - \mathbf{d}_3^T \epsilon(\Phi) \Big) \mathrm{d}Y. \end{aligned} \tag{6.29}$$

Case b) $k = l = 2$. Letting $\chi_1^{22} = \Psi_1$, $\chi_2^{22} = \Psi_2$, and $\chi_3^{22} = \Psi_3$. Doing as done in the previous section for case a) we find

$$\int_Y \epsilon(v)^T \mathbf{C} \epsilon(\Psi) \mathrm{d}Y = \int_Y \epsilon^T(v) \mathbf{d}_2 \mathrm{d}Y, \tag{6.30}$$

and the homogenized properties

$$\begin{aligned} C_{12}^H &= \frac{1}{|Y|}\int_Y \Big(C_{12} - \mathbf{d}_1^T \epsilon(\Psi) \Big) \mathrm{d}Y, \\ C_{22}^H &= \frac{1}{|Y|}\int_Y \Big(C_{22} - \mathbf{d}_2^T \epsilon(\Psi) \Big) \mathrm{d}Y, \\ C_{32}^H &= \frac{1}{|Y|}\int_Y \Big(C_{32} - \mathbf{d}_3^T \epsilon(\Psi) \Big) \mathrm{d}Y. \end{aligned} \tag{6.31}$$

Case c) $k = 1$,$l = 2$. Letting $\chi_1^{12} = \Theta_1$, $\chi_2^{12} = \Theta_2$, and $\chi_3^{12} = \Theta_3$, we find

$$\int_Y \epsilon(v)^T \mathbf{C} \epsilon(\Theta) \mathrm{d}Y = \int_Y \epsilon^T(v) \mathbf{d}_6 \mathrm{d}Y, \tag{6.32}$$

and the homogenized properties

$$C_{66}^H = \frac{1}{|Y|}\int_Y \Big(C_{66} - \mathbf{d}_6^T \epsilon(\Theta)\Big) \mathrm{d}Y. \tag{6.33}$$

Case d) $k = 1$ **,**$l = 3$. Letting $\chi_1^{13} = \Omega_1$, $\chi_2^{13} = \Omega_2$, and $\chi_3^{13} = \Omega_3$, we find

$$\int_Y \epsilon(v)^T \mathbf{C} \epsilon(\Omega) \mathrm{d}Y = \int_Y \epsilon^T(v) \mathbf{d}_5 \mathrm{d}Y, \tag{6.34}$$

and the homogenized properties

$$C_{55}^H = \frac{1}{|Y|}\int_Y \Big(C_{55} - \mathbf{d}_5^T \epsilon(\Omega)\Big) \mathrm{d}Y. \tag{6.35}$$

Case e) $k = 2$ **,**$l = 3$. Letting $\chi_1^{23} = \Gamma_1$, $\chi_2^{23} = \Gamma_2$, and $\chi_3^{23} = \Gamma_3$, we find

$$\int_Y \epsilon(v)^T \mathbf{C} \epsilon(\Gamma) \mathrm{d}Y = \int_Y \epsilon^T(v) \mathbf{d}_4 \mathrm{d}Y, \tag{6.36}$$

and the homogenized properties

$$C_{44}^H = \frac{1}{|Y|}\int_Y \Big(C_{44} - \mathbf{d}_4^T \epsilon(\Gamma)\Big) \mathrm{d}Y. \tag{6.37}$$

Case f) $k = l = 3$. Letting $\chi_1^{33} = \Upsilon_1$, $\chi_2^{33} = \Upsilon_2$, and $\chi_3^{33} = \Upsilon_3$, we find

$$\int_Y \epsilon(v)^T \mathbf{C} \epsilon(\Upsilon) \mathrm{d}Y = \int_Y \epsilon^T(v) \mathbf{d}_3 \mathrm{d}Y, \tag{6.38}$$

and the homogenized properties

$$\begin{aligned} C_{13}^H &= \frac{1}{|Y|}\int_Y \Big(C_{13} - \mathbf{d}_1^T \epsilon(\Upsilon)\Big) \mathrm{d}Y, \\ C_{23}^H &= \frac{1}{|Y|}\int_Y \Big(C_{23} - \mathbf{d}_2^T \epsilon(\Upsilon)\Big) \mathrm{d}Y, \\ C_{33}^H &= \frac{1}{|Y|}\int_Y \Big(C_{33} - \mathbf{d}_3^T \epsilon(\Upsilon)\Big) \mathrm{d}Y. \end{aligned} \tag{6.39}$$

There is some overlap in the cases, for instance we expect the moduli $C_{13}^H = C_{31}^H$, which can be compared by using cases **a** and **f**. This can provide as a first check on correct implementation of the theory. Next finite elements are reviewed and used in this theory and a comparison study is done.

6.2.2 FEM application

Consider case a) (k=l=1) which yields the governing equation (6.28). We took the displacements $\chi_i^{11} = \Phi_i$ and let $\mathbf{\Phi} = \begin{bmatrix} \Phi_1 & \Phi_2 & \Phi_3 \end{bmatrix}^T$, using the finite element method displacements take the form [72]

$$\Phi_i(\mathbf{y}) = \sum N_{iK}(\mathbf{y}) \hat{\mathbf{\Phi}}_K^e, \tag{6.40}$$

where summation is taken over all elements, N_{iK} are interpolation functions known as the shape functions and depend on the type of element used and $\hat{\mathbf{\Phi}}_K^e$ are the nodal displacements of element e. The strains are then

$$\epsilon(\mathbf{\Phi})_{ij} = \sum A_{ijK} \hat{\mathbf{\Phi}}_K^e = \sum \mathbf{B} \hat{\mathbf{\Phi}}^e, \tag{6.41}$$

where $\mathbf{B}$ is known as the strain-displacement matrix and

$$A_{ijK} = \frac{1}{2}\left(\frac{\partial N_{iK}}{\partial y_j} + \frac{\partial N_{jK}}{\partial y_i}\right). \tag{6.42}$$

Applying equation (6.41) to (6.28) we find [1, 70]

$$\int_Y \mathbf{B}^T \mathbf{C} \mathbf{B} \, \mathrm{d}\, Y \hat{\mathbf{\Phi}} = \int_Y B^T \mathbf{d}_1 \, \mathrm{d}\, Y, \tag{6.43}$$

where all of the element nodal displacements, $\hat{\mathbf{\Phi}}^e$, have been assembled into a global displacement vector, $\hat{\mathbf{\Phi}}$. Equation (6.43) is rewritten as

$$\mathbf{K} \hat{\mathbf{\Phi}} = \mathbf{f}, \tag{6.44}$$

where

$$\mathbf{K} = \int_Y \mathbf{B}^T \mathbf{C} \mathbf{B} \, \mathrm{d}\, Y, \quad \text{and} \quad \mathbf{f} = \int_Y B^T \mathbf{d}_1 \, \mathrm{d}\, Y, \tag{6.45}$$

which is the global set of equations used in the finite element analysis. As noted by [70] if we consider just a single element the force vector has the form

$$\mathbf{f}_i^e = \int_{Y^e} \mathbf{B}_i^{e^T} \mathbf{d}_1 \, \mathrm{d}\, Y, \tag{6.46}$$

where i denotes the node of element e and $\mathbf{B}_i^{e^T}$ is the strain-displacement matrix for node i of element e. When the force vector in equation (6.46) is compared to an initial strain loading defined as [73]

$$\{f_i^{\varepsilon^0}\}^e = \int_{Y^e} \mathbf{B}^{e^T} \mathbf{C} \varepsilon^0 \, \mathrm{d}\, Y, \tag{6.47}$$

we find

$$\mathbf{C}\varepsilon^0 = \mathbf{d}_1 \quad \rightarrow \quad \begin{bmatrix} C_{11} & C_{12} & C_{13} & 0 & 0 & 0 \\ C_{12} & C_{22} & C_{23} & 0 & 0 & 0 \\ C_{13} & C_{23} & C_{33} & 0 & 0 & 0 \\ 0 & 0 & 0 & C_{44} & 0 & 0 \\ 0 & 0 & 0 & 0 & C_{55} & 0 \\ 0 & 0 & 0 & 0 & 0 & C_{66} \end{bmatrix} . \begin{bmatrix} \varepsilon^0_{11} \\ \varepsilon^0_{22} \\ \varepsilon^0_{33} \\ 2\varepsilon^0_{23} \\ 2\varepsilon^0_{13} \\ 2\varepsilon^0_{12} \end{bmatrix} = \begin{bmatrix} C_{11} \\ C_{12} \\ C_{13} \\ 0 \\ 0 \\ 0 \end{bmatrix}, \tag{6.48}$$

which implies

$$\varepsilon^0_{11} = 1, \quad \text{else} \quad \varepsilon^0_{ij} = 0, \tag{6.49}$$

note that this was case a) for $k = l = 1$. Similarly if we continue the analysis on the other cases we find for each case

$$\varepsilon^0_{kl} = 1, \quad \text{else} \quad \varepsilon^0_{ij} = 0, \quad \text{for case } k, l. \tag{6.50}$$

That is for case b) $k = l = 2 \rightarrow \varepsilon^0_{22} = 1$, for c) $k = 1, l = 2 \rightarrow \varepsilon^0_{12} = 1$, and so on. Unfortunately many FEM packages do not come with an initial strain loading option but recent versions of COMSOL have added this capability. Lastly it should be noted that the boundary conditions for this analysis are periodic conditions on the displacements such that for a cubic unit cell the left and right sides have the same displacement, the top and bottom, and the front and back pairs.

Triangular elements

We first used MATLAB to implement the finite element homogenization technique and benchmarked our results with [1]. Using the PDE toolbox in MATLAB a mesh containing two dimensional triangular elements can be made. The periodic structure consists of a unit square cell containing a 0.4 x 0.6 void. This example was studied by both [1] and [2]. Figure 6.5 contains the geometry and was created and meshed using the PDE toolbox in MATLAB. Next we must review triangular finite elements to form the matrix equations and to apply the unit initial strains for the various cases. It should be noted that in two dimensions only the cases $k = l = 1$, $k = l = 2$ and $k = 1, l = 2$

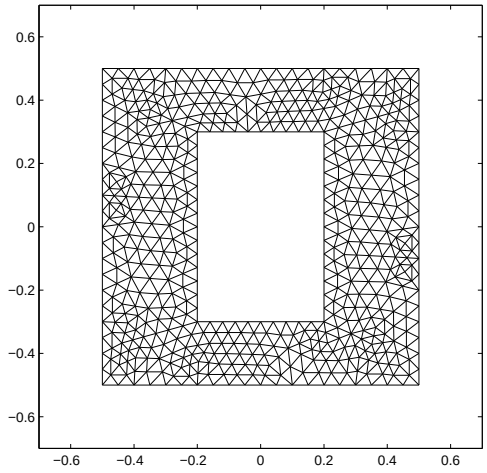

Figure 6.5: Unit cell studied in [1] consists of a unit square containing a 0.4 x 0.6 void, figure was created and meshed using the PDE toolbox in MATLAB

need to be studied. As a reference on finite elements [3] was used for theory as well as codes which were adapted for the homogenization problem. Consider the triangular

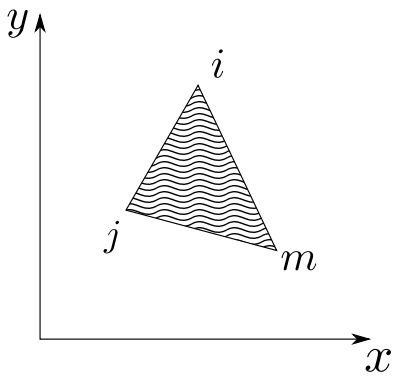

Figure 6.6: Triangular element with nodes i, j, and m, reference [3] used here.

element of figure 6.6 for which node i has coordinates (x_i, y_i). The strain-displacement

matrix for this element is

$$\mathbf{B}^e = \frac{1}{2A}\begin{bmatrix} y_j - y_m & 0 & y_m - y_i & 0 & y_i - y_j & 0 \\ 0 & x_m - x_j & 0 & x_i - x_m & x_j - x_i & \\ x_m - x_j & y_j - y_m & x_i - x_m & y_m - y_i & x_j - x_i & y_i - y_j \end{bmatrix}. \tag{6.51}$$

Next we apply equation (6.46) to find the forces needed on each element to produce a unit initial strain which is then

$$\mathbf{f}^e = A^e \mathbf{B}^{e^T} \mathbf{d}_i, \tag{6.52}$$

where A^e is the area of the element and $\mathbf{d}_i$ is the vector of elastic constants corresponding to the case being evaluated. For instance in two dimensions and considering plane strain problems, that is that the depth of the geometry into the page is relatively large compared to other dimensions, we have

$$\mathbf{C} = \frac{E}{1-\nu^2}\begin{bmatrix} 1 & \nu & 0 \\ \nu & 1 & 0 \\ 0 & 0 & \frac{1-\nu}{2} \end{bmatrix} = \begin{bmatrix} C_{11} & C_{12} & 0 \\ C_{12} & C_{22} & 0 \\ 0 & 0 & C_{66} \end{bmatrix} = \begin{bmatrix} \mathbf{d}_1 & \mathbf{d}_2 & \mathbf{d}_3 \end{bmatrix}, \tag{6.53}$$

where E is the material's Young's modulus and ν the Poisson ratio. The element stiffness is found by

$$\mathbf{k}^e = A^e \mathbf{B}^{e^T} \mathbf{C} \mathbf{B}^e. \tag{6.54}$$

Then the global matrix equation (6.44) can be formed by assembling the forces from equation (6.52) and stiffnesses from equation (6.54). The boundary conditions on the unit cell are periodic and as derived in [1] they can be broken down into two cases. As noted before for the two dimensional problem only cases $(k = l = 1)$, $(k = l = 2)$, and $(k = 1, l = 2)$ need to be solved, for $(k = l = 1)$ and $(k = l = 2)$ the boundary conditions are rollers on the outer edge of the unit cell, that is the displacement normal to the edges is zero. For the case $(k = 1, l = 2)$ the condition is perpendicular rollers, meaning on the boundary displacement parallel to the edge is zero. These conditions can be easily applied to the global equation by setting the corresponding nodal displacements to zero which has the effect of removing rows and columns corresponding to that degree of freedom. After the nodal displacements are found the homogenized properties given

in equation (6.29) are found by summing, for example

$$C_{11}^H = \frac{1}{|Y|}\sum C_{11} - \mathbf{d}_1^T \mathbf{B}^e \mathbf{\Phi}^e, \tag{6.55}$$

where the summation is taken over all the elements.

For the example given by [2, 1] the elastic properties of the material used were $C_{11} = C_{22} = 30$ and $C_{12} = C_{66} = 10$, with these properties the homogenization technique produced the results of table 6.1. Implementing the homogenization theory

Elements	C_{11}^H	C_{12}^H	C_{22}^H	C_{66}^H	Reference
20x20 4-node	13.015	3.241	17.552	2.785	[2]
3rd adapt.	12.844	3.131	17.421	2.668	[2]
436 8-node	12.839	3.139	17.422	2.648	[1]

Table 6.1: Table is directly from [1] for which the unit cell of figure 6.5 was used and compared against the results of [2].

using MATLAB with 3-node triangular elements resulted in table 6.2 for which we see agreement. Note that using lower order elements such as the linear triangular element used here requires more elements than those reported by [1] or [2] as they used higher order quadrilateral elements. Lastly using MATLAB for finite element analysis is quite tedious as FEM packages such as ANSYS and COMSOL have efficient solvers capable of inverting equation (6.44) quickly and have the added benefit of a graphics user interface. Our last example using 16,256 elements required approximately 268 minutes to compute.

Elements	C_{11}^H	C_{12}^H	C_{22}^H	C_{66}^H
242	13.385	3.404	17.810	3.065
1,016	13.035	3.250	17.562	2.794
4,064	12.903	3.177	17.469	2.695
16,256	12.844	3.140	17.425	2.652

Table 6.2: Results based on a MATLAB code using linear triangular elements. Nodal displacement solutions located in figures 6.7, 6.8 and 6.9.

Quadrilateral elements

The limitations of MATLAB previously described are eliminated through the use of ANSYS Mechanical APDL FEM package, which features an optimized solver that can

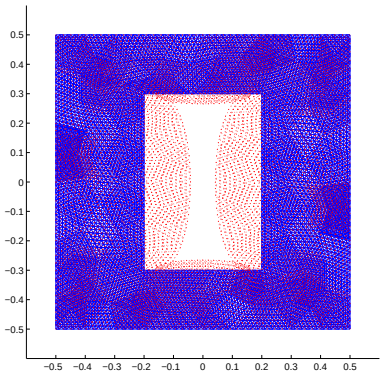

Figure 6.7: Displacement solution for $(k = l = 1)$ corresponding to $\varepsilon^0_{11} = 1$.

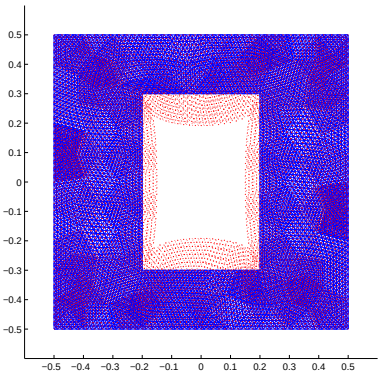

Figure 6.8: Displacement solution for $(k = l = 2)$ corresponding to $\varepsilon^0_{22} = 1$.

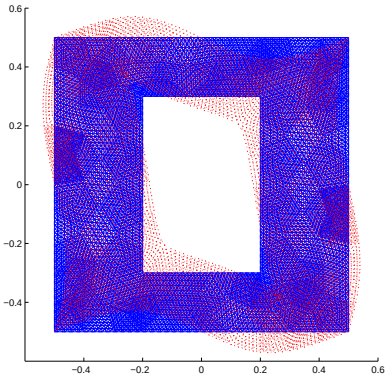

Figure 6.9: Displacement solution for $(k = 1, l = 2)$ corresponding to $\varepsilon^0_{12} = 1$.

implement more complex elements. Unfortunately the version of ANSYS available did not have a built in method of implementing a unit initial strain. The strategy devised was to use ANSYS to construct the geometry and mesh then export the mesh data into a MATLAB code which would compute the nodal forces necessary to implement a unit initial strain found from equation (6.46). The nodal forces are then inserted back into ANSYS in a quick manner by using batch mode. Then solving the system the strains and areas necessary to compute the homogenized properties are exported back into MATLAB following equation (6.55).

In order to find the nodal forces we detail the derivation here using 4-node quadrilateral elements. In the previous section we used triangular elements for which the

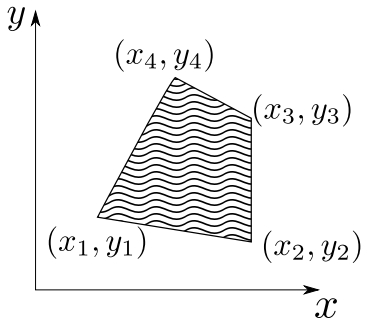

Figure 6.10: Quadrilateral element in terms of the global coordinates (x_i, y_i).

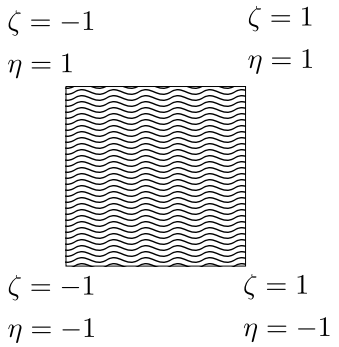

Figure 6.11: Quadrilateral element in terms of the natural coordinates (ζ, η).

strain-displacement matrix can be obtained easily due to the simplicity of the element, here we will have to use the shape functions and natural coordinates. The natural coordinates are used to map an irregular element in global coordinates (x_i, y_i), figure 6.10, to a unit square in (ζ, η) coordinates, figure 6.11, which helps simplify the analysis. The shape functions in natural coordinates are [3]

$$\begin{aligned} N_1 &= \frac{1}{4}(1-\zeta)(1-\eta), \quad N_2 = \frac{1}{4}(1+\zeta)(1-\eta), \\ N_3 &= \frac{1}{4}(1+\zeta)(1+\eta), \quad N_4 = \frac{1}{4}(1-\zeta)(1+\eta). \end{aligned} \tag{6.56}$$

We can find the nodal forces necessary to implement a unit strain by defining

$$\mathbf{B} = \begin{bmatrix} \mathbf{B}_1 & \mathbf{B}_2 & \mathbf{B}_3 & \mathbf{B}_4 \end{bmatrix}, \tag{6.57}$$

where

$$\mathbf{B}_i = \begin{bmatrix} a\frac{\partial N_i}{\partial \zeta} - b\frac{\partial N_i}{\partial \eta} & 0 \\ 0 & c\frac{\partial N_i}{\partial \eta} - d\frac{\partial N_i}{\partial \zeta} \\ c\frac{\partial N_i}{\partial \eta} - d\frac{\partial N_i}{\partial \zeta} & a\frac{\partial N_i}{\partial \zeta} - b\frac{\partial N_i}{\partial \eta} \end{bmatrix} \tag{6.58}$$

, and

$$\begin{aligned} a &= \frac{1}{4}\big(y_1(\zeta-1)+y_2(-1-\zeta)+y_3(1+\zeta)+y_4(1-\zeta)\big),\\ b &= \frac{1}{4}\big(y_1(\eta-1)+y_2(1-\eta)+y_3(1+\eta)+y_4(-1-\eta)\big),\\ c &= \frac{1}{4}\big(x_1(\eta-1)+x_2(1-\eta)+x_3(1+\eta)+x_4(-1-\eta)\big),\\ d &= \frac{1}{4}\big(x_1(\zeta-1)+x_2(-1-\zeta)+x_3(1+\zeta)+x_4(1-\zeta)\big). \end{aligned} \tag{6.59}$$

Following equation (6.47), let

$$\mathbf{d}_i = \mathbf{C}\varepsilon_i^0, \tag{6.60}$$

where for the given case ε_i^0 takes on the values

$$\begin{bmatrix}1\\0\\0\end{bmatrix}, \quad \begin{bmatrix}0\\1\\0\end{bmatrix}, \quad \begin{bmatrix}0\\0\\1\end{bmatrix}. \tag{6.61}$$

Lastly the integral of equation (6.47) is done in the natural coordinates as

$$\mathbf{f}^e = \int_{-1}^{1}\int_{-1}^{1} \mathbf{B}^T\mathbf{d}_i \,\mathrm{d}\,\zeta\,\mathrm{d}\,\eta. \tag{6.62}$$

Following this procedure the nodal force vector required to implement an initial strain for the 4-node quadrilateral element is

$$\mathbf{f}^e = \frac{1}{2}\begin{bmatrix}(y_2-y_4)d_1+(x_4-x_2)d_3\\(x_4-x_2)d_2+(y_2-y_4)d_3\\(y_3-y_1)d_1+(x_1-x_3)d_3\\(x_1-x_3)d_2+(y_3-y_1)d_3\\(y_4-y_2)d_1+(x_2-x_4)d_3\\(x_2-x_4)d_2+(y_4-y_2)d_3\\(y_1-y_3)d_1+(x_3-x_1)d_3\\(x_3-x_1)d_2+(y_1-y_3)d_3\end{bmatrix} = \begin{bmatrix}f_{1x}\\f_{1y}\\f_{2x}\\f_{2y}\\f_{3x}\\f_{3y}\\f_{4x}\\f_{4y}\end{bmatrix}, \tag{6.63}$$

where d_j is the j^{th} element of $\mathbf{d}_i$ from equation (6.60) corresponding to the particular case of initial strain and f_{mx} is the nodal force at node m in the x direction and f_{my} the nodal force at node m in the y direction. It should be noted that equation (6.63) is in terms of the global coordinates.

Elements	C_{11}^H	C_{12}^H	C_{22}^H	C_{66}^H
304	12.941	3.201	17.496	2.732
1,282	12.857	3.149	17.436	2.664
11,889	12.814	3.118	17.402	2.630
107,001	12.801	3.107	17.392	2.620

Table 6.3: Results from ANSYS using the 4-node quadrilateral element.

Hassani example using COMSOL

The last FEM package we turned to was COMSOL which has a built in method of adding desired initial strains. Using the same example as before, figure 6.5, we benchmark our application of the static homogenization for which table 6.4 shows convergence based on the number of elements used. Here we see quicker convergence since we are using 6-node quadratic triangular elements. It should be noted that this method is easily implemented in COMSOL where the homogenization integral, for example equation (6.29), is done within COMSOL and as compared with the MATLAB implementation the longest solution time was on the order of half a minute. This ends the review of static methods that produce the effective elastic moduli of periodic structures. The next chapter focuses on reviewing methods that can perform this homogenization task in a dynamic sense by considering Bloch-Floquet conditions on a unit cell.

Elements	C_{11}^H	C_{12}^H	C_{22}^H	C_{66}^H
70	13.083	3.292	17.603	2.801
500	12.887	3.173	17.459	2.680
4,940	12.819	3.123	17.407	2.633
19,330	12.807	3.112	17.397	2.624
77,328	12.801	3.107	17.392	2.620

Table 6.4: Results from COMSOL using triangular elements.

Chapter 7

Dynamic homogenization

This chapter focuses on the problem of solving dispersion relations which characterizes the relation between the wave vector and frequency dependence, $\omega(\mathbf{k})$, for periodic structures. First the concept of the Brillouin zone is discussed in section 7.1. It is used to describe the range of wave vectors that should be considered when analyzing a medium with periodic structure. In section 7.2 the plane wave expansion method is reviewed for structures made from fluids only. In looking for solid structures that can accommodate Pentamode behavior elastic models are studied. The first being a lattice constructed of masses and springs, where the work in [74] is reviewed in section 7.3. In section 7.4 we review beam theories including Euler-Bernoulli, Rayleigh and Timoshenko. This is done as beams are used as the building blocks of the theories used in sections 7.5, 7.6, and 7.7. The work in section 7.5 uses Euler-Bernoulli beams and has not been seen in the literature. For comparison to more standard procedures, section 7.6 deals with Timoshenko beams and the development of reflection and transmission matrices, here the work of [6] is reviewed. Lastly, section 7.7 reviews the implementation of Bloch-Floquet problems using finite elements, where the work of [75] is reviewed. The motivation of this chapter is to understand the derivation of theories used to create dispersion curves. This will give us a tool to further investigate material properties of periodic media as well as a check on the static properties that the theories of chapter 6 produce.

7.1 The Brillouin zone and k space

In Bloch-Floquet problems we seek dispersion curves which define at what frequencies a medium will allow for wave propagation as a function of the wave vector. As written

by Léon Brillouin in [4] the wave vector, $\mathbf{k}$, can be confined to a k-space defined by the irreducible Brillouin zone such that any solution involving $\mathbf{k}$ outside this zone is repeated via a reflection based on the symmetry of the structure. These zones are found by considering a structure's direct and reciprocal lattice vectors. The direct lattice vectors, defined by $\mathbf{d}_i \; \forall \; i \; \in \; \{1, 2, 3\}$ in three dimensions, define a structure's geometry and class such as cubic or hexagonal. For example the direct lattice vectors of a two dimensional hexagonal lattice are shown in Figure 7.1. The vectors are such that any point defined by $n_1\mathbf{d}_1 + n_2\mathbf{d}_2$ for n_i being an integer is another lattice point. The structure is then found by connecting the lattice points and drawing perpendicular bisecting lines, as done in Figure 7.1. The Brillouin zone is then defined by the

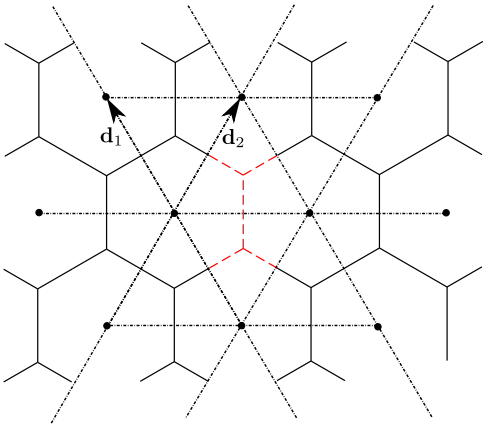

Figure 7.1: Direct lattice space with direct lattice vectors $\mathbf{d}_1$ and $\mathbf{d}_2$. The connection between the lattice points and the structure they define is made by connecting lattice points, shown here with dashed lines, and drawing perpendicular bisecting lines between two lattice points. Also defined here in red dashed lines is a possible choice of a primitive cell to be considered.

reciprocal lattice vectors, $\mathbf{b}_i$, $i \in \{1, 2, 3\}$, which have the property $\mathbf{b}_i \cdot \mathbf{d}_j = \delta_{ij}$ (or $\mathbf{b}_i \cdot \mathbf{d}_j = 2\pi\delta_{ij}$ depending on the formulation), where δ_{ij} is the Kronecker delta function. In two dimensions we can define the matrices

$$\mathbf{D} = \begin{pmatrix} d_{1x} & d_{1y} \\ d_{2x} & d_{2y} \end{pmatrix} \quad \text{and} \quad \mathbf{B} = \begin{pmatrix} b_{1x} & b_{2x} \\ b_{1y} & d_{2y} \end{pmatrix}, \tag{7.1}$$

then

$$\mathbf{B} \cdot \mathbf{D} = \mathbf{I}, \rightarrow \mathbf{B} = \mathbf{D}^{-1}. \tag{7.2}$$

Alternatively if we consider three dimensional problems then the relation between the direct and reciprocal lattice vectors is written as [76]

$$\mathbf{b}_1 = \frac{\mathbf{d}_2 \times \mathbf{d}_3}{\mathbf{d}_1 \cdot (\mathbf{d}_2 \times \mathbf{d}_3)}, \quad \mathbf{b}_2 = \frac{\mathbf{d}_3 \times \mathbf{d}_1}{\mathbf{d}_1 \cdot (\mathbf{d}_2 \times \mathbf{d}_3)}, \quad \mathbf{b}_3 = \frac{\mathbf{d}_1 \times \mathbf{d}_2}{\mathbf{d}_1 \cdot (\mathbf{d}_2 \times \mathbf{d}_3)}. \tag{7.3}$$

A plane wave traveling through the medium will have the form

$$\psi = Ae^{i(\omega t - 2\pi \mathbf{a}\cdot\mathbf{x})}, \tag{7.4}$$

where $\mathbf{x}$ is a position vector and $\mathbf{a}$ defines the direction and wavelength of the propagating wave, such that

$$|\mathbf{a}|^2 = a_1^2 + a_2^2 = \frac{1}{\lambda^2}, \tag{7.5}$$

where λ is the wavelength. Since the medium may be discontinuous we let the position vector be defined only at lattice points $\mathbf{x} = n_1\mathbf{d}_1 + n_2\mathbf{d}_2$. We then simplify equation (7.4) by taking

$$2\pi\mathbf{a}\cdot\mathbf{x} = 2\pi\mathbf{a}\cdot(n_1\mathbf{d}_1 + n_2\mathbf{d}_2) = n_1k_1 + n_2k_2, \tag{7.6}$$

where $k_1 = 2\pi\mathbf{a}\cdot\mathbf{d}_1$ and $k_2 = 2\pi\mathbf{a}\cdot\mathbf{d}_2$. Equation (7.4) may then be rewritten as

$$\psi = Ae^{i(\omega t - k_1n_1 - k_2n_2)}. \tag{7.7}$$

The importance of Brillouin zones comes into play since we can replace the components of the wave vector, $\mathbf{k} = \begin{bmatrix} k_i & k_j \end{bmatrix}^T$, by

$$k_i^{'} = k_i + 2\pi m_i, \quad \forall \quad m_i = \text{integers}, \tag{7.8}$$

without changing the plane wave in equation (7.7). This is because

$$\begin{aligned} e^{i(-k_1n_1 - k_2n_2)} &= e^{i(-(k_1+2\pi m_1)n_1 - (k_2+2\pi m_2)n_2)} = e^{i(-k_1n_1-k_2n_2)}e^{i(-2\pi m_1n_1)}e^{i(-2\pi m_2n_2)} \\ &= e^{i(-k_1n_1-k_2n_2)}, \end{aligned} \tag{7.9}$$

since m_i and n_i are both integers. The change to $k_i^{'}$ corresponds to the wave vector changing to

$$\mathbf{a}^{'} = \mathbf{a} + m_1\mathbf{b}_1 + m_2\mathbf{b}_2, \tag{7.10}$$

which is seen from equation (7.6) and the property $\mathbf{d}_i \cdot \mathbf{b}_j = \delta_{ij}$. Looking back at equation (7.4) we see that the direction of the wave and magnitude of the wave length,

equation (7.5), now depends on the integers m_1 and m_2 that define $\mathbf{a}'$. Any wave vector of the form $\mathbf{a}' = \mathbf{a}+m_1\mathbf{b}_2+m_2\mathbf{b}_2$ corresponds to the same plane wave traveling through the medium, figure 7.2 details this ambiguity pictorially. Brillouin then constructed

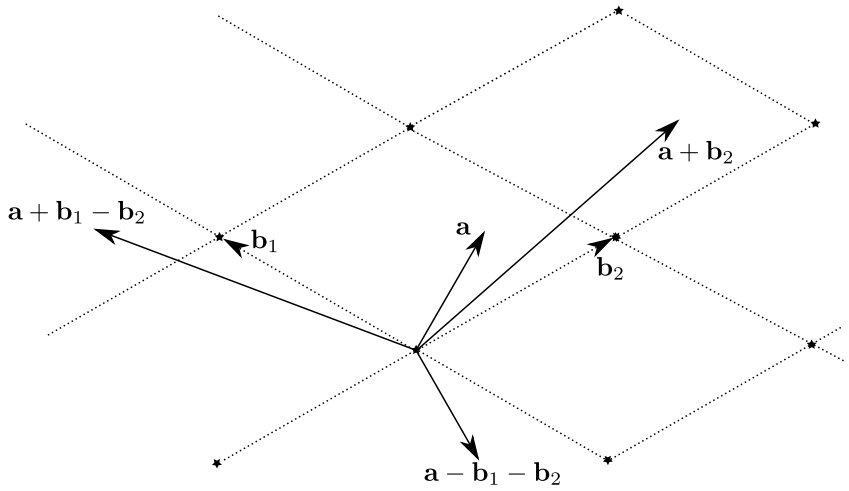

Figure 7.2: As stated by Brillouin, [4], this example shows the ambiguity of the wave vector, $\mathbf{a}$, in reciprocal lattice space created due to the integers m_1 and m_2 in equation (7.9). Any choice of the wave vector $\mathbf{a}' = \mathbf{a} + m_1\mathbf{b}_1 + m_2\mathbf{b}_2$ corresponds to the same plane wave traveling through the medium.

rules for choosing the area for which the wave vector must be confined, they include that the area be independent of the basis coordinates, allow for wave propagation in all directions, and requires that the longest wave length must be accommodated for [4]. This means that a complete period for every possible direction of propagation is contained within the zone. To construct a zone that accomplishes these requirements Brillouin placed the origin in the center of the zone and confined the space by drawing perpendicular bisectors of the lines joining each point in the reciprocal lattice space, as shown in figure 7.3. If the lattice structure contains symmetries the zones can be further restricted to an irreducible Brillouin zone, this lets us consider a smaller k-space that contains all solutions of the wave and whose perimeter is known as the k-path. In two dimensions there are several examples including those in figure 7.4. It is important to note that in figure 7.4 the definition of the reciprocal lattice vectors is $\mathbf{d}_i \cdot \mathbf{b}_j = 2\pi\delta_{ij}$, this eliminates having to multiply the reciprocal space by a factor of 2π as Brillouin did [5].

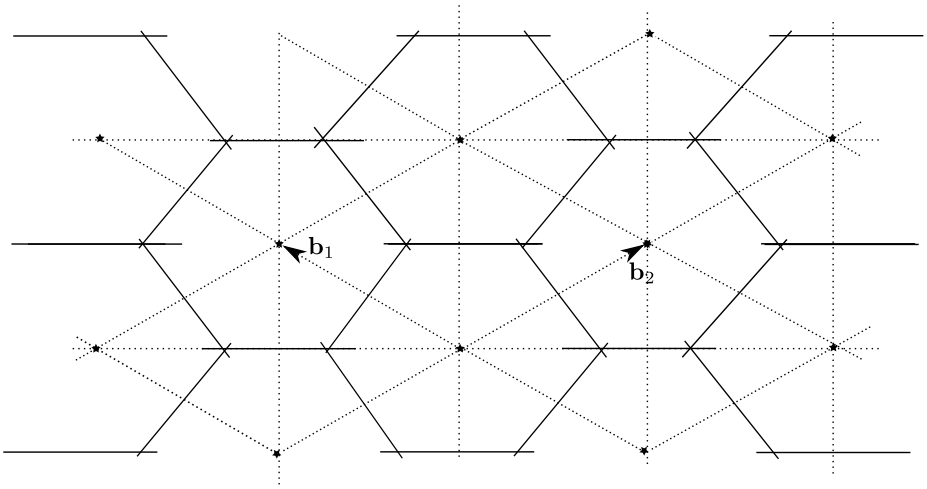

Figure 7.3: Like constructing a structure in direct lattice space as done in figure 7.1. The Brillouin zones are constructed much the same way only now done in reciprocal lattice space where perpendicular bisecting lines are drawn to construct the zones. Brillouin zones shown by enclosed regions of solid lines.

7.2 Plane wave expansion for acoustic media

Here we use the plane wave expansion method to formulate the Bloch Floquet problem using acoustic media. Although we do not use this method later in the thesis for development of metamaterial devices it is an important first step in learning how to implement Bloch-Floquet conditions. We start with a simple analysis of one dimensional structures in section 7.2.1 and then continue on to structures with two or more dimensions in section 7.2.2. As expected the problem boils down to solving a generalized eigenvalue problem. Simple examples are considered however numerical solutions are left to be conducted by the reader.

7.2.1 One dimension

We start with the simplest example of Bloch-Floquet problems in in one dimension using the plane wave expansion method. The goal of this section is to understand the dynamic properties of one dimensional metamaterials made from at least two differing fluids, characterized by a density and bulk modulus, with periodic structure. In using the plane wave expansion method geometric details are dealt with by a Fourier expansion. Consider figure 7.5 and let α be the material properties, either the bulk modulus K_i

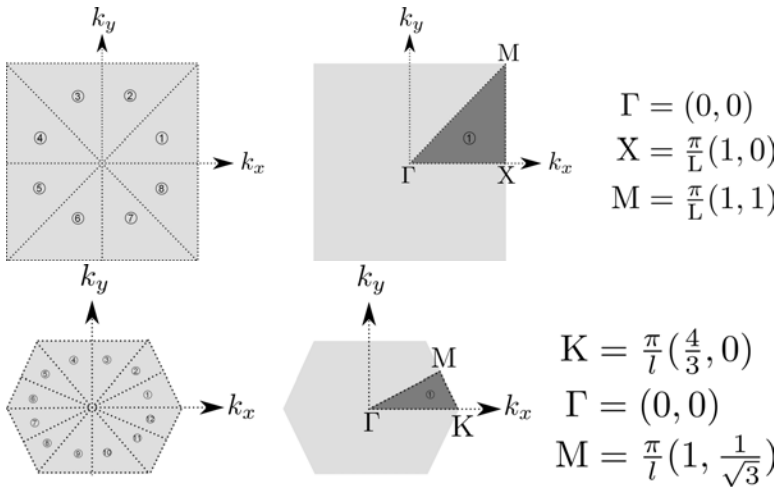

Figure 7.4: Irreducible Brillouin zones for square and hexagonal lattice structures, additional zones can be found in [5]. Here the definition of the reciprocal lattice vectors is $\mathbf{d}_i \cdot \mathbf{b}_j = 2\pi\delta_{ij}$, this eliminates having to multiply the reciprocal space by a factor of 2π as Brillouin did.

or the density ρ_i. Due to the periodic nature of the system, $\alpha(x) = \alpha(x+L)$, where L is the period of the structure. We can then write the bulk modulus and density as a Fourier series for which

$$\begin{aligned} K(x) &= \sum_{n=-\infty}^{\infty} K_n e^{ig_n x}, \quad K_n = \frac{1}{L}\int_0^L K(x)e^{-ig_n x}\,\mathrm{d}\,x, \\ \rho(x) &= \sum_{n=-\infty}^{\infty} \rho_n e^{ig_n x}, \quad \rho_n = \frac{1}{L}\int_0^L \rho(x)e^{-ig_n x}\,\mathrm{d}\,x, \end{aligned} \tag{7.11}$$

where

$$g_n = \frac{2n\pi}{L}. \tag{7.12}$$

In the example for figure 7.5 we find

$$\begin{aligned} K_n &= \frac{1}{L}\Big[\int_0^{x_1} K_1 e^{-ig_n x}\,\mathrm{d}\,x + \int_{x_1}^{x_2} K_2 e^{-ig_n x}\,\mathrm{d}\,x\Big] \\ &= \frac{1}{L}\Big[\frac{K_1}{ig_n}(1-e^{-ig_n x_1}) + \frac{K_2}{ig_n}(e^{-ig_n x_1} - e^{-ig_n x_2})\Big], \\ \rho_n &= \frac{1}{L}\Big[\int_0^{x_1} \rho_1 e^{-ig_n x}\,\mathrm{d}\,x + \int_{x_1}^{x_2} \rho_2 e^{-ig_n x}\,\mathrm{d}\,x\Big] \\ &= \frac{1}{L}\Big[\frac{\rho_1}{ig_n}(1-e^{-ig_n x_1}) + \frac{\rho_2}{ig_n}(e^{-ig_n x_1} - e^{-ig_n x_2})\Big]. \end{aligned} \tag{7.13}$$

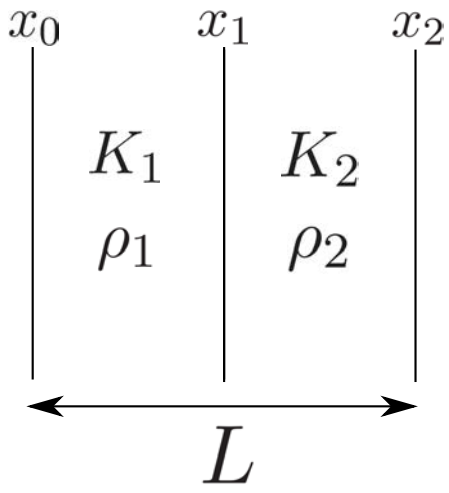

Figure 7.5: Example of one dimensional, periodic structure to be considered.

Next the acoustic equation is reduced to an eigenvalue problem through the application of Bloch-Floquet conditions. The acoustic equation in one dimension is

$$\nabla \cdot \sigma = \rho \ddot{\mathbf{u}}, \quad \rightarrow \quad \frac{\mathrm{d}}{\mathrm{d}\,x}(K(x)\frac{\mathrm{d}\,u}{\mathrm{d}\,x}) + \rho(x)\omega^2 u = 0, \tag{7.14}$$

instead of writing it in one line we can split it up into two equations where

$$\sigma = K(x)\frac{\mathrm{d}\,u}{\mathrm{d}\,x}, \qquad \frac{\mathrm{d}}{\mathrm{d}\,x}\sigma = -\rho(x)\omega^2 u. \tag{7.15}$$

Then we write the displacement, $u(x)$, and the stress, $\sigma(x)$, as

$$u(x) = U(x)e^{ikx}, \qquad \sigma(x) = S(x)e^{ikx}, \tag{7.16}$$

where $U(x)$ and $S(x)$ are periodic functions with the form

$$U(x) = \sum_{n=-\infty}^{\infty} U_n e^{ig_n x}, \qquad S(x) = \sum_{n=-\infty}^{\infty} S_n e^{ig_n x}. \tag{7.17}$$

Combining equations (7.11), $(7.15)_1$, (7.16), and (7.17) we find

$$\sum_n S_n e^{ig_n x} = \sum_m K_m e^{ig_m x} \sum_l i(k_l + k) U_l e^{ig_l x}. \tag{7.18}$$

Comparing coefficients in the exponential terms we find $n = l + m$, which means

$$S_n = \sum_l i(k + k_l) K_{n-l} U_l. \tag{7.19}$$

Then by combining equations (7.11), $(7.15)_2$, (7.16), and (7.17) we find

$$\sum_n i(g_n + k) S_n e^{ig_n x} = -\omega^2 \sum_m \rho_m e^{ig_m x} \sum_l U_l e^{ig_l x}, \tag{7.20}$$

which leads to

$$i(g_n + k)S_n = -\omega^2 \sum_l \rho_{n-l} U_l. \tag{7.21}$$

Combining equations (7.19) and (7.21) yields

$$\sum_l \left[(k + g_l) K_{n-l} (k + g_n) - \rho_{n-l} \omega^2 \right] U_l = 0, \tag{7.22}$$

which is a general eigenvalue problem and can be solved for the example shown in figure 7.5 by using equations $(7.13)_1$ and $(7.13)_2$. Next we reformulate equation (7.22) into a matrix equation by taking a discrete summation in equation (7.22) for the indices l and n over $\{-N, -N+1, \ldots, N-1, N\}$. The matrix equation is then

$$[\mathbf{DAD} - \omega^2 \mathbf{B}]\mathbf{U} = 0, \tag{7.23}$$

where $\mathbf{D}$ is a diagonal matrix with entries $\{D_1, D_2, \ldots, D_{2N+1}\}$, and $\mathbf{A}$, $\mathbf{D}$, $\mathbf{B}$ are all of size $(2N+1)$ by $(2N+1)$. We then arrange $\mathbf{U}$ as follows

$$\mathbf{U} = \begin{bmatrix} U_{-N} \\ U_{-N+1} \\ \vdots \\ U_{N-1} \\ U_N \end{bmatrix}, \tag{7.24}$$

the structure of the first term of equation (7.23) is then

$$\mathbf{DAD} = \begin{bmatrix} D_1 A_{11} D_1 & D_1 A_{12} D_2 & \ldots & D_1 A_{1(2N+1)} D_{2N+1} \\ D_2 A_{21} D_1 & \ldots & \ldots & D_2 A_{2(2N+1)} D_{2N+1} \\ \vdots & \vdots & \vdots & \vdots \\ D_{2N+1} A_{(2N+1)1} & \ldots & \ldots & D_{(2N+1)} A_{(2N+1)(2N+1)} D_{2N+1} \end{bmatrix}. \tag{7.25}$$

Comparison of equations (7.25) and (7.22) gives

$$\mathbf{D} = \mathrm{diag}\{D_1 = k + g_{-N},\ D_2 = k + g_{-N+1},\ \ldots,\ D_{2N} = k + g_{N-1},\ D_{2N+1} = k + g_N\}, \tag{7.26}$$

and the form of $\mathbf{A}$ is then

$$\mathbf{A} = \begin{bmatrix} K_0 & K_{-1} & K_{-2} & \dots & K_{-2N+1} & K_{-2N} \\ K_1 & K_0 & K_{-1} & \dots & K_{-2N+2} & K_{-2N+1} \\ K_2 & K_1 & K_0 & \dots & K_{-2N+3} & K_{-2N+2} \\ \vdots & \vdots & \vdots & \vdots & \vdots & \vdots \\ K_{2N-1} & K_{2N-2} & K_{2N-3} & \dots & K_0 & K_{-1} \\ K_{2N} & K_{2N-1} & K_{2N-2} & \dots & K_1 & K_0 \end{bmatrix}. \tag{7.27}$$

Since we are using complex Fourier expansions we see that $\mathbf{A}$ is Hermitian from equation (7.27), because of this we can make use of the toeplitz MATLAB command. We can then solve equation (7.23) for k and ω pairs yielding the dispersion relations of the metamaterial, from there important characteristics can be found such as band gaps and material group velocities. We leave the discussion there and continue the development further.

7.2.2 Two or more dimensions

Again we must expand the material parameters by a Fourier series, for which we have the periodicity

$$f(\mathbf{x}) = f(\mathbf{x} + \mathbf{X}), \tag{7.28}$$

where $\mathbf{x}$ is a vector describing a spatial coordinate and $\mathbf{X}$ is a vector describing the dimensions of a single periodic cell. The Fourier series expansion in multiple dimensions is written as

$$f(\mathbf{x}) = \sum_{\mathbf{k}} f_{\mathbf{k}} e^{i\mathbf{k}\cdot\mathbf{x}}, \quad f_{\mathbf{k}} = \frac{1}{V} \int_V f(\mathbf{x}) e^{-i\mathbf{k}\cdot\mathbf{x}} \, \mathrm{d}\, V, \tag{7.29}$$

where V is either the volume of the unit cell in three dimensions or the area of the unit cell in two dimensions [77]. Also note that this definition requires that $\mathbf{k} \cdot \mathbf{X} = 2\pi n$ for integer n, this is from the periodicity condition (7.28). In multiple dimensions the displacement is written in the form

$$u = U(x) e^{i\mathbf{k}\cdot\mathbf{x}}, \quad U(x) = \sum_{\mathbf{g}} U_{\mathbf{g}} e^{i\mathbf{g}\cdot\mathbf{x}}, \tag{7.30}$$

where as an example in two dimensions, $\mathbf{g}$ may be written as

$$\mathbf{g} = g_1\mathbf{e}_1 + g_2\mathbf{e}_2 = \frac{2n\pi}{a}\mathbf{e}_1 + \frac{2m\pi}{b}\mathbf{e}_2. \tag{7.31}$$

where a is the dimension of the unit cell in the 1 direction and b is the dimension of the unit cell in the 2 direction. This means the summation in equation (7.30) is really a double summation over m and n. The strain, $\varepsilon = \nabla u \leftrightarrow \varepsilon_i = \frac{\partial u}{\partial x_i}$, is then

$$\varepsilon = \sum_{\mathbf{g}} i(\mathbf{g}+\mathbf{k})U_{\mathbf{g}}e^{i(\mathbf{g}\cdot\mathbf{x}+\mathbf{k}\cdot\mathbf{x})}. \tag{7.32}$$

The relation for the stress is $\sigma = \mu\cdot\varepsilon \leftrightarrow \sigma_i = \mu_{ij}\varepsilon_j$, where

$$\mu = \sum_{\mathbf{g}'} \mu_{\mathbf{g}'}e^{i\mathbf{g}'\cdot\mathbf{x}}, \tag{7.33}$$

the stress is then

$$\sigma = \sum_{\mathbf{g}'}\sum_{\mathbf{g}} U_{\mathbf{g}}\mu_{\mathbf{g}'}\cdot i(\mathbf{g}+\mathbf{k})e^{i(\mathbf{g}'+\mathbf{g})\cdot\mathbf{x}}e^{i\mathbf{k}\cdot\mathbf{x}}. \tag{7.34}$$

We rewrite the stress in order to simplify the summation where we let

$$\sigma = \sum_{\mathbf{g}''}\sigma_{\mathbf{g}''}e^{i\mathbf{g}''\cdot\mathbf{x}}e^{i\mathbf{k}\cdot\mathbf{x}}, \quad \sigma_{\mathbf{g}''} = \sum_{\mathbf{g}}\mu_{\mathbf{g}''-\mathbf{g}}\cdot i(\mathbf{g}+\mathbf{k})U_{\mathbf{g}}. \tag{7.35}$$

Next we use the equilibrium equation, $\nabla\cdot\sigma = \rho\ddot{u}$, which gives

$$\sum_{\mathbf{g}} i(\mathbf{k}+\mathbf{g})\cdot\sigma_{\mathbf{g}}e^{i(\mathbf{g}+\mathbf{k})\cdot\mathbf{x}} = -\omega^2\sum_{\mathbf{g}'}\sum_{\mathbf{g}''}\rho_{\mathbf{g}'}e^{i\mathbf{g}'\cdot\mathbf{x}}U_{\mathbf{g}''}e^{i(\mathbf{g}''+\mathbf{k})\cdot\mathbf{x}}, \tag{7.36}$$

analysis of the exponential factors of (7.36) has $\mathbf{g} = \mathbf{g}' + \mathbf{g}''$, which allows us to write

$$i(\mathbf{k}+\mathbf{g})\cdot\sigma_{\mathbf{g}} = -\omega^2\sum_{\mathbf{g}''}\rho_{\mathbf{g}-\mathbf{g}''}U_{\mathbf{g}''}. \tag{7.37}$$

Combining equations (7.35) and (7.37) we find the generalized eigenvalue problem for which

$$\sum_{\mathbf{g}'}\left[(\mathbf{k}+\mathbf{g})\cdot\mu_{\mathbf{g}-\mathbf{g}'}\cdot(\mathbf{k}+\mathbf{g}') - \omega^2\rho_{\mathbf{g}-\mathbf{g}'}\right]U_{\mathbf{g}'} = 0. \tag{7.38}$$

Again solving equation (7.38) yields the dispersion relations for $\omega(\mathbf{k})$. We consider the two dimensional example shown in figure 7.6. First we analyze the terms of μ, and

consider an acoustic medium by allowing the shear modulus to go to zero. The normal stresses in the medium are $\sigma_i = \mu_{ij}\varepsilon_j$ which can be written in matrix notation with

$$\begin{bmatrix}\sigma_1\\ \sigma_2\end{bmatrix} = K(x,y)\begin{bmatrix}1 & 0\\ 0 & 1\end{bmatrix}\begin{bmatrix}\varepsilon_1\\ \varepsilon_2\end{bmatrix}. \tag{7.39}$$

Analyzing equation (7.38) we will take the following definitions

$$\mathbf{k} = k_1\mathbf{e}_1 + k_2\mathbf{e}_2, \quad \mathbf{g} = \frac{2m\pi}{a}\mathbf{e}_1 + \frac{2n\pi}{b}\mathbf{e}_2, \quad \mathbf{g}' = \frac{2r\pi}{a}\mathbf{e}_1 + \frac{2s\pi}{b}\mathbf{e}_2, \tag{7.40}$$

and rewrite it as

$$\begin{aligned}\sum_r\sum_s\Bigg[K_{m-r,n-s}\Big[(k_1+g_m^{(x)})(k_1+g_r^{(x)}) + (k_2+g_n^{(y)})(k_2+g_s^{(y)})\Big]\\ - \omega^2\rho_{m-r,n-s}\Bigg]U_{r,s} = 0,\end{aligned} \tag{7.41}$$

with

$$g_r^{(x)} = \frac{2\pi r}{a}, \quad g_m^{(x)} = \frac{2\pi m}{a}, \quad g_s^{(y)} = \frac{2\pi s}{b}, \quad g_n^{(y)} = \frac{2\pi n}{b}. \tag{7.42}$$

We then find $K_{i,j}$ and $\rho_{i.j}$ for equation (7.41) by considering the example shown in figure 7.6. The Fourier coefficients of the bulk modulus are

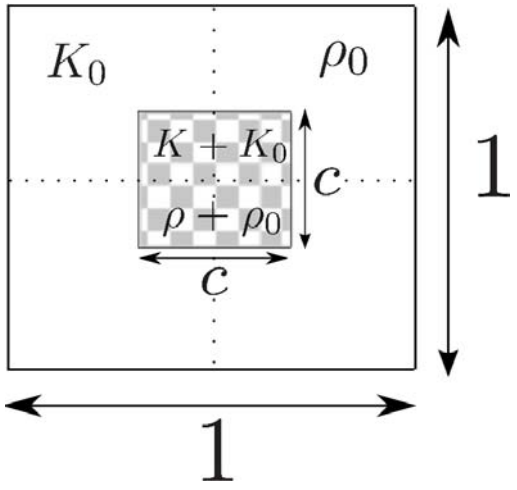

Figure 7.6: Example of two dimensional, unit cell for a periodic structure consisting of centered inclusion of material with constant bulk modulus, $K+K_0$, and density, $\rho+\rho_0$, surrounded by material with bulk modulus, K_0, and density, ρ_0.

$$K_{i,j} = \int_{-1/2}^{1/2}\int_{-1/2}^{1/2} K_0 e^{-i(g_i x + g_j y)}\,\mathrm{d}\,x\,\mathrm{d}\,y + \int_{-c/2}^{c/2}\int_{-c/2}^{c/2} K e^{-i(g_i x + g_j y)}\,\mathrm{d}\,x\,\mathrm{d}\,y, \tag{7.43}$$

we then find

$$
\begin{aligned}
K_{0,0} &= K_0 + c^2 K, \\
K_{i,0} &= \frac{2cK \sin \frac{g_i c}{2}}{g_i}, \quad \text{for} \quad \{i\} \neq 0 \\
K_{0,j} &= \frac{2cK \sin \frac{g_j c}{2}}{g_j}, \quad \text{for} \quad \{j\} \neq 0 \\
K_{i,j} &= \frac{4K \sin \frac{cg_i}{2} \sin \frac{cg_j}{2}}{g_i g_j} \quad \text{for} \quad \{i,j\} \neq 0.
\end{aligned}
$$

Similarly

$$
\begin{aligned}
\rho_{0,0} &= \rho_0 + c^2 \rho, \\
\rho_{i,0} &= \frac{2c\rho \sin \frac{g_i c}{2}}{g_i}, \quad \text{for} \quad \{i\} \neq 0 \\
\rho_{0,j} &= \frac{2c\rho \sin \frac{g_j c}{2}}{g_j}, \quad \text{for} \quad \{j\} \neq 0 \\
\rho_{i,j} &= \frac{4\rho \sin \frac{cg_i}{2} \sin \frac{cg_j}{2}}{g_i g_j} \quad \text{for} \quad \{i,j\} \neq 0.
\end{aligned}
$$

This approach allows for the study of metamaterials created by fluids only. We leave the discussion there with numerical examples being left for the reader to solve. In the next section we consider materials described by networks of masses and springs.

7.3 Mass spring model

Here we consider an analysis which only uses masses and the longitudinal stiffness of the elements of the primitive cell similar to the study conducted in [74]. We consider structures that have only three associated struts connected to a center junction. This is the property of hexagonal foam structures, studied in section 6.1. We will later consider adding more complexity to the problem but here this is done as a learning experience of developing models and applying Bloch-Floquet conditions. The equation of motion of a spring is

$$
m \frac{\mathrm{d}^2 x}{\mathrm{d}\, t^2} = -\mu_j x, \tag{7.44}
$$

where x is the amount of stretch in the spring and m is an attached mass. Applying this equilibrium equation to the reference configuration of the unit cell in figure 7.7 we find the wave equation at the point $\mathbf{a}_0$ will be

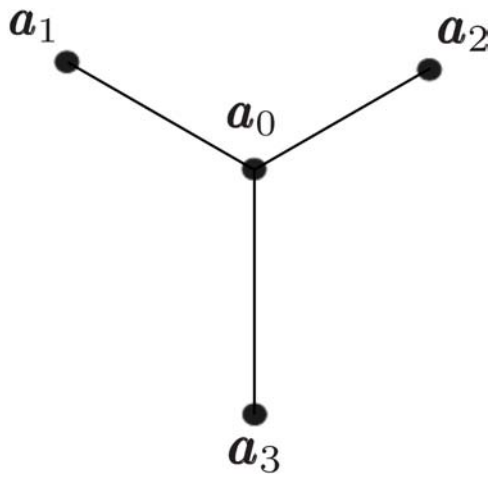

Figure 7.7: Periodic cell geometry to be considered.

$$\sum_{j=1}^{3} \mu_j \mathbf{A}_j(\mathbf{u}_0 - \mathbf{u}_j) = \omega^2 m_0 \mathbf{u}_0, \tag{7.45}$$

where

$$\mathbf{A}_j = (\mathbf{a}_0 - \mathbf{a}_j)(\mathbf{a}_0 - \mathbf{a}_j)^T \quad \forall \quad j = 1, 2, 3, \tag{7.46}$$

and μ_j is the stiffness of segment $[\mathbf{a}_0, \mathbf{a}_j]$. The Floquet periodic conditions are

$$\mathbf{u}_j = e^{i\mathbf{k}\cdot\mathbf{g}_j}\mathbf{u}_1, \tag{7.47}$$

where $\mathbf{g}_j = \mathbf{a}_j - \mathbf{a}_1$. Using equation (7.47) in (7.45) leads to

$$\sum_{j=1}^{3} \mu_j \mathbf{A}_j \mathbf{u}_0 - \sum_{j=1}^{3} e^{i\mathbf{k}\cdot\mathbf{g}_j} \mu_j \mathbf{A}_j \mathbf{u}_1 = \omega^2 m_0 \mathbf{u}_0. \tag{7.48}$$

The wave equation at point $\mathbf{a}_1 = \mathbf{a}_0^{'}$ is

$$\sum_{j=1}^{3} \mu_j^{'} \mathbf{B}_j(\mathbf{u_0}^{'} - \mathbf{u}_j^{'}) = \omega^2 m_1 \mathbf{u}_0^{'}, \tag{7.49}$$

where $\mathbf{B}_j = (\mathbf{a}_0^{'} - \mathbf{a}_j^{'})(\mathbf{a}_0^{'} - \mathbf{a}_j^{'})^T$ and $\mu_j^{'}$ is the stiffness of segment $[\mathbf{a}_0^{'}, \mathbf{a}_j^{'}]$. It is clear that $\mu_j = \mu_j^{'}$. Comparing elements of $\mathbf{B}_j$ and $\mathbf{A}_j$ we write the positions

$$\begin{gathered} \mathbf{a}_0 = \begin{bmatrix} 0 \\ 0 \end{bmatrix} = \mathbf{a}_1^{'}, \quad \mathbf{a}_1 = L \begin{bmatrix} \cos\theta \\ \sin\theta \end{bmatrix} = \mathbf{a}_0^{'}, \quad \mathbf{a}_2 = L \begin{bmatrix} -\cos\theta \\ \sin\theta \end{bmatrix}, \\ \mathbf{a}_3 = L \begin{bmatrix} 0 \\ -1 \end{bmatrix}, \quad \mathbf{a}_2^{'} = L \begin{bmatrix} 2\cos\theta \\ 0 \end{bmatrix}, \quad \mathbf{a}_3^{'} = L \begin{bmatrix} \cos\theta \\ 1 + \sin\theta \end{bmatrix}, \end{gathered} \tag{7.50}$$

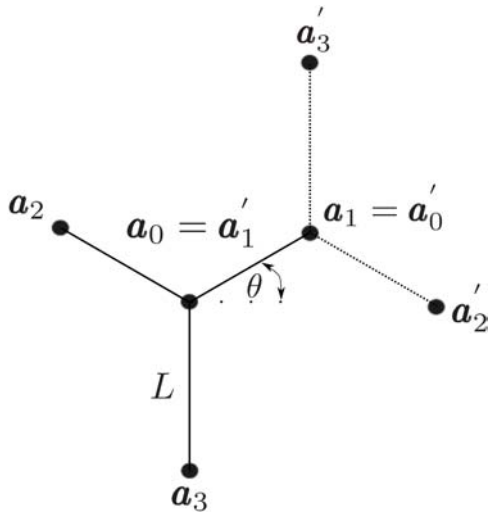

Figure 7.8: Periodic cell geometry to be considered.

and find

$$\mathbf{A}_j = \mathbf{B}_j. \tag{7.51}$$

We can then rewrite equation (7.49) as

$$\sum_{j=1}^{3} \mu_j \mathbf{A}_j (\mathbf{u}_1 - \mathbf{u}_j^{'}) = \omega^2 m_1 \mathbf{u}_1, \tag{7.52}$$

Floquet periodic conditions are now

$$\mathbf{u}_j^{'} = e^{i\mathbf{k}\cdot\mathbf{g}_j^{'}} \mathbf{u}_0, \quad \mathbf{g}_j^{'} = \mathbf{a}_j^{'} - \mathbf{a}_0, \tag{7.53}$$

comparing $\mathbf{g}_j^{'}$ and $\mathbf{g}_j$ we find

$$\mathbf{g}_j = -\mathbf{g}_j^{'}, \tag{7.54}$$

equation (7.53) can then be written as

$$\mathbf{u}_j^{'} = e^{-i\mathbf{k}\cdot\mathbf{g}_j} \mathbf{u}_0, \tag{7.55}$$

then the wave equation at point $\mathbf{a}_1$ is

$$-\sum_{j=1}^{3} e^{-i\mathbf{k}\cdot\mathbf{g}_j} \mu_j \mathbf{A}_j \mathbf{u}_0 + \sum_{j=1}^{3} \mu_j \mathbf{A}_j \mathbf{u}_1 = \omega^2 m_1 \mathbf{u}_1. \tag{7.56}$$

Combining equations (7.48) and (7.56) we find

$$\begin{pmatrix} \sum\limits_{j=1}^{3} \mu_j \mathbf{A}_j & -\sum\limits_{j=1}^{3} e^{i\mathbf{k}\cdot\mathbf{g}_j} \mu_j \mathbf{A}_j \\ -\sum\limits_{j=1}^{3} e^{-i\mathbf{k}\cdot\mathbf{g}_j} \mu_j \mathbf{A}_j & \sum\limits_{j=1}^{3} \mu_j \mathbf{A}_j \end{pmatrix} \begin{pmatrix} \mathbf{u}_0 \\ \mathbf{u}_1 \end{pmatrix} = \omega^2 \begin{pmatrix} m_0 \mathbf{u}_0 \\ m_1 \mathbf{u}_1 \end{pmatrix}. \tag{7.57}$$

Which can be simplified into a more standard form with

$$\left(\mathbf{K} - \omega^2 \mathbf{M}\right) \begin{pmatrix} \mathbf{u}_0 \\ \mathbf{u}_1 \end{pmatrix} = 0, \quad \mathbf{M} = \mathrm{diag}(m_0, m_1), \tag{7.58}$$

where

$$\mathbf{K} = \sum_{j=1}^{3} \mathbf{K}_j, \quad \mathbf{K}_j = \mu_j \mathbf{v}_j \mathbf{v}_j^{+} \mathrm{diag}(\mathbf{A}_j, \mathbf{A}_j), \quad \mathbf{v}_j = \begin{pmatrix} 1 \\ -\exp(-i\mathbf{k} \cdot \mathbf{g}_j) \end{pmatrix}. \tag{7.59}$$

Note that $\mathbf{K}_j = \mathbf{K}_j^{+} \Rightarrow \mathbf{K} = \mathbf{K}^{+}$, where superscript $^{+}$ denotes Hermitian transpose. Again numeric examples are left for the reader and we wish to add the physics of bending into the system and to do so we start by reviewing beam theories next.

7.4 Review of beam theories

In this section we review the derivation for several different types of beam theories using [78] as reference. Longitudinal motion is reviewed in section 7.4.1 and transverse bending is covered in section 7.4.2. Beam theories covered include Euler-Bernoulli, Rayleigh and Timoshenko. The Euler-Bernoulli model is used in section 7.5, while Timoshenko theory is used later in section 7.6 in application to transmission and reflection matrices.

7.4.1 Longitudinal motion

We consider elastic rods with cross-sectional area $A(x)$, density $\rho(x)$, Young's modulus $E(x)$, and applied distributed axial forces $p(x,t)$. An equilibrium of the axial forces on a differential beam element is shown in figure 7.9. In this theory we neglect Poisson's

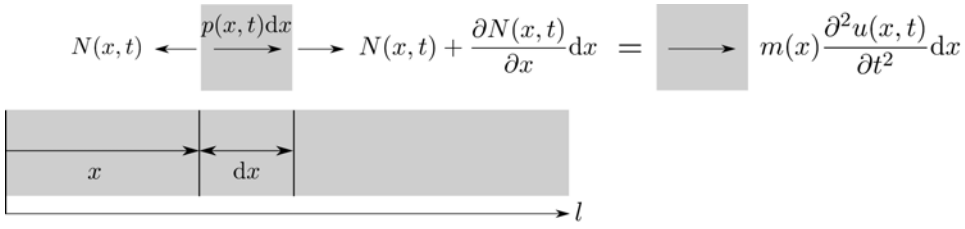

Figure 7.9: Equilibrium of the balance of axial forces on a differential beam element. $N(x,t)$ is an axial force and $p(x,t)$ is a distributed axial load.

effect and understand the beam as a one-dimensional continuous medium where the

axial stress is written as

$$\sigma(x,t) = E(x)\varepsilon(x,t) = E(x)\frac{\partial u(x,t)}{\partial x}, \tag{7.60}$$

such that the axial force is

$$N(x,t) = A(x)\sigma(x,t) = E(x)A(x)\frac{\partial u(x,t)}{\partial x}. \tag{7.61}$$

Force balance on a differential element as depicted in figure 7.9 yields

$$p(x,t)\mathrm{d}x + \frac{\partial N(x,t)}{\partial x}\mathrm{d}x = m(x)\frac{\partial^2 u(x,t)}{\partial t^2}\mathrm{d}x, \tag{7.62}$$

rearranging terms and using equation (7.61) we find

$$m(x)\frac{\partial^2 u(x,t)}{\partial t^2} - \frac{\partial}{\partial x}\big(E(x)A(x)\frac{\partial u(x,t)}{\partial x}\big) = p(x,t). \tag{7.63}$$

This is the full equation of longitudinal motion in a beam.

7.4.2 Transverse motion in beams

We start with Kirchhoff's assumptions which are: 1) normals remain straight, 2) normals remain unstretched, and 3) normals remain normal. Under these assumptions

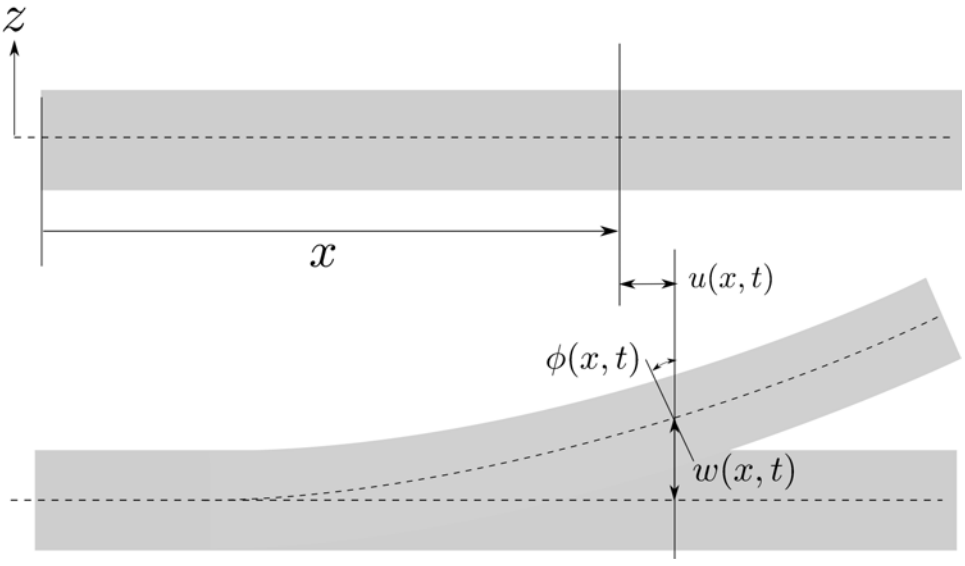

Figure 7.10: Motion of a beam under Kirchoff's three assumptions, where $u(x,t)$ is the axial displacement and $w(x,t)$ is the transverse displacement as measured from the neutral ($z = 0$) surface.

the displacements are taken as

$$\begin{aligned} u_x(x,z,t) &= u(x,t) - z\phi(x,t), \\ u_z(x,z,t) &= w(x,t), \end{aligned} \tag{7.64}$$

where $\phi(x,t)$ is the rotation of the cross section of the beam, $u(x,t)$ and $w(x,t)$ are the axial and transverse displacements respectively as measured from the neutral axis, $z=0$ surface. The strain $\varepsilon_x = \frac{\partial u_x}{\partial x}$ is then

$$\varepsilon_x(x,z,t) = \frac{\partial u(x,t)}{\partial x} - z\kappa(x,t), \quad \kappa(x,t) = \frac{\partial \phi(x,t)}{\partial x}, \tag{7.65}$$

where $\kappa(x,t)$ is the curvature of the neutral axis of the beam. Also note that the shear strain is

$$\varepsilon_{xz}(x,z,t) = \frac{1}{2}\big(\frac{\partial u_x(x,z,t)}{\partial z} + \frac{\partial u_z(x,z,t)}{\partial x}\big) = \frac{1}{2}\big(\frac{\partial w(x,t)}{\partial x} - \phi(x,t)\big). \tag{7.66}$$

Then to find the axial force in the beam, $N(x,t)$ we have

$$N(x,t) = \int_A E(x)\varepsilon_x(x,z,t)\mathrm{d}A = E(x)\frac{\partial u(x,t)}{\partial(x)}A(x) - E(x)\kappa(x,t)\int_A z\,\mathrm{d}\,A, \tag{7.67}$$

since z is measured from the x-axis which is located at the neutral axis or area centroid of the beam we find $\int_A z\,\mathrm{d}\,A = 0$. We then have

$$N(x,t) = E(x)A(x)\frac{\partial u(x,t)}{\partial x}. \tag{7.68}$$

The resultant moment in the beam is

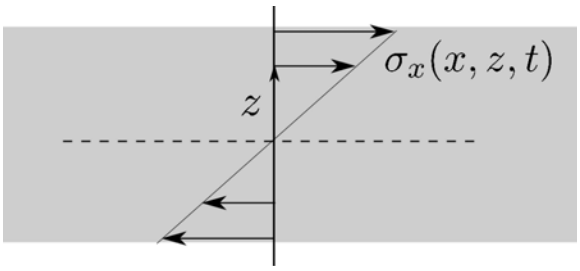

Figure 7.11: Axial stress distribution within the beam.

$$M(x,t) = \int_A \sigma_x(x,z,t)z\,\mathrm{d}\,A, \quad \sigma_x(x,z,t) = E(x)\varepsilon_x(x,z,t), \tag{7.69}$$

inserting the result of equation (7.65) we have

$$\begin{aligned} M(x,t) &= E(x)\frac{\partial u(x,t)}{\partial x}\int_A z\,\mathrm{d}\,A - E(x)\frac{\partial \phi(x,t)}{\partial x}\int_A z^2\,\mathrm{d}\,A, \\ &= -E(x)I(x)\frac{\partial \phi(x,t)}{\partial x} \quad I(x) = \int_A z^2\,\mathrm{d}\,A. \end{aligned} \tag{7.70}$$

where I is the moment of inertia. Lastly the resultant shear force on a section of the beam is

$$Q(x,t) = \int_A \sigma_{xz}(x,z,t)\,\mathrm{d}\,A. \tag{7.71}$$

We next consider the equilibrium of the moments and transverse forces on a differential element of the beam, as shown in figure 7.12, which yields

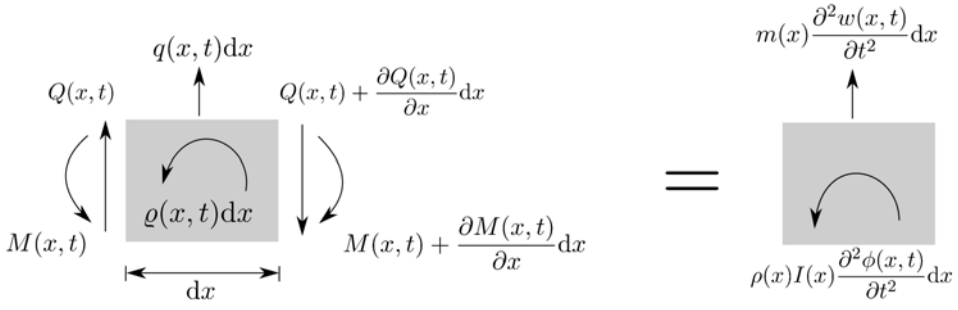

Figure 7.12: Equilibrium balance of transverse forces and moments on a differential beam element. $\varrho(x,t)$ is an applied moment, $q(x,t)$ is an applied transverse force.

$$\begin{aligned} q(x,t) + \frac{\partial Q(x,t)}{\partial x} &= m(x)\frac{\partial^2 w(x,t)}{\partial t^2}, \\ \varrho(x,t) - \frac{\partial M(x,t)}{\partial x} + Q(x,t) + \frac{1}{2}\frac{\partial Q(x,t)}{\partial x}\,\mathrm{d}\,x &= \rho(x)I(x)\frac{\partial^2 \phi(x,t)}{\partial t^2}. \end{aligned} \tag{7.72}$$

The first equation of (7.72) is the balance of transverse forces the second is the balance of moments. Considering linear theory the term $\frac{1}{2}\frac{\partial Q(x,t)}{\partial x}\,\mathrm{d}\,x$ is dropped from the balance of moments. We then have as our equilibrium equations

$$\begin{aligned} q(x,t) + \frac{\partial Q(x,t)}{\partial x} &= m(x)\frac{\partial^2 w(x,t)}{\partial t^2}, \\ Q(x,t) &= \frac{\partial M(x,t)}{\partial x} + \rho(x)I(x)\frac{\partial^2 \phi(x,t)}{\partial t^2} - \varrho(x,t). \end{aligned} \tag{7.73}$$

Combining the two balances and using $M(x,t) = -E(x)I(x)\frac{\partial \phi(x,t)}{\partial x}$, we find

$$\begin{aligned} q(x,t) - \frac{\partial \varrho(x,t)}{\partial x} - \frac{\partial^2}{\partial x^2}\big(E(x)I(x)\frac{\partial \phi(x,t)}{\partial x}\big) \\ = m(x)\frac{\partial^2 w(x,t)}{\partial t^2} - \frac{\partial}{\partial x}\big(\rho(x)I(x)\frac{\partial^2 \phi(x,t)}{\partial t^2}\big), \end{aligned} \tag{7.74}$$

which is the full equation of bending motion for a beam.

Euler-Bernoulli theory

In this theory small angle approximation is used such that

$$\phi(x,t) \approx \frac{\partial w(x,t)}{\partial x}, \tag{7.75}$$

note that this approximation causes the shear strain ε_{xz} as defined in (7.66) to be zero, which means shear deformation is neglected. Additionally the effect of rotary inertia is ignored, i.e. $I_\rho = \rho(x)I(x)$ is assumed to be zero. Applying these approximations to equation (7.74) yields

$$m(x)\frac{\partial^2 w(x,t)}{\partial t^2} + \frac{\partial^2}{\partial x^2}\big(E(x)I(x)\frac{\partial^2 w(x,t)}{\partial x^2}\big) = q(x,t) - \frac{\partial \varrho(x,t)}{\partial x}. \tag{7.76}$$

Rayleigh theory

Similar to the Euler theory the small angle approximation is used, $\phi(x,t) = \frac{\partial w(x,t)}{\partial x}$, and we keep the effects of rotary inertia. Applying this to equation (7.74) gives

$$\begin{aligned} m(x)\frac{\partial^2 w(x,t)}{\partial t^2} - \frac{\partial}{\partial x}\big(\rho(x)I(x)\frac{\partial^3 w(x,t)}{\partial x \partial t^2}\big) \\ + \frac{\partial^2}{\partial x^2}\big(E(x)I(x)\frac{\partial^2 w(x,t)}{\partial x^2}\big) = q(x,t) - \frac{\partial \varrho(x,t)}{\partial x}. \end{aligned} \tag{7.77}$$

7.4.3 Timoshenko theory

Unlike Euler and Rayleigh theories the effect of shear deformation is included in Timoshenko beam theory. We start with the stress strain relation for the shear

$$\sigma_{xz}(x,z,t) = 2\mu(x)\varepsilon_{xz}(x,z,t), \tag{7.78}$$

where $\mu(x)$ is the shear modulus. In order to reduce the theory to one dimension we consider the shear angle $\gamma(x,t)$ such that

$$\gamma(x,t) = \frac{1}{\mathcal{K}A(x)}\int_A 2\varepsilon_{xz}(x,z,t)\,\mathrm{d}\,A, \tag{7.79}$$

where $\mathcal{K}$ is a shape factor, dependent on the geometry of the cross-section. The resultant shear force can then be found as

$$Q(x,t) = \int_A \sigma_{xz}(x,z,t)\,\mathrm{d}\,A = \mu(x)A(x)\mathcal{K}\gamma(x,t). \tag{7.80}$$

Now we have two angles one caused by the bending stress, $\phi(x,t)$ and one caused by the shear stress $\gamma(x,t)$, let the total angle be defined by

$$\psi(x,t) = \phi(x,t) + \gamma(x,t) \approx \frac{\partial w(x,t)}{\partial x}, \tag{7.81}$$

where again we have used the small angle approximation for the total angle, $\psi(x,t)$. Combining equations (7.70) and (7.81) we find the resultant moment,

$$M(x,t) = -E(x)I(x)\frac{\partial}{\partial x}\big(\frac{\partial w(x,t)}{\partial x} - \gamma(x,t)\big). \tag{7.82}$$

Lastly, we combine equations (7.80) and (7.82) and use equation (7.73) to find

$$\begin{gathered} m(x)\frac{\partial^2 w(x,t)}{\partial t^2} - \frac{\partial}{\partial x}\left[\mathcal{K}A(x)\mu(x)\big(\frac{\partial w(x,t)}{\partial x} - \phi(x,t)\big)\right] = q(x,t), \\ \rho(x)I(x)\frac{\partial^2 \phi(x,t)}{\partial t^2} - \mathcal{K}A(x)\mu(x)\big(\frac{\partial w(x,t)}{\partial x} - \phi(x,t)\big) - \\ \frac{\partial}{\partial x}\big(E(x)I(x)\frac{\partial \phi(x,t)}{\partial x} = \varrho(x,t). \end{gathered} \tag{7.83}$$

Reference [79] derives the shape factor $\mathcal{K}$ for various cross-sections and for a rectangular section

$$\mathcal{K}_{\text{rect}} = \frac{10(1+\nu)}{12+11\nu}, \tag{7.84}$$

where ν is Poisson's ratio. With the beam theories reviewed we can now use these models in the application of two dimensional periodic media.

7.5 An Euler-Bernoulli model with inertial mass junctions

The method considered here involves a Bloch-Floquet formulation using Euler-Bernoulli beams that has not been seen in the literature. We consider elements as depicted in figure 7.13 where we denote connecting rods of points $\mathbf{a}_i$ and $\mathbf{a}_j$ by $[\mathbf{a}_i, \mathbf{a}_j]$ with length, $l_{ij} = |\mathbf{a}_i - \mathbf{a}_j|$ and direction $\mathbf{e}_{ij} = l_{ij}^{-1}(\mathbf{a}_i - \mathbf{a}_j)$ where the density, stiffness and beam coefficients are ρ_{ij}, μ_{ij}, l_{ij}. We have also added a beam moment, I_i, at point $\mathbf{a}_i$. Each node has a displacement vector defined by

$$\mathbf{u}_i = \begin{bmatrix} u_1 \\ u_2 \\ \theta \end{bmatrix}_i, \tag{7.85}$$

describing the displacement in the 1 and 2 directions as well as the rotation about the 3 direction.

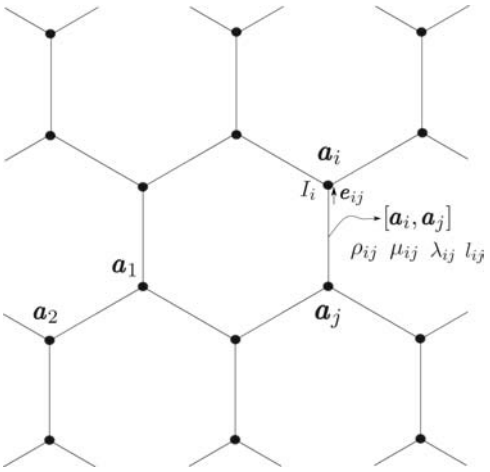

Figure 7.13: Periodic cell geometry to be considered.

7.5.1 Longitudinal motion

Displacement of rod $[\mathbf{a}_i, \mathbf{a}_j]$ is taken as a function of x, which is the one dimensional linear parameter that takes values of 0 to l_{ij} such that $u_{ij} = u_{ij}(x,t)$. The longitudinal wave motion of the rod, first derived in equation (7.63), is described by

$$\rho_{ij}(x)\frac{\partial^2 u_{ij}(x,t)}{\partial t^2} - \frac{\partial}{\partial x}\mu^l_{ij}(x)\frac{\partial u_{ij}(x,t)}{\partial x} = p_{ij}(x,t), \tag{7.86}$$

where $p_{ij}(x,t)$ is a distributed axial load, with units force per unit length, and $\mu^l_{ij}(x)$ is the axial stiffness usually taken as $\mu^l_{ij}(x) = E(x)A(x)$, where $E(x)$ is the Young's Modulus and $A(x)$ is the cross-sectional area. Taking time dependence $e^{i\omega t}$, such that $u_{ij}(x,t) = u_{ij}(x)e^{i\omega t}$, keeping the stiffness constant along each rod, $\mu^l_{ij}(x) = \mu^l_{ij}$, and taking $p_{ij}(x,t) = 0$ we have

$$\mu^l_{ij}\frac{\partial^2 u_{ij}(x)}{\partial x^2} = -\omega^2\rho_{ij}u_{ij}(x), \tag{7.87}$$

with boundary conditions

$$u_{ij}(0) = \mathbf{e}_{ij}\cdot\mathbf{u}_i, \quad u_{ij}(l_{ij}) = \mathbf{e}_{ij}\cdot\mathbf{u}_j. \tag{7.88}$$

The solution of equation (7.87) is then

$$u_{ij}(x) = \mathbf{e}_{ij}\cdot\mathbf{u}_i\cos(s_{ij}\omega x) + \frac{\mathbf{e}_{ij}\cdot\mathbf{u}_j - \mathbf{e}_{ij}\cdot\mathbf{u}_i\cos(s_{ij}\omega l_{ij})}{\sin(s_{ij}\omega l_{ij})}\sin(s_{ij}\omega x), \tag{7.89}$$

where $s_{ij} = \sqrt{\frac{\rho_{ij}}{\mu^l_{ij}}}$. The force due to longitudinal motion at point $\mathbf{a}_i$ is found from equation (7.61) with

$$\mathbf{f}_{ij\ long} = \mu^l_{ij}\frac{\partial u_{ij}(0)}{\partial x}\mathbf{e}_{ij} = \frac{\mathbf{A}_{ij}\mathbf{u}_j - \mathbf{A}_{ij}\mathbf{u}_i\cos(s_{ij}\omega l_{ij})}{\sin(s_{ij}\omega l_{ij})}\mu^l_{ij}s_{ij}\omega, \tag{7.90}$$

where $\mathbf{A}_{ij} = \mathbf{e}_{ij}\mathbf{e}^T_{ij}$.

7.5.2 Transverse motion

The equation describing the transverse displacement of Euler-Bernoulli beams was derived in equation (7.76). Here the transverse displacement equation is

$$\rho_{ij}(x)\frac{\partial^2 w_{ij}(x,t)}{\partial t^2} + \frac{\partial^2}{\partial x^2}\mu^b_{ij}(x)\frac{\partial^2}{\partial x^2}w_{ij}(x,t) = q_{ij}(x,t) - \frac{\partial \beta_{ij}}{\partial x}, \tag{7.91}$$

where $w_{ij}(x)$ is the transverse displacement of rod $[\mathbf{a}_i, \mathbf{a}_j]$, $q_{ij}(x,t)$ are the distributed transverse forces, β_{ij} are the body couples and $\mu^b_{ij}(x)$ is the bending stiffness usually taken as $\mu^b_{ij}(x) = E(x)I(x)$. Simplifying (7.91) by taking zero loading conditions, taking material properties as uniform in the rod and using time dependence $e^{i\omega t}$ we attain

$$\mu^b_{ij}\frac{\partial^4 w_{ij}(x)}{\partial x^4} = \rho_{ij}\omega^2 w_{ij}(x), \tag{7.92}$$

with boundary conditions

$$\begin{aligned} &w_{ij}(0) = \mathbf{e}^\perp_{ij}\cdot\mathbf{u}_i, \quad w_{ij}(l_{ij}) = \mathbf{e}^\perp_{ij}\cdot\mathbf{u}_j, \\ &w'_{ij}(0) = \mathbf{e}_3\cdot\mathbf{u}_i = \theta_i, \quad w'_{ij}(l_{ij}) = \mathbf{e}_3\cdot\mathbf{u}_j = \theta_j, \end{aligned} \tag{7.93}$$

where $\mathbf{e}^\perp_{ij} = \mathbf{e}_3 \times \mathbf{e}_{ij}$. The force at point $\mathbf{a}_i$ due to bending is then

$$\mathbf{f}_{ij\ bend} = -\mu^b_{ij}\frac{\partial^3 w_{ij}(x)}{\partial x^3}\mathbf{e}^\perp_{ij} + \mu^b_{ij}\frac{\partial^2 w_{ij}(x)}{\partial x^2}\mathbf{e}_3, \tag{7.94}$$

where the first term arises from the transverse shear force and the second from the bending moment generated in the beam. The solution of equation (7.92), describing flexural motion, is found by writing it in the form

$$\frac{\partial^4 w_{ij}(x)}{\partial x^4} - \gamma^4_{ij}w_{ij}(x) = 0, \quad x \in [0, l_{ij}], \tag{7.95}$$

where we set $\gamma^4 = \gamma^4_{ij} = \frac{\rho_{ij}}{\mu^b_{ij}}\omega^2$ for simplicity. The general solution to equation (7.95) is

$$w_{ij}(x) = c_1 e^{-\gamma x} + c_2 e^{\gamma x} + c_3\sin\gamma x + c_4\cos\gamma x. \tag{7.96}$$

Applying boundary conditions from equation (7.93) we find the transverse displacement and subsequent derivatives used to be

$$\begin{aligned} w_{ij}(x) = \frac{1}{2(1-cc_h)}\Big\{ &\big[(c-c_h)(\cos\gamma x-\cosh\gamma x)+(s+s_h)(\sin\gamma x-\sinh\gamma x)\big]w_{ij}(l_{ij}) \\ &+\frac{1}{\gamma}\big[(s_h-s)(\cos\gamma x-\cosh\gamma x)+(c-c_h)(\sin\gamma x-\sinh\gamma x)\big]w_{ij}^{'}(l) \\ &+\big[(1-cc_h+ss_h)\cos\gamma x+(1-cc_h-ss_h)\cosh\gamma x+(cs_h+sc_h)(\sinh\gamma x-\sin\gamma x)\big]w_{ij}(0) \\ &+\frac{1}{\gamma}\big[(sc_h-cs_h)(\cos\gamma x-\cosh\gamma x)+(1-cc_h-ss_h)\sin\gamma x+(1-cc_h+ss_h)\sinh\gamma x\big]w_{ij}^{'}(0)\Big\}, \end{aligned} \tag{7.97}$$

$$\begin{aligned} w_{ij}^{'}(x) = \frac{\gamma}{2(1-cc_h)}\Big\{ &\big[(c-c_h)(-\sin\gamma x-\sinh\gamma x)+(s+s_h)(\cos\gamma x-\cosh\gamma x)\big]w_{ij}(l_{ij}) \\ &+\frac{1}{\gamma}\big[(s_h-s)(-\sin\gamma x-\sinh\gamma x)+(c-c_h)(\cos\gamma x-\cosh\gamma x)\big]w_{ij}^{'}(l) \\ &+\big[-(1-cc_h+ss_h)\sin\gamma x+(1-cc_h-ss_h)\sinh\gamma x+(cs_h+sc_h)(\cosh\gamma x-\cos\gamma x)\big]w_{ij}(0) \\ &+\frac{1}{\gamma}\big[(sc_h-cs_h)(-\sin\gamma x-\sinh\gamma x)+(1-cc_h-ss_h)\cos\gamma x+(1-cc_h+ss_h)\cosh\gamma x\big]w_{ij}^{'}(0)\Big\}, \end{aligned} \tag{7.98}$$

$$\begin{aligned} w_{ij}^{''}(x) = \frac{\gamma^2}{2(1-cc_h)}\Big\{ &\big[(c-c_h)(-\cos\gamma x-\cosh\gamma x)+(s+s_h)(-\sin\gamma x-\sinh\gamma x)\big]w_{ij}(l_{ij}) \\ &+\frac{1}{\gamma}\big[(s_h-s)(-\cos\gamma x-\cosh\gamma x)+(c-c_h)(-\sin\gamma x-\sinh\gamma x)\big]w_{ij}^{'}(l) \\ &+\big[-(1-cc_h+ss_h)\cos\gamma x+(1-cc_h-ss_h)\cosh\gamma x+(cs_h+sc_h)(\sinh\gamma x+\sin\gamma x)\big]w_{ij}(0) \\ &+\frac{1}{\gamma}\big[(sc_h-cs_h)(-\cos\gamma x-\cosh\gamma x)-(1-cc_h-ss_h)\sin\gamma x+(1-cc_h+ss_h)\sinh\gamma x\big]w_{ij}^{'}(0)\Big\}, \end{aligned} \tag{7.99}$$

$$\begin{aligned} w_{ij}^{'''}(x) = \frac{\gamma^3}{2(1-cc_h)}\Big\{ &\big[(c-c_h)(\sin\gamma x-\sinh\gamma x)+(s+s_h)(-\cos\gamma x-\cosh\gamma x)\big]w_{ij}(l_{ij}) \\ &+\frac{1}{\gamma}\big[(s_h-s)(\sin\gamma x-\sinh\gamma x)+(c-c_h)(-\cos\gamma x-\cosh\gamma x)\big]w_{ij}^{'}(l) \\ &+\big[(1-cc_h+ss_h)\sin\gamma x+(1-cc_h-ss_h)\sinh\gamma x+(cs_h+sc_h)(\cosh\gamma x+\cos\gamma x)\big]w_{ij}(0) \\ &+\frac{1}{\gamma}\big[(sc_h-cs_h)(\sin\gamma x-\sinh\gamma x)-(1-cc_h-ss_h)\cos\gamma x+(1-cc_h+ss_h)\cosh\gamma x\big]w_{ij}^{'}(0)\Big\}, \end{aligned} \tag{7.100}$$

where $c=\cos\gamma l$, $s=\sin\gamma l$, $c_h=\cosh\gamma l$, $s_h=\sinh\gamma l$. The forces in equation (7.94) can be found by simplifying the above into matrix form with

$$\begin{bmatrix} w^{'''}(0) \\ -w^{''}(0) \\ -w^{'''}(l) \\ w^{''}(l) \end{bmatrix} = \frac{1}{1-cc_h}\begin{bmatrix} \gamma^3(cs_h+sc_h) & \gamma^2 ss_h & -\gamma^3(s+s_h) & \gamma^2(c_h-c) \\ \gamma^2 ss_h & \gamma(sc_h-cs_h) & \gamma^2(c-c_h) & \gamma(s_h-s) \\ -\gamma^3(s+s_h) & \gamma^2(c-c_h) & \gamma^3(cs_h+sc_h) & -\gamma^2 ss_h \\ \gamma^2(c_h-c) & \gamma(s_h-s) & -\gamma^3 ss_h & \gamma(sc_h-cs_h) \end{bmatrix}\begin{bmatrix} w(0) \\ w^{'}(0) \\ w(l) \\ w^{'}(l) \end{bmatrix}, \tag{7.101}$$

which is simplified further by

$$\begin{bmatrix} w'''(0) \\ -w''(0) \\ -w'''(l) \\ w''(l) \end{bmatrix} = \begin{bmatrix} \mathbf{K}_1 & \mathbf{K_2} \\ \mathbf{K}_2^T & \mathbf{K}_3 \end{bmatrix} \begin{bmatrix} \mathbf{e}_{ij}^{\perp} \cdot \mathbf{u}_i \\ \mathbf{e}_3 \cdot \mathbf{u}_i \\ \mathbf{e}_{ij}^{\perp} \cdot \mathbf{u}_j \\ \mathbf{e}_3 \cdot \mathbf{u}_j \end{bmatrix}. \tag{7.102}$$

Note that $\mathbf{K}_3$ has the property

$$\mathbf{K}_3 = \begin{pmatrix} 1 & 0 \\ 0 & -1 \end{pmatrix} \mathbf{K}_1 \begin{pmatrix} 1 & 0 \\ 0 & -1 \end{pmatrix}, \tag{7.103}$$

where the relation is that $\mathbf{K}_1$ and $\mathbf{K}_3$ are the same except for a minus sign in the off diagonal terms.

7.5.3 Application of Bloch-Floquet periodic conditions

As we have found repeatedly in previous sections the usual form of Bloch Floquet problems is solved by an eigenvalue problem in the form

$$\mathbf{Hu} = \omega^2 \mathbf{Mu} \quad \rightarrow \quad \det(\mathbf{H} - \omega^2 \mathbf{M}) = 0. \tag{7.104}$$

This is derived by noting the equilibrium equation of point $\mathbf{a}_i$ is

$$\sum_{j \in \mathcal{N}_i} \mathbf{f}_{ij} = -\omega^2 \mathbf{M}_i \mathbf{u}_i, \tag{7.105}$$

where $\mathcal{N}_i$ are the points connected with $\mathbf{a}_i$ and the mass matrix has the form

$$\mathbf{M}_i = \begin{bmatrix} m_i & 0 & 0 \\ 0 & m_i & 0 \\ 0 & 0 & I_i \end{bmatrix}, \tag{7.106}$$

where m_i is the mass located at point $\mathbf{a}_i$ and I_i is the beam moment remembering the displacement has the form $\mathbf{u}_i = \begin{bmatrix} u_1, & u_2, & \theta \end{bmatrix}_i^T$. The force at point $\mathbf{a}_i$ is found from summing equations (7.90) and (7.94) for which we have

$$\mathbf{f}_{ij} = \mu_{ij}^l \frac{\partial u_{ij}(0)}{\partial x} \mathbf{e}_{ij} - \mu_{ij}^b \frac{\partial^3 w_{ij}(0)}{\partial x^3} \mathbf{e}_{ij}^{\perp} + \mu_{ij}^b \frac{\partial^2 w_{ij}(0)}{\partial x^2} \mathbf{e}_3. \tag{7.107}$$

In terms of $\mathbf{u}_i$ and $\mathbf{u}_j$ we find

$$\begin{aligned}\mathbf{f}_{ij} &= \frac{\mathbf{A}_{ij}\mathbf{u}_j - \mathbf{A}_{ij}\mathbf{u}_i\cos(s_{ij}\omega l_{ij})}{\sin(s_{ij}\omega l_{ij})}\mu^l_{ij}s_{ij}\omega \\ &- \frac{\mu^b_{ij}}{1-cc_h}\big[\gamma^3(cs_h+sc_h)\mathbf{e}^\perp_{ij}\cdot\mathbf{u}_i + \gamma^2 ss_h\mathbf{e}_3\cdot\mathbf{u}_i - \gamma^3(s+s_h)\mathbf{e}^\perp_{ij}\cdot\mathbf{u}_j + \gamma^2(c_h-c)\mathbf{e}_3\cdot\mathbf{u}_j\big]\mathbf{e}^\perp_{ij} \\ &+ \frac{\mu^b_{ij}}{1-cc_h}\big[-\gamma^2 ss_h\mathbf{e}^\perp_{ij}\cdot\mathbf{u}_i - \gamma(sc_h-cs_h)\mathbf{e}_3\cdot\mathbf{u}_i - \gamma^2(c-c_h)\mathbf{e}^\perp_{ij}\cdot\mathbf{u}_j - \gamma(s_h-s)\mathbf{e}_3\cdot\mathbf{u}_j\big]\mathbf{e}_3\end{aligned} \tag{7.108}$$

Grouping terms involving $\mathbf{u}_i$ and $\mathbf{u}_j$ and taking

$$\mathbf{A}_{ij} = \mathbf{e}_{ij}\mathbf{e}^T_{ij}, \quad \mathbf{A}^\perp_{ij} = \mathbf{e}^\perp_{ij}\mathbf{e}^{\perp^T}_{ij}, \quad \mathbf{A}^{\perp 3}_{ij} = \mathbf{e}^\perp_{ij}\mathbf{e}^T_3, \quad \mathbf{A}^{3\perp}_{ij} = \mathbf{e}_3\mathbf{e}^{\perp^T}_{ij}, \quad \mathbf{A}_3 = \mathbf{e}_3\mathbf{e}^T_3, \tag{7.109}$$

the force is then

$$\begin{aligned}\mathbf{f}_{ij} &= \bigg[\frac{\mathbf{A}_{ij}}{\sin(s_{ij}\omega l_{ij})}\mu^l_{ij}s_{ij}\omega + \\ &\frac{\mu^b_{ij}}{1-cc_h}\big(\gamma^3(s+s_h)\mathbf{A}^\perp_{ij} + \gamma^2(c-c_h)(\mathbf{A}^{\perp 3}_{ij} - \mathbf{A}^{3\perp}_{ij}) - \gamma(s_h-s)\mathbf{A}_3\big)\bigg]\mathbf{u}_j \\ &- \bigg[\mathbf{A}_{ij}\frac{\cos(s_{ij}\omega l_{ij})}{\sin(s_{ij}\omega l_{ij})}\mu^l_{ij}s_{ij}\omega + \\ &\frac{\mu^b_{ij}}{1-cc_h}\bigg(\gamma^3(cs_h+sc_h)\mathbf{A}^\perp_{ij} + \gamma^2 ss_h(\mathbf{A}^{\perp 3}_{ij} + \mathbf{A}^{3\perp}_{ij}) + \gamma(sc_h-cs_h)\mathbf{A}_3\bigg)\bigg]\mathbf{u}_i, \\ &= \mathbf{P}^{(2)}_{ij}\mathbf{u}_j - \mathbf{P}^{(1)}_{ij}\mathbf{u}_i,\end{aligned} \tag{7.110}$$

where $\mathbf{P}^{(n)}_{ij}\ \forall\ n = 1,2,3$ as

$$\begin{aligned}\mathbf{P}^{(1)}_{ij} &= \tilde{\mu}_{ij}\hat{s}_{ij}\cot(\hat{s}_{ij})\mathbf{A}_{ij} + \mu^b_{ij}\big(\mathbf{e}^\perp_{ij},\mathbf{e}_3\big)\mathbf{K}_1\big(\mathbf{e}^\perp_{ij},\mathbf{e}_3\big)^T, \\ \mathbf{P}^{(2)}_{ij} &= \tilde{\mu}_{ij}\hat{s}_{ij}\csc(\hat{s}_{ij})\mathbf{A}_{ij} - \mu^b_{ij}\big(\mathbf{e}^\perp_{ij},\mathbf{e}_3\big)\mathbf{K}_2\big(\mathbf{e}^\perp_{ij},\mathbf{e}_3\big)^T, \\ \mathbf{P}^{(3)}_{ij} &= \tilde{\mu}_{ij}\hat{s}_{ij}\cot(\hat{s}_{ij})\mathbf{A}_{ij} + \mu^b_{ij}\big(\mathbf{e}^\perp_{ij},\mathbf{e}_3\big)\mathbf{K}_3\big(\mathbf{e}^\perp_{ij},\mathbf{e}_3\big)^T.\end{aligned} \tag{7.111}$$

We defined $\mathbf{P}^{(3)}_{ij}$ for simplification later and take

$$\hat{s}_{ij} = s_{ij}l_{ij}\omega, \quad \text{and} \quad \tilde{\mu}_{ij} = \mu^l_{ij}/l_{ij}. \tag{7.112}$$

7.5.4 Hexagonal lattice

Next we apply the Floquet periodic conditions on the displacements by considering the unit cell located in figure 7.14. As seen there are two points in the unit cell, $\mathbf{a}_1$ and $\mathbf{a}_2$ each having three connecting links. The Floquet periodic conditions are then

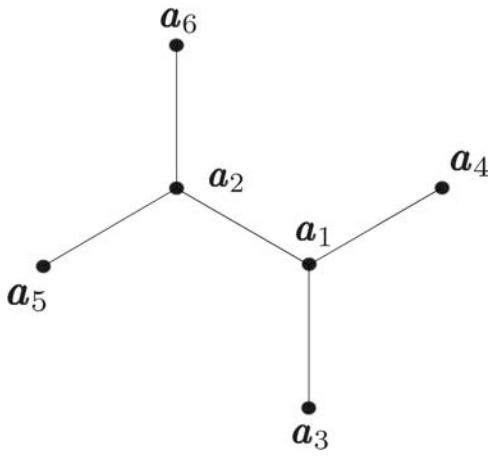

Figure 7.14: Periodic cell

$$\begin{aligned} \mathbf{u}_j &= e^{i\mathbf{k}\cdot\mathbf{g}_j}\mathbf{u}_1, \quad \mathbf{g}_j = \mathbf{a}_j - \mathbf{a}_1, \quad j \in \mathcal{N}_2, \\ \mathbf{u}_j &= e^{i\mathbf{k}\cdot\mathbf{g}_j}\mathbf{u}_2, \quad \mathbf{g}_j = \mathbf{a}_j - \mathbf{a}_2, \quad j \in \mathcal{N}_1, \end{aligned} \tag{7.113}$$

where $\mathcal{N}_1 = \{2, 3, 4\}$ and $\mathcal{N}_2 = \{1, 5, 6\}$. Applying equations (7.110) and (7.113) to the equilibrium equation, (7.105), we find

$$\begin{aligned} \sum_{j=2,3,4} \left(\mathbf{P}_{1j}^{(2)} e^{i\mathbf{k}\cdot\mathbf{g}_j}\mathbf{u}_2 - \mathbf{P}_{1j}^{(1)}\mathbf{u}_1\right) &= -\omega^2\mathbf{M}_1\mathbf{u}_1, \\ \sum_{j=1,5,6} \left(\mathbf{P}_{2j}^{(2)} e^{i\mathbf{k}\cdot\mathbf{g}_j}\mathbf{u}_1 - \mathbf{P}_{2j}^{(1)}\mathbf{u}_2\right) &= -\omega^2\mathbf{M}_2\mathbf{u}_2. \end{aligned} \tag{7.114}$$

Written into matrix form this becomes

$$\begin{bmatrix} \left[P_{12}^{(1)} + P_{13}^{(1)} + P_{14}^{(1)}\right] & -\left[P_{12}^{(2)} e^{i\mathbf{k}\cdot\mathbf{g}_2} + P_{13}^{(2)} e^{i\mathbf{k}\cdot\mathbf{g}_3} + P_{14}^{(2)} e^{i\mathbf{k}\cdot\mathbf{g}_4}\right] \\ -\left[P_{21}^{(2)} e^{i\mathbf{k}\cdot\mathbf{g}_1} + P_{25}^{(2)} e^{i\mathbf{k}\cdot\mathbf{g}_5} + P_{26}^{(2)} e^{i\mathbf{k}\cdot\mathbf{g}_6}\right] & \left[P_{21}^{(1)} + P_{25}^{(1)} + P_{26}^{(1)}\right] \end{bmatrix} \begin{bmatrix} \mathbf{u}_1 \\ \mathbf{u}_2 \end{bmatrix} = \omega^2 \begin{bmatrix} \mathbf{M}_1 & 0 \\ 0 & \mathbf{M}_2 \end{bmatrix} \begin{bmatrix} \mathbf{u}_1 \\ \mathbf{u}_2 \end{bmatrix}, \tag{7.115}$$

which is rewritten into the familiar general eigenvalue problem with

$$\mathbf{H}(\omega, \mathbf{k})\mathbf{u} = \omega^2\mathbf{M}\mathbf{u}, \tag{7.116}$$

where (ω, $\mathbf{k}$) pairs must satisfy

$$\det\Big(\mathbf{H}(\omega, \mathbf{k}) - \omega^2\mathbf{M}\Big) = 0. \tag{7.117}$$

Note that this is a more difficult problem than the standard forms found in earlier sections due to the dependence of $\mathbf{H}(\omega, \mathbf{k})$ on ω, however solution pairs can still be

found by numerical means. Alternatively we may take the summation strictly over $\mathcal{N}_1$ since

$$\sum_{j\in\mathcal{N}_2} \mathbf{P}_{2j}^{(1)} = \sum_{j\in\mathcal{N}_1} \mathbf{P}_{1j}^{(3)}, \tag{7.118}$$

and

$$\left[\sum_{j\in\mathcal{N}_1} \mathbf{P}_{1j}^{(2)} e^{i\mathbf{k}\cdot\mathbf{g}_j}\right] = \left[\sum_{j\in\mathcal{N}_2} \mathbf{P}_{2j}^{(2)} e^{i\mathbf{k}\cdot\mathbf{g}_j}\right]^{+}. \tag{7.119}$$

Equation (7.114) is rewritten to attain

$$\mathbf{H}_1 = \sum_{j\in\mathcal{N}_1} \mathbf{P}_{1j}^{(1)}, \quad \mathbf{H}_2 = -\sum_{j\in\mathcal{N}_1} \mathbf{P}_{1j}^{(2)} e^{i\mathbf{k}\cdot\mathbf{g}_j}, \quad \mathbf{H}_3 = \sum_{j\in\mathcal{N}_1} \mathbf{P}_{1j}^{(3)}, \tag{7.120}$$

where

$$\mathbf{H}(\omega,\mathbf{k}) = \begin{pmatrix} \mathbf{H}_1 & \mathbf{H}_2 \\ \mathbf{H}_2^{+} & \mathbf{H}_3 \end{pmatrix}, \tag{7.121}$$

where superscript $^{+}$ denotes the Hermitian transpose. Next we consider a simpler structure using a rectangular lattice and later show numerical examples with comparison to COMSOL results.

7.5.5 Rectangular lattice

Here we consider the rectangular lattice structure shown in figure 7.15. The equations

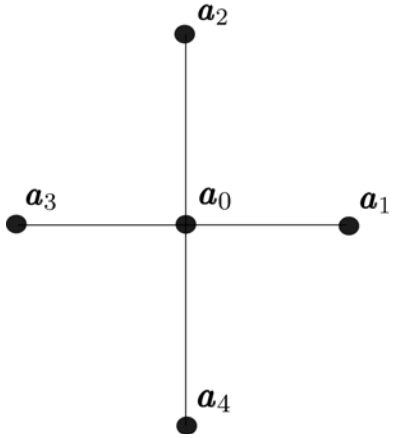

Figure 7.15: Unit Cell for the rectangular lattice.

of motion for this structure are

$$\sum_{j=1,2,3,4} \left(\mathbf{P}_{0j}^{(1)} - \mathbf{P}_{0j}^{(2)} \mathbf{e}^{i\mathbf{k}\cdot\mathbf{g}_j}\right)\mathbf{u}_0 = \omega^2 \mathbf{M}_0 \mathbf{u}_0, \tag{7.122}$$

where

$$
\begin{aligned}
\mathbf{P}_{01}^{(1)} &= \tilde{\mu}_{01}\hat{s}_{01}\cot(\hat{s}_{01})\begin{bmatrix}1&0&0\\0&0&0\\0&0&0\end{bmatrix} + \mu_{01}^{b}\begin{bmatrix}0&0&0\\0&K_{11}&-K_{12}\\0&-K_{21}&K_{22}\end{bmatrix},\\
\mathbf{P}_{02}^{(1)} &= \tilde{\mu}_{02}\hat{s}_{02}\cot(\hat{s}_{02})\begin{bmatrix}0&0&0\\0&1&0\\0&0&0\end{bmatrix} + \mu_{02}^{b}\begin{bmatrix}K_{11}&0&K_{12}\\0&0&0\\K_{21}&0&K_{22}\end{bmatrix},\\
\mathbf{P}_{03}^{(1)} &= \tilde{\mu}_{03}\hat{s}_{03}\cot(\hat{s}_{03})\begin{bmatrix}1&0&0\\0&0&0\\0&0&0\end{bmatrix} + \mu_{03}^{b}\begin{bmatrix}0&0&0\\0&K_{11}&K_{12}\\0&K_{21}&K_{22}\end{bmatrix},\\
\mathbf{P}_{04}^{(1)} &= \tilde{\mu}_{04}\hat{s}_{04}\cot(\hat{s}_{04})\begin{bmatrix}0&0&0\\0&1&0\\0&0&0\end{bmatrix} + \mu_{04}^{b}\begin{bmatrix}K_{11}&0&-K_{12}\\0&0&0\\-K_{21}&0&K_{22}\end{bmatrix},
\end{aligned}
\tag{7.123}
$$

$$
\begin{aligned}
\mathbf{P}_{01}^{(2)} &= \tilde{\mu}_{01}\hat{s}_{01}\csc(\hat{s}_{01})\begin{bmatrix}1&0&0\\0&0&0\\0&0&0\end{bmatrix} - \mu_{01}^{b}\begin{bmatrix}0&0&0\\0&K_{13}&-K_{14}\\0&-K_{23}&K_{24}\end{bmatrix},\\
\mathbf{P}_{02}^{(2)} &= \tilde{\mu}_{02}\hat{s}_{02}\csc(\hat{s}_{02})\begin{bmatrix}0&0&0\\0&1&0\\0&0&0\end{bmatrix} - \mu_{02}^{b}\begin{bmatrix}K_{13}&0&K_{14}\\0&0&0\\K_{23}&0&K_{24}\end{bmatrix},\\
\mathbf{P}_{03}^{(2)} &= \tilde{\mu}_{03}\hat{s}_{03}\csc(\hat{s}_{03})\begin{bmatrix}1&0&0\\0&0&0\\0&0&0\end{bmatrix} - \mu_{03}^{b}\begin{bmatrix}0&0&0\\0&K_{13}&K_{14}\\0&K_{23}&K_{24}\end{bmatrix},\\
\mathbf{P}_{04}^{(2)} &= \tilde{\mu}_{04}\hat{s}_{04}\csc(\hat{s}_{04})\begin{bmatrix}0&0&0\\0&1&0\\0&0&0\end{bmatrix} - \mu_{04}^{b}\begin{bmatrix}K_{13}&0&-K_{14}\\0&0&0\\-K_{23}&0&K_{24}\end{bmatrix}.
\end{aligned}
\tag{7.124}
$$

Taking all members to be of the same properties such that $\tilde{\mu}_{ij} = \tilde{\mu}$, $\hat{s}_{ij} = \hat{s}$ and $\mu^b_{ij} = \mu^b$ we find the summations used in equation (7.122) are

$$\begin{aligned}
\sum_{j=1,2,3,4} \left(\mathbf{P}^{(1)}_{0j}\right) &= \tilde{\mu}\hat{s}\cot(\hat{s}) \begin{bmatrix} 2 & 0 & 0 \\ 0 & 2 & 0 \\ 0 & 0 & 0 \end{bmatrix} + \mu^b \begin{bmatrix} 2K_{11} & 0 & 0 \\ 0 & 2K_{11} & 0 \\ 0 & 0 & 4K_{22} \end{bmatrix}, \\
\sum_{j=1,2,3,4} \left(\mathbf{P}^{(2)}_{0j} e^{i\mathbf{k}\cdot\mathbf{g}_j}\right) &= 2\tilde{\mu}\hat{s}\csc(\hat{s}) \begin{bmatrix} \cos(\hat{k}_x) & 0 & 0 \\ 0 & \cos(\hat{k}_y) & 0 \\ 0 & 0 & 0 \end{bmatrix} \\
&\quad - 2\mu^b \begin{bmatrix} K_{13}\cos(\hat{k}_y) & 0 & iK_{14}\sin(\hat{k}_y) \\ 0 & K_{13}\cos(\hat{k}_x) & -iK_{14}\sin(\hat{k}_x) \\ iK_{23}\sin(\hat{k}_y) & -iK_{23}\sin(\hat{k}_x) & K_{24}(\cos(\hat{k}_x)+\cos(\hat{k}_y)) \end{bmatrix}.
\end{aligned} \tag{7.125}$$

Simplifying the problem further we take the lattice to be square such that joining points have distance l between them. The non-dimensional wave vector components are then

$$\hat{k}_x = lk_x, \quad \hat{k}_y = lk_y. \tag{7.126}$$

From equation (7.122) we find

$$\begin{aligned}
&\Bigg(2\tilde{\mu}\hat{s} \begin{bmatrix} \cot(\hat{s}) - \csc(\hat{s})\cos(\hat{k}_x) & 0 & 0 \\ 0 & \cot(\hat{s}) - \csc(\hat{s})\cos(\hat{k}_y) & 0 \\ 0 & 0 & 0 \end{bmatrix} \\
&+ 2\mu^b \begin{bmatrix} K_{11} + K_{13}\cos(\hat{k}_y) & 0 & iK_{14}\sin(\hat{k}_y) \\ 0 & K_{11} + K_{13}\cos(\hat{k}_x) & -iK_{14}\sin(\hat{k}_x) \\ iK_{23}\sin(\hat{k}_y) & -iK_{23}\sin(\hat{k}_x) & 2K_{22} + K_{24}(\cos(\hat{k}_x)+\cos(\hat{k}_y)) \end{bmatrix}\Bigg)\mathbf{u}_0 \\
&= \omega^2 \mathbf{M}_0 \mathbf{u}_0,
\end{aligned} \tag{7.127}$$

We know for a square lattice the irreducible Brillouin zone is triangular, as shown in figure 7.4, if we consider the case along $\mathbf{\Gamma} - \mathbf{X}$ for which $\hat{k}_y = 0$ we find

$$\begin{aligned}
&\Bigg(2\tilde{\mu}\hat{s} \begin{bmatrix} \cot(\hat{s}) - \csc(\hat{s})\cos(\hat{k}_x) & 0 & 0 \\ 0 & \cot(\hat{s}) - \csc(\hat{s}) & 0 \\ 0 & 0 & 0 \end{bmatrix} \\
&+ 2\mu^b \begin{bmatrix} K_{11} + K_{13} & 0 & 0 \\ 0 & K_{11} + K_{13}\cos(\hat{k}_x) & -iK_{14}\sin(\hat{k}_x) \\ 0 & -iK_{23}\sin(\hat{k}_x) & 2K_{22} + K_{24}(\cos(\hat{k}_x)+1) \end{bmatrix}\Bigg)\mathbf{u}_0 = \omega^2 \mathbf{M}_0 \mathbf{u}_0,
\end{aligned} \tag{7.128}$$

Then the solution is found from

$$\text{Det}\begin{bmatrix} B_1 & 0 & 0 \\ 0 & B_2 & B_3 \\ 0 & B_4 & B_5 \end{bmatrix} = 0, \tag{7.129}$$

where

$$\begin{aligned} B_1 &= \tilde{\mu}\hat{s}[\cot(\hat{s}) - \csc(\hat{s})\cos(\hat{k}_x)] + \mu^b[K_{11} + K_{13}] - \frac{1}{2}m_0\omega^2, \\ B_2 &= \tilde{\mu}\hat{s}[\cot(\hat{s}) - \csc(\hat{s})] + \mu^b[K_{11} + K_{13}\cos(\hat{k}_x)] - \frac{1}{2}m_0\omega^2, \\ B_3 &= -i\mu^b K_{14}\sin(\hat{k}_x), \quad B_4 = i\mu^b K_{14}\sin(\hat{k}_x), \\ B_5 &= \mu^b[2K_{22} + K_{24}(\cos(\hat{k}_x) + 1)] - \frac{1}{2}I_0\omega^2, \end{aligned} \tag{7.130}$$

and the simplification $K_{23} = -K_{14}$ was used. Taking the determinant, the equation to be solved is

$$\begin{aligned} &\left[\tilde{\mu}\hat{s}[\cot(\hat{s}) - \csc(\hat{s})\cos(\hat{k}_x)] + \mu^b[K_{11} + K_{13}] - \frac{1}{2}m_0\omega^2\right]\times \\ &\Big[\big(\tilde{\mu}\hat{s}[\cot(\hat{s}) - \csc(\hat{s})] + \mu^b[K_{11} + K_{13}\cos(\hat{k}_x)] - \frac{1}{2}m_0\omega^2\big)\big(\mu^b[2K_{22} \\ &+ K_{24}(\cos(\hat{k}_x) + 1)] - \frac{1}{2}I_0\omega^2\big) - \big(\mu^b K_{14}\sin(\hat{k}_x)\big)^2\Big] = 0. \end{aligned} \tag{7.131}$$

This equation has the form $a * (bd - c^2) = 0$, where solutions are $a = 0$ and or $bd = c^2$. We start with a, which is

$$\tilde{\mu}\hat{s}[\cot(\hat{s}) - \csc(\hat{s})\cos(\hat{k}_x)] + \mu^b[K_{11} + K_{13}] - \frac{1}{2}m_0\omega^2 = 0. \tag{7.132}$$

Since $\hat{s}$ and K_{ij} are rather complicated functions of ω we solve for $\hat{k}_x$ instead of ω, for which we find

$$\cos(\hat{k}_x) = \cos(\hat{s}) + \frac{\mu^b\sin(\hat{s})}{\tilde{\mu}\hat{s}}[K_{11} + K_{13}] - \frac{m_0\omega^2}{2\tilde{\mu}\hat{s}}\sin(\hat{s}), \tag{7.133}$$

noting that k_x must be real for real ω we have the constraint

$$|\cos(\hat{s}) + \frac{\mu^b\sin(\hat{s})}{\tilde{\mu}\hat{s}}[K_{11} + K_{13}] - \frac{m_0\omega^2}{2\tilde{\mu}\hat{s}}\sin(\hat{s})| \leq 1. \tag{7.134}$$

As a check the units of the variables have proportionality $\gamma \propto 1/m, \quad \tilde{\mu} \propto N/m, \quad \mu^b \propto Nm^2$. Working on the second part of equation (7.131), the $bd = c^2$, we find

$$\cos(\hat{k}_x)\Big[\tilde{\mu}\hat{s}\mu^b K_{24}[\cot(\hat{s}) - \csc(\hat{s})] + (\mu^b)^2[2K_{22}K_{13} + K_{24}K_{11} + K_{24}K_{13}] - \frac{\mu^b}{2}\omega^2[K_{13}I_0 + K_{24}m_0]\Big] + \cos^2(\hat{k}_x)(\mu^b)^2K_{24}K_{13} - \sin^2(\hat{k}_x)(\mu^b)^2K_{14}^2 = -\tilde{\mu}\hat{s}\mu^b[\cot(\hat{s}) - \csc(\hat{s})](2K_{22} + K_{24}) + \frac{\tilde{\mu}\hat{s}}{2}[\cot(\hat{s}) - \csc(\hat{s})]I_0\omega^2 - (\mu^b)^2[2K_{22}K_{11} + K_{24}K_{11}] + \frac{\mu^b}{2}K_{11}I_0\omega^2 + \mu^b K_{22}m_0\omega^2 + \frac{\mu^b}{2}K_{24}m_0\omega^2 - \frac{1}{4}m_0I_0\omega^4. \tag{7.135}$$

The above equation is in the form

$$a\cos(x) + b\cos^2(x) + c\sin^2(x) = d, \tag{7.136}$$

the solution for x is then

$$x = \cos^{-1}\left(\frac{-a \pm \sqrt{a^2 - 4(b-c)(c-d)}}{2(b-c)}\right). \tag{7.137}$$

7.5.6 Examples

Examples using this theory are shown in figures 7.16 and 7.17. The numeric computations are based on the properties in table 7.1 for the square lattice and table 7.2 for the hexagonal lattice. For the square lattice we plot the solutions for equations (7.133) and (7.135) which were found using $k_y = 0$, that is solutions along $\mathbf{\Gamma} - \mathbf{X}$ of the Brillouin zone located in figure 7.4. For the hexagonal lattice the path of the wave vector taken is along the perimeter of the Brillouin zone from figure 7.4.

E (GPa)	ν	ρ^V (kg/m^3)	L (m)	t (m)
210	.25	$25 \cdot 10^3$	.25	.0125

Table 7.1: Parameters of the square lattice for the example shown in figure 7.16.

E (GPa)	ν	ρ^V (kg/m^3)	l (mm)	t (mm)
69	.33	$2.7 \cdot 10^3$	4.39	0.35

Table 7.2: Hexagonal lattice parameters for the example shown in figure 7.17.

The dispersion curves in figure 7.17 (top) were obtained using a combination of minimum value threshold and minimum peak finding methods for the 6×6 determinant

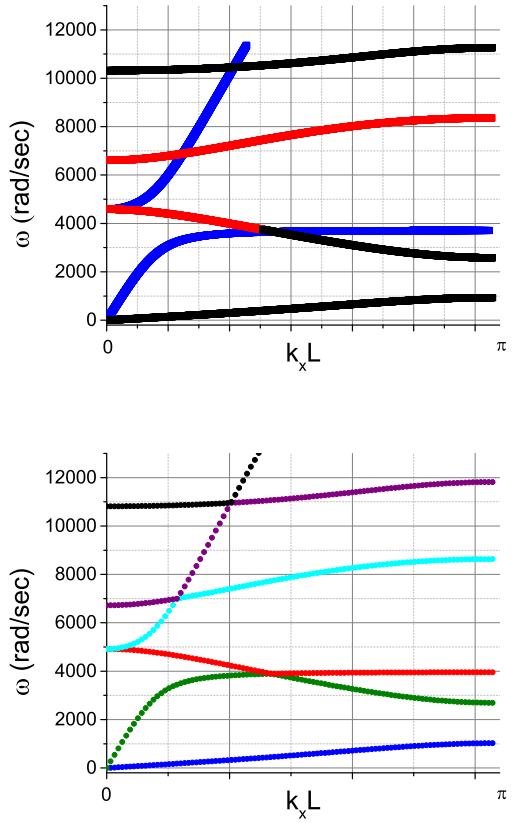

Figure 7.16: Dispersion curves of the square lattice for $k_y = 0$. Properties located in table 7.1. In the top figure the black curves correspond to quasi-longitudinal motion described by equation (7.133); the blue and red curves correspond to the pair of quasi-transverse solutions described by equation (7.135). The bottom dispersion curves were calculated using COMSOL.

evaluated on a discretized grid of wave vector and frequency parameters. This provides a fast solution technique, which can be refined by taking smaller grid steps. Figure 7.17 (bottom) shows that the dispersion curves computed by the present simplified theory agree well with those found using FEM. A close comparison shows some small deviations from the FEM results (which can safely be considered as an accurate benchmark) but the overall agreement is remarkable considering the simplicity of the present approach. We next review a more standard approach seen in the literature that uses reflection and transmission matrices with Timoshenko beam elements.

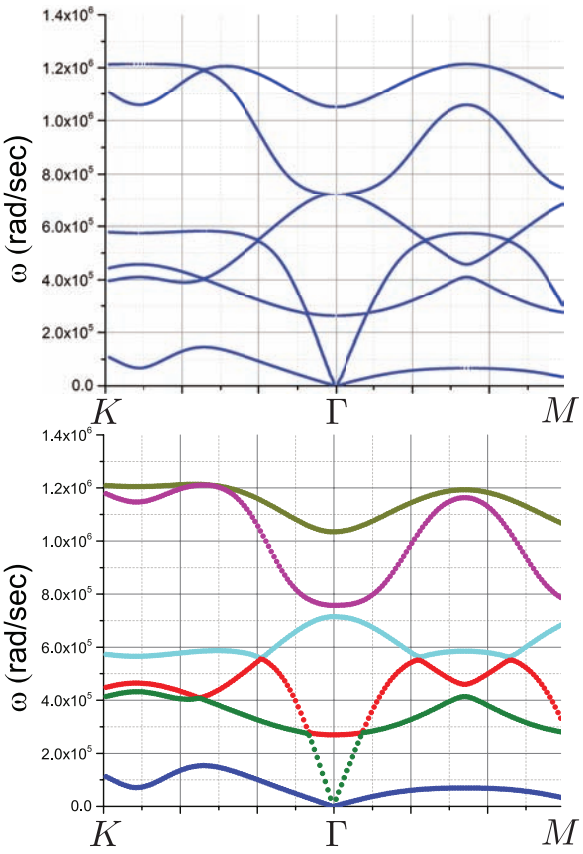

Figure 7.17: Dispersion curves of the regular hexagonal lattice with properties located in table 7.2. Shown are the first six Floquet branches for wave-vector along the perimeter of the Brillouin zone. Top figure is found using the theory of this section while the bottom curves were calculated using COMSOL.

7.6 Reflection/transmission matrices of Timoshenko beams

In this section the work of [6] is heavily reviewed. This is for accuracy but more importantly for the understanding and derivation of another method used in solving for dispersion behavior. The method of producing reflection and transmission matrices for beam structures is more standardly found in the literature [80, 81, 82]. It comes down to considering incoming and exiting waves at an intersection. We review this method here as a comparison to the previous one of section 7.5. The equations of free vibration for a Timoshenko beam were derived in section 7.4 and are located in equations (7.83) and (7.63). Uniform beams are considered here, where $E(x) = E,\ I(x) = I,\ A(x) =$

A, $\rho(x) = \rho$, and $\mu(x) = \mu$, this gives

$$\mu A\mathcal{K}\big(\frac{\partial\phi(x,t)}{\partial x} - \frac{\partial^2 w(x,t)}{\partial x^2}\big) + \rho A\frac{\partial^2 w(x,t)}{\partial t^2} = 0, \tag{7.138}$$

$$EI\frac{\partial^2\phi(x,t)}{\partial x^2} + \mu A\mathcal{K}\big(\frac{\partial w(x,t)}{\partial x} - \phi(x,t)\big) - \rho I\frac{\partial^2\phi(x,t)}{\partial t^2} = 0, \tag{7.139}$$

$$\rho A\frac{\partial^2 u(x,t)}{\partial t^2} - EA\frac{\partial^2 u(x,t)}{\partial x^2} = 0. \tag{7.140}$$

The general solutions which satisfy these equilibrium equations for the axial displacement, $u(x,t)$, the transverse displacement, $w(x,t)$, and the angle due to bending, $\phi(x,t)$, are

$$w(x,t) = \Big(a_1^+ e^{-ik_1x} + a_2^+ e^{-k_2x} + a_1^- e^{ik_1x} + a_2^- e^{k_2x}\Big)e^{i\omega t}, \tag{7.141}$$

$$\phi(x,t) = \Big(-iPa_1^+ e^{-ik_1x} - Na_2^+ e^{-k_2x} + iPa_1^- e^{ik_1x} + Na_2^- e^{k_2x}\Big)e^{i\omega t}, \tag{7.142}$$

$$u(x,t) = \Big(c^+ e^{-ik_3x} + c^- e^{ik_3x}\Big)e^{i\omega t}, \tag{7.143}$$

where the coefficients $a_i^\pm$, P, N, and $c^\pm$ will be solved for later. The derivatives of these solutions that are needed are

$$\begin{aligned}
\frac{\partial w(x,t)}{\partial x} =& \Big(-ik_1a_1^+ e^{-ik_1x} - k_2a_2^+ e^{-k_2x} + ik_1a_1^- e^{ik_1x} + k_2a_2^- e^{k_2x}\Big)e^{i\omega t},\\
\frac{\partial^2 w(x,t)}{\partial x^2} =& \Big(-k_1^2a_1^+ e^{-ik_1x} + k_2^2a_2^+ e^{-k_2x} - k_1^2a_1^- e^{ik_1x} + k_2^2a_2^- e^{k_2x}\Big)e^{i\omega t},\\
\frac{\partial\phi(x,t)}{\partial x} =& \Big(-k_1Pa_1^+ e^{-ik_1x} + k_2Na_2^+ e^{-k_2x} - k_1Pa_1^- e^{ik_1x} + k_2Na_2^- e^{k_2x}\Big)e^{i\omega t},\\
\frac{\partial^2\phi(x,t)}{\partial x^2} =& \Big(ik_1^2Pa_1^+ e^{-ik_1x} - k_2^2Na_2^+ e^{-k_2x} - ik_1^2Pa_1^- e^{ik_1x} + k_2^2Na_2^- e^{k_2x}\Big)e^{i\omega t},\\
\frac{\partial u(x,t)}{\partial x} =& \Big(-ik_3c^+ e^{-ik_3x} + ik_3c^- e^{ik_3x}\Big)e^{i\omega t},\\
\frac{\partial^2 u(x,t)}{\partial x^2} =& \Big(-k_3^2c^+ e^{-ik_3x} - k_3^2c^- e^{ik_3x}\Big)e^{i\omega t},
\end{aligned} \tag{7.144}$$

applying these to the equations of motion, equations (7.138)-(7.140), we find

$$\begin{aligned}
&\big[a_1^+ e^{-ik_1x} + a_1^- e^{ik_1x}\big]\big[\mu\mathcal{K}(k_1^2 - k_1P) - \rho\omega^2\big]\\
&+ \big[a_2^+ e^{-k_2x} + a_2^- e^{k_2x}\big]\big[\mu\mathcal{K}(k_2N - k_2^2) - \rho\omega^2\big] = 0,\\
&\big[a_1^+ e^{-ik_1x} - a_1^- e^{ik_1x}\big]\big[iPEIk_1^2 + \mu A\mathcal{K}i(-k_1 + P) - iP\rho I\omega^2\big] +\\
&\big[a_2^+ e^{-k_2x} - a_2^- e^{k_2x}\big]\big[-NEIk_2^2 + \mu A\mathcal{K}(-k_2 + N) - N\rho I\omega^2\big] = 0,\\
&\big[c^+ e^{-ik_3x} + c^- e^{ik_3x}\big]\big[EAk_3^2 - \rho A\omega^2\big] = 0.
\end{aligned} \tag{7.145}$$

The first equation of (7.145) implies

$$P = k_1\big(1 - \frac{\omega^2}{k_1^2 C_s^2}\big), \quad N = k_2\big(1 + \frac{\omega^2}{k_2^2 C_s^2}\big), \tag{7.146}$$

where

$$C_s = \sqrt{\frac{\mu\mathcal{K}}{\rho}}. \tag{7.147}$$

Plugging equations (7.146) and (7.147) into the second and third equations of (7.145) yields

$$\begin{aligned} k_1^2 &= \frac{\omega^2}{2}\big[(\frac{1}{C_s})^2 + (\frac{C_r}{C_b})^2\big] \pm \sqrt{(\frac{\omega}{C_b})^2 + \frac{\omega^4}{4}\big[(\frac{1}{C_s})^2 - (\frac{C_r}{C_b})^2\big]^2}, \\ k_2^2 &= -\frac{\omega^2}{2}\big[(\frac{1}{C_s})^2 + (\frac{C_r}{C_b})^2\big] \pm \sqrt{(\frac{\omega}{C_b})^2 + \frac{\omega^4}{4}\big[(\frac{1}{C_s})^2 - (\frac{C_r}{C_b})^2\big]^2}, \\ k_3^2 &= \frac{\rho\omega^2}{E} = (\frac{C_r}{C_b})^2\omega^2, \end{aligned} \tag{7.148}$$

where

$$C_b = \sqrt{\frac{EI}{\rho A}}, \quad C_r = \sqrt{\frac{I}{A}}. \tag{7.149}$$

Now the solutions, equations (7.141), (7.142) and (7.143), can be written in terms of known material properties, the circular frequency ω and six unknown coefficients. The coefficients can be found from a given set of boundary conditions which define resultant shear, moment and axial forces at a given location. As found in section 7.4 they are

$$\begin{gathered} Q(x,t) = \mu A\mathcal{K}\big(\frac{\partial w(x,t)}{\partial x} - \phi(x,t)\big), \quad M(x,t) = -EI\frac{\partial \phi(x,t)}{\partial x}, \\ F(x,t) = EA\frac{\partial u(x,t)}{\partial x}. \end{gathered} \tag{7.150}$$

7.6.1 Joint continuity and the propagation matrix

As done in the work of [6], the square lattice is considered for which there are four cases of transmission and reflection waves at the joint intersection, as depicted in figure 7.18. Each wave represented is traveling in one direction having only three associated coefficients, this is seen from equations (7.141)-(7.143). Vectors of coefficients to describe

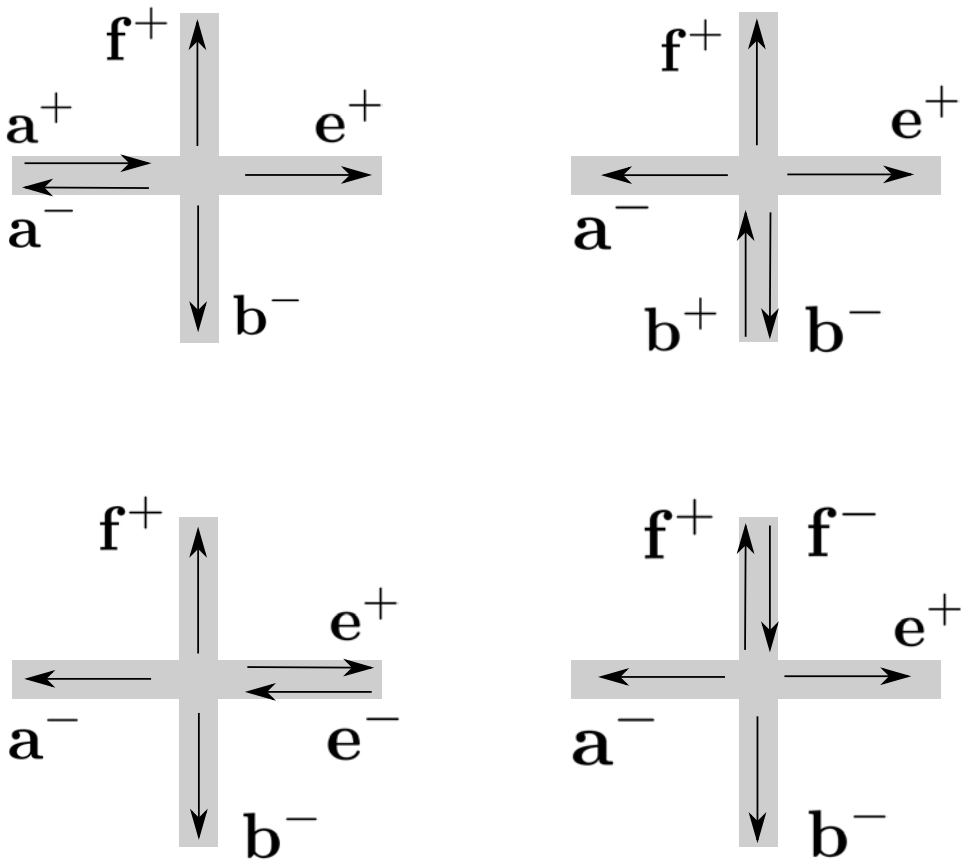

Figure 7.18: As done by [6] the four cases of reflection and transmission of waves entering the joint section from the right, bottom, left, or top are shown. The variables $\mathbf{a}^+$, $\mathbf{a}^-$, and so on are vectors of coefficients as described by equation (7.151)

transmission and reflection waves are defined by

$$\begin{aligned}
\mathbf{a}^+ &= \begin{bmatrix} a_1^+ \\ a_2^+ \\ c^+ \end{bmatrix}, \quad \mathbf{a}^- = \begin{bmatrix} a_1^- \\ a_2^- \\ c^- \end{bmatrix}, \quad \mathbf{b}^+ = \begin{bmatrix} b_1^+ \\ b_2^+ \\ d^+ \end{bmatrix}, \quad \mathbf{b}^- = \begin{bmatrix} b_1^- \\ b_2^- \\ d^- \end{bmatrix}, \\
\mathbf{e}^+ &= \begin{bmatrix} e_1^+ \\ e_2^+ \\ g^+ \end{bmatrix}, \quad \mathbf{e}^- = \begin{bmatrix} e_1^- \\ e_2^- \\ g^- \end{bmatrix}, \quad \mathbf{f}^+ = \begin{bmatrix} f_1^+ \\ f_2^+ \\ h^+ \end{bmatrix}, \quad \mathbf{f}^- = \begin{bmatrix} f_1^- \\ f_2^- \\ h^- \end{bmatrix}.
\end{aligned} \tag{7.151}$$

Labeling the four cases, **Case 1**: wave $\mathbf{a}^+$ causing reflection and transmission waves $\mathbf{a}^-$, $\mathbf{b}^-$, $\mathbf{e}^+$, $\mathbf{f}^+$. **Case 2**: wave $\mathbf{b}^+$ causing reflection and transmission waves $\mathbf{a}^-$, $\mathbf{b}^-$, $\mathbf{e}^+$, $\mathbf{f}^+$. **Case 3**: wave $\mathbf{e}^-$ causing reflection and transmission waves $\mathbf{a}^-$, $\mathbf{b}^-$, $\mathbf{e}^+$, $\mathbf{f}^+$. **Case 4**: wave $\mathbf{f}^-$ causing reflection and transmission waves $\mathbf{a}^-$, $\mathbf{b}^-$, $\mathbf{e}^+$, $\mathbf{f}^+$. Next

we consider the forces and moments acting at an orthogonal joint, as shown in figure 7.19, where for simplicity we take thicknesses $h_1 = h_3$ and $h_2 = h_4$. The equilibrium

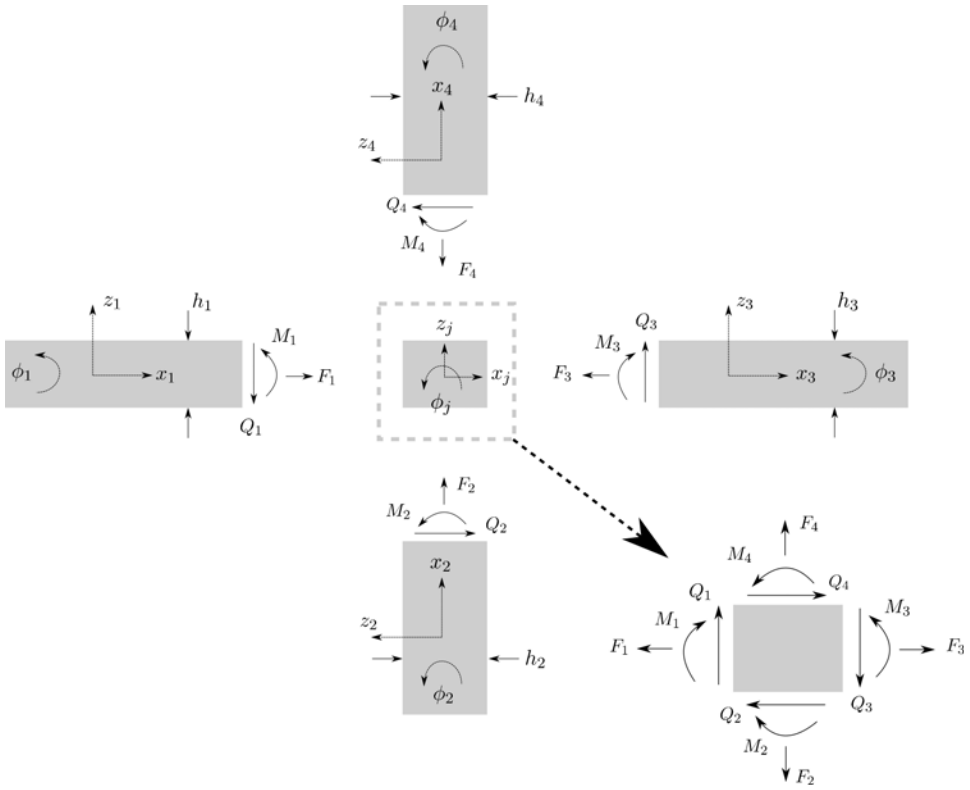

Figure 7.19: Free body diagram of orthogonal joint intersection.

conditions are

$$\begin{aligned} Q_1 - Q_3 + F_4 - F_2 &= m\ddot{w}_j, \\ Q_4 - Q_2 + F_3 - F_1 &= m\ddot{u}_j, \\ M_3 + M_4 - M_1 - M_2 - \frac{h_2}{2}(Q_1 + Q_3) - \frac{h_1}{2}(Q_2 + Q_4) &= \rho I \ddot{\phi}_j, \end{aligned} \tag{7.152}$$

where m, I, and ρ are the mass, moment of inertia, and density of the joint. Evaluating the shear, moment and axial forces at time $t = 0$ and position $x = 0$ or $y = 0$ yields

$$\begin{aligned} Q_1(x=0,t=0) &= (\mu A\mathcal{K})_1\big[(-ik_{1_1} + iP_1)(a_1^+ - a_1^-) + (-k_{2_1} + N_1)(a_2^+ - a_2^-)\big], \\ Q_2(y=0,t=0) &= (\mu A\mathcal{K})_2\big[(-ik_{1_2} + iP_2)(b_1^+ - b_1^-) + (-k_{2_2} + N_2)(b_2^+ - b_2^-)\big], \\ Q_3(x=0,t=0) &= (\mu A\mathcal{K})_3\big[(-ik_{1_3} + iP_3)(e_1^+ - e_1^-) + (-k_{2_3} + N_3)(e_2^+ - e_2^-)\big], \\ Q_4(y=0,t=0) &= (\mu A\mathcal{K})_4\big[(-ik_{1_4} + iP_4)(f_1^+ - f_1^-) + (-k_{2_4} + N_4)(f_2^+ - f_2^-)\big], \end{aligned} \tag{7.153}$$

$$
\begin{aligned}
M_1(x=0,t=0) &= -(EI)_1\big[-k_{1_1}P_1a_1^+ + k_{2_1}N_1a_2^+ - k_{1_1}P_1a_1^- + k_{2_1}N_1a_2^-\big],\\
M_2(y=0,t=0) &= -(EI)_2\big[-k_{1_2}P_2b_1^+ + k_{2_2}N_2b_2^+ - k_{1_2}P_2b_1^- + k_{2_2}N_2b_2^-\big],\\
M_3(x=0,t=0) &= -(EI)_3\big[-k_{1_3}P_3e_1^+ + k_{2_3}N_3e_2^+ - k_{1_3}P_3e_1^- + k_{2_3}N_3e_2^-\big],\\
M_4(y=0,t=0) &= -(EI)_4\big[-k_{1_4}P_4f_1^+ + k_{2_4}N_4f_2^+ - k_{1_4}P_4f_1^- + k_{2_4}N_4f_2^-\big],
\end{aligned}
\tag{7.154}
$$

$$
\begin{aligned}
F_1(x=0,t=0) &= (EA)_1(c^- - c^+)ik_{3_1},\\
F_2(y=0,t=0) &= (EA)_2(d^- - d^+)ik_{3_2},\\
F_3(x=0,t=0) &= (EA)_3(g^- - g^+)ik_{3_3},\\
F_4(y=0,t=0) &= (EA)_4(h^- - h^+)ik_{3_4},
\end{aligned}
\tag{7.155}
$$

where $(\mu A\mathcal{K})_i = \mu_i A_i \mathcal{K}_i$, $(EA)_i = E_i A_i$, and k_{l_m} is the wave number where l represents the direction, 1 or 2, and m is to identify for which beam the wave number is associated. We also have continuity of the displacements at the joint such that

$$
\begin{gathered}
u_1 = u_j, \quad u_2 = w_j, \quad u_3 = u_j, \quad u_4 = w_j,\\
w_1 = w_j - \frac{h_2}{2}\phi_j, \quad w_2 = -u_j - \frac{h_1}{2}\phi_j,\\
w_3 = w_j + \frac{h_2}{2}\phi_j, \quad w_4 = -u_j + \frac{h_1}{2}\phi_j,\\
\phi_1 = \phi_2 = \phi_3 = \phi_4 = \phi_j.
\end{gathered}
\tag{7.156}
$$

Using the equilibrium equations at the joint, equation (7.152), and the continuity conditions, equation (7.156), we find the matrix form of the equations of motion at the joint to be

$$
\mathbf{Q}_2^+\mathbf{b}^+ + \mathbf{Q}_2^-\mathbf{b}^- + \mathbf{Q}_3^+\mathbf{e}^+ + \mathbf{Q}_3^-\mathbf{e}^- + \mathbf{Q}_4^+\mathbf{f}^+ + \mathbf{Q}_4^-\mathbf{f}^- = \mathbf{Q}_1^+\mathbf{a}^+ + \mathbf{Q}_1^-\mathbf{a}^-, \tag{7.157}
$$

where

$$
\begin{aligned}
\mathbf{Q}_2^+ &= \begin{bmatrix} 0 & 0 & (EA)_2 ik_{3_2} \\ -(\mu A\mathcal{K})_2 i(-k_{1_2}+P_2) & -(\mu A\mathcal{K})_2(-k_{2_2}+N_2) & 0 \\ -(EI)_2 k_{1_2} P_2 - \frac{h_1}{2}(\mu A\mathcal{K})_2 i(-k_{1_2}+P_2) & (EI)_2 k_{2_2} N_2 - \frac{h_1}{2}(\mu A\mathcal{K})_2(-k_{2_2}+N_2) & 0 \end{bmatrix}, \\
\mathbf{Q}_2^- &= \begin{bmatrix} 0 & 0 & -(EA)_2 ik_{3_2} \\ (\mu A\mathcal{K})_2 i(-k_{1_2}+P_2) & (\mu A\mathcal{K})_2(-k_{2_2}+N_2) & 0 \\ -(EI)_2 k_{1_2} P_2 + \frac{h_1}{2}(\mu A\mathcal{K})_2 i(-k_{1_2}+P_2) & (EI)_2 k_{2_2} N_2 + \frac{h_1}{2}(\mu A\mathcal{K})_2(-k_{2_2}+N_2) & 0 \end{bmatrix}, \\
\mathbf{Q}_3^+ &= \begin{bmatrix} -(\mu A\mathcal{K})_3 i(-k_{1_3}+P_3) & -(\mu A\mathcal{K})_3(-k_{2_3}+N_3) & 0 \\ 0 & 0 & -(EA)_3 ik_{3_3} \\ (EI)_3 k_{1_3} P_3 - \frac{h_2}{2}(\mu A\mathcal{K})_3 i(-k_{1_3}+P_3) & -(EI)_3 k_{2_3} N_3 - \frac{h_2}{2}(\mu A\mathcal{K})_3(-k_{2_3}+N_3) & 0 \end{bmatrix}, \\
\mathbf{Q}_3^- &= \begin{bmatrix} (\mu A\mathcal{K})_3 i(-k_{1_3}+P_3) & (\mu A\mathcal{K})_3(-k_{2_3}+N_3) & 0 \\ 0 & 0 & (EA)_3 ik_{3_3} \\ (EI)_3 k_{1_3} P_3 + \frac{h_2}{2}(\mu A\mathcal{K})_3 i(-k_{1_3}+P_3) & -(EI)_3 k_{2_3} N_3 + \frac{h_2}{2}(\mu A\mathcal{K})_3(-k_{2_3}+N_3) & 0 \end{bmatrix}, \\
\mathbf{Q}_4^+ &= \begin{bmatrix} 0 & 0 & -(EA)_4 ik_{3_4} \\ (\mu A\mathcal{K})_4 i(-k_{1_4}+P_4) & (\mu A\mathcal{K})_4(-k_{2_4}+N_4) & 0 \\ (EI)_4 k_{1_4} P_4 - \frac{h_1}{2}(\mu A\mathcal{K})_4 i(-k_{1_4}+P_4) & -(EI)_4 k_{2_4} N_4 - \frac{h_1}{2}(\mu A\mathcal{K})_4(-k_{2_4}+N_4) & 0 \end{bmatrix}, \\
\mathbf{Q}_4^- &= \begin{bmatrix} 0 & 0 & (EA)_4 ik_{3_4} \\ -(\mu A\mathcal{K})_4 i(-k_{1_4}+P_4) & -(\mu A\mathcal{K})_4(-k_{2_4}+N_4) & 0 \\ (EI)_4 k_{1_4} P_4 + \frac{h_1}{2}(\mu A\mathcal{K})_4 i(-k_{1_4}+P_4) & -(EI)_4 k_{2_4} N_4 + \frac{h_1}{2}(\mu A\mathcal{K})_4(-k_{2_4}+N_4) & 0 \end{bmatrix},
\end{aligned}
\tag{7.158}
$$

and

$$
\begin{aligned}
\mathbf{Q}_1^+ &= \begin{bmatrix} Q_{11}^+ & Q_{12}^+ & 0 \\ 0 & 0 & Q_{23}^+ \\ Q_{31}^+ & Q_{32}^+ & 0 \end{bmatrix}, \\
\mathbf{Q}_1^- &= \begin{bmatrix} Q_{11}^- & Q_{12}^- & 0 \\ 0 & 0 & Q_{23}^- \\ Q_{31}^- & Q_{32}^- & 0 \end{bmatrix},
\end{aligned}
\tag{7.159}
$$

where

$$
\begin{aligned}
Q_{11}^+ &= -\omega^2 m - \frac{h_2}{2} iP_1 - (\mu A\mathcal{K})_1 i(-k_{1_1}+P_1), \\
Q_{12}^+ &= -\omega^2 m - \frac{h_2}{2} N_1 - (\mu A\mathcal{K})_1(-k_{2_1}+N_1), \\
Q_{23}^+ &= -\omega^2 m - (EA)_1 ik_{3_1}, \\
Q_{31}^+ &= \omega^2 \rho I iP_1 + (EI)_1 k_{1_1} P_1 + \frac{h_2}{2}(\mu A\mathcal{K})_1 i(-k_{1_1}+P_1), \\
Q_{32}^+ &= \omega^2 \rho I N_1 - (EI)_1 k_{2_1} N_1 + \frac{h_2}{2}(\mu A\mathcal{K})_1(-k_{2_1}+N_1),
\end{aligned}
\tag{7.160}
$$

$$
\begin{aligned}
Q_{11}^{-} &= -\omega^2 m + \frac{h_2}{2} i P_1 + (\mu A \mathcal{K})_1 i(-k_{1_1} + P_1),\\
Q_{12}^{-} &= -\omega^2 m + \frac{h_2}{2} N_1 + (\mu A \mathcal{K})_1 (-k_{2_1} + N_1),\\
Q_{23}^{-} &= -\omega^2 m + (EA)_1 i k_{3_1},\\
Q_{31}^{-} &= -\omega^2 \rho I i P_1 + (EI)_1 k_{1_1} P_1 - \frac{h_2}{2}(\mu A \mathcal{K})_1 i(-k_{1_1} + P_1),\\
Q_{32}^{-} &= -\omega^2 \rho I N_1 - (EI)_1 k_{2_1} N_1 - \frac{h_2}{2}(\mu A \mathcal{K})_1 (-k_{2_1} + N_1).
\end{aligned}
\tag{7.161}
$$

Eliminating w_j, ϕ_j and u_j from the continuity conditions at the joint gives

$$
\mathbf{U}_1 = \begin{bmatrix} 0 & -\frac{h_2}{2} & 1 \\ 0 & 1 & 0 \\ -1 & -\frac{h_1}{2} & 0 \end{bmatrix} \mathbf{U}_2 = \begin{bmatrix} 1 & -h_2 & 0 \\ 0 & 1 & 0 \\ 0 & 0 & 1 \end{bmatrix} \mathbf{U}_3 = \begin{bmatrix} 0 & -\frac{h_2}{2} & 1 \\ 0 & 1 & 0 \\ -1 & \frac{h_1}{2} & 0 \end{bmatrix} \mathbf{U}_4, \tag{7.162}
$$

which is rewritten as

$$
\mathbf{U}_1 = \mathbf{R}_{11}\mathbf{U}_2 = \mathbf{R}_{12}\mathbf{U}_3 = \mathbf{R}_{13}\mathbf{U}_4, \tag{7.163}
$$

where $\mathbf{U}_i = \begin{bmatrix} w_i & \phi_i & u_i \end{bmatrix}^T$, $\forall\ i = \{1,2,3,4,j\}$. With this we are in a position to develop transmission and reflection matrices.

Case 1: Wave $\mathbf{a}^+$ causes reflection and transmission waves $\mathbf{a}^-$, $\mathbf{b}^-$, $\mathbf{e}^+$, $\mathbf{f}^+$. The displacement vectors for each beam are

$$
\begin{gathered}
\mathbf{U}_1 = \mathbf{X}_1^+ \mathbf{a}^+ + \mathbf{X}_1^- \mathbf{a}^-,\\
\mathbf{U}_2 = \mathbf{Y}_2^- \mathbf{b}^-, \quad \mathbf{U}_3 = \mathbf{X}_3^+ \mathbf{e}^+, \quad \mathbf{U}_4 = \mathbf{Y}_4^+ \mathbf{f}^+,
\end{gathered}
\tag{7.164}
$$

where

$$
\begin{aligned}
\mathbf{X}_m^+ &= \begin{bmatrix} e^{-ik_{1_m}x} & e^{-k_{2_m}x} & 0 \\ -iP_m e^{-ik_{1_m}x} & -N_m e^{-k_{2_m}x} & 0 \\ 0 & 0 & e^{-ik_{3_m}x} \end{bmatrix}, \quad \mathbf{X}_m^- = \begin{bmatrix} e^{ik_{1_m}x} & e^{k_{2_m}x} & 0 \\ iP_m e^{ik_{1_m}x} & N_m e^{k_{2_m}x} & 0 \\ 0 & 0 & e^{ik_{3_m}x} \end{bmatrix},\\
\mathbf{Y}_m^+ &= \begin{bmatrix} e^{-ik_{1_m}y} & e^{-k_{2_m}y} & 0 \\ -iP_m e^{-ik_{1_m}y} & -N_m e^{-k_{2_m}y} & 0 \\ 0 & 0 & e^{-ik_{3_m}y} \end{bmatrix}, \quad \mathbf{Y}_m^- = \begin{bmatrix} e^{ik_{1_m}y} & e^{k_{2_m}y} & 0 \\ iP_m e^{ik_{1_m}y} & N_m e^{k_{2_m}y} & 0 \\ 0 & 0 & e^{ik_{3_m}y} \end{bmatrix}.
\end{aligned}
\tag{7.165}
$$

Applying continuity of displacements, equation (7.162), gives

$$\begin{aligned}\mathbf{b}^- &= \Big[\mathbf{R}_{11}\mathbf{Y}_2^-\Big]^{-1}\Big[\mathbf{X}_1^+\mathbf{a}^+ + \mathbf{X}_1^-\mathbf{a}^-\Big],\\ \mathbf{e}^+ &= \Big[\mathbf{R}_{12}\mathbf{X}_3^+\Big]^{-1}\Big[\mathbf{X}_1^+\mathbf{a}^+ + \mathbf{X}_1^-\mathbf{a}^-\Big],\\ \mathbf{f}^+ &= \Big[\mathbf{R}_{13}\mathbf{Y}_4^+\Big]^{-1}\Big[\mathbf{X}_1^+\mathbf{a}^+ + \mathbf{X}_1^-\mathbf{a}^-\Big].\end{aligned} \tag{7.166}$$

Lastly the equilibrium equations at the joint, equation (7.157), where for this case we only consider $\mathbf{a}^+$, $\mathbf{a}^-$, $\mathbf{b}^-$, $\mathbf{e}^+$, and $\mathbf{f}^+$, gives

$$\mathbf{Q}_2^-\mathbf{b}^- + \mathbf{Q}_3^+\mathbf{e}^+ + \mathbf{Q}_4^+\mathbf{f}^+ = \mathbf{Q}_1^+\mathbf{a}^+ + \mathbf{Q}_1^-\mathbf{a}^-. \tag{7.167}$$

Using equations (7.166) and (7.167) we can reduce everything to one vector of coefficients such that we can find the transmission $\mathbf{t}_{ij}$ and reflection matrices $\mathbf{r}_{ij}$ where

$$\mathbf{a}^- = \mathbf{r}_{11}\mathbf{a}^+, \quad \mathbf{b}^- = \mathbf{t}_{12}\mathbf{a}^+, \quad \mathbf{e}^+ = \mathbf{t}_{13}\mathbf{a}^+, \quad \mathbf{f}^+ = \mathbf{t}_{14}\mathbf{a}^+, \tag{7.168}$$

where

$$\begin{aligned}\mathbf{a}^- =&\Bigg[\Bigg(\mathbf{Q}_2^-\Big[\mathbf{R}_{11}\mathbf{Y}_2^-\Big]^{-1} + \mathbf{Q}_3^+\Big[\mathbf{R}_{12}\mathbf{X}_3^+\Big]^{-1} + \mathbf{Q}_4^+\Big[\mathbf{R}_{13}\mathbf{Y}_4^+\Big]^{-1}\Bigg)\mathbf{X}_1^- - \mathbf{Q}_1^-\Bigg]^{-1}\times\\ &\Bigg[\mathbf{Q}_1^+ - \Bigg(\mathbf{Q}_2^-\Big[\mathbf{R}_{11}\mathbf{Y}_2^-\Big]^{-1} + \mathbf{Q}_3^+\Big[\mathbf{R}_{12}\mathbf{X}_3^+\Big]^{-1} + \mathbf{Q}_4^+\Big[\mathbf{R}_{13}\mathbf{Y}_4^+\Big]^{-1}\Bigg)\mathbf{X}_1^+\Bigg]\mathbf{a}^+,\end{aligned} \tag{7.169}$$

then

$$\begin{aligned}\mathbf{r}_{11} = &\Bigg[\Bigg(\mathbf{Q}_2^-\Big[\mathbf{R}_{11}\mathbf{Y}_2^-\Big]^{-1} + \mathbf{Q}_3^+\Big[\mathbf{R}_{12}\mathbf{X}_3^+\Big]^{-1} + \mathbf{Q}_4^+\Big[\mathbf{R}_{13}\mathbf{Y}_4^+\Big]^{-1}\Bigg)\mathbf{X}_1^- - \mathbf{Q}_1^-\Bigg]^{-1}\times\\ &\Bigg[\mathbf{Q}_1^+ - \Bigg(\mathbf{Q}_2^-\Big[\mathbf{R}_{11}\mathbf{Y}_2^-\Big]^{-1} + \mathbf{Q}_3^+\Big[\mathbf{R}_{12}\mathbf{X}_3^+\Big]^{-1} + \mathbf{Q}_4^+\Big[\mathbf{R}_{13}\mathbf{Y}_4^+\Big]^{-1}\Bigg)\mathbf{X}_1^+\Bigg],\end{aligned} \tag{7.170}$$

and

$$\begin{aligned}\mathbf{t}_{12} &= \Big[\mathbf{R}_{11}\mathbf{Y}_2^-\Big]^{-1}\Big[\mathbf{X}_1^+ + \mathbf{X}_1^-\mathbf{r}_{11}\Big],\\ \mathbf{t}_{13} &= \Big[\mathbf{R}_{12}\mathbf{X}_3^+\Big]^{-1}\Big[\mathbf{X}_1^+ + \mathbf{X}_1^-\mathbf{r}_{11}\Big],\\ \mathbf{t}_{14} &= \Big[\mathbf{R}_{13}\mathbf{Y}_4^+\Big]^{-1}\Big[\mathbf{X}_1^+ + \mathbf{X}_1^-\mathbf{r}_{11}\Big].\end{aligned} \tag{7.171}$$

Case 2: Following the same procedure from above, we consider the case of wave $\mathbf{b}^+$ causing reflection and transmission waves $\mathbf{a}^-$, $\mathbf{b}^-$, $\mathbf{e}^+$, $\mathbf{f}^+$. The displacements of each beam are

$$\begin{aligned}\mathbf{U}_2 &= \mathbf{Y}_2^+\mathbf{b}^+ + \mathbf{Y}_2^-\mathbf{b}^-,\\ \mathbf{U}_1 = \mathbf{X}_1^-\mathbf{a}^-, &\quad \mathbf{U}_3 = \mathbf{X}_3^+\mathbf{e}^+, \quad \mathbf{U}_4 = \mathbf{Y}_4^+\mathbf{f}^+.\end{aligned} \tag{7.172}$$

Applying continuity of displacements, equation (7.162), is rewritten in terms of $\mathbf{U}_2$, with

$$\mathbf{U}_2 = \begin{bmatrix} 0 & -\frac{h_1}{2} & -1 \\ 0 & 1 & 0 \\ 1 & \frac{h_2}{2} & 0 \end{bmatrix} \mathbf{U}_1 = \begin{bmatrix} 0 & -\frac{h_1}{2} & -1 \\ 0 & 1 & 0 \\ 1 & -\frac{h_2}{2} & 0 \end{bmatrix} \mathbf{U}_3 = \begin{bmatrix} 1 & -h_1 & 0 \\ 0 & 1 & 0 \\ 0 & 0 & 1 \end{bmatrix} \mathbf{U}_4, \tag{7.173}$$

which we take equivalent to

$$\mathbf{U}_2 = \mathbf{R}_{21}\mathbf{U}_1 = \mathbf{R}_{22}\mathbf{U}_3 = \mathbf{R}_{23}\mathbf{U}_4. \tag{7.174}$$

The coefficients are

$$\begin{aligned} \mathbf{a}^- &= \Big[\mathbf{R}_{21}\mathbf{X}_1^-\Big]^{-1}\Big[\mathbf{Y}_2^+\mathbf{b}^+ + \mathbf{Y}_2^-\mathbf{b}^-\Big], \\ \mathbf{e}^+ &= \Big[\mathbf{R}_{22}\mathbf{X}_3^+\Big]^{-1}\Big[\mathbf{Y}_2^+\mathbf{b}^+ + \mathbf{Y}_2^-\mathbf{b}^-\Big], \\ \mathbf{f}^+ &= \Big[\mathbf{R}_{23}\mathbf{Y}_4^+\Big]^{-1}\Big[\mathbf{Y}_2^+\mathbf{b}^+ + \mathbf{Y}_2^-\mathbf{b}^-\Big]. \end{aligned} \tag{7.175}$$

Lastly we use the equilibrium equations at the joint, equation (7.157), where for this case we only consider $\mathbf{b}^+$, $\mathbf{a}^-$, $\mathbf{b}^-$, $\mathbf{e}^+$, and $\mathbf{f}^+$, this gives

$$\mathbf{Q}_2^+\mathbf{b}^+ + \mathbf{Q}_2^-\mathbf{b}^- + \mathbf{Q}_3^+\mathbf{e}^+ + \mathbf{Q}_4^+\mathbf{f}^+ = \mathbf{Q}_1^-\mathbf{a}^-. \tag{7.176}$$

Using equations (7.175) and (7.176) we can reduce everything in terms of one vector of coefficients

$$\mathbf{a}^- = \mathbf{t}_{21}\mathbf{b}^+, \quad \mathbf{b}^- = \mathbf{r}_{22}\mathbf{b}^+, \quad \mathbf{e}^+ = \mathbf{t}_{23}\mathbf{b}^+, \quad \mathbf{f}^+ = \mathbf{t}_{24}\mathbf{b}^+, \tag{7.177}$$

where the transmission $\mathbf{t}_{ij}$ and reflection matrices $\mathbf{r}_{ij}$ are

$$\begin{aligned} \mathbf{r}_{22} = \Bigg[\mathbf{Q}_2^- + \Bigg(&- \mathbf{Q}_1^-\big[\mathbf{R}_{21}\mathbf{X}_1^-\big]^{-1} + \mathbf{Q}_4^+\big[\mathbf{R}_{23}\mathbf{Y}_4^+\big]^{-1} + \mathbf{Q}_3^+\big[\mathbf{R}_{22}\mathbf{X}_3^+\big]^{-1}\Bigg)\mathbf{Y}_2^-\Bigg]^{-1} \times \\ \Bigg[&- \mathbf{Q}_2^+ + \Bigg(- \mathbf{Q}_3^+\big[\mathbf{R}_{22}\mathbf{X}_3^+\big]^{-1} - \mathbf{Q}_4^+\big[\mathbf{R}_{23}\mathbf{Y}_4^+\big]^{-1} + \mathbf{Q}_1^-\big[\mathbf{R}_{21}\mathbf{X}_1^-\big]^{-1}\Bigg)\mathbf{Y}_2^+\Bigg], \end{aligned} \tag{7.178}$$

and

$$\begin{aligned} \mathbf{t}_{21} &= \Big[\mathbf{R}_{21}\mathbf{X}_1^-\Big]^{-1}\Big[\mathbf{Y}_2^+ + \mathbf{Y}_2^-\mathbf{r}_{22}\Big], \\ \mathbf{t}_{23} &= \Big[\mathbf{R}_{22}\mathbf{X}_3^+\Big]^{-1}\Big[\mathbf{Y}_2^+ + \mathbf{Y}_2^-\mathbf{r}_{22}\Big], \\ \mathbf{t}_{24} &= \Big[\mathbf{R}_{23}\mathbf{Y}_4^+\Big]^{-1}\Big[\mathbf{Y}_2^+ + \mathbf{Y}_2^-\mathbf{r}_{22}\Big]. \end{aligned} \tag{7.179}$$

Case 3: Wave $\mathbf{e}^-$ causes reflection and transmission waves $\mathbf{a}^-$, $\mathbf{b}^-$, $\mathbf{e}^+$, $\mathbf{f}^+$. The displacements of each beam are

$$\begin{gathered}\mathbf{U}_3 = \mathbf{X}_3^+\mathbf{e}^+ + \mathbf{X}_3^-\mathbf{e}^-, \\ \mathbf{U}_1 = \mathbf{X}_1^-\mathbf{a}^-, \quad \mathbf{U}_2 = \mathbf{Y}_2^-\mathbf{b}^-, \quad \mathbf{U}_4 = \mathbf{Y}_4^+\mathbf{f}^+.\end{gathered} \tag{7.180}$$

Applying continuity of displacements, equation (7.162) is rewritten in terms of $\mathbf{U}_3$,

$$\mathbf{U}_3 = \begin{bmatrix} 1 & h_2 & 0 \\ 0 & 1 & 0 \\ 0 & 0 & 1 \end{bmatrix} \mathbf{U}_1 = \begin{bmatrix} 0 & \frac{h_2}{2} & 1 \\ 0 & 1 & 0 \\ -1 & -\frac{h_1}{2} & 0 \end{bmatrix} \mathbf{U}_2 = \begin{bmatrix} 0 & \frac{h_2}{2} & 1 \\ 0 & 1 & 0 \\ -1 & \frac{h_1}{2} & 0 \end{bmatrix} \mathbf{U}_4, \tag{7.181}$$

which is taken as

$$\mathbf{U}_3 = \mathbf{R}_{31}\mathbf{U}_1 = \mathbf{R}_{32}\mathbf{U}_2 = \mathbf{R}_{33}\mathbf{U}_4, \tag{7.182}$$

with

$$\begin{aligned}\mathbf{a}^- &= \left[\mathbf{R}_{31}\mathbf{X}_1^-\right]^{-1}\left[\mathbf{X}_3^+\mathbf{e}^+ + \mathbf{X}_3^-\mathbf{e}^-\right], \\ \mathbf{b}^- &= \left[\mathbf{R}_{32}\mathbf{Y}_2^-\right]^{-1}\left[\mathbf{X}_3^+\mathbf{e}^+ + \mathbf{X}_3^-\mathbf{e}^-\right], \\ \mathbf{f}^+ &= \left[\mathbf{R}_{33}\mathbf{Y}_4^+\right]^{-1}\left[\mathbf{X}_3^+\mathbf{e}^+ + \mathbf{X}_3^-\mathbf{e}^-\right].\end{aligned} \tag{7.183}$$

The equilibrium equations at the joint, equation (7.157), where for this case we only consider $\mathbf{e}^-$, $\mathbf{a}^-$, $\mathbf{b}^-$, $\mathbf{e}^+$, and $\mathbf{f}^+$, become

$$\mathbf{Q}_2^-\mathbf{b}^- + \mathbf{Q}_3^+\mathbf{e}^+ + \mathbf{Q}_3^-\mathbf{e}^- + \mathbf{Q}_4^+\mathbf{f}^+ = \mathbf{Q}_1^-\mathbf{a}^-. \tag{7.184}$$

Then using equations (7.183) and (7.184) we can reduce everything in terms of one vector of coefficients

$$\mathbf{a}^- = \mathbf{t}_{31}\mathbf{e}^-, \quad \mathbf{b}^- = \mathbf{t}_{32}\mathbf{e}^-, \quad \mathbf{e}^+ = \mathbf{r}_{33}\mathbf{e}^-, \quad \mathbf{f}^+ = \mathbf{t}_{34}\mathbf{e}^-, \tag{7.185}$$

where the transmission $\mathbf{t}_{ij}$ and reflection matrices $\mathbf{r}_{ij}$ are

$$\begin{aligned}\mathbf{r}_{33} = &\left[\left(\mathbf{Q}_2^-\left[\mathbf{R}_{32}\mathbf{Y}_2^-\right]^{-1} + \mathbf{Q}_4^+\left[\mathbf{R}_{33}\mathbf{Y}_4^+\right]^{-1} - \mathbf{Q}_1^-\left[\mathbf{R}_{31}\mathbf{X}_1^-\right]^{-1}\right)\mathbf{X}_3^+ + \mathbf{Q}_3^+\right]^{-1} \times \\ &\left[\left(\mathbf{Q}_1^-\left[\mathbf{R}_{31}\mathbf{X}_1^-\right]^{-1} - \mathbf{Q}_2^-\left[\mathbf{R}_{32}\mathbf{Y}_2^-\right]^{-1} - \mathbf{Q}_4^+\left[\mathbf{R}_{33}\mathbf{Y}_4^+\right]^{-1}\right)\mathbf{X}_3^- - \mathbf{Q}_3^-\right],\end{aligned} \tag{7.186}$$

and

$$\begin{aligned}\mathbf{t}_{31} &= \left[\mathbf{R}_{31}\mathbf{X}_1^-\right]^{-1}\left[\mathbf{X}_3^+\mathbf{r}_{33}+\mathbf{X}_3^-\right],\\ \mathbf{t}_{32} &= \left[\mathbf{R}_{32}\mathbf{Y}_2^-\right]^{-1}\left[\mathbf{X}_3^+\mathbf{r}_{33}+\mathbf{X}_3^-\right],\\ \mathbf{t}_{34} &= \left[\mathbf{R}_{33}\mathbf{Y}_4^+\right]^{-1}\left[\mathbf{X}_3^+\mathbf{r}_{33}+\mathbf{X}_3^-\right].\end{aligned} \tag{7.187}$$

Case 4: Wave $\mathbf{f}^-$ causes reflection and transmission waves $\mathbf{a}^-$, $\mathbf{b}^-$, $\mathbf{e}^+$, $\mathbf{f}^+$. The displacements of each beam are

$$\begin{aligned}\mathbf{U}_4 &= \mathbf{Y}_4^+\mathbf{f}^+ + \mathbf{Y}_4^-\mathbf{f}^-,\\ \mathbf{U}_1 = \mathbf{X}_1^-\mathbf{a}^-,\quad \mathbf{U}_2 &= \mathbf{Y}_2^-\mathbf{b}^-,\quad \mathbf{U}_3 = \mathbf{X}_3^+\mathbf{e}^+.\end{aligned} \tag{7.188}$$

Applying continuity of displacements, we rewrite (7.162) in terms of $\mathbf{U}_4$,

$$\mathbf{U}_4 = \begin{bmatrix}0 & \frac{h_1}{2} & -1\\ 0 & 1 & 0\\ 1 & \frac{h_2}{2} & 0\end{bmatrix}\mathbf{U}_1 = \begin{bmatrix}1 & h_1 & 0\\ 0 & 1 & 0\\ 0 & 0 & 1\end{bmatrix}\mathbf{U}_2 = \begin{bmatrix}0 & \frac{h_1}{2} & -1\\ 0 & 1 & 0\\ 1 & -\frac{h_2}{2} & 0\end{bmatrix}\mathbf{U}_3, \tag{7.189}$$

which we rewrite as

$$\mathbf{U}_4 = \mathbf{R}_{41}\mathbf{U}_1 = \mathbf{R}_{42}\mathbf{U}_2 = \mathbf{R}_{43}\mathbf{U}_3, \tag{7.190}$$

$$\begin{aligned}\mathbf{a}^- &= \left[\mathbf{R}_{41}\mathbf{X}_1^-\right]^{-1}\left[\mathbf{Y}_4^+\mathbf{f}^+ + \mathbf{Y}_4^-\mathbf{f}^-\right],\\ \mathbf{b}^- &= \left[\mathbf{R}_{42}\mathbf{Y}_2^-\right]^{-1}\left[\mathbf{Y}_4^+\mathbf{f}^+ + \mathbf{Y}_4^-\mathbf{f}^-\right],\\ \mathbf{e}^+ &= \left[\mathbf{R}_{43}\mathbf{X}_3^+\right]^{-1}\left[\mathbf{Y}_4^+\mathbf{f}^+ + \mathbf{Y}_4^-\mathbf{f}^-\right].\end{aligned} \tag{7.191}$$

Lastly the equilibrium equations at the joint, equation (7.157), where for this case we only consider $\mathbf{f}^-$, $\mathbf{a}^-$, $\mathbf{b}^-$, $\mathbf{e}^+$ and $\mathbf{f}^+$, are

$$\mathbf{Q}_2^-\mathbf{b}^- + \mathbf{Q}_3^+\mathbf{e}^+ + \mathbf{Q}_4^+\mathbf{f}^+ + \mathbf{Q}_4^-\mathbf{f}^- = \mathbf{Q}_1^-\mathbf{a}^-. \tag{7.192}$$

Using equations (7.191) and (7.192) we can reduce everything to one vector of coefficients such that we can find the transmission $\mathbf{t}_{ij}$ and reflection matrices $\mathbf{r}_{ij}$ where

$$\mathbf{a}^- = \mathbf{t}_{41}\mathbf{f}^-,\quad \mathbf{b}^- = \mathbf{t}_{42}\mathbf{f}^-,\quad \mathbf{e}^+ = \mathbf{t}_{43}\mathbf{f}^-,\quad \mathbf{f}^+ = \mathbf{r}_{44}\mathbf{f}^-, \tag{7.193}$$

where

$$\mathbf{r}_{44} = \left[\left(\mathbf{Q}_2^-\left[\mathbf{R}_{42}\mathbf{Y}_2^-\right]^{-1} + \mathbf{Q}_3^+\left[\mathbf{R}_{43}\mathbf{X}_3^+\right]^{-1} - \mathbf{Q}_1^-\left[\mathbf{R}_{41}\mathbf{X}_1^-\right]^{-1}\right)\mathbf{Y}_4^+ + \mathbf{Q}_4^+\right]^{-1} \times \left[\left(\mathbf{Q}_1^-\left[\mathbf{R}_{41}\mathbf{X}_1^-\right]^{-1} - \mathbf{Q}_2^-\left[\mathbf{R}_{42}\mathbf{Y}_2^-\right]^{-1} - \mathbf{Q}_3^+\left[\mathbf{R}_{43}\mathbf{X}_3^+\right]^{-1}\right)\mathbf{Y}_4^- - \mathbf{Q}_4^-\right], \tag{7.194}$$

and

$$\begin{aligned}
\mathbf{t}_{41} &= \left[\mathbf{R}_{41}\mathbf{X}_1^-\right]^{-1}\left[\mathbf{Y}_4^+\mathbf{r}_{44} + \mathbf{Y}_4^-\right], \\
\mathbf{t}_{42} &= \left[\mathbf{R}_{42}\mathbf{Y}_2^-\right]^{-1}\left[\mathbf{Y}_4^+\mathbf{r}_{44} + \mathbf{Y}_4^-\right], \\
\mathbf{t}_{43} &= \left[\mathbf{R}_{43}\mathbf{X}_3^+\right]^{-1}\left[\mathbf{Y}_4^+\mathbf{r}_{44} + \mathbf{Y}_4^-\right].
\end{aligned} \tag{7.195}$$

Total reflection and transmission relations

Having gone through all four cases the total orthogonal joint relations are the sum of the four cases such that we sum equations (7.168) (7.177) (7.185) (7.193) to find

$$\begin{aligned}
\mathbf{a}^- &= \mathbf{r}_{11}\mathbf{a}^+ + \mathbf{t}_{21}\mathbf{b}^+ + \mathbf{t}_{31}\mathbf{e}^- + \mathbf{t}_{41}\mathbf{f}^-, \\
\mathbf{b}^- &= \mathbf{t}_{12}\mathbf{a}^+ + \mathbf{r}_{22}\mathbf{b}^+ + \mathbf{t}_{32}\mathbf{e}^- + \mathbf{t}_{42}\mathbf{f}^-, \\
\mathbf{e}^+ &= \mathbf{t}_{13}\mathbf{a}^+ + \mathbf{t}_{23}\mathbf{b}^+ + \mathbf{r}_{33}\mathbf{e}^- + \mathbf{t}_{43}\mathbf{f}^-, \\
\mathbf{f}^+ &= \mathbf{t}_{14}\mathbf{a}^+ + \mathbf{t}_{24}\mathbf{b}^+ + \mathbf{t}_{34}\mathbf{e}^- + \mathbf{r}_{44}\mathbf{f}^-.
\end{aligned} \tag{7.196}$$

Next we apply the Bloch-Floquet conditions.

7.6.2 Bloch-Floquet conditions

Referring to figure 7.20 we have the following relationships

$$\begin{aligned}
\mathbf{A}^+ &= \mathbf{X}_1^+(x = \frac{l_1}{2})\mathbf{a}^+, \quad \mathbf{a}^- = \mathbf{X}_1^-(x = \frac{l_1}{2})\mathbf{A}^-, \\
\mathbf{E}^+ &= \mathbf{X}_3^+(x = \frac{l_3}{2})\mathbf{e}^+, \quad \mathbf{e}^- = \mathbf{X}_3^-(x = \frac{l_3}{2})\mathbf{E}^-, \\
\mathbf{b}^+ &= \mathbf{Y}_2^+(y = \frac{l_2}{2})\mathbf{B}^+, \quad \mathbf{B}^- = \mathbf{Y}_2^-(y = \frac{l_2}{2})\mathbf{b}^-, \\
\mathbf{F}^+ &= \mathbf{Y}_4^+(y = \frac{l_4}{2})\mathbf{f}^+, \quad \mathbf{f}^- = \mathbf{Y}_4^-(y = \frac{l_4}{2})\mathbf{F}^-,
\end{aligned} \tag{7.197}$$

where $\mathbf{X}_m^\pm$ and $\mathbf{Y}_m^\pm$ are defined in equation (7.165). The Bloch conditions are

$$\mathbf{F}^+ = \mathbf{B}^+e^{-ik_2}, \quad \mathbf{F}^- = \mathbf{B}^-e^{-ik_2}, \quad \mathbf{E}^+ = \mathbf{A}^+e^{-ik_1}, \quad \mathbf{E}^- = \mathbf{A}^-e^{-ik_1}. \tag{7.198}$$

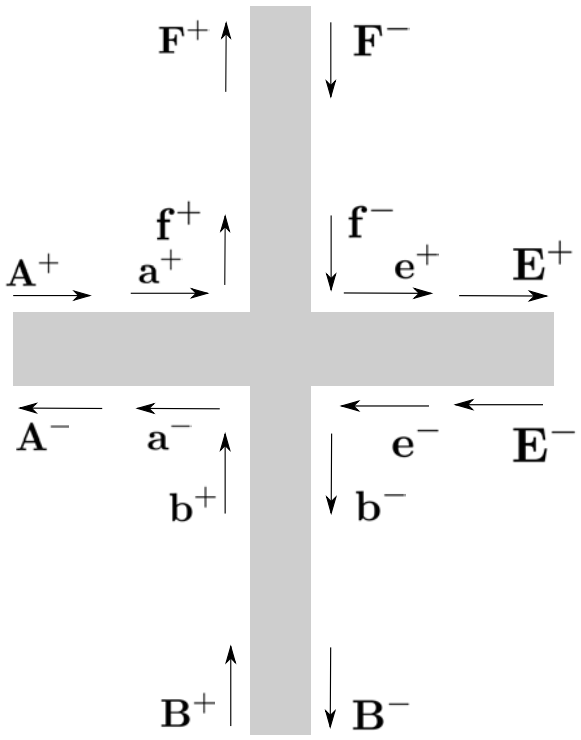

Figure 7.20: Waves to be considered of the square periodic cell.

The last step is to combine equations (7.197), (7.196), and (7.198) into the eigenvalue problem

$$\mathcal{A}(\omega, \mathbf{k})\mathbf{Z} = \mathbf{0}, \tag{7.199}$$

where we can find the elements

$$\begin{gathered}
\mathcal{A}_{1,1}=\mathbf{I},\quad \mathcal{A}_{1,2}=-\mathbf{X}_1^+(\frac{l_1}{2}),\quad \mathcal{A}_{2,3}=-X_1^-(\frac{l_1}{2}),\quad \mathcal{A}_{2,4}=\mathbf{I},\\
\mathcal{A}_{3,9}=\mathbf{I},\quad \mathcal{A}_{3,10}=-\mathbf{X}_3^+(\frac{l_3}{2}),\quad \mathcal{A}_{4,11}=-\mathbf{X}_3^-(\frac{l_3}{2}),\quad \mathcal{A}_{4,12}=\mathbf{I},\\
\mathcal{A}_{5,5}=-\mathbf{Y}_2^+(\frac{l_2}{2}),\quad \mathcal{A}_{5,6}=\mathbf{I},\quad \mathcal{A}_{6,7}=\mathbf{I},\quad \mathcal{A}_{6,8}=-\mathbf{Y}_2^-(\frac{l_2}{2}),\\
\mathcal{A}_{7,13}=\mathbf{I},\quad \mathcal{A}_{7,14}=-\mathbf{Y}_4^+(\frac{l_4}{2}),\quad \mathcal{A}_{8,15}=-\mathbf{Y}_{\mathbf{4}}^-(\frac{l_4}{2}),\quad \mathcal{A}_{8,16}=\mathbf{I},\\
\mathcal{A}_{9,2}=\mathbf{r}_{11},\quad \mathcal{A}_{9,4}=-\mathbf{I},\quad \mathcal{A}_{9,6}=\mathbf{t}_{21},\quad \mathcal{A}_{9,12}=\mathbf{t}_{31},\quad \mathcal{A}_{9,16}=\mathbf{t}_{41},\\
\mathcal{A}_{10,2}=\mathbf{t}_{12},\quad \mathcal{A}_{10,6}=\mathbf{r}_{22},\quad \mathcal{A}_{10,8}=-\mathbf{I},\quad \mathcal{A}_{10,12}=\mathbf{t}_{32},\quad \mathcal{A}_{10,16}=\mathbf{t}_{42},\\
\mathcal{A}_{11,2}=\mathbf{t}_{13},\quad \mathcal{A}_{11,6}=\mathbf{t}_{23},\quad \mathcal{A}_{11,10}=-\mathbf{I},\quad \mathcal{A}_{11,12}=\mathbf{r}_{33},\quad \mathcal{A}_{11,16}=\mathbf{t}_{43},\\
\mathcal{A}_{12,2}=\mathbf{t}_{14},\quad \mathcal{A}_{12,6}=\mathbf{t}_{24},\quad \mathcal{A}_{12,12}=\mathbf{t}_{34},\quad \mathcal{A}_{12,14}=-\mathbf{I},\quad \mathcal{A}_{12,16}=\mathbf{r}_{44},\\
\mathcal{A}_{13,5}=-\mathbf{I}e^{-ik_2},\quad \mathcal{A}_{13,13}=\mathbf{I},\quad \mathcal{A}_{14,7}=-\mathbf{I}e^{-ik_2},\quad \mathcal{A}_{14,15}=\mathbf{I},\\
\mathcal{A}_{15,1}=-\mathbf{I}e^{-ik_1},\quad \mathcal{A}_{15,9}=\mathbf{I},\quad \mathcal{A}_{16,3}=-\mathbf{I}e^{-ik_1},\quad \mathcal{A}_{16,11}=\mathbf{I},
\end{gathered} \tag{7.200}$$

otherwise $\mathcal{A}_{i,j}=\mathbf{0}$, and the coefficient matrix is

$$\mathbf{Z}=\begin{bmatrix}\mathbf{A}^+\\ \mathbf{a}^+\\ \mathbf{A}^-\\ \mathbf{a}^-\\ \mathbf{B}^+\\ \mathbf{b}^+\\ \mathbf{B}^-\\ \mathbf{b}^-\\ \mathbf{E}^+\\ \mathbf{e}^+\\ \mathbf{E}^-\\ \mathbf{e}^-\\ \mathbf{F}^+\\ \mathbf{f}^+\\ \mathbf{F}^-\\ \mathbf{f}^-\end{bmatrix}^T. \tag{7.201}$$

We note that each block of $\mathcal{A}_{i,j}$ is a 3×3. This method can be extended to other lattice types such as the hexagonal lattice done in [6]. We have reviewed this method as a comparison tool against that of section 7.5. Here Timoshenko beams were used which adds more complexity to the problem as the effect of shear deformation is included into the theory. It is also apparent that the reflection transmission method produces much larger matrices that must be solved for, this is seen in the square lattice example of section 7.5.5, where only a 3×3 matrix system needs to be solved.

7.7 Finite element approach

Using the standard stiffness and mass matrices of finite elements we can formulate the Bloch-Floquet problem by establishing constraints on the boundary nodal degrees of freedom of a unit cell. We review the work of Phani et al. [75] where hexagonal honeycomb structures made from Timoshenko beam elements is studied. The nodal displacements of point j on the lattice are defined by

$$\mathbf{q}_j = \begin{bmatrix} u_j \\ v_j \\ \phi_j \end{bmatrix}, \tag{7.202}$$

where u_j, v_j represent displacement along the x and y directions and ϕ_j represents a rotation about the z axis, which would disappear when working with solid elements. The periodic condition on the boundary nodes of the unit cell is

$$\mathbf{q}_j = \mathbf{q}_i e^{i(\mathbf{k}\cdot\mathbf{r}_{ij} - \omega t)}, \tag{7.203}$$

where $\mathbf{r}_{ij} = \mathbf{r}_j - \mathbf{r}_i$, is the vector between the two lattice points i and j. The standard equation of motion in finite elements is

$$\mathbf{M}\ddot{\mathbf{q}} + \mathbf{K}\mathbf{q} = \mathbf{f}, \tag{7.204}$$

where $\mathbf{M}$, $\mathbf{K}$ and $\mathbf{f}$ are the standard mass, stiffness and forcing matrices of the finite element method. For free wave motion we set $\mathbf{f}$ to zero and taking $e^{-i\omega t}$ time dependence we have

$$[-\omega^2\mathbf{M} + \mathbf{K}]\mathbf{q} = \mathbf{0}, \tag{7.205}$$

which is the standard eigenfrequency analysis. In order to produce the Bloch-Floquet analysis equation (7.205) is manipulated using a transformation matrix, $\mathbf{T}$, which is easiest to describe by an example. Consider the primitive cell given in figure 7.21 with nodal points $\mathbf{a}_i$ for $i = 1..6$. By the Bloch-Floquet conditions

$$\begin{aligned} \mathbf{q}_2 &= \mathbf{q}_5 e^{i\mathbf{k}\cdot\mathbf{r}_{25}}, \quad \mathbf{r}_{25} = \mathbf{a}_2 - \mathbf{a}_5, \\ \mathbf{q}_6 &= \mathbf{q}_1 e^{i\mathbf{k}\cdot\mathbf{r}_{61}}, \quad \mathbf{r}_{61} = \mathbf{a}_6 - \mathbf{a}_1. \end{aligned} \tag{7.206}$$

We apply the conditions via a matrix in the following manner

$$\mathbf{q} = \mathbf{T}\tilde{\mathbf{q}} \rightarrow \begin{bmatrix} \mathbf{q}_1 \\ \mathbf{q}_2 \\ \mathbf{q}_3 \\ \mathbf{q}_4 \\ \mathbf{q}_5 \\ \mathbf{q}_6 \end{bmatrix} = \begin{bmatrix} \mathbf{I} & \mathbf{0} & \mathbf{0} & \mathbf{0} \\ \mathbf{0} & \mathbf{I}e^{i\mathbf{k}\cdot\mathbf{r}_{25}} & \mathbf{0} & \mathbf{0} \\ \mathbf{0} & \mathbf{0} & \mathbf{I} & \mathbf{0} \\ \mathbf{0} & \mathbf{0} & \mathbf{0} & \mathbf{I} \\ \mathbf{0} & \mathbf{I} & \mathbf{0} & \mathbf{0} \\ \mathbf{I}e^{i\mathbf{k}\cdot\mathbf{r}_{61}} & \mathbf{0} & \mathbf{0} & \mathbf{0} \end{bmatrix} \begin{bmatrix} \mathbf{q}_1 \\ \mathbf{q}_5 \\ \mathbf{q}_3 \\ \mathbf{q}_4 \end{bmatrix}. \tag{7.207}$$

Then in order to change the eigenfrequency analysis from a single unit to a periodic structure with Bloch-Floquet conditions we transform equation (7.205) using the $\mathbf{T}$ matrix by taking

$$\mathbf{T}^H[-\omega^2\mathbf{M} + \mathbf{K}]\mathbf{T}\mathbf{q} = \mathbf{0}, \tag{7.208}$$

which is the general eigenvalue problem, where superscript ^{H} is the Hermitian transpose [75]. Solving the eigenvalue problem of equation (7.208) yields the dispersion behavior of the periodic structure. Next we write out a few stiffness and mass matrices for different types of beam elements. For the plane truss (PT) element

$$\mathbf{K}_{PT} = \frac{AE}{L}\begin{bmatrix} c^2 & cs & -c^2 & -cs \\ cs & s^2 & -cs & -s^2 \\ -c^2 & -cs & c^2 & cs \\ -cs & -s^2 & cs & s^2 \end{bmatrix}, \tag{7.209}$$

where A is the cross-sectional area, E the Young's modulus, L the length, $s = \sin\theta$, $c = \cos\theta$, and θ is the angle measured from the horizontal. The mass matrix is

$$\mathbf{M}_{PT} = \frac{\rho AL}{6}\begin{bmatrix} 2c^2 & 2cs & c^2 & cs \\ 2cs & 2s^2 & cs & s^2 \\ c^2 & cs & 2c^2 & 2cs \\ cs & s^2 & 2cs & 2s^2 \end{bmatrix}, \tag{7.210}$$

where ρ is the density of the element[3]. Lastly the elements must be assembled into a global matrix system and Bloch-Floquet conditions can be implemented. For plane frame (PF) elements the stiffness matrix is given as follows

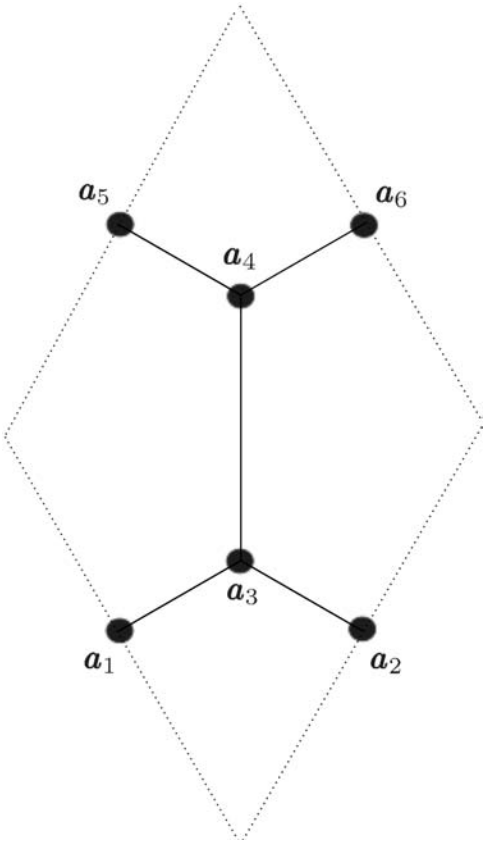

Figure 7.21: Elements of the primitive cell.

$$\mathbf{K}_{PF} = \frac{E}{L}\begin{bmatrix} AC^2 + \frac{12I}{L^2}S^2 & (A - \frac{12I}{L^2})CS & -\frac{6I}{L}S & -(AC^2 + \frac{12I}{L^2}S^2) & -(A - \frac{12I}{L^2})CS & -\frac{6I}{L}S \\ & AS^2 + \frac{12I}{L^2}C^2 & \frac{6I}{L}C & -(A - \frac{12I}{L^2})CS & -(AS^2 + \frac{12I}{L^2}C^2) & \frac{6I}{L}C \\ & & 4I & \frac{6I}{L}S & -\frac{6I}{L}C & 2I \\ & SYM.. & & AC^2 + \frac{12I}{L^2}S^2 & (A - \frac{12I}{L^2})CS & \frac{6I}{L}S \\ & & & & AS^2 + \frac{12I}{L^2}C^2 & -\frac{6I}{L}C \\ & & & & & 4I \end{bmatrix}, \tag{7.211}$$

where $\mathbf{K}_{PF}$ is written in global coordinates with $C = \cos\theta$ and $S = \sin\theta$. The mass matrix for this element is

$$\mathbf{M}'_{PF} = \frac{\rho AL}{420}\begin{bmatrix} 140 & 0 & 0 & 70 & 0 & 0 \\ 0 & 156 & 22L & 0 & 54 & -13L \\ 0 & 22L & 4L^2 & 0 & 13L & -3L^2 \\ 70 & 0 & 0 & 140 & 0 & 0 \\ 0 & 54 & 13L & 0 & 156 & -22L \\ 0 & -13L & -3L^2 & 0 & -22L & 4L^2 \end{bmatrix}, \tag{7.212}$$

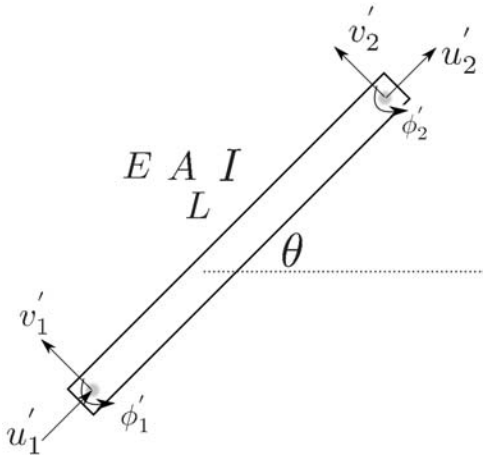

Figure 7.22: Plane frame element where prime denotes local coordinates.

which is written in local coordinates and can be transformed to the global coordinates using the transformation matrix

$$\mathbf{R} = \begin{bmatrix} C & S & 0 & 0 & 0 & 0 \\ -S & C & 0 & 0 & 0 & 0 \\ 0 & 0 & 1 & 0 & 0 & 0 \\ 0 & 0 & 0 & C & S & 0 \\ 0 & 0 & 0 & -S & C & 0 \\ 0 & 0 & 0 & 0 & 0 & 1 \end{bmatrix}, \tag{7.213}$$

such that

$$\mathbf{M} = \mathbf{R}^T \mathbf{M}' \mathbf{R}. \tag{7.214}$$

Next we derive the finite element matrices for Timoshenko beams.

7.7.1 Timoshenko beam element

The one dimensional finite element matrices for the Timoshenko beam are give in [83] as $\mathbf{K} = \mathbf{K}_b + \mathbf{K}_s$ where

$$\mathbf{K}_b = \frac{EI}{L} \begin{bmatrix} 0 & 0 & 0 & 0 \\ 0 & 1 & 0 & -1 \\ 0 & 0 & 0 & 0 \\ 0 & -1 & 0 & 1 \end{bmatrix}, \quad \mathbf{K}_s = \frac{\mu GA}{4l} \begin{bmatrix} 4 & 2l & -4 & 2l \\ 2l & l^2 & -2l & l^2 \\ -4 & -2l & 4 & -2l \\ 2l & l^2 & -2l & l^2 \end{bmatrix} \tag{7.215}$$

with μ being a correction shear factor usually taken as 5/6 for rectangular sections and with Poisson's ratio close to one third.

In two dimensions we go through the derivation of the finite element matrices as done in [75] and seek to explicitly write out the terms. We define $\mathbf{q}_r(t)$ as having the six nodal degrees of freedom at the two nodes of each element with

$$\mathbf{q}_r(t) = \Big[u_1(t), \quad v_1(t), \quad \theta_{z1}(t), \quad u_2(t), \quad v_2(t), \quad \theta_{z2}(t)\Big]^T. \tag{7.216}$$

The displacements at a position x and time t are given by

$$u(x,t) = \sum_{r=1}^{6} a_r(x) q_r(t), \quad v(x,t) = \sum_{r=1}^{6} b_r(x) q_r(t), \quad \theta_z(x,t) = \sum_{r=1}^{6} c_r(x) q_r(t), \tag{7.217}$$

where the shape functions $a_r,\ b_r,\ c_r$ for $r = 1..6$ are given by

$$\begin{aligned}
&a_1 = \frac{1}{2}(1-\zeta), \quad a_2 = 0, \quad a_3 = 0, \quad a_4 = \frac{1}{2}(1+\zeta), \quad a_5 = 0, \quad a_6 = 0,\\
&b_1 = 0, \quad b_2 = \frac{1}{4(1+3\beta)}[2+6\beta-3(1+2\beta)\zeta+\zeta^3],\\
&b_3 = \frac{1}{4(1+3\beta)}[1+3\beta-\zeta-(1+3\beta)\zeta^2+\zeta^3], \quad b_4 = 0,\\
&b_5 = \frac{1}{4(1+4\beta)}[2+6\beta+3(1+2\beta)\zeta-\zeta^3],\\
&b_6 = \frac{1}{4(1+3\beta)}[-(1+3\beta)-\zeta+(1+3\beta)\beta^2+\zeta^3],\\
&c_1 = 0, \quad c_2 = \frac{1}{4(1+3\beta)}(-3+3\zeta^2),\\
&c_3 = \frac{1}{4(1+3\beta)}[-1+6\beta-(2+6\beta)\zeta+3\zeta^2], \quad c_4 = 0,\\
&c_5 = \frac{1}{4(1+3\beta)}(3-3\zeta^2), \quad c_6 = \frac{1}{4(1+3\beta)}[-1+6\beta+(2+6\beta)\zeta+3\zeta^2],
\end{aligned} \tag{7.218}$$

with

$$\zeta = \frac{x}{L}, \quad \text{and} \quad \beta = \frac{EI_z}{\kappa GAL^2}, \tag{7.219}$$

again κ is the shear correction factor in Timoshenko beam theory. The kinetic and potential energies per unit thickness are

$$\begin{aligned}
T &= \frac{1}{2}\int_{-L/2}^{L/2} \rho d\dot{u}^2 \,\mathrm{d}\,x + \frac{1}{2}\int_{-L/2}^{L/2} \rho d\dot{v}^2 \,\mathrm{d}\,x + \frac{1}{2}\int_{-L/2}^{L/2} \rho I_z \dot{\theta_z}^2 \,\mathrm{d}\,x,\\
U &= \frac{1}{2}\int -L/2^{L/2} Ed\Big(\frac{\mathrm{d}\,u}{\mathrm{d}\,x}\Big)^2 \,\mathrm{d}\,x + \frac{1}{2}\int_{-L/2}^{L/2} EI_z\Big(\frac{\mathrm{d}\,\theta_z}{\mathrm{d}\,x}\Big)^2 \,\mathrm{d}\,x + \frac{1}{2}\int_{-L/2}^{L/2} \kappa dG\Big(\frac{\mathrm{d}\,v}{\mathrm{d}\,x} - \theta_z\Big)^2 \,\mathrm{d}\,x.
\end{aligned} \tag{7.220}$$

Applying equation (7.217) to equation (7.220) we have

$$\begin{aligned} T &= \frac{1}{2}\sum_{r=1}^{6}\sum_{s=1}^{6}\dot{q}_r\dot{q}_s\int_{-L/2}^{L/2}\rho(da_ra_s + db_rb_s + I_zc_rc_s)\,\mathrm{d}\,x, \\ U &= \frac{1}{2}\sum_{r=1}^{6}\sum_{s=1}^{6}q_rq_s\int_{-L/2}^{L/2}[Eda_r^{'}a_s^{'} + EI_zb_r^{''}b_s^{''} + \kappa Gd(b_r^{'} - c_r)(b_s^{'} - c_s)]\,\mathrm{d}\,x. \end{aligned} \tag{7.221}$$

Then by using the Euler-Lagrangian equations of motion

$$\frac{\mathrm{d}}{\mathrm{d}\,t}\Big(\frac{\partial\mathcal{L}}{\partial\dot{q}_r}\Big) - \frac{\partial\mathcal{L}}{\partial q_r} = f_r, \tag{7.222}$$

where $\mathcal{L} = T - U$, or

$$\frac{\mathrm{d}}{\mathrm{d}\,t}\Big(\frac{\partial T}{\partial\dot{q}_r}\Big) - \frac{\partial U}{\partial q_r} = f_r, \tag{7.223}$$

we can generate the mass and stiffness matrices. These matrices are left to be assembled however the terms $\frac{\partial T}{\partial\dot{q}_r}$ and $\frac{\partial U}{\partial q_r}$ have been found where

$$\begin{aligned}
&\frac{\partial U}{\partial q_1} = \frac{Ed(q_1 - q_4)}{4L}, \\
&\frac{\partial U}{\partial q_2} = \frac{1}{1280L^3(1+3\beta)^2}\Big[\\
&\quad q_2(240EI_z + \kappa GdL^2(-1218L + 609(1+L^2) + 2640\beta + 2880\beta^2 - 2640L\beta)) + \\
&\quad q_3(240EI_z + \kappa GdL^2(-338L + 169(1+L^2) + 360\beta - 1320L^2\beta + 960L\beta + 2880L\beta^2)) + \\
&\quad q_5(-240EI_z + \kappa GdL^2(-2880\beta^2 - 609(1+L^2) + 1218L - 2640\beta + 2640L\beta)) + \\
&\quad q_6(240EI_z + \kappa GdL^2(960L\beta + 2880L\beta^2 + 169(1+L^2) - 338L + 360\beta - 1320L^2\beta))\Big], \\
&\frac{\partial U}{\partial q_3} = \frac{1}{3840L^3(1+3\beta)^2}\Big[\\
&\quad q_2(720EI_z + \kappa GdL^2(-1014L + 507(1+L^2) - 3960L^2\beta + 8640L\beta^2 + 1080\beta + 2880L\beta)) + \\
&\quad q_3(EI_z(1680 + 5760\beta + 8640\beta^2) + \kappa GdL^2(-454L + 227(1+L^2) + 720\beta^2 + \\
&\quad 9360L^2\beta^2 + 480\beta - 1680L^2\beta + 1200L\beta - 1440L\beta^2)) + \\
&\quad q_5(-720EI_z + \kappa GdL^2(1014L - 507(1+L^2) + 3960L^2\beta - 8640L\beta^2 - 1080\beta - 2880L\beta)) + \\
&\quad q_6(720EI_z + \kappa GdL^2(2640L\beta + 720L\beta^2 + 147 + 67L^2 - 214L + 7920L^2\beta^2 - 2640L^2\beta))\Big], \\
&\frac{\partial U}{\partial q_4} = \frac{Ed(q_4 - q_1)}{4L}, \\
&\frac{\partial U}{\partial q_5} = \frac{-1}{1280L^3(1+3\beta)^2}\Big[\\
&\quad q_2(240EI_z + \kappa GdL^2(-1218L + 609(1+L^2) + 2640\beta + 2880\beta^2 - 2640L\beta)) + \\
&\quad q_3(240EI_z + \kappa GdL^2(-338L + 169(1+L^2) + 360\beta - 1320L^2\beta + 960L\beta + 2880L\beta^2)) + \\
&\quad q_5(-240EI_z + \kappa GdL^2(-2880\beta^2 - 609(1+L^2) + 1218L - 2640\beta + 2640L\beta)) + \\
&\quad q_6(240EI_z + \kappa GdL^2(960L\beta + 2880L\beta^2 + 169(1+L^2) - 338L + 360\beta - 1320L^2\beta))\Big], \\
&\frac{\partial U}{\partial q_6} = \frac{1}{3840L^3(1+3\beta)^2}\Big[\\
&\quad q_2(720EI_z + \kappa GdL^2(-1014L + 507(1+L^2) - 3960L^2\beta + 8640L\beta^2 + 1080\beta + 2880L\beta)) + \\
&\quad q_3(720EI_z + \kappa GdL^2(-214L + 67L^2 + 7920L^2\beta^2 + 147 - 2640L^2\beta + 2640L\beta + 720L\beta^2)) \\
&\quad q_5(-720EI_z + \kappa GdL^2(1014L - 507(1+L^2) + 3960L^2\beta - 8640L\beta^2 - 1080\beta - 2880L\beta)) + \\
&\quad q_6(720EI_z + \kappa GdL^2(2160L\beta + 147 - 294L + 227L^2 + 9360L^2\beta^2 - 1680L^2\beta))\Big],
\end{aligned} \tag{7.224}$$

$$
\begin{aligned}
\frac{\partial T}{\partial \dot{q}_1} &= \frac{\rho d L(13\dot{q}_1 + 11\dot{q}_4)}{48}, \\
\frac{\partial T}{\partial \dot{q}_2} &= \frac{\rho L}{107520(1+3\beta)^2}\Big[\\
&\quad \dot{q}_2\big(51156 I_z + d(31431 + 180432\beta + 262080\beta^2)\big) + \\
&\quad \dot{q}_3\big(I_z(14196 - 110880\beta) + d(13679 + 76776\beta + 110880\beta^2)\big) + \\
&\quad \dot{q}_5\big(-51156 I_z + d(22329 + 142128\beta + 221760\beta^2)\big) + \\
&\quad \dot{q}_6\big(I_z(14196 - 110880\beta) + d(-12081 - 77784\beta - 107520\beta^2 + 80640\beta^3 + 120960\beta^4)\big)\Big], \\
\frac{\partial T}{\partial \dot{q}_3} &= \frac{\rho L}{107520(1+3\beta)^2}\Big[\\
&\quad \dot{q}_2\big(I_z(14196 - 110880\beta) + d(13679 + 76776\beta + 110880\beta^2)\big) + \\
&\quad \dot{q}_3\big(I_z(6356 - 47040\beta + 262080\beta^2) + d(6091 + 34104\beta + 51156\beta^2)\big) + \\
&\quad \dot{q}_5\big(I_z(-14196 + 110880\beta) + d(10961 + 71064\beta + 110880\beta^2)\big) + \\
&\quad \dot{q}_6\big(I_z(1876 - 73920\beta + 221760\beta^2) + d(-5753 - 36960\beta - 49280\beta^2 + 36960\beta^3 + 55440\beta^4)\big)\Big], \\
\frac{\partial T}{\partial \dot{q}_4} &= \frac{\rho d L(11\dot{q}_1 + 13\dot{q}_4)}{48}, \\
\frac{\partial T}{\partial \dot{q}_5} &= \frac{\rho L}{107520(1+3\beta)^2}\Big[\\
&\quad \dot{q}_2\big(-51156 I_z + d(22329 + 142128\beta + 221760\beta^2)\big) + \\
&\quad \dot{q}_3\big(I_z(-14196 + 110880\beta) + d(10961 + 71064\beta + 110880\beta^2)\big) + \\
&\quad \dot{q}_5\big(51156 I_z + d(31431 + 180432\beta + 262080\beta^2)\big) + \\
&\quad \dot{q}_6\big(I_z(-14196 + 110880\beta) + d(-14799 - 83496\beta - 107520\beta^2 + 80640\beta^3 + 120960\beta^4)\big)\Big], \\
\frac{\partial T}{\partial \dot{q}_6} &= \frac{\rho L}{107520(1+3\beta)^2}\Big[\\
&\quad \dot{q}_2\big(I_z(14196 - 110880\beta) + d(-12081 - 77784\beta - 107520\beta^2 + 80640\beta^3 + 120960\beta^4)\big) + \\
&\quad \dot{q}_3\big(I_z(1876 - 73920\beta + 221760\beta^2) + d(-5753 - 36960\beta - 49280\beta^2 + 36960\beta^3 + 55440\beta^4)\big) + \\
&\quad \dot{q}_5\big(I_z(-14196 + 110880\beta) + d(-14799 - 83496\beta - 107520\beta^2 + 80640\beta^3 + 120960\beta^4)\big) + \\
&\quad \dot{q}_6\big(I_z(6356 - 47040\beta + 262080\beta^2) + d(7127 + 40320\beta + 47040\beta^2 - 80640\beta^3 \\
&\quad - 114240\beta^4 + 40320\beta^5 + 60480\beta^6)\big)\Big].
\end{aligned}
\tag{7.225}
$$

Again by plugging these terms into equation (7.223) the mass and stiffness matrices can be found. This is reviewed here to give another method to compare to. It also gives the reader some insight into what is occurring in finite element packages and can be implemented in MATLAB for relatively simple structures. Also noted here is that the spacing of nodes when discretizing structures with finite elements should be one sixth of the wavelength or smaller. That is for a wave to be accurately registered by the method in the structure there should be at least six nodes per wavelength. We leave this section as a review which can be used in future investigation. Lastly further research of Bloch-Floquet problems using finite elements, in this thesis, is used with COMSOL using solid elements. We use the results of section 7.5 later as a comparison tool for when the geometry becomes more complicated as is the case when developing Metal Water which is described in the next chapter.

Chapter 8

Designing Metal Water I

Having reviewed static homogenization methods in chapter 6 and dynamic methods in chapter 7 we are equipped with the tools necessary to design and evaluate metamaterial devices. As a first step we focus the objective to finding a metallic foam that has the same acoustic properties of water. We call this material Metal Water. Since water is isotropic and inviscid the first requirement is that the material also be isotropic and have very small shear modulus compared with it's bulk modulus. Small shear modulus is a defining characteristic of pentamode materials required for transformation acoustics as discussed in section 5.1. The other requirement is that the solid have the same overall density as the fluid. The design process for creating a structured material that can mimic the acoustic properties of water consists of utilizing the analytic static homogenization theory of section 6.1 until a design that can closely match the elastic and density properties of water comes about. This is done in section 8.1. To finalize the design an iterative process is done using the finite element homogenization technique of Hinton and Hassani [69, 70, 71] which was heavily reviewed in section 6.2. Results of the static finite element method are shown in section 8.2. Once the design is finalized we further investigate dynamic properties of the prototype by generating dispersion curves using the Bloch-Floquet theories discussed in chapter 7, however COMSOL is used primarily for this process, results are shown in section 8.3. Additional designs that are easier to produce are considered in section 8.4.

8.1 Analytical static homogenization

Designs for Metal Water are first proposed and evaluated using the static homogenization technique of section 6.1. This first step in prototyping gives a quick estimation on

the elastic properties of proposed structures. Density properties can quickly be determined from the ratio of solid to void filling space in a unit cell design. Furthermore we are considering water as an isotropic material with zero shear modulus, as it is a type of pentamode material as discussed in section 5.1. Designs that have regular hexagonal structure are considered as analysis of equation (6.5) with associated figure 8.1 and subsequent analysis from figure 6.3 displays this result. The regular hexagon has $h = l$

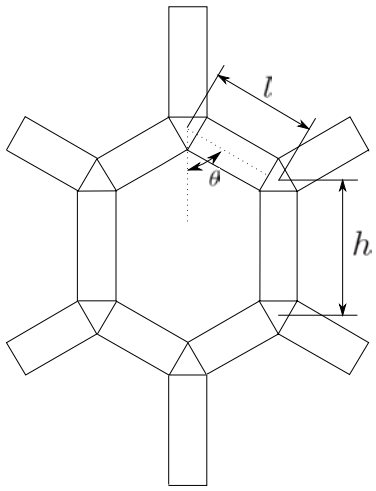

Figure 8.1: General cellular structure.

and $\theta = \pi/3$ with parameters shown in figure 8.1. Using equations (6.1), (6.2) and (6.3) we have isotropy, with $E_1^* = E_2^* = E^*$, $\nu_{12}^* = \nu_{21}^* = \nu^*$ and $E^* = 2G^*(1 + \nu^*)$, where

$$E^* = \frac{2}{\sqrt{3}b(N' + 3M)}, \quad \nu^* = \frac{N_l' - M_l}{N' + 3M}, \tag{8.1}$$

and $N' = N_l' = N_h'$, $M = M_l = M_h$. These moduli are for plane strain which is a good approximation as we expect to create materials that have relatively large thickness compared to other cell dimensions. Using equation (6.4), the effective elasticity of a regular hexagonal foam is therefore

$$\mathbf{C} = \frac{\sqrt{3}}{12M(N' + M)b} \begin{pmatrix} N' + 3M & N' - M & 0 \\ N' - M & N' + 3M & 0 \\ 0 & 0 & 2M \end{pmatrix}, \tag{8.2}$$

which is the same result reported by [84] but with N replaced by N'. The effective elasticity is isotropic since $C_{11} = C_{22} \equiv \lambda_* + 2\mu_*$ and $C_{66} = \frac{1}{2}(C_{11} - C_{12}) = G^* \equiv \mu_*$,

where λ_*, μ_*, are the effective Lamé moduli. Hence,

$$\lambda_* = \frac{\sqrt{3}}{12Mb}\left(\frac{1-\delta}{1+\delta}\right), \quad \mu_* = \frac{2\delta\lambda_*}{1-\delta}, \quad \text{where } \delta = \frac{M}{N'}. \tag{8.3}$$

Note that the effective Poisson's ratio, defined by $\lambda_*/\mu_* = 2\nu_*/(1-2\nu_*)$, is related to the plane strain one by $\nu_* = \nu^*/(1+\nu^*)$. So, $\nu_* \approx \frac{1}{2}$, indicating the near-incompressibility of the foam relative to the ease of shearing. In order to mimic the acoustic properties of water we first match the group velocity as studied previously in section 2.2.2. Using equation (2.51) the group velocity for longitudinal wave motion in elastic media is $c_P = \sqrt{C_{11}/\rho}$ where for a fluid the speed is given by $\sqrt{K/\rho}$, where K is the fluid's bulk modulus. In matching the density we must also equate $C_{11} = K$ in order to get the same wave speed behavior. Using equation (8.2) the effective bulk modulus is

$$K = \frac{\sqrt{3}(N'+3M)}{12M(N'+M)b}. \tag{8.4}$$

A simple geometry with uniform thickness function, $t(x) = t$, using figure 8.2 as reference, means the axial and bending compliance are

$$M = \frac{l}{2btE}, \quad N = \frac{l^3}{2bt^3E}. \tag{8.5}$$

For this case using equation (6.2) we see $N' \approx N$ and we can take the parameter $\delta = \frac{t^2}{l^2}$, which is expected to be small in order for the theories of section 6.1 to be valid. The area fraction of solid is $\phi = A_m/A$, where A_m and A are the area of material and the total area of the fundamental unit cell respectively. Using figure 8.2 the area fraction

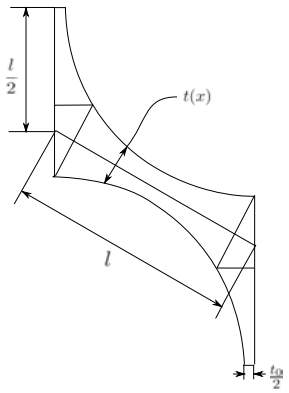

Figure 8.2: Quarter unit cell configuration. Thickness is symmetric about the center line of each member.

can be found where

$$\phi = \frac{2}{\sqrt{3}}\frac{t}{l} \quad \Rightarrow \quad \delta = \frac{3}{4}\phi^2. \tag{8.6}$$

The acoustic fluid has density ρ_f and elasticity defined by

$$\mathbf{C} = \begin{pmatrix} K & K & 0 \\ K & K & 0 \\ 0 & 0 & 0 \end{pmatrix}, \tag{8.7}$$

where K is the fluid bulk modulus. Fluid-like behavior therefore requires

$$\rho_{eff} \approx \rho_f, \quad C_{11} \approx C_{12} \approx K, \quad C_{66} \ll C_{11}, \tag{8.8}$$

where we have taken C_{66} to be small compared to other elasticity components in order to have pentamode like behavior while finding structures that can maintain shape. Using $\rho_{eff} = \phi\rho_s$, where ρ_s is the density of solid material, the three conditions of equation (8.8) are satisfied if

$$\frac{\rho_f}{\rho_s} = \phi, \quad \frac{K}{E} = \frac{1}{4}\phi, \quad \phi \ll 1. \tag{8.9}$$

Hence, we must have

$$\rho_s \gg \rho_f \quad \text{and} \quad \frac{E}{\rho_s} = 4\frac{K}{\rho_f}. \tag{8.10}$$

The first condition is satisfied if the foam is made of a much heavier material than the fluid. The second condition will not in general be satisfied, since it requires a very special relation between the solid and the fluid properties. Additionally trying to equate, $C_{11} = C_{22} = C_{12} = K$, is not possible as setting $C_{11} = C_{12}$ from (8.2) yields $4M = 0$. This means for hexagonal foams it is impossible to have $C_{11} = C_{12}$ exactly, so instead we minimize the function

$$F = \big[(C_{11} - K)^2 + (C_{12} - K)^2\big] = \frac{1}{24}\big[48K^2 + \frac{1}{M^2} - \frac{8\sqrt{3}K}{M} + \frac{4}{(M + N')^2}\big]. \tag{8.11}$$

In order to minimize F we take $\partial F/\partial M = 0$ and $\partial F/\partial N^{'} = 0$ resulting in

$$\begin{aligned} \frac{\partial F}{\partial M} &= \frac{1}{24}\big[\frac{8\sqrt{3}KM - 2}{M^3} - \frac{8}{(M + N')^3}\big] = 0, \\ \frac{\partial F}{\partial N'} &= -\frac{1}{3(M + N')^3} = 0, \end{aligned} \tag{8.12}$$

the second relation gives $M + N^{'} >> 1$ the first yields

$$8\sqrt{3}KM - 2 = \left(\frac{2M}{M + N'}\right)^3. \tag{8.13}$$

Trying a perturbation based on a small parameter ϵ where $N^{'} >> M$ in general, we take $N^{'} \propto \mathcal{O}(\frac{1}{\epsilon})$ and $M \propto \mathcal{O}(1)$. We see $\frac{\partial F}{\partial N'} \propto \mathcal{O}(\epsilon^3)$. Setting $N^{'} = \epsilon^{-1}n$ we rewrite equation (8.13) as

$$8\sqrt{3}KM - 2 - \frac{8\epsilon^3 M^3}{(M\epsilon + n)^3} = 0. \tag{8.14}$$

If we take the perturbation expansion of M as $M \approx M_0 + \epsilon M_1 + \epsilon^2 M_2 + \mathcal{O}(\epsilon^3)$. Equation (8.14) becomes

$$8\sqrt{3}K(M_0 + \epsilon M_1 + \epsilon^2 M_2) - 2 = \left(\frac{2(M_0 + \epsilon M_1 + \epsilon^2 M_2)}{M_0 + \epsilon M_1 + \epsilon^2 M_2 + N'}\right)^3, \tag{8.15}$$

which yields the following equations in orders of ϵ

$$\begin{aligned}
\mathcal{O}(\epsilon^0) \quad & 8\sqrt{3}KM_0^4 - 2N^{'3} + 2M_0N^{'2}(-3 + 4\sqrt{3}KN^{'}) + 6M_0^2N^{'}(-1 + 4\sqrt{3}KN^{'}) + 2M_0^3(-5 + 12\sqrt{3}KN^{'}) = 0, \\
\mathcal{O}(\epsilon) \quad & 2M_1(4\sqrt{3}K(M_0 + N^{'})^2(4M_0 + N^{'}) - 3(5M_0^2 + 2M_0N^{'} + N^{'2})) = 0, \\
\mathcal{O}(\epsilon^2) \quad & 6M_1^2(-5M_0 - N^{'} + 4\sqrt{3}K(M_0 + N^{'})(2M_0 + N^{'})) + 2M_2(4\sqrt{3}K(M_0 + N^{'})^2(4M_0 + N^{'}) \\
& - 3(5M_0^2 + 2M_0N^{'} + N^{'2})) = 0.
\end{aligned} \tag{8.16}$$

Solving the equations of (8.16) gives $M_1 = M_2 = 0$, such that we can take $M \approx M_0$ and find equation (8.14) becomes

$$8\sqrt{3}KM - 2 = \left(\frac{2M}{M + N'}\right)^3. \tag{8.17}$$

This relation between M and $N^{'}$ minimizes equation (8.11) which allows for the C_{11} and C_{12} moduli to be closely valued.

8.1.1 Hexagonal foams with varying thickness

The analysis of the previous section suggests that a hex-metal foam with uniformly thick struts will not work unless the metal happens to satisfy equation (8.10), which is unlikely. Considering beams with thickness, $t(x)$, that varies along the length the axial and bending compliances are

$$M = \frac{1}{E}\int_0^{l/2} \frac{\mathrm{d}\,x}{A(x)}, \quad N = \frac{1}{E}\int_0^{l/2} \frac{x^2\,\mathrm{d}\,x}{I(x)}, \tag{8.18}$$

where $A(x) = bt(x)$ and $I(x) = \frac{1}{12}bt^3(x)$. The area of the unit cell is unchanged since it only depends on l, which is seen from figure 8.2. The area of the unit cell is $A = \frac{3\sqrt{3}l^2}{4}$ and the area the material occupies within the unit cell is approximately

$$A_m \approx \int_0^{l/2} \frac{t(x)}{2}\,\mathrm{d}\,x + \int_{-l/2}^{l/2} t(x)\,\mathrm{d}\,x + \int_0^{l/2} \frac{t(x)}{2}\,\mathrm{d}\,x = 3\int_0^{l/2} t(x)\,\mathrm{d}\,x, \tag{8.19}$$

where we have ignored the junction. The area fraction of solid, $\phi = A_m/A$, is

$$\phi \approx \frac{4}{l^2\sqrt{3}} \int_0^{l/2} t(x)\,\mathrm{d}\,x. \tag{8.20}$$

The main conditions are matching the density, equation $(8.9)_1$, $K \approx \lambda_*$, equation (8.3), and that the shear modulus is small, which requires

$$\frac{\rho_f}{\rho_s} = \frac{2}{\sqrt{3}} \frac{\int_0^l t\,\mathrm{d}\,x}{l^2}, \quad \frac{K}{E} = \frac{\sqrt{3}}{12b} \frac{1}{\int_0^l t^{-1}\,\mathrm{d}\,x}, \quad \delta \ll 1. \tag{8.21}$$

For a given fluid (water) and metal, these define constraints on the tapering of the beams. Considering the joints are not accounted for in the stiffness analysis Kim and Al-Hassani [85] introduced an effective half length L_j to attain more accurate results. Close inspection of the area integrals or for the equations that calculate M and N we see some parts of the geometry are integrated twice while others are left out. The proposed effective half wall length is

$$L_j = \frac{l}{2} - \frac{t}{2\cos(\theta)} j, \tag{8.22}$$

where j, the joint stiffening factor, can be obtained from comparison with results of finite element analysis and t, here, is the thickness at the cell wall joint.

8.1.2 Hex foam with circular holes

Looking for simple geometry that is easily machinable we consider a thickness function that comes about from drilling holes into a plate. The geometry is represented in figure 8.2, with examples located in figures 8.5 and 8.6. The holes are of radius r and the minimum thickness is t_0, located at the center of a strut member. The area fraction of solid is then

$$\phi = 1 - \frac{\pi}{2\sqrt{3}}\big(1 + \frac{t_0}{2r}\big)^{-2} = 1 - \frac{2\pi}{3\sqrt{3}}\big(\frac{r}{l}\big)^2, \tag{8.23}$$

which must satisfy the condition $\phi > \phi_0$, where ϕ_0 would represent the area fraction when t_0 goes to zero. The minimum is $\phi_0 = 1 - \frac{\pi}{2\sqrt{3}} = 0.0931$, for $t_0 = 0$. Thus,

$$\phi = 1 - \frac{1-\phi_0}{\alpha^2} \quad \text{with} \quad \alpha = 1 + \frac{t_0}{2r}. \tag{8.24}$$

The normalized bulk modulus from equation (8.21) is

$$\gamma \equiv \frac{K}{E} = \frac{\sqrt{3}}{12}\Big(\int_0^{l/2} \frac{\mathrm{d}\,x}{t(x)}\Big)^{-1}, \tag{8.25}$$

where the thickness function for the circular hole pattern is

$$t(x) = 2r\big(\alpha - \sqrt{1-(x/r)^2}\big). \tag{8.26}$$

Applying equation (8.26) to (8.25) the normalized bulk modulus is

$$\gamma = \frac{\sqrt{3}}{6}\left\{\frac{2\alpha}{\sqrt{\alpha^2-1}}\tan^{-1}\left(\sqrt{\frac{\alpha+1}{\alpha-1}}\tan\frac{\psi}{2}\right) - \psi\right\}^{-1}, \ \psi = \psi_j, \tag{8.27}$$

where, $\sin\psi_j \equiv \frac{L_j}{r}$.

Evaluation of M and N for the circular hole model

We note that

$$l = \frac{2}{\sqrt{3}}(r + \frac{t_0}{2}). \tag{8.28}$$

The expression for M follows from equations (8.18) and (8.26), using the substitution $x = r\sin\psi$,

$$\begin{aligned} M &= \frac{1}{E}\int_0^{L_j}\frac{\mathrm{d}\,x}{A(x)} = \frac{1}{bE}\int_0^{L_j}\frac{\mathrm{d}\,x}{t(x)} = \frac{1}{2bEr}\int_0^{L_j}\frac{\mathrm{d}\,x}{\alpha - \sqrt{1-(\frac{x}{r})^2}} \\ &= \frac{1}{2bE}\int_0^{\psi_j}\frac{\cos\psi\,\mathrm{d}\,\psi}{\alpha-\cos\psi}, \end{aligned} \tag{8.29}$$

where ψ_j is defined in equation (8.27). Similarly, the expression for N is

$$N = \frac{1}{E}\int_0^{L_j}\frac{x^2\,\mathrm{d}\,x}{I(x)} = \frac{12}{bE}\int_0^{L_j}\frac{x^2}{t(x)^3}\,\mathrm{d}\,x = \frac{3}{2bE}\int_0^{\psi_j}\frac{\sin^2\psi\cos\psi}{(\alpha-\cos\psi)^3}\,\mathrm{d}\,\psi. \tag{8.30}$$

The basic integral identity used is

$$\int\frac{\mathrm{d}\,\psi}{\alpha-\cos\psi} = \frac{2}{\sqrt{\alpha^2-1}}\tan^{-1}\big(\sqrt{\frac{\alpha+1}{\alpha-1}}\tan\frac{\psi}{2}\big), \tag{8.31}$$

which immediately gives

$$\boxed{M = \frac{1}{bE}\left[\frac{\alpha}{\sqrt{\alpha^2-1}}\tan^{-1}\left[\sqrt{\frac{\alpha+1}{\alpha-1}}\tan(\frac{\psi}{2})\right] - \frac{\psi}{2}\right]\Bigg|_0^{\sin^{-1}(\frac{L_j}{r})}}. \tag{8.32}$$

To simplify the integral for N note that

$$N = \frac{3}{2bE}\frac{1}{2}\frac{\mathrm{d}^2}{\mathrm{d}\,\alpha^2}\int \frac{\sin^2\psi\cos\psi}{\alpha-\cos\psi}\,\mathrm{d}\,\psi, \tag{8.33}$$

which can be rewritten using the identity

$$\frac{\sin^2\psi\cos\psi}{\alpha-\cos\psi} = \alpha^2 + \alpha\cos\psi - \sin^2\psi - \frac{\alpha(\alpha^2-1)}{\alpha-\cos\psi}, \tag{8.34}$$

as

$$N = \frac{3}{2bE}\big(\psi - \frac{\mathrm{d}^2 I_1}{\mathrm{d}\,\alpha^2}\big), \tag{8.35}$$

where

$$I_1 = \frac{1}{2}\int \frac{\alpha(\alpha^2-1)}{\alpha-\cos\psi}\,\mathrm{d}\,\psi = \alpha\sqrt{\alpha^2-1}\tan^{-1}\left(\sqrt{\frac{\alpha+1}{\alpha-1}}\tan\frac{\psi}{2}\right). \tag{8.36}$$

Explicit differentiation yields

$$\frac{\mathrm{d}\,I_1}{\mathrm{d}\,\alpha} = -\frac{\sin\psi}{2} + \frac{\sin\psi\cos\psi}{2(\cos\psi-\alpha)} + \frac{(2\alpha^2-1)}{\alpha(\alpha^2-1)}I_1, \tag{8.37}$$

and

$$\begin{aligned}\frac{\mathrm{d}^2 I_1}{\mathrm{d}\,\alpha^2} &= \frac{\sin\psi\cos\psi}{2(\cos\psi-\alpha)^2} - \frac{(2\alpha^4-\alpha^2+1)}{\alpha^2(\alpha^2-1)^2}I_1 + \frac{(2\alpha^2-1)}{\alpha(\alpha^2-1)}\frac{\mathrm{d}\,I_1}{\mathrm{d}\,\alpha}\\ &= \frac{\sin\psi\cos\psi}{2(\cos\psi-\alpha)^2} + \frac{(2\alpha^2-1)}{\alpha(\alpha^2-1)}\frac{\sin\psi}{2}\left[-1+\frac{\cos\psi}{\cos\psi-\alpha}\right]\\ &\quad + \big[(2\alpha^2-1)^2 - (2\alpha^4-\alpha^2+1)\big]\frac{I_1}{\alpha^2(\alpha^2-1)^2}\\ &= \frac{\sin\psi}{2(\cos\psi-\alpha)}\big[\frac{2\alpha^2-1}{\alpha^2-1} + \frac{\cos\psi}{\cos\psi-\alpha}\big] + \frac{(2\alpha^2-3)}{(\alpha^2-1)^2}I_1.\end{aligned}$$

Finally, N follows from equations (8.35), (8.36) and (8.38) as

$$\boxed{N = \frac{3}{2bE}\Big[\psi - \frac{\sin\psi}{2(\cos\psi-\alpha)}\big[\frac{2\alpha^2-1}{\alpha^2-1}+\frac{\cos\psi}{\cos\psi-\alpha}\big] - \frac{\alpha(2\alpha^2-3)}{(\alpha^2-1)^{3/2}}\tan^{-1}\big[\sqrt{\frac{\alpha+1}{\alpha-1}}\tan(\frac{\psi}{2})\big]\Big]\Bigg|_0^{\sin^{-1}(\frac{L_j}{r})}}. \tag{8.38}$$

For small thickness, $a \equiv \alpha - 1 \ll 1$, we have

$$\phi = \phi_0 + \mathrm{O}(a), \quad \gamma = \frac{\sqrt{a}}{\pi\sqrt{6}} + \mathrm{O}(a) = \frac{\sqrt{t_0/r}}{2\pi\sqrt{3}} + \mathrm{O}(t_0/r). \tag{8.39}$$

This will work if the metal has relative density (specific gravity) greater than $1/\phi_0$. If it is larger than $1/\phi_0$ then additional holes can be made into the junction area of the

solid part to reduce the density without changing the γ parameter much. If the specific gravity is less than $1/\phi_0$ then mass has to be somehow added. Either way, the idea is to select a to give the right value of γ for the metal. Since we are trying to match the bulk modulus of water where $K \approx 2.25\ GPa$, and metals have E in the many GPa, it means that a must be small. Very small a could be a problem in machining, so that suggests we want large specific gravity, and relatively small E.

An example for an aluminum plate where the density of aluminum is roughly 2700 kg/m^3 and the Young's modulus is 69 GPa gives $\phi_{Al} = 1/2.7 = 0.37$ and $\gamma_{Al} = 2.25/69 = 0.0326$. Equation (8.24) gives $\phi = 1/2.7$ if $a = 0.2$ ($t_0 = 0.4r$), and this value of a gives $\gamma = 0.058$, using equation (8.39). This is too big, but could be reduced by additional thinning of the strut thickness without reducing ϕ much.

Numerical analysis

We analyze equations (8.24) and (8.27) in order to determine what density of solid material, ρ_s, and what Young's modulus, E, could be used to build a foam with the smallest possible unit cell size. First we find a useful range for α, defined in equation $(8.24)_2$, which implies, using equations (8.23) and $(8.27)_2$, that

$$\frac{l}{r} = \frac{2\alpha}{\sqrt{3}} \quad \text{and} \quad \sin\psi_j \approx \frac{l}{2r} = \frac{\alpha}{\sqrt{3}}. \tag{8.40}$$

In order for ψ_j to remain real we must impose $\alpha \leq \sqrt{3}$, also in order for the design to remain physically consistent we must have $\alpha \geq 1$, so we allow

$$1 \leq \alpha \leq \sqrt{3} \quad \Leftrightarrow \quad \phi_0 \approx 0.0931 \leq \phi \leq 0.6977. \tag{8.41}$$

Applying equations (8.24) and (8.27), figures 8.3 and 8.4 were created by considering $t_0 = 1mm$. To gain a physical understanding of the structure at these extremes, for $\alpha = 1.01$ and $\alpha = \sqrt{3}$, figures 8.5 and 8.6 were created.

In order to have smaller unit cell sizes we wish α to be close to $\sqrt{3}$ however such structures with relatively high thickness compared to strut length ratios may not be characterized by this analysis, since we are assuming that the thickness is much smaller compared to the strut length. This result is seen when the equations for M and N,

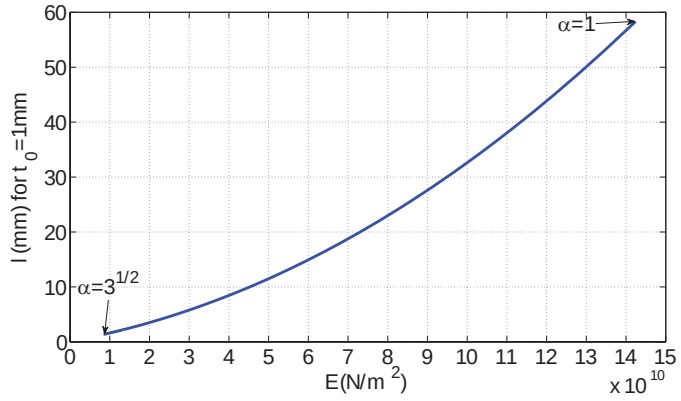

Figure 8.3: Plot of the estimated Young's modulus, E, and expected dimension size, l.

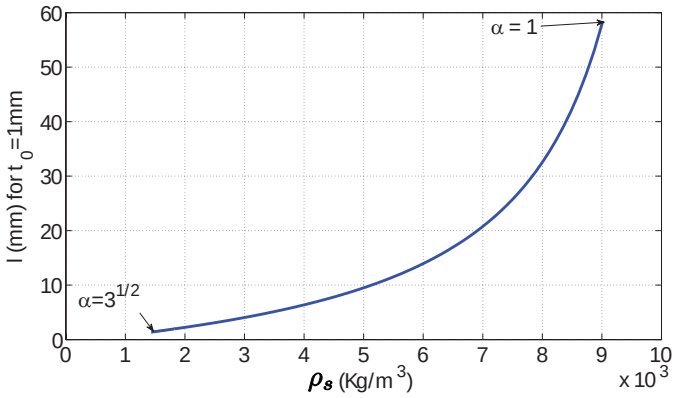

Figure 8.4: Plot of the estimated density, ρ_s, and expected dimension size, l.

equations (8.32) and (8.38), are used in (6.5), the shear correction term, k, in equation (6.2) has a very strong influence on the strength for such structures. Possibly an FEM analysis may gain further insight into how well the foam mechanics theory captures the behavior for relatively high thickness.

8.1.3 Modified triangular penetration pattern

Here we consider the geometry of figure 8.7 for which we have a triangular penetration pattern with straight thin sections notched into the middle of the members, this will have the impact of decreasing bending capacity. The thickness function is

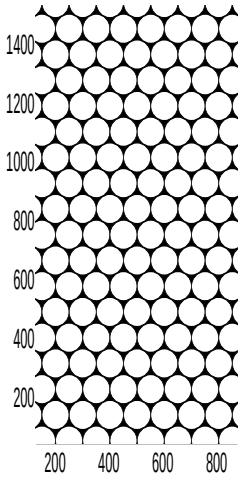

Figure 8.5: Structure for $\alpha = 1.01$

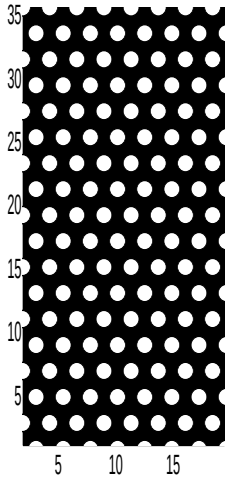

Figure 8.6: Structure for $\alpha = \sqrt{3}$

$$t_\eta(x) = \begin{cases} t_1, & 0 \le |x| < r\sin\eta, \\ t(x), & r\sin\eta \le |x| < \frac{l}{2}, \end{cases} \tag{8.42}$$

where $t_1 = t_0 - t_s$ is the thickness of the notched section, the angular extent is $0 < \eta < \frac{\pi}{6}$ and $t(x)$ is the undeformed thickness function of (8.26). The amount of area being subtracted is then

$$\int_0^{r\sin\eta} (t(x) - t_1)\mathrm{d}x = r^2 a_s, \quad \text{where} \quad a_s \equiv \big(\frac{t_s}{r} + 2 - \cos\eta\big)\sin\eta - \eta. \tag{8.43}$$

The relative (area) density ϕ is now given by

$$\phi = 1 - \frac{\pi + 6a_s}{2\sqrt{3}\alpha^2}. \tag{8.44}$$

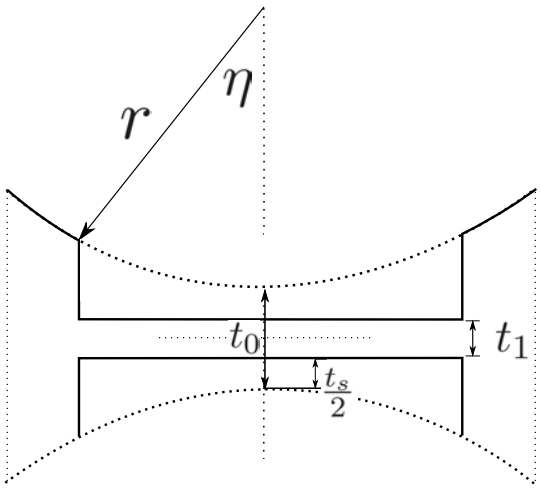

Figure 8.7: A single member of the modified triangular penetration pattern in discussion, described by θ, r and t_1, where equation (8.26) describes the thickness of the circular cut-out region.

The axial and bending compliances of the cell wall are then, respectively,

$$\begin{aligned}
M =& \frac{1}{bE}\Big[\int_0^{r\sin\eta}\frac{\mathrm{d}x}{t_1}+\int_{r\sin\eta}^{L_j}\frac{1}{2r(\alpha-\sqrt{1-(\frac{x}{r})^2})}\mathrm{d}x\Big]\\
=& \frac{r\sin\eta}{bEt_1}+\frac{1}{2bE}\Big[\eta-\psi_j+\frac{2\alpha}{\sqrt{\alpha^2-1}}\big[\tan^{-1}\big(\sqrt{\frac{\alpha+1}{\alpha-1}}\tan(\frac{\psi_j}{2})\big)-\tan^{-1}\big(\sqrt{\frac{\alpha+1}{\alpha-1}}\tan(\frac{\eta}{2})\big)\big]\Big],\\
N =& \frac{12}{bE}\Big(\int_0^{r\sin\eta}\frac{x^2\mathrm{d}x}{t_1^3}+\int_{r\sin\eta}^{L_j}\frac{x^2\mathrm{d}x}{\big(2r(\alpha-\sqrt{1-(\frac{x}{r})^2})\big)^3}\Big),\\
=& \frac{3}{2bE}\Big[\psi_j-\frac{\sin\psi_j}{2(\cos\psi_j-\alpha)}\big[\frac{2\alpha^2-1}{\alpha^2-1}+\frac{\cos\psi_j}{\cos\psi_j-\alpha}\big]+\frac{\alpha(3-2\alpha^2)}{(\alpha^2-1)^{3/2}}\tan^{-1}\big(\sqrt{\frac{\alpha+1}{\alpha-1}}\tan\frac{\psi_j}{2}\big)\Big]\\
&-\frac{3}{2bE}\Big[\eta-\frac{\sin\eta}{2(\cos\eta-\alpha)}\big[\frac{2\alpha^2-1}{\alpha^2-1}+\frac{\cos\eta}{\cos\eta-\alpha}\big]+\frac{\alpha(3-2\alpha^2)}{(\alpha^2-1)^{3/2}}\tan^{-1}\big(\sqrt{\frac{\alpha+1}{\alpha-1}}\tan\frac{\eta}{2}\big)\Big]\\
&+\frac{4}{bE}\big(\frac{r\sin\eta}{t_1}\big)^3.
\end{aligned}\tag{8.45}$$

We want the area fraction, ϕ, of equation (8.44) to equal $\phi_w = \rho_w/\rho$, the value that gives the density of water. Putting $\phi = \phi_w$ implies that

$$\frac{t_0}{r} = 2\left[\frac{\sqrt{3}}{1-\phi_w}\left(\frac{\pi}{6}+(\frac{t_s}{r}+2-\cos\eta)\sin\eta-\eta\right)\right]^{1/2}-2. \tag{8.46}$$

Note that the function $[(2-\cos\eta)\sin\eta-\eta]$ has maximum value of 0.0434 at $\eta=\pi/6$. If $\frac{t_s}{r}$ is small then the numerator is essentially $\pi/3$, and therefore,

$$\frac{t_0}{r}\approx\left(\frac{2\pi}{\sqrt{3}(1-\phi_w)}\right)^{1/2}-2. \tag{8.47}$$

In other words, if $\frac{t_s}{r}$ is small, the ratio $\frac{t_0}{r}$ is insensitive to t_s and η, and is essentially determined by the density of the metal. We want $\frac{t_0}{r}$ not to be too small. For $\phi\approx\phi_0=$

$1 - \frac{\pi}{2\sqrt{3}} = 0.0931$ we can use the slope of the function to get

$$\frac{t_0}{r} \approx \left(\frac{2\sqrt{3}}{\pi}\right)^{1/2}\left(\phi_w - \phi_0\right) = 1.0501\left(\phi_w - \phi_0\right). \tag{8.48}$$

This is a good approximation for brass but doesn't do as well for aluminum. The idea with aluminum is that we can get a relatively large $\frac{t_0}{r}$, which is very good. The $C_{11} = K$ condition is then met by choosing t_s and η. Unfortunately under closer inspection of the moduli produced using equations (8.45) for M and N, defined in equation (6.5), and the density found using this geometry we are not able to simultaneously match the bulk modulus and density properties required. We further tweak the design in the next section.

8.1.4 Straight-edged design

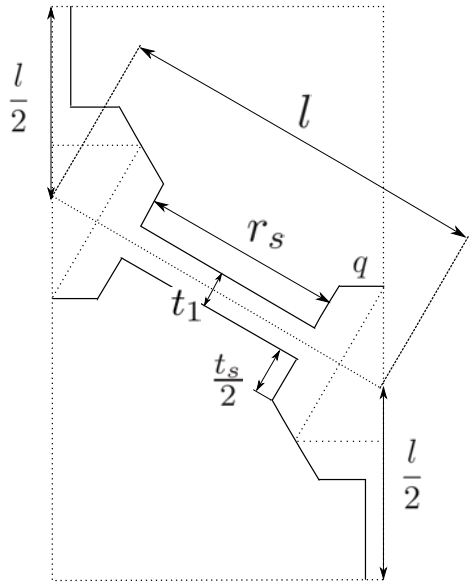

Figure 8.8: Straight-edged design unit cell configuration. Thickness is symmetric about the center line of each member.

The geometry of figure 8.8 is considered here. This unit cell is defined by the six parameters l, r_s, q, t_0, , t_1 and t_s, of which only four are independent since they satisfy the two relations:

$$\begin{aligned} t_0 &= t_1 + t_s, \\ l &= r_s + \frac{1}{\sqrt{3}}(t_0 + 4q). \end{aligned} \tag{8.49}$$

The length l alone defines the unit cell size, while the fine details of unit cell depend on the relative sizes of $t_0 > 0$, $q \geq 0$, $r_s \geq 0$ and $t_1 > 0$. The limit $q = 0$, or equivalently, $\sqrt{3}(l - r_s) = t_0$ is seemingly equivalent to $\eta = \pi/6$ in the previous design. The fractional area of solid is

$$\begin{aligned}\phi &= \frac{4}{3l^2}\big(q^2 + 2qt_0 + \frac{t_0^2}{4} + \frac{\sqrt{3}}{2}t_1 r_s\big) \\ &= \frac{1}{4l^2}\bigg((l - r_s)^2 - t_0^2 + 2\sqrt{3}(l - r_s)t_0 + \frac{8}{\sqrt{3}}t_1 r_s\bigg).\end{aligned} \tag{8.50}$$

The thickness function is

$$t_t(x) = \begin{cases} t_1, & 0 \leq |x| < \frac{r_s}{2}, \\ t_0 + \frac{2}{\sqrt{3}}\big(x - \frac{r_s}{2}\big), & \frac{r_s}{2} \leq |x| < \frac{l}{2}, \end{cases} \tag{8.51}$$

using this function the compliances are found as

$$\begin{aligned} M &= \frac{1}{bE}\bigg(\int_0^{\frac{r_s}{2}} \frac{\mathrm{d}x}{t_1} + \int_{\frac{r_s}{2}}^{L_j} \frac{\mathrm{d}x}{t_t(x)}\bigg) = \frac{1}{2bE}\bigg(\frac{r_s}{t_1} + \sqrt{3}\int_1^{\gamma_1} \frac{\mathrm{d}\,y}{y}\bigg), \\ N &= \frac{12}{bE}\bigg(\int_0^{\frac{r_s}{2}} \frac{x^2}{t_1^3}\,\mathrm{d}\,x + \int_{\frac{r_s}{2}}^{L_j} \frac{x^2}{t_t^3(x)}\,\mathrm{d}\,x\bigg) = \frac{1}{2bE}\bigg(\frac{r_s^3}{t_1^3} + 9\sqrt{3}\int_1^{\gamma_1} \frac{(y + \gamma_2)^2}{y^3}\,\mathrm{d}\,y\bigg), \end{aligned} \tag{8.52}$$

where

$$\gamma_1 = 1 + \frac{(2L_j - r_s)}{\sqrt{3}t_0}, \quad \gamma_2 = \frac{r_s}{\sqrt{3}t_0} - 1. \tag{8.53}$$

Simplifying equation (8.52) gives

$$\begin{aligned} M &= \frac{1}{2bE}\bigg(\frac{r_s}{t_1} + \sqrt{3}\ln\gamma_1\bigg), \\ N &= \frac{1}{2bE}\bigg(\frac{r_s^3}{t_1^3} + 9\sqrt{3}\bigg[\ln\gamma_1 + \frac{(\gamma_1 - 1)\gamma_2^2}{2\gamma_1}\big(1 + \frac{1}{\gamma_1} + \frac{4}{\gamma_2}\big)\bigg]\bigg). \end{aligned} \tag{8.54}$$

In order to organize and solve the system we define the nondimensional parameters

$$\chi_1 = \frac{r_s}{l}, \quad \chi_2 = \frac{t_0}{l}, \quad \chi_3 = \frac{t_1}{r_s}. \tag{8.55}$$

Then the area fraction is

$$\phi = \frac{1}{4}\bigg((1 - \chi_1)^2 - \chi_2^2 + 2\sqrt{3}(1 - \chi_1)\chi_2 + \frac{8}{\sqrt{3}}\chi_1^2\chi_3\bigg). \tag{8.56}$$

The parameter χ_3 should be very small to ensure that $N \gg M$, in which case C_{11} depends on M, essentially, and they are all basically a function of χ_3:

$$M \approx \frac{1}{2bE}\chi_3^{-1}, \quad N \approx \frac{1}{2bE}\chi_3^{-3}. \tag{8.57}$$

A solution can be found to closely match the properties of water by using $\frac{l}{t_1} = \frac{1}{\chi_1 \chi_3}$, we have for aluminum

$$\text{Aluminum}: \quad \chi_1 \approx 0.4095, \quad \chi_2 \approx 1.023, \quad \chi_3 \approx 0.11 \quad \Rightarrow \quad \frac{l}{t_1} \approx 22. \tag{8.58}$$

Using these parameters figure 8.9 was created. The effective elasticity is

$$\mathbf{C}_{FM} = \begin{bmatrix} 2.12 & 2.02 & 0 \\ 2.02 & 2.12 & 0 \\ 0 & 0 & 0.05 \end{bmatrix} GPa, \tag{8.59}$$

where subscript $_{FM}$ stands for the foam mechanics theory result, equation (8.2).

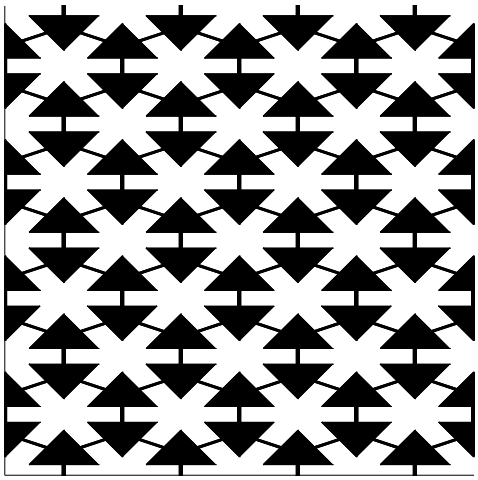

Figure 8.9: Straight edge design using the parameters in equation (8.58).

A more precise evaluation can be made using the full relations for M and N. Fixing χ_2, the two identities $\phi = \phi_w$ and $C_{11} = K$ can be simultaneously solved numerically to give χ_1 and χ_3. Then varying χ_2 one finds a unique value that gives a minimum for $\frac{l}{t_1} = \frac{1}{\chi_1 \chi_3}$. The values of the latter for aluminum and brass were found to be 21.4 and 19.8, respectively. In each case the optimal design has q very close to zero, which means the junction region is essentially an equilateral triangle of side $3a_0$ where

$$l - r_s = \sqrt{3} a_0, \tag{8.60}$$

this is seen in figure 8.9. Noting that q is close to zero in the solutions for brass and

aluminum we tweak the design again to utilize more of the space in the cell to acquire a greater density in a smaller unit cell size.

8.1.5 Metal Water I

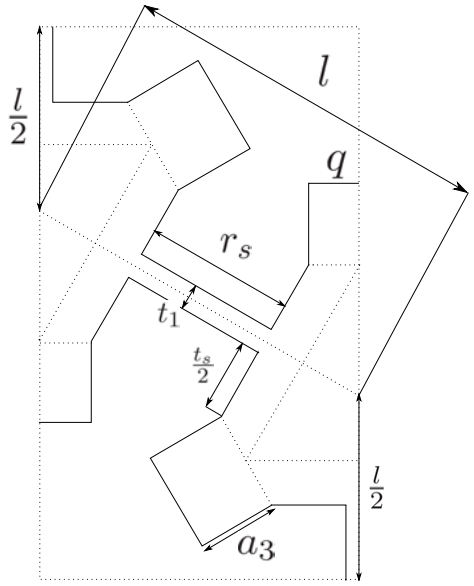

Figure 8.10: Metal Water I design.

The results for the straight edged design show that for aluminum in particular that the mass is concentrated in the equilateral triangles at the junctions. This is not an optimal junction shape for space filling. Here we explore a variation on the previous design that starts with the equilateral triangle junction but modifies it to reduce the unit cell size, that is, to reduce $\frac{l}{t_1}$. This model has the same axial and bending compliance as the previous one described by equation (8.54) but here the idea is to insert a $2q$ by a_3 rectangular region into the hexagonal joint as shown in figure 8.10. By inspection $a_3 \leq r_s$ and

$$\begin{aligned}\phi &= \frac{4}{3l^2}(2qt_0 + q^2 + \frac{t_0^2}{4} + \frac{\sqrt{3}}{2}r_s t_1 + 2\sqrt{3}qa_3) \\ &= \frac{1}{4l^2}\big((l-r_s)^2 - t_0^2 + 2\sqrt{3}t_0(l-r_s) + \frac{8}{\sqrt{3}}r_s t_1 + 8a_3(l-r_s) - \frac{8}{\sqrt{3}}t_0 a_3\big) \\ &= \frac{1}{4}\big((1-\chi_1)^2 - \chi_2^2 + 2\sqrt{3}\chi_2(1-\chi_1) + \frac{8}{\sqrt{3}}\chi_1^2\chi_3 + 8\chi_4(1-\chi_1) - \frac{8}{\sqrt{3}}\chi_2\chi_4\big),\end{aligned}$$

with $\chi_4 = \frac{a_3}{l}$ and χ_1, χ_2 and χ_3 defined in equation (8.55). Also required is that $\frac{\chi_4}{\chi_1} \leq 1$

in order for $a_3 \leq r_s$. For $a_3 = 2q$, $\chi_4 = \frac{1}{2}\big(\sqrt{3}(1-\chi_1) - \chi_2\big)$ and

$$\begin{aligned}\phi &= \frac{4}{3l^2}\big(a_3^2(\sqrt{3}+\frac{1}{4}) + a_3 t_0 + \frac{t_0^2}{4} + \frac{\sqrt{3}}{2} r_s t_1\big) \\ &= \frac{4}{3}\big(\chi_4^2(\sqrt{3}+\frac{1}{4}) + \chi_2\chi_4 + \frac{1}{4}\chi_2^2 + \frac{\sqrt{3}}{2}\chi_1^2\chi_3\big). \end{aligned} \tag{8.61}$$

Completing the square, we can write equation (8.61) as

$$3\big(\frac{t_0}{2} + q + \frac{a_3}{\sqrt{3}}\big)^2 - \big(\frac{t_0}{2} - q + \sqrt{3}a_3\big)^2 = \frac{3}{2}\phi l^2 - \sqrt{3} r_s t_1 - 2a_3^2, \tag{8.62}$$

or equivalently,

$$\left(\frac{t_0}{2} + (2-\sqrt{3})q + a_3\right)\left(\frac{t_0}{2} + (2+\sqrt{3})q - a_3\right) = \frac{3}{4}\phi l^2 - \frac{\sqrt{3}}{2} r_s t_1 - a_3^2. \tag{8.63}$$

With this model we are able to make better use in the filling space of a unit cell while matching the density and elastic properties required to mimic water. The elastic properties are very much based on the uniform strut thickness while the junction is used to match density properties while adding some additional strength. Ideally if we could machine petals at the junction that only minimally contact the struts we could further decouple the mass and elasticity problem. However we do not further tweak this design as machinability is also a concern.

A MATLAB code was written using equations (8.61), (8.54) and (6.6) in order to simultaneously match the bulk modulus and density using aluminum. The parameter $t_1 = 1\ mm$ was chosen in order to shrink the unit cell size while maintaining a dimension that could still be machined. It was found that when this analysis is compared with FEM results the foam mechanics theory generally underestimates the results by $5-10\%$. We then chose to lower the required bulk modulus to $K \approx 2.0\ GPa$ in searching for solution parameters. The set of dimensions found are located in table 8.1, where the density is perfectly matched. The effective elasticity was found to be

$t_1 = 1.00$	$t_0 = 1.42$	$l = 12.89$	$a_3 = 6.05$
$t_s = 0.42$	$r_s = 8.58$	$q = 1.51$	

Table 8.1: Optimized parameters for the Metal Water I design of figure 8.10, using $E = 69\ GPa$ and $\nu = 1/3$. All dimensions given in millimeters.

$$\mathbf{C}_{FM} = \begin{bmatrix} 1.98 & 1.87 & 0 \\ 1.87 & 1.98 & 0 \\ 0 & 0 & 0.051 \end{bmatrix} GPa, \tag{8.64}$$

where subscript $_{FM}$ denotes the result using the foam mechanics theory used here and first reviewed in section 6.1. Figure 8.11 shows what this material looks like. Colored in blue is the added section for mass between the previous design of section 8.1.4 and the current.

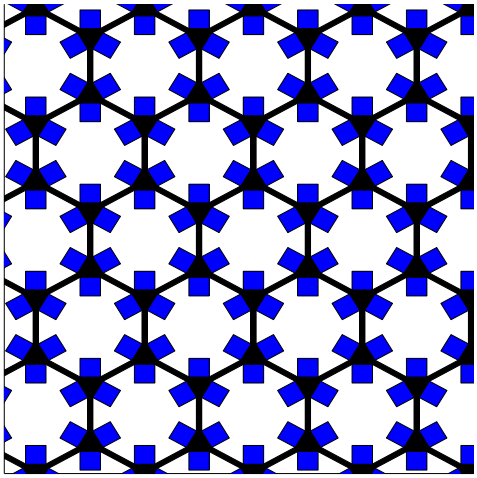

Figure 8.11: Metal Water I design based on MATLAB solution, parameters located in table 8.1.

8.2 Static finite element homogenization

In this section we iterate the designs using the static homogenization technique of section 6.2 until we can more perfectly match the elasticity and density requirements. From the discussion in the previous section we choose to search for structures made from aluminum as it seems to be better suited for achieving our goals.

8.2.1 The straight-edged design

Here the straight edged-design of section 8.1.4 is used with the finite element homogenization technique. We start with the parameters found in equation (8.58) for this

design and iterate using the finite element homogenization method. The optimized parameters are reported in table 8.2, where density is perfectly matched. Using these

$t_1 = 1.00$	$t_0 = 21.00$	$l = 21.42$
$t_s = 20.00$	$r_s = 8.77$	$q = 0.23$

Table 8.2: Optimized parameters for the design of figure 8.10, using $E = 69\ GPa$ and $\nu = 1/3$. All dimensions given in millimeters.

parameters the expected elasticity found by finite element homogenization is

$$\mathbf{C}_{FEM} = \begin{bmatrix} 2.20 & 2.089 & 0 \\ 2.089 & 2.20 & 0 \\ 0 & 0 & 0.056 \end{bmatrix} GPa. \tag{8.65}$$

We also used slightly different elastic properties for aluminum with Young's modulus given by $E = 75.5\ GPa$ and Poisson's ratio as $\nu = 0.35$. This is done to determine the sensitivity of the geometry to the elasticity of the aluminum slab being machined. The optimized parameters are reported in table 8.3. We see some difference between the parameters located in tables 8.2 and 8.3 however they're not too far off, each time the density of aluminum is taken as $\rho_{Al} = 2700\ kg/m^3$. Using the parameters of table

$t_1 = 1.00$	$t_0 = 23.09$	$l = 23.56$
$t_s = 22.09$	$r_s = 9.60$	$q = 0.27$

Table 8.3: Optimized parameters for the design of figure 8.10, using $E = 75.5\ GPa$ and $\nu = 0.35$. All dimensions given in millimeters.

8.3, the expected elasticity was found to be

$$\mathbf{C}_{FEM} = \begin{bmatrix} 2.20 & 2.11 & 0 \\ 2.11 & 2.20 & 0 \\ 0 & 0 & 0.047 \end{bmatrix}. \tag{8.66}$$

8.2.2 Metal Water I

Here the Metal Water I design of section 8.1.5 is used. We note this design is capable of more optimally filling space reducing the cell size needed. Using $E = 69\ GPa$ and $\nu = 1/3$ the optimized parameters are located in table 8.1. The expected elasticity is

then

$$\mathbf{C}_{FEM} = \begin{bmatrix} 2.22 & 2.11 & 0 \\ 2.11 & 2.22 & 0 \\ 0 & 0 & 0.053 \end{bmatrix} GPa, \tag{8.67}$$

where we see about a 10% underestimation from the foam mechanics theory result in equation (8.64). The figures in 8.12 show the displacement solutions and stresses using the finite element homogenization theory with the parameters of table 8.1 used. A quarter cell was used as we have symmetry about the x and y axes. The simulation was also done using the full cell yielding the same elastic moduli as shown in equation (8.67).

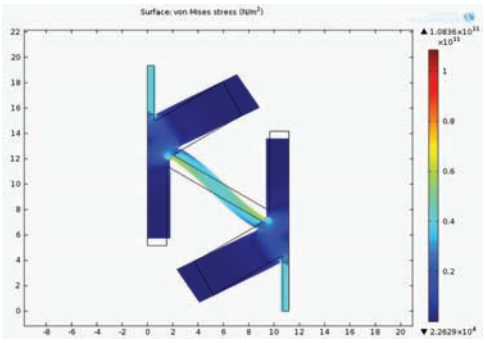

$\varepsilon^0_{11} = 1.$

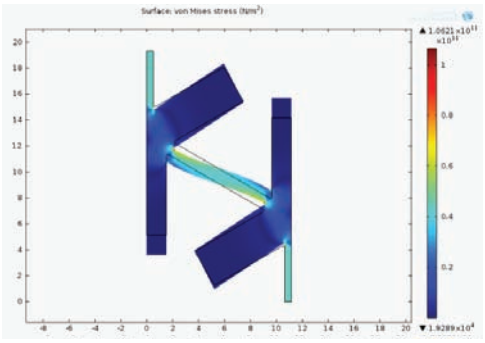

$\varepsilon^0_{22} = 1.$

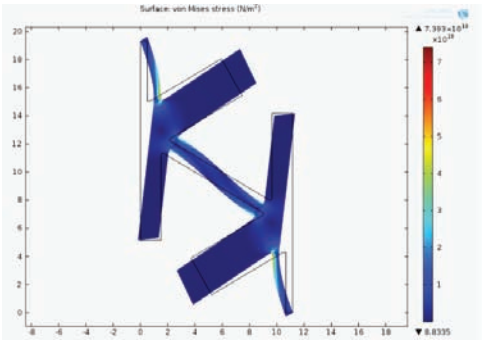

$\varepsilon^0_{12} = 1.$

Figure 8.12: Static homogenization implementation using COMSOL, as described in section 6.2, using the parameters of table 8.1 with aluminum.

These are quite spectacular results as the elasticity matrix for aluminum, using

Young's modulus, $E = 69\ GPa$ and Poisson's ratio of $\nu = 1/3$ has the components

$$\mathbf{C}_{alum} = \begin{bmatrix} 102.09 & 50.28 & 0 \\ 50.28 & 102.09 & 0 \\ 0 & 0 & 25.90 \end{bmatrix} GPa, \tag{8.68}$$

using plane strain. This means we are able to take a solid slab of aluminum and machine it in a particular fashion in order to mimic the elastic and density properties of water. Processes investigated for the physical machining included: Wire EDM (electrical discharge machining), CNC milling, and Waterjet. While Wire EDM has the best precision by far it comes with the steepest cost. In the end the Metal Water I prototype was fabricated by waterjet machining by the WhitCraft Group, shown in figure 8.13. It has since been sent to the Naval Research Laboratory in Washington D.C. for testing.

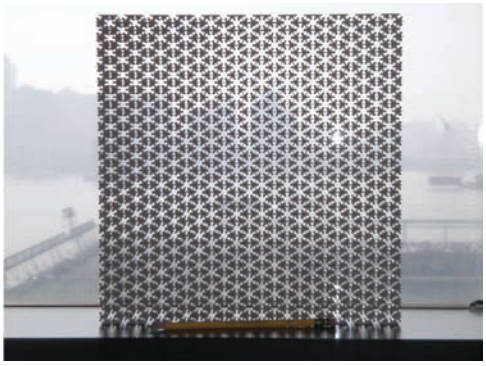

Figure 8.13: Manufactured Metal Water I prototype produced by waterjet machining by the WhitCraft Group.

8.3 Dynamic study of Metal Water I

The finalized version of Metal Water I, with dimensional parameters located in table 8.1, is used with Bloch-Floquet theory in COMSOL. We have a hexagonal lattice structure such that the wave vector, $\mathbf{k}$, is taken along the perimeter of figure 7.4_b. Additionally as we are considering two dimensional geometry the lowest branch emerging from the origin of the wave vector represents shear waves and the second lowest represents longitudinal waves. The tangent to the dispersion curve at any point gives the group velocity, such

that

$$c_j = \frac{\mathrm{d}\,\omega(\mathbf{k})}{\mathrm{d}\,|\mathbf{k}|}, \tag{8.69}$$

where j depends on the branch under investigation [75]. The dispersion behavior for

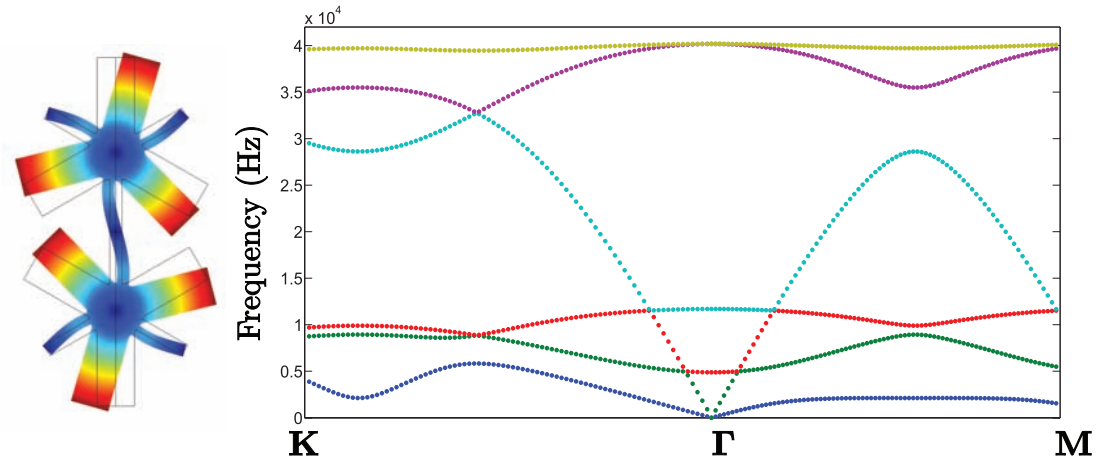

Figure 8.14: Dispersion curves found by COMSOL using Bloch-Floquet analysis.

Metal Water I is shown in figure 8.14, the group velocity for shear waves was found to be $c_s = 230\ m/s$ along both $\mathbf{\Gamma} - \mathbf{K}$ and $\mathbf{\Gamma} - \mathbf{M}$. The longitudinal wave speed was found to be $c_L = 1491\ m/s$ along both directions. This shows the material behaves isotropically at low frequency however we do see some anisotropy in these speeds when considering all directions of the wave vector. As a check we use the discussion of material group velocities from section 2.2.2 which allows two independent checks on the results from the static finite element homogenization theory and Bloch Floquet when applied in COMSOL. Using the previous results, equation (8.67), and taking $c_L = \sqrt{C_{11}/\rho}$ and $c_s = \sqrt{C_{66}/\rho}$ we attain exactly the same results using $\rho = 1000\ kg/m^3$ which is the density of water which we matched the structure to. We also see that the structure has a frequency homogenization limit for the pure longitudinal mode around $25,000$ Hz. Between roughly $25,000$ to $35,000$ Hz and along the $\mathbf{\Gamma} - \mathbf{M}$ path we have a partial band gap and do not expect any propagation of waves. This is a consequence of the unit cell size, using figure 8.1 where we are using regular hexagons with $l = 12.89\ mm$ the vertical height of one entire cell is around 61 mm. Using the wave speed of water as 1500 m/s and the unit cell size as the wavelength the expected homogenization frequency limit is

roughly $24,500$ Hz, which is similar to the behavior seen in the dispersion curves. The dispersion curves were also found using the method of section 7.5, as shown in figure 8.15. Here Euler-Bernoulli beams are used as the building blocks of the structure. The junctions in Metal Water I are then turned into point masses with associated moment of inertia. As expected there is better agreement between figures 8.14 and 8.15 at

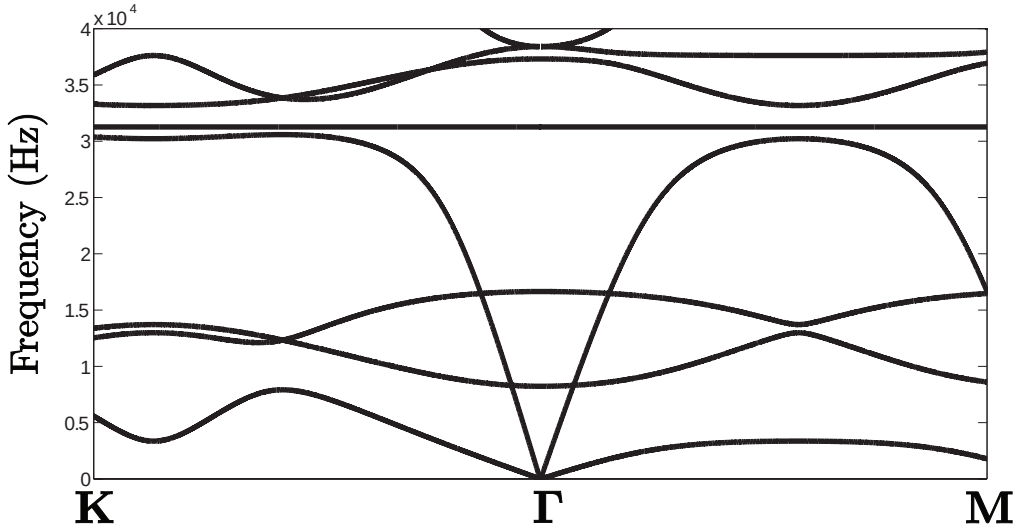

Figure 8.15: Dispersion curves found by method of section 7.5.

lower frequencies. The branches of figure 8.15 are shifted upward compared to the FEM results.

8.3.1 Negative index lens

An interesting phenomenon of the dispersion curves of figure 8.14 is that the longitudinal branch intersects branches with a negative group velocity, shown more clearly in figure 8.16. As the wave vector increases from $\mathbf{\Gamma}$ outward there are modes that have negative slope and by equation (8.69) they also have negative group velocity. This was investigated by a group at Institut d'lectronique de microlectronique et de nanotechnologie (IEMN) [86, 87], where numerical as well as physical testing on the Metal Water I design was conducted. There is difficulty, however, in coupling modes at these frequencies as the slab is intended for wavelengths on the order of the unit cell size. Here we mention the wave vector location of the intersection between the longitudinal

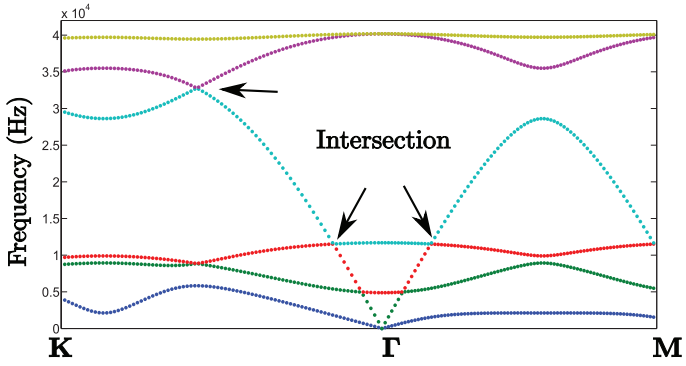

Figure 8.16: Intersections of longitudinal branch to branches with negative wave speed.

branch and the first branch with negative velocity. We vary the wave vector by angle ψ as shown in figure 8.17 and note the location, results shown in table 8.4. It should

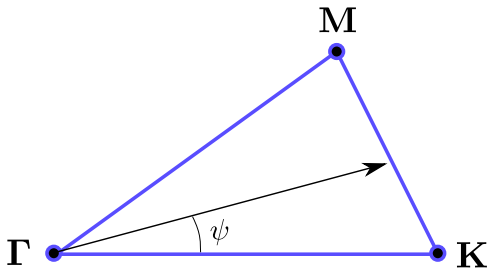

Figure 8.17: Varying wave vector along the irreducible Brillouin zone to find the longitudinal-negative branch intersections.

be noted that the study done in [87] considered the second intersection.

8.4 Metal Water II: A corrugated design

Having designed and fabricated Metal Water I we next look for structures that are more readily producible. This design considers the folding and bonding of metallic sheets inspired by the production capability of Cellular Materials Inc. (CMI). A quarter cell is shown in figure 8.18, note that when the cell is mirrored we have vertical struts of thickness $2t$ while struts along the angle keep thickness t only. Mass is then added by adhering lead wire in various locations. Several designs were found using a variety of materials including: aluminum, brass, and lead for the extra mass needed to match

ψ (rad)	$\mathbf{k}$ (m^{-1})
$0\pi/60$	$[48.99, 0.00]$
$1\pi/60$	$[50.25, 2.63]$
$2\pi/60$	$[49.90, 5.24]$
$3\pi/60$	$[49.56, 7.85]$
$4\pi/60$	$[49.24, 10.47]$
$5\pi/60$	$[47.35, 12.69]$
$6\pi/60$	$[47.06, 15.29]$
$7\pi/60$	$[46.77, 17.95]$
$8\pi/60$	$[44.94, 20.01]$
$9\pi/60$	$[44.67, 22.76]$
$10\pi/60$	$[42.87, 24.75]$

Table 8.4: Wave vector value at the intersect of the longitudinal branch and the first negative branch.

density. The properties used in calculations for these materials are

$$\begin{aligned} \text{Aluminum} &\begin{cases} E = 69\ GPa, \quad \nu = 0.33, \quad \rho = 2,700\ kg/m^3, \end{cases} \\ \text{Brass} &\begin{cases} E = 100\ GPa, \quad \nu = 0.40, \quad \rho = 8,400\ kg/m^3, \end{cases} \\ \text{Lead} &\begin{cases} E = 16\ GPa, \quad \nu = 0.44, \quad \rho = 11,340\ kg/m^3. \end{cases} \end{aligned} \tag{8.70}$$

Three unique designs were studied where each has the dimension $l = 4.387\ mm$ and then the thickness was found by trying to match the bulk modulus. For aluminum the thickness must be $t = 0.35\ mm$ and for brass it must be $t = 0.23\ mm$, found using the foam mechanics theory of section 6.1. Lead was used to add mass and was attached in the COMSOL model by taking a 10 % overlay into the strut thickness. Figures 8.19, 8.20, and 8.21 show the COMSOL dispersion curves and geometry of where lead mass was added for each design. Longitudinal and shear wave speeds are also found in the figures. We note that a more perfect matching for the longitudinal speed could be found by iterating the design further in COMSOL. Interestingly, Design 1, figure 8.19 using aluminum seems to be the best design. This is because the third branch is higher and the frequency range for which there is only the longitudinal mode present is the greatest. Lastly physical production of this material by CMI is an issue due to the required bonding of corrugated sheets.

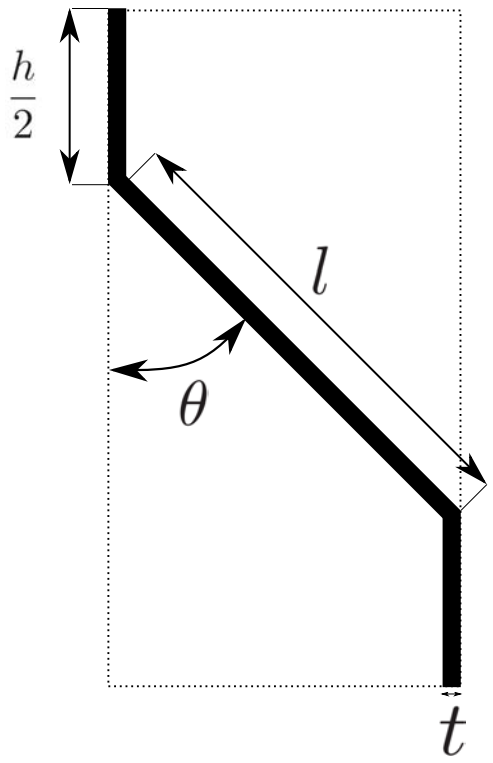

Figure 8.18: Quarter cell design to be considered for CMI production. Thickness in the quarter cell is constant described by dimension t. Missing is added masses that can be tacked on in a variety of locations.

8.5 Application to cloaking

All of the methods used to create Metal Water I worked in the Cartesian coordinate system and produced a unit cell with rectangular shape. In application to cloaking theory the unit cell will need to be slightly deformed in order for a circular section to come about. This can be done by a mapping of the r direction to y and θ direction to x. This approximation is made as the unit cell size is expected to be small compared to the global scale of the cloak. The next step is to remove the constraints $h = l$ and $\theta = \pi/3$ in reference to figure 8.1. This has the consequence of creating anisotropic structures while maintaining small shear modulus. This is needed as the cloaking theory reviewed in section 5.2 requires anisotropic pentamode behavior defined by equations (5.5) and (5.6). The procedure then comes down to finding a suitable structure with parameters that can accommodate the transformation function, $f(r)$, that is used to define the elastic and density properties of the cloak as a function of the radius, r. Then

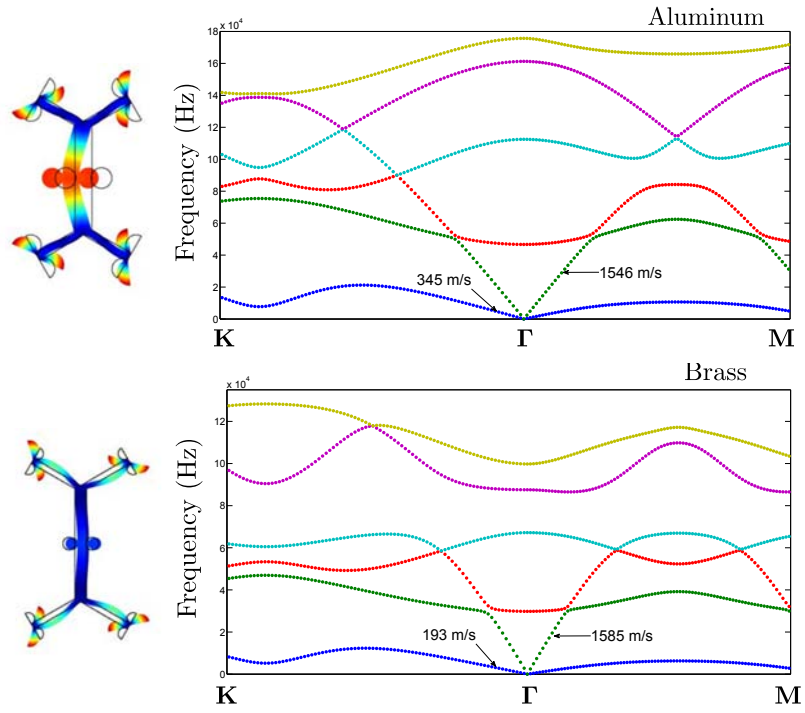

Figure 8.19: Design 1 using (top) aluminum and (bottom) brass. Each design has added lead masses located at the center of the struts.

by taking a discrete number of layers and following the steps of figure 8.22 a cloaking medium can come about [88]. Such an example was done for two unique layers in figure 8.23 using the foam mechanics model.

In relation to inertial cloaks the inverse problem was found in which using a structure which layers three unique fluids a mapping function $f(r)$ could be found [19]. Finding the inverse problem for the pentamode cloak, that is finding a mapping function which depends on the designed microstructure of the material would be extremely useful for future development of cloaks and other devices that utilize transformation acoustics. Instead of finding designs that suit the mapping function $f(r)$, we find relations based on the cell geometry that define the mapping function. This type of analysis is left for future work but would be of great use in determining the proficiency of a proposed cell design in application to producing an acoustic cloaking device. The development of two dimensional structures is left here, the next chapter will focus on producing three dimensional structures that again mimic the acoustic properties of water.

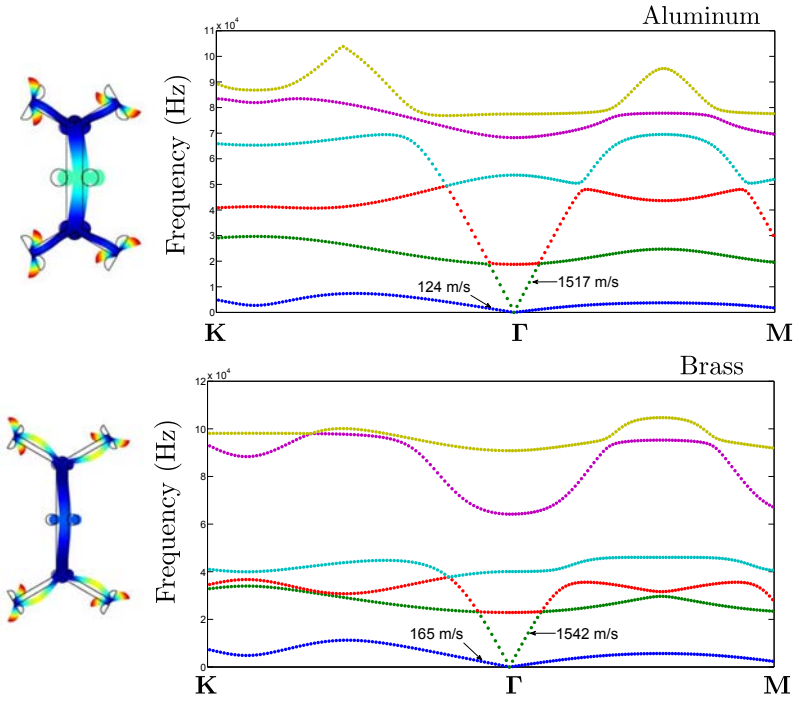

Figure 8.20: Design 2 using (top) aluminum and (bottom) brass. Each design has added lead masses located at the center of the struts as well as the junction.

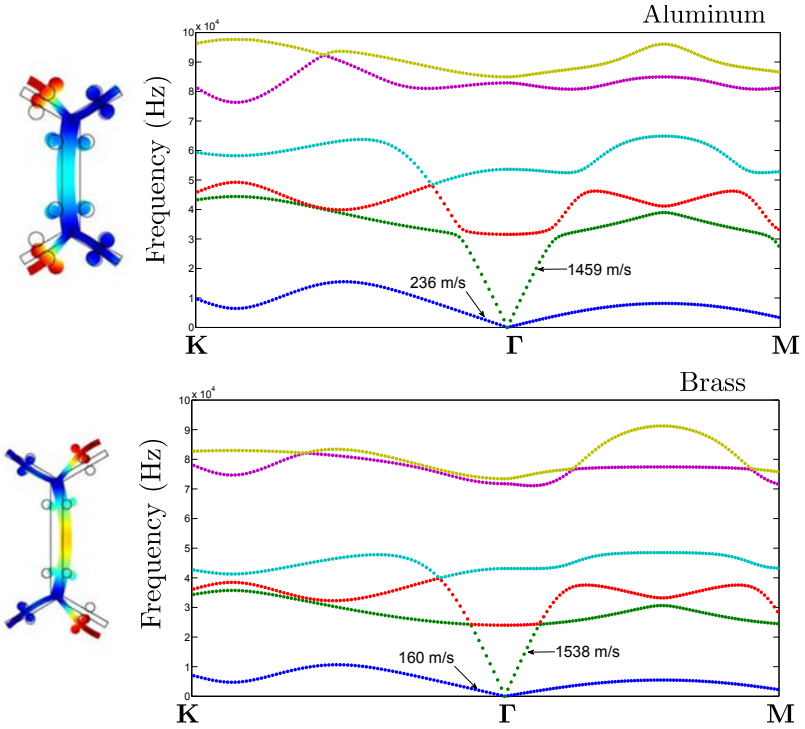

Figure 8.21: Design 3 using (top) aluminum and (bottom) brass. Each design has added lead masses located one third the distance plus and minus of the center of each strut.

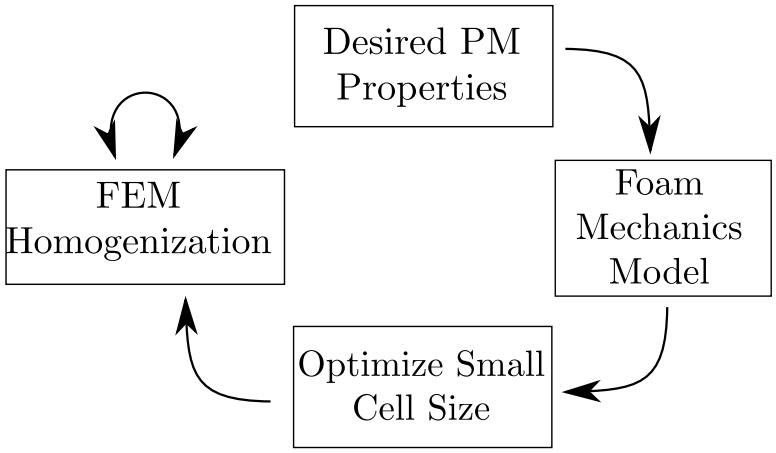

Figure 8.22: Process for creating additional metamaterials.

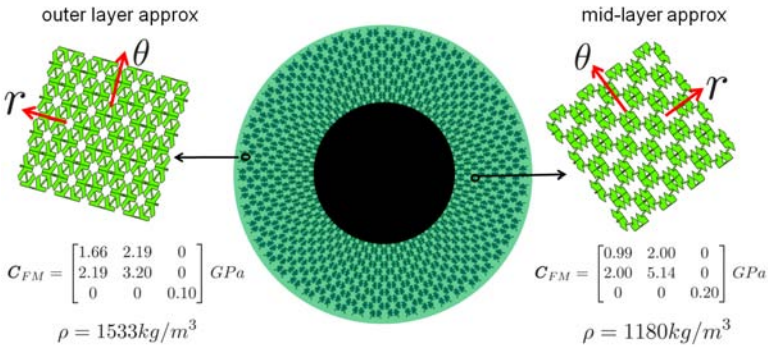

Figure 8.23: Example of achieving a cloaking medium. Here the foam mechanics theory was used to develop two unique layers based on a mapping function $f(r)$ that defines the elastic and density properties required, equation (5.5).

Chapter 9

Designing three dimensional Metal Water

Having developed two dimensional structures that mimic the acoustic properties of water in the previous chapter we investigate further by doing the same in three dimensions. The diamond lattice structure is chosen here as it only has four struts intersecting at a joint. This is a minimum requirement for three dimensional structures and it should be able to produce a smaller shear modulus as compared to other structures, it should also be able to offer better isotropy in its effective moduli. Section 9.1 begins with a brief derivation of the effective bulk modulus for cubic lattice structures, after which the work of Warren and Kraynik [65], which undergoes a strength of materials approach to deriving the effective moduli of the diamond lattice is reviewed. The section is ended by listing the results of Norris [7], which aims to more accurately find the effective moduli. The Warren and Kraynik results are used thereafter as they estimate both the bulk and shear modulus. In section 9.2 the effective elasticity equations are parameterized in terms of strut geometry and several different lattice materials are studied in order to reduce the shear modulus while maintaining a match in the bulk modulus with water. Bloch-Floquet analysis is accomplished in COMSOL and group velocities in the quasi-static limit are calculated for several different designs. Analysis of changing the strut geometry is completed in sections 9.2.3 through 9.2.6. Lastly section 9.3 considers matching the acoustic properties of water using the cubic lattice in one direction, where the wave speed and density are matched. It is done only in one direction as the cubic lattice has rather large anisotropy. Application to cloaking theory is left out however the analysis used here for producing materials with desired macroscopic elastic and density properties can easily be applied to such a theory.

9.1 Analytical static homogenization

We first investigate the cubic lattice using the strain energy method to find the effective bulk modulus. The strain energy in a strut of length L due to bending moment $\mathcal{M}(x)$,

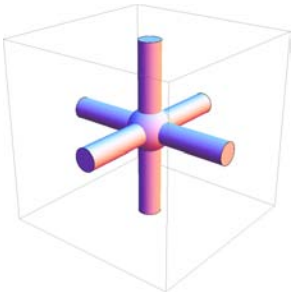

Figure 9.1: Cubic lattice unit cell geometry, each strut has length L.

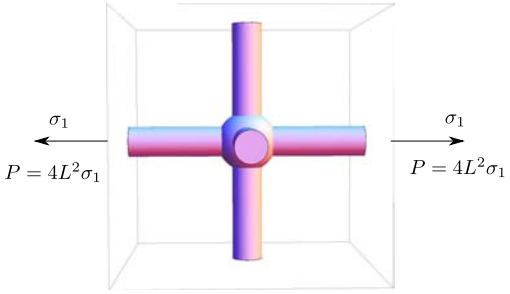

Figure 9.2: Applying σ_1 to the cubic lattice. Each face has area $4L^2$.

axial load $\mathcal{R}$ and shear load $\mathcal{V}$ is [89]

$$U = \int_0^L \frac{\mathcal{M}^2(x)}{2EI(x)}\,\mathrm{d}\,x + \int_0^L \frac{\mathcal{R}^2}{2EA(x)}\,\mathrm{d}\,x + \int_0^L \frac{k\mathcal{V}^2}{2GA(x)}\,\mathrm{d}\,x, \tag{9.1}$$

where k is a shear correction factor. When load σ_1 is applied to the unit cell, as shown in figure 9.2, we find the strain energy to be

$$U_1 = P^2 M/2, \quad \text{where} \quad M = \int_0^L \frac{\mathrm{d}\,x}{EA(x)}. \tag{9.2}$$

The displacement and strain in the 1 direction is then

$$\delta_1 = \frac{\partial U_1}{\partial P} = PM, \quad \epsilon_1 = \frac{2\delta_1}{2L} = PM/L. \tag{9.3}$$

The effective Young's modulus can be found using

$$E_1^* = \frac{\sigma_1}{\epsilon_1} = \frac{1}{4LM}. \tag{9.4}$$

In order to find the effective bulk modulus we can load the unit cell with a hydrostatic pressure, σ, and then do the same analysis. This means there are three directions in which the strain written in equation (9.3) occurs. The change in volume due to hydrostatic loading is then

$$\Delta = \epsilon_{ii} = 3PM/L. \tag{9.5}$$

Finally using the definition of the bulk modulus, $K = \sigma/\epsilon_{ii}$,

$$K = \frac{\sigma L}{3PM} = \frac{1}{12LM}. \tag{9.6}$$

We leave the cubic case for now and return to it later using COMSOL simulation. Furthermore isotropic elasticity is not expected and higher shear moduli as compared to the diamond lattice will occur.

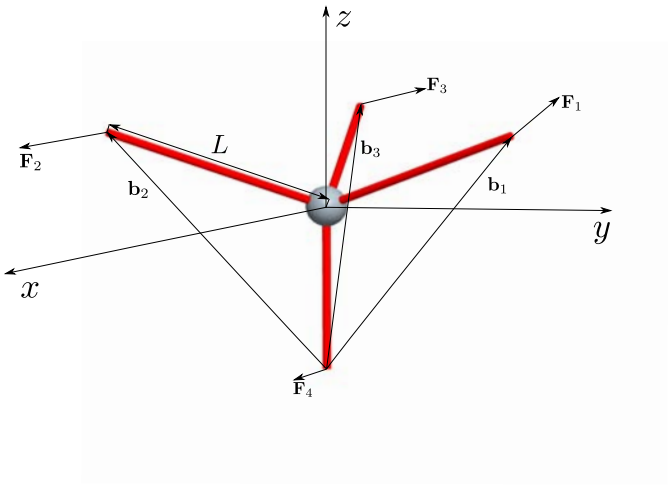

Figure 9.3: Geometry associated with the Warren and Kraynik model. The unit cell consists of four half-struts of equal length, L.

Following the work of Warren and Kraynik [65], the effective elastic properties of a tetrahedral structure are reviewed. This structure is the building block of the diamond lattice and it can be used to find its effective elastic properties. As shown in figure 9.3 the geometry consists of a tetrahedral unit cell with four half struts of equal length L. The forces acting on the midpoints of each strut are considered in components parallel and normal to each strut,

$$\mathbf{F}_i = (\mathbf{F}_i \cdot \mathbf{e}_i)\mathbf{e}_i + (\mathbf{e}_i \times \mathbf{F}_i) \times \mathbf{e}_i, \qquad i = 1 \cdots 4, \tag{9.7}$$

where the unit vector $\mathbf{e}_i$ is taken parallel to the i^{th} strut. Displacements of the midpoints are taken as

$$\boldsymbol{\Delta}_i = M(\mathbf{F}_i \cdot \mathbf{e}_i)\mathbf{e}_i + N(\mathbf{e}_i \times \mathbf{F}_i) \times \mathbf{e}_i + L\psi \times \mathbf{e}_i, \tag{9.8}$$

where M is the axial compliance, N is the bending compliance and ψ is a rigid body rotation of the entire cell. The strut midpoints are defined by the undeformed position, $\mathbf{b}_i^0$, plus a deformation $\delta_i = \boldsymbol{\Delta}_i - \boldsymbol{\Delta}_4$, such that

$$\mathbf{b}_i = \mathbf{b}_i^0 + \delta_i. \tag{9.9}$$

Lastly equilibrium of forces and moments require

$$\sum_{i=1}^{4} \mathbf{F}_i = \mathbf{0}, \quad \sum_{i=1}^{4} \mathbf{e}_i \times \mathbf{F}_i = \mathbf{0}. \tag{9.10}$$

Cutting the volume element in figure 9.4 along $x = 0$ and finding a force balance on

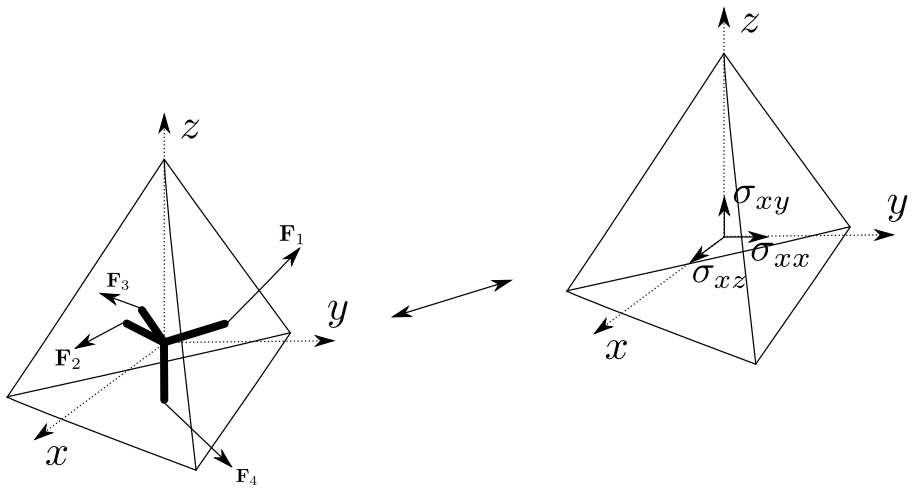

Figure 9.4: Figure to relate forces, $\mathbf{F}_i$, to stresses σ_{ij}.

the remaining volume yields the relation

$$12\sqrt{2}L^2(\sigma_{xx}\mathbf{i} + \sigma_{xy}\mathbf{j} + \sigma_{xz}\mathbf{k}) = \mathbf{F}_2 - \mathbf{F}_3. \tag{9.11}$$

Cutting along $y = 0$ gives

$$12\sqrt{6}L^2(\sigma_{xy}\mathbf{i} + \sigma_{yy}\mathbf{j} + \sigma_{yz}\mathbf{k}) = -3(\mathbf{F}_2 + \mathbf{F}_3) - 2\mathbf{F}_4, \tag{9.12}$$

lastly along $z = -L$ gives

$$6\sqrt{3}L^2(\sigma_{xz}\mathbf{i} + \sigma_{zy}\mathbf{j} + \sigma_{zz}\mathbf{k}) = -\mathbf{F}_4. \tag{9.13}$$

These relations can be plugged into the equilibrium equation, (9.10), to find further relations. Taking a case of pure shear where $\delta_i = \gamma(\mathbf{b}_i^0 \cdot \mathbf{k})\mathbf{j}$, where γ is the magnitude of the shearing strain. The relation

$$\sigma_{yz} = \frac{\gamma M}{D}[3(17N + 7M) + (N - M)(f_1 + f_2)], \tag{9.14}$$

can be found where f_i are functions that deal with the three dimensional orientation of the structure, found in equation (9.17). Similarly taking a case of uniaxial extension, $\delta_i = \varepsilon(\mathbf{b}_i^0 \cdot \mathbf{k})\mathbf{k}$, the normal stress is

$$\sigma_{xx} = \frac{\varepsilon(N - M)}{D}[(16N + 11M) + M(f_1 - f_2)], \tag{9.15}$$

where

$$D = 288\sqrt{3}LMN(2M + N). \tag{9.16}$$

Unlike the motivation behind [65], where the lattice was unstructured and took random orientations, which is common in production metallic foams, we do not wish to average over all possible orientation angles. The functions $f_i(\theta, \phi, \psi)$ and $f_i^*(\theta, \phi, \psi)$ are evaluated at $f_i(0, 0, 0)$ and $f_i^*(0, 0, 0)$ where

$$\begin{aligned}
f_1(\theta, \phi) &= 4\sqrt{2}(2\sin 2\theta - \sin 4\theta)\cos 3\phi - (4\cos 2\theta + 7\cos 4\theta), \\
f_2(\theta, \phi, \psi) &= (3 + 4\cos 2\theta - 7\cos 4\theta)\cos 2\psi + 4\sqrt{2}(3\sin 3\theta - \sin\theta)\sin 3\phi \sin 2\psi \\
&\quad - 4\sqrt{2}(2\sin 2\theta + \sin 4\theta)\cos 3\phi \cos 2\psi, \\
f_3(\theta, \phi, \psi) &= (2\sin 2\theta + 7\sin 4\theta)\sin\psi + 4\sqrt{2}(\cos 2\theta - \cos 4\theta)\cos 3\phi \sin\psi \\
&\quad + 6\sqrt{2}(\cos\theta - \cos 3\theta)\sin 3\phi \cos\psi, \\
f_4(\theta, \phi, \psi) &= 7(2\sin 2\theta - \sin 4\theta)\sin 3\psi + 4\sqrt{2}(7\cos 2\theta + \cos 4\theta)\cos 3\phi \sin 3\psi \\
&\quad + 2\sqrt{2}(7\cos\theta + 9\cos 3\theta)\sin 3\phi \cos 3\psi,
\end{aligned} \tag{9.17}$$

and f_i^* is found from f_i by replacing $(\sin p\psi, \cos p\psi)$ by $(\cos p\psi, -\sin p\psi)$. Evaluating $f_i(0, 0, 0)$ and $f_i^*(0, 0, 0)$ yields

$$\begin{aligned}
f_1 = -11, \quad f_2 = 0, \quad f_3 = 0, \quad f_4 = 0, \\
f_1^* = -11, \quad f_2^* = 0, \quad f_3^* = 0, \quad f_4^* = 32\sqrt{2}.
\end{aligned} \tag{9.18}$$

Then for the case of pure shear

$$\sigma_{yz} = \mu\gamma, \qquad \rightarrow \qquad \mu_{WK} = \frac{M}{D}(40N + 32M), \tag{9.19}$$

and for the case of uniaxial extension

$$\sigma_{xx} = \lambda\varepsilon, \qquad \rightarrow \qquad \lambda_{WK} = \frac{N-M}{D}16N. \tag{9.20}$$

where subscript $_{WK}$ denotes the result of Warren and Kraynik.

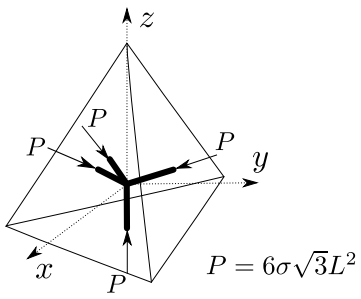

Figure 9.5: Regular tetrahedral unit cell for determining the bulk modulus using strain energy formulation. Note for a regular tetrahedral structure, i.e. diamond lattice, the edge length of the unit tetrahedron, a, to the half-strut length, L, are related by $4L = a\sqrt{2/3}$, then the area of each face, A_0, in terms of L is $A_0 = 6\sqrt{3}L^2$. The volume of the tetrahedron is $V = 8\sqrt{3}L^3$.

Using figure 9.5 the results of [65], equations (9.19) and (9.20), can be independently checked by finding the bulk modulus using a strain energy formulation. Consider the origin, which is the junction point between all struts, as fixed. The strain energy of one of the struts is

$$U_1 = P^2M/2. \tag{9.21}$$

The displacement of the strut in the direction of P, which is axial deformation, is

$$\delta_1 = \frac{\partial U_1}{\partial P} = PM. \tag{9.22}$$

The total strut length after stress σ is applied is then $L' = L - PM$. Considering load P is applied to all struts the deformed volume, using the equation for the volume of a tetrahedron, $V = 8\sqrt{3}L^3$, is

$$\begin{aligned} V' &= 8\sqrt{3}(L-PM)^3 = 8\sqrt{3}\big[L^3 - 3L^2PM + 3LP^2M^2 - P^3M^3\big] \\ &\approx 8\sqrt{3}\big[L^3 - 3L^2PM\big], \end{aligned} \tag{9.23}$$

where the approximation is used assuming infinitesimal deformation. The change in volume of the unit cell is then

$$\Delta V = 8\sqrt{3}L^3 - 8\sqrt{3}\big[L^3 - 3L^2PM\big] = 24\sqrt{3}L^2PM. \tag{9.24}$$

The bulk modulus can be easily determined by

$$K = \frac{V\sigma}{\Delta V} = \frac{8\sqrt{3}L^3\sigma}{24\sqrt{3}L^2PM}. \tag{9.25}$$

This can be simplified by using $P = 6\sigma\sqrt{3}L^2$, which is found by taking the stress, σ, applied to one of the faces on the unit cell having area $6\sqrt{3}L^2$. The effective bulk modulus is then

$$K = \frac{1}{18\sqrt{3}LM}, \tag{9.26}$$

which is the result that Warren and Kraynik [65] found for a randomly oriented configuration of unit cells. It should be noted that by taking the Lamé parameters of equations (9.19) and (9.20) and assuming $N \gg M$ an approximate bulk modulus can be found, where

$$\lambda_{WK} \propto \frac{1}{18\sqrt{3}LM}, \quad \mu_{WK} \propto \frac{40M}{N}, \quad \rightarrow K_{WK} \approx \frac{1}{18\sqrt{3}LM}, \tag{9.27}$$

which agrees with the result of the strain energy method as shear is not accounted for. A problem with these results is that the volume used for the tetrahedron should not be used since tetrahedrons are not capable of filling three dimensional space. Instead the volume for the diamond lattice should be used where for the regular diamond structure

$$V = \frac{64\sqrt{3}L^3}{9}. \tag{9.28}$$

This changes the results and was compensated for by the work of Norris [7]. In that work the effective elasticity was found to be

$$\begin{bmatrix} C_{11} & C_{12} & 0 \\ C_{12} & C_{22} & 0 \\ 0 & 0 & C_{66} \end{bmatrix} \approx C_0 \begin{bmatrix} \varpi & 1 & 0 \\ 1 & \varpi^{-1} & 0 \\ 0 & 0 & 0 \end{bmatrix}, \tag{9.29}$$

with

$$C_0 = \frac{d}{d-1}\frac{cs^2R_2(R_1+cR_2)}{V(M_2+dc^2M_1)}, \quad \varpi = \frac{(d-1)c(R_1+cR_2)}{s^2R_2}, \tag{9.30}$$

where $d = 2, 3$ corresponding to two and three dimensions, $c = \cos\theta$, $s = \sin\theta$, V is the volume, and the parameters R_1, R_2, θ are shown in figure 9.6. The volume, for the diamond lattice used here, is

$$V = 6\sqrt{3}(sR_2)^{d-1}(R_1 + cR_2). \tag{9.31}$$

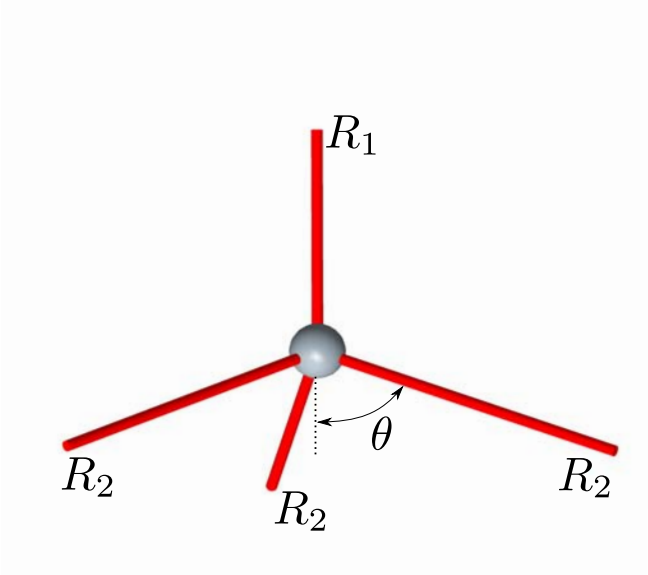

Figure 9.6: Unit cell used in the work of Norris [7], where there are three identical struts with length R_2 all oriented an angle θ away from the opposite direction of the fourth strut with length R_1.

For the case of the regular tetrahedral structure, $R_1 = R_2 = L$, $\theta = \cos^{-1}\frac{1}{3}$. This gives isotropic behavior as $\varpi = 1$ in equation (9.29). The volume is then the same as equation (9.28). Looking for materials with small shear modulus the approximation $\lambda \approx C_{11}$ is used, giving

$$\lambda_N = \frac{1}{16\sqrt{3}LM}, \tag{9.32}$$

where subscript $_N$ denotes the result of Norris. This is similar to the Warren and Kraynik result shown in equation (9.27).

Using equation (9.30) the equations can be reformulated using an elastic filling fraction, ϕ^{el}, which will refer to the volume fraction of material necessary to achieve the desired bulk modulus. The axial compliances are $M_1 = M_2 = \frac{L}{AE}$, where A is the rod cross-sectional area. C_0 of equation (9.30) gives

$$C_0 = \frac{4}{9}\frac{AEL}{V} = \frac{\phi^{el}E}{9}. \tag{9.33}$$

In order to match the bulk modulus of water we take $C_0 = K \approx 2.2GPa$ then for steel, for which Young's modulus is $E \approx 193GPa$, we find $\phi^{el}_{steel} \approx 1/10$. This result means that in order to match just the strength of water we must fill approximately 10% of the volume of the unit cell assuming uniform circular cross-section struts.

9.2 Parameterization

Here the results of Warren and Kraynik, which gave an approximation on both the effective bulk and shear moduli, are parameterized into a simpler form. Assuming rods of constant circular cross-section the axial compliance, M, and bending compliance, N, are given by

$$M = \int_0^L \frac{\mathrm{d}\,x}{EA}, \quad N = \int_0^L \frac{x^2\,\mathrm{d}\,x}{EI}, \tag{9.34}$$

where for a rod $I = \pi r^4/4$, this results in

$$M = \frac{L}{E\pi r^2}, \quad N = \frac{4L^3}{3E\pi r^4}. \tag{9.35}$$

Simplifying the first lamé parameter, found in equation (9.20), gives

$$\lambda_{WK} = \frac{(N-M)16N}{288\sqrt{3}LMN(2M+N)} = E\pi\frac{\frac{4}{3}\alpha^2 - 1}{18\sqrt{3}\alpha^2(2+\frac{4}{3}\alpha^2)}, \tag{9.36}$$

where $\alpha = L/r$ and r is the rod radius. The shear modulus is taken as

$$\mu_{WK} = \frac{M(40N+32M)}{288\sqrt{3}LMN(2M+N)} = E\pi\frac{5\alpha^2+3}{36\sqrt{3}\alpha^4(2+\frac{4}{3}\alpha^2)}. \tag{9.37}$$

The approximation, $\lambda_{WK} \approx K_{H_2O}$, could be used since relatively long thin rods are expected which will mean $\mu_{WK} \ll \lambda_{WK}$. However, if the small amount of shear modulus is taken into account then the bulk modulus is

$$K_{H_2O} = \lambda_{WK} + \frac{2}{3}\mu_{WK} = E\pi\frac{4\alpha^4+2\alpha^2+3}{36\sqrt{3}\alpha^4(2\alpha^2+3)}. \tag{9.38}$$

The density can be found by using the volume and number of elements, rods and masses in the unit cell. Referring to figure 9.7, the unit cell consists of 16 full length rods, that is each rod has a full length of $2L$, and 8 masses, points that we may add a specified amount of mass to and the volume these components occupy is $V_{tot} = \frac{512\sqrt{3}}{9}L^3$. The density is then

$$\rho_{H_2O} = \frac{9\rho_{rod}\pi}{16\sqrt{3}\alpha^2} + \frac{9m}{64\sqrt{3}L^3}, \tag{9.39}$$

where m is the mass located at each vertex. Parameters created are a non-dimensional $\alpha = L/r$ and a dimensional $\beta = m/L^3$ having units of density. The ratio between λ and μ is computed for comparison in terms of α where

$$\frac{\mu_{WK}}{\lambda_{WK}} = \frac{3+5\alpha^2}{2\alpha^2(\frac{4}{3}\alpha^2-1)}. \tag{9.40}$$

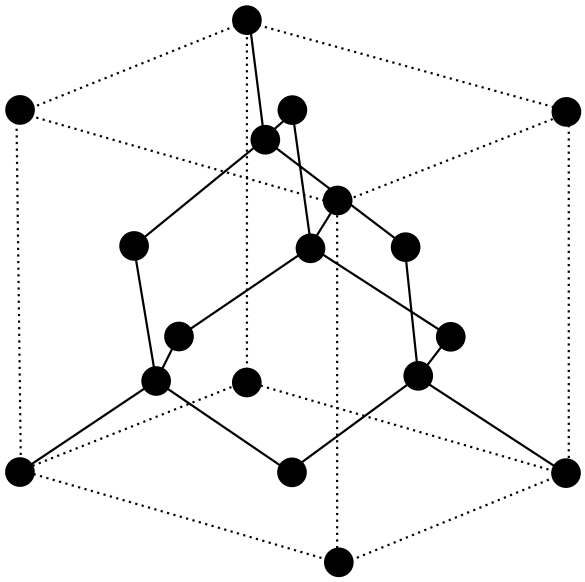

Figure 9.7: Full unit cell of the diamond lattice. It consists of 16 rods and 8 masses.

Clearly as $\alpha = L/r$ becomes greater the shear modulus must become smaller. Solving equation (9.38) for the bulk modulus of water and equation (9.39) for the density examples were considered for a variety of materials. Using steel where Young's modulus is $E_{steel} = 193\ GPa$ and $\rho_{steel} = 8000\ kg/m^3$ a solution is found with

$$\alpha_{steel} = 2.828, \qquad \beta_{steel} = -255.2\ kg/m^3, \tag{9.41}$$

where $\rho_{H_2O} = 1000\ kg/m^3$ and the bulk modulus of water as $K_{H_2O} = 2.2\ GPa$ was used. Since β is negative we must find materials that are lighter but keep relatively large stiffness. The contribution of just the steel rods to the density, i.e. the first term in equation (9.39), is $1020.7\ kg/m^3$, so if we took β to be zero we would not be too far off. The effective Lamé parameters using steel are $\lambda_{steel} \approx 1.86\ GPa$ and $\mu_{steel} \approx 0.51\ GPa$. For aluminum the results are

$$\alpha_{alum} = 1.616, \qquad \beta_{alum} = -670.25\ kg/m^3, \tag{9.42}$$

where $E_{alum} = 69\ GPa$ and $\rho_{alum} = 2700\ kg/m^3$. This results in a high shear stiffness material, where the lamé parameters are $\lambda_{alum} \approx 1.21\ GPa$ and $\mu_{alum} \approx 1.49\ GPa$. This is due to the relatively small α which means the rods are rather short compared to the radius. In order to increase α higher stiffness materials are required, for ceramic

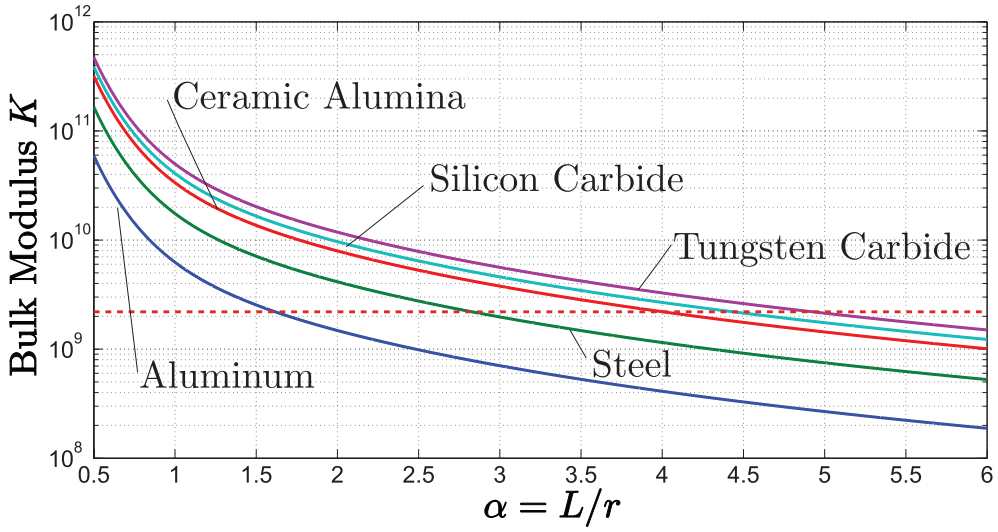

Figure 9.8: Predicted bulk modulus using equation (9.38), for steel, aluminum, ceramic alumina, and silicon carbide (SiC) rods where $E_{steel} = 193\ GPa$, $E_{alum} = 69\ GPa$, $E_{ceram} = 370\ GPa$ and $E_{SiC} = 450\ GPa$. Red dashed line represents the bulk modulus of water, $K_{H_2O} \approx 2.2\ GPa$.

alumina a solution is found with

$$\alpha_{ceram} = 4.00, \qquad \beta_{ceram} = 9242.9\ kg/m^3, \tag{9.43}$$

where $E_{ceram} = 370\ GPa$ and $\rho_{ceram} = 3920\ kg/m^3$. Figure 9.8 was generated using equation (9.38) and plots the effective bulk modulus as a function of α using several different materials. Clearly a three dimensional material will be very difficult to produce as high stiffness but lighter materials are required by the theory. These results are valid for larger α corresponding to longer and thinner rods. Lastly it should be noted that the filling factor, which is the proportional amount of space that could be occupied by spheres in point contact with each sphere centered at the vertices of the lattice, is $\frac{\pi\sqrt{3}}{16} \approx 0.34$ for the diamond lattice [90]. This result means that the lattice geometry has difficulty in filling space and is the reason that very stiff materials are needed. In two dimensions we only needed a material that was on the order of ten times the stiffness of water, here in three dimensions we need something on the order of one hundred times the stiffness.

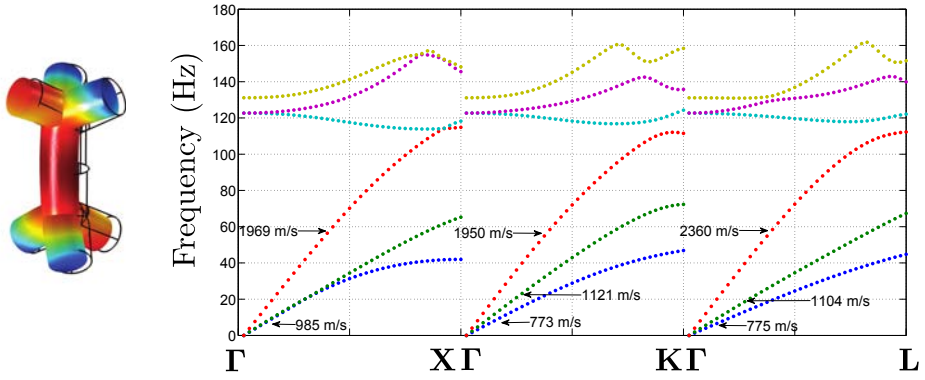

Figure 9.9: Using equation (9.38) for steel, $\alpha = 2.828$, which creates the geometry shown to the left. Dispersion curves found from Bloch-Floquet analysis using COMSOL are on the right. Shown are various wave speeds for longitudinal and transverse motion along paths of the Brillouin zone that have the point $\mathbf{\Gamma}$.

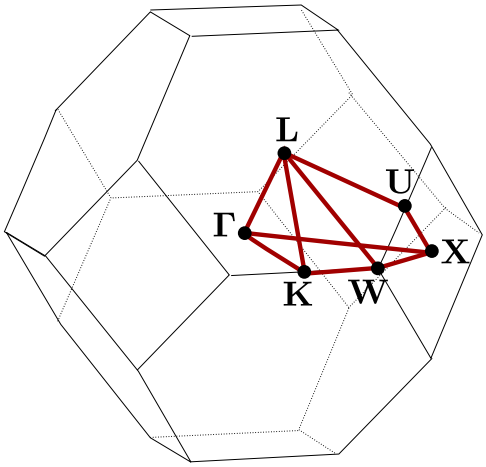

Figure 9.10: Brillouin zone for the diamond lattice [8]. The irreducible region is enclosed by the points $\mathbf{\Gamma}$, $\mathbf{X}$, $\mathbf{L}$, $\mathbf{W}$, $\mathbf{K}$, and $\mathbf{U}$ listed in equation (9.44).

9.2.1 Comparison using FEM

Next the results of Warren and Kraynik are compared using COMSOL. Instead of using the static homogenization technique, reviewed in section 6.2, we go straight to Bloch-Floquet analysis. Looking for quasi-static wave speeds by taking the derivative of the frequency with respect to the wave vector, as shown in equation (8.69), we take small steps away from $\mathbf{\Gamma}$ in the irreducible Brillouin zone, shown in figure 9.10 for the

diamond lattice. The points are defined by [8]

$$\begin{aligned} \mathbf{\Gamma} &= \begin{bmatrix} 0 \\ 0 \\ 0 \end{bmatrix}, \quad \mathbf{X} = c_0 \begin{bmatrix} 1 \\ 0 \\ 0 \end{bmatrix}, \quad \mathbf{L} = \frac{c_0}{2} \begin{bmatrix} 1 \\ 1 \\ 1 \end{bmatrix}, \\ \mathbf{W} &= c_0 \begin{bmatrix} 1 \\ 1/2 \\ 0 \end{bmatrix}, \quad \mathbf{K} = \frac{3c_0}{4} \begin{bmatrix} 1 \\ 1 \\ 0 \end{bmatrix}, \quad \mathbf{U} = c_0 \begin{bmatrix} 1 \\ 1/4 \\ 1/4 \end{bmatrix}, \end{aligned} \tag{9.44}$$

where $c_0 = \sqrt{3}\pi/(4L)$. Using the steel result of equation (9.41), where the density is not too far off, figure 9.9 was generated. Longitudinal and transverse wave speeds are shown in the dispersion curve figures along various directions. The longitudinal wave speed is about 2000 m/s and for water we desire 1500 m/s. Iterating the Bloch-Floquet analysis just for the desired wave speed and neglecting the density requirement we find $\alpha_{steel} \approx 22.4$. However this does not solve the problem since we are only finding

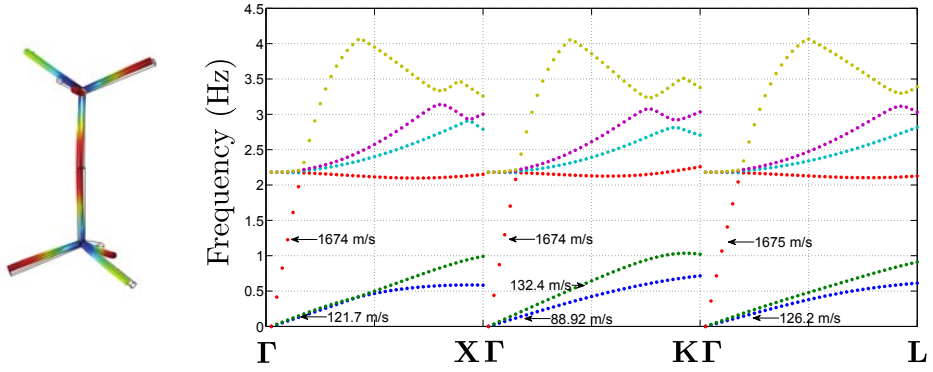

Figure 9.11: Right side shows the geometry for $\alpha = 22.4$. Dispersion curves shown on left using steel.

solutions for which $c = \sqrt{\frac{K}{\rho}} \approx 1500\ m/s$. In order to be water like we require both the density and the bulk modulus be equivalent to water, this ensures that the medium is matched both in impedance and speed. For $\alpha = 22.4$, figure 9.11 was generated. The bulk modulus is found by noting the filling fraction for this example is $\phi^{el} = 0.00203$, which for steel gives an effective density of 16 kg/m^3. The bulk modulus as calculated by Bloch-Floquet analysis via COMSOL is then; $K^{FEM} = 44.83\ MPa$, whereas the Warren and Kraynik result, equation (9.38), gives $K^{pred} = 38.68\ MPa$, which is close

to the FEM result. Likewise for $\alpha = 2.83$, shown in figure 9.9, we found $\phi^{el} = 0.128$, which means the effective density is 1024 kg/m^3 and the bulk modulus calculated by FEM is $K^{FEM} = 4.49\ GPa$ and that calculated by (9.38) gives $K^{pred} = 2.2\ GPa$. This puts light to the fact that the theory is valid for thin members, in the example of $\alpha = 22.4$ we were to able to find closer agreement of the calculated bulk modulus between the analytical and FEM results however for $\alpha = 2.8$ the results are quite off.

9.2.2 Examples using tetrahedral and spherical shaped masses

In order to match the density masses are added to the strut intersections. Using an all steel design where the rod is simulated as being in full contact with the tetrahedral shaped mass figures 9.12, 9.13, and 9.14 were generated. So far the dispersion curves in this chapter have been taken with an unrealistic rod radius of 1 m, which explains the rather low frequencies seen in the dispersion curves. The cell size can be scaled down which has the effect of raising the frequencies in the band diagrams without changing the wave speeds shown in the figures. This is seen between figures 9.13 and 9.14, where the geometry is exactly the same except in figure 9.14 the rod radius was scaled down to 1 cm. After enough iterations figure 9.15 was created which matches the density and wave speed very closely. Unfortunately the shear wave speed is high meaning there is not much of a frequency range where only the purely longitudinal mode is present, which is the desired goal of producing a material that mimics water-like behavior.

The next design considers using spherical masses where, in order to reduce the materials effective shear modulus, rods are not in full contact with the sphere. The geometry is shown in figure 9.16. The rod material was changed to silicon carbide which is much stiffer than steel. This has the effect of increasing α which lowers the expected shear modulus of the material. The spherical masses are taken as steel. Doing this resulted in figure 9.17, which is matched to water in speed and density. The shear speed is still rather high with an effective shear moduli of $G \approx 0.25\ GPa$. Using a stiffer material such as tungsten carbide, where the material properties are $E = 550$ GPa and $\rho = 15,630\ kg/m^3$, figure 9.18 was created. We investigate further by looking into changing the rod geometry.

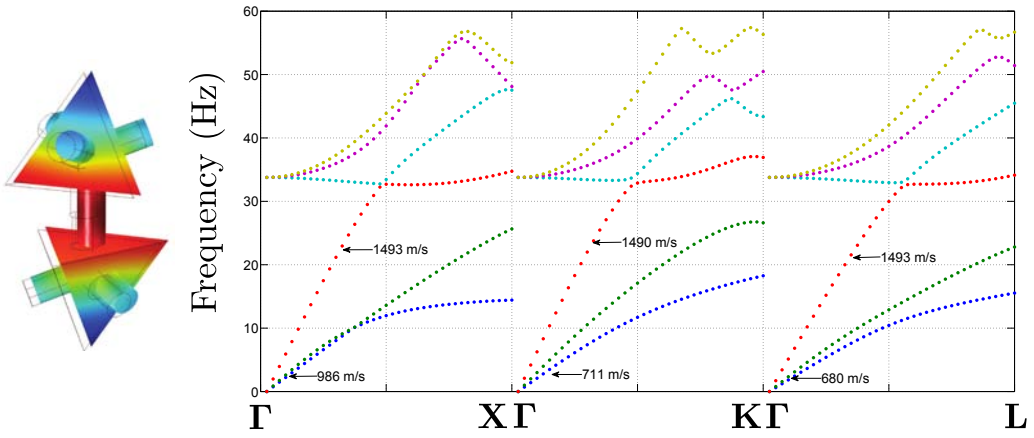

Figure 9.12: Dispersion curves found from Bloch-Floquet analysis using COMSOL. Using all steel design with $\alpha = 4.2$, this gives an effective density of $\rho = 1126\ kg/m^3$.

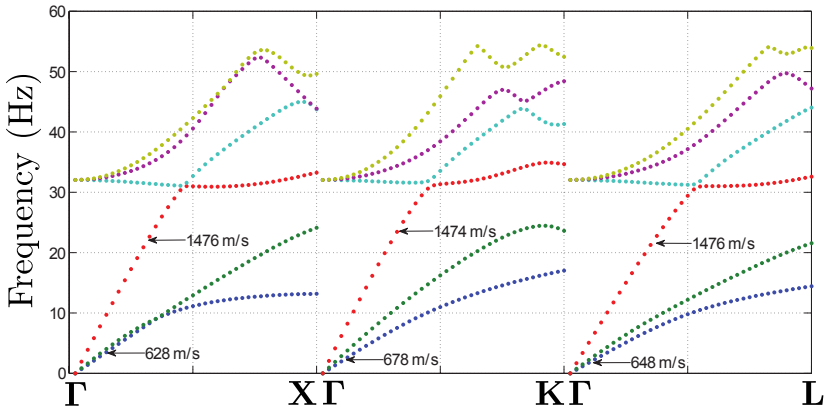

Figure 9.13: Dispersion curves for $\alpha = 4.4$ using tetrahedral masses, geometry shape similar to figure 9.12 left. Using all steel design the effective density is 996 kg/m^3.

9.2.3 Hollow Rods

Here rods consisting of inner radius r_i and outer radius r are considered. Again the axial compliance, M, and bending compliance, N, are given by

$$M = \int_0^L \frac{\mathrm{d}\,x}{EA}, \quad N = \int_0^L \frac{x^2\,\mathrm{d}\,x}{EI}, \tag{9.45}$$

where I is the moment of inertia, for a beam $I = bt^3/12$ and for a rod $I = \pi r^4/4$. For a hollow rod $I = \frac{\pi}{4}(r^4 - r_i^4)$ then

$$M = \frac{L}{E\pi(r^2 - r_i^2)}, \quad N = \frac{4L^3}{3E\pi(r^4 - r_i^4)}. \tag{9.46}$$

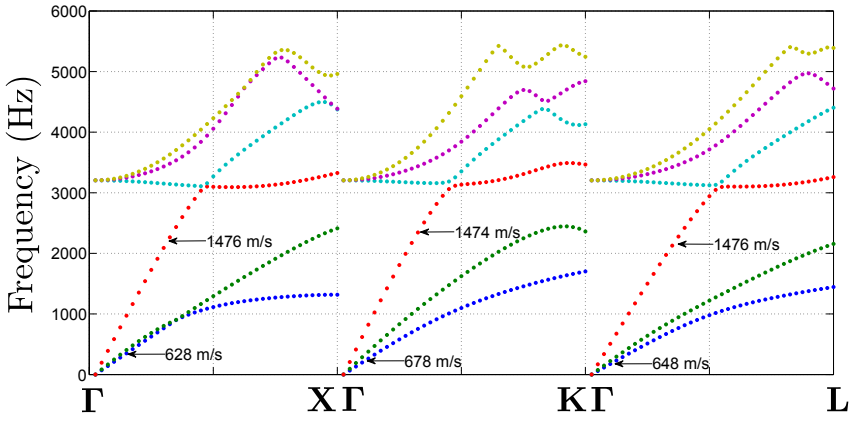

Figure 9.14: Dispersion curves for all steel design. Geometry same as in figure 9.13 with $\alpha = 4.4$ however here $r = 1\ cm$.

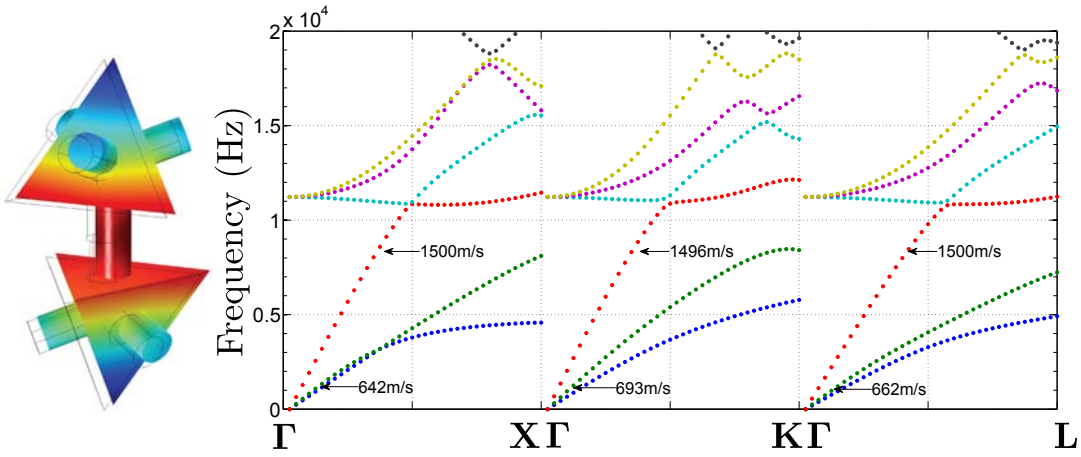

Figure 9.15: Finalized version of the all steel design with tetrahedral masses in full contact. Parameters are $\alpha = 4.32$, $L = 13\ cm$, $\rho = 1000\ kg/m^3$.

The effective moduli are

$$\lambda_{WK} = \frac{(N-M)16N}{288\sqrt{3}LMN(2M+N)} = E\pi\frac{(r^2-r_i^2)(4L^2-3(r^2+r_i^2))}{36\sqrt{3}L^2(2L^2+3(r^2+r_i^2))}, \tag{9.47}$$

$$\mu_{WK} = \frac{M(40N+32M)}{288\sqrt{3}LMN(2M+N)} = E\pi\frac{(r^4-r_i^4)(5L^2+3(r^2+r_i^2))}{24\sqrt{3}L^4(2L^2+3(r^2+r_i^2))}, \tag{9.48}$$

and the bulk modulus is

$$K_{H_2O} = E\pi\frac{(r^2-r_i^2)(4L^4+2L^2(r^2+r_i^2)+3(r^2+r_i^2)^2)}{36\sqrt{3}L^4(2L^2+3(r^2+r_i^2))}, \tag{9.49}$$

because the term $(r^2-r_i^2)$ shows in the numerator taking hollow cylinders is of no help.

The density is

$$\rho_{H_2O} = \frac{9\rho_{rod}\pi(r^2-r_i^2)}{16\sqrt{3}L^2} + \frac{9m}{64\sqrt{3}L^3}. \tag{9.50}$$

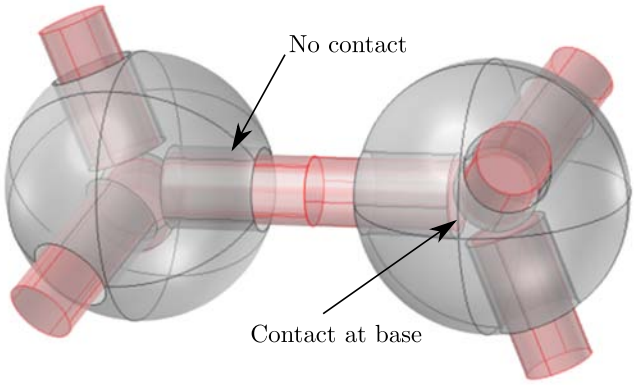

Figure 9.16: Geometry using spherical masses with limited contact region. Used to create figure 9.17.

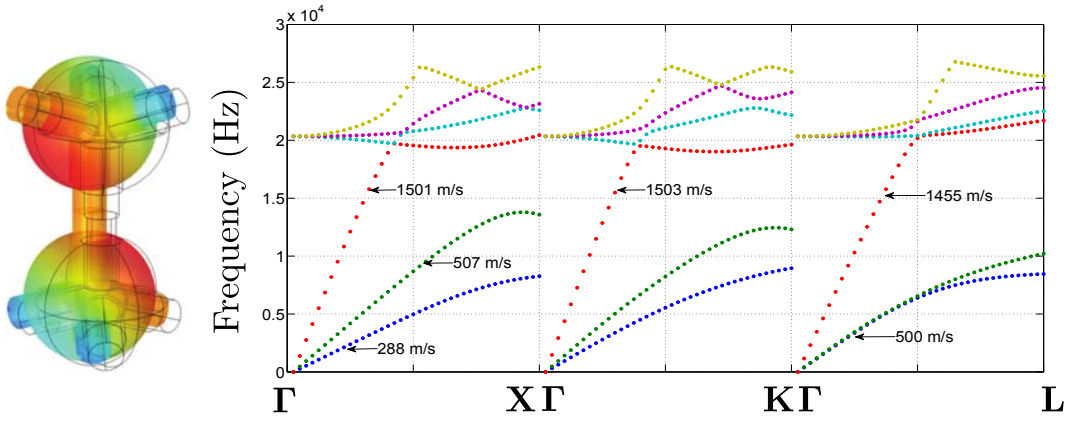

Figure 9.17: Silicon carbide rods with steel masses. Rod radius is $r = 1.16\ mm$. Effective properties are $\rho = 1000\ kg/m^3$, $G \approx 0.25\ GPa$, and $\nu \approx 0.45$.

9.2.4 Double coned rods

Trying the coned shape geometry, as seen in [24], in order to investigate if a reduction in shear modulus occurs. The rod geometry is shown in figure 9.19, the axial and bending compliances are

$$M = \int_0^L \frac{\mathrm{d}\,x}{EA} = \frac{L}{E\pi r R}, \tag{9.51}$$

$$N = \int_0^L \frac{x^2\,\mathrm{d}\,x}{EI} = \frac{4L^3}{3E\pi R r^3}. \tag{9.52}$$

Using equations (9.19) and (9.20) the effective moduli are

$$\lambda_{WK} = \frac{(N-M)16N}{288\sqrt{3}LMN(2M+N)} = E\pi r R\frac{4L^2-3r^2}{36\sqrt{3}L^2(2L^2+3r^2)}, \tag{9.53}$$

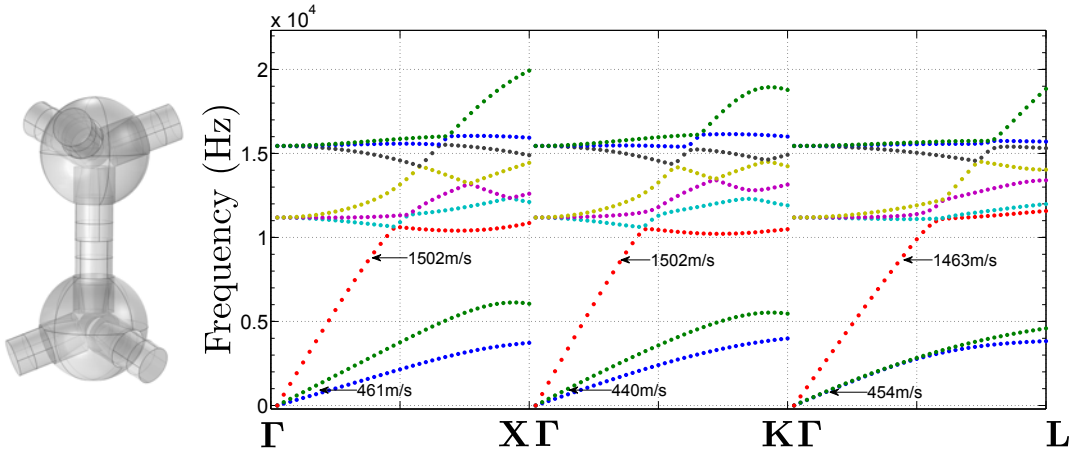

Figure 9.18: Tungsten carbide rods with steel masses. Parameters: $L = 13\ mm$, $\alpha = 5.6$, effective density, $\rho = 1000\ kg/m^3$.

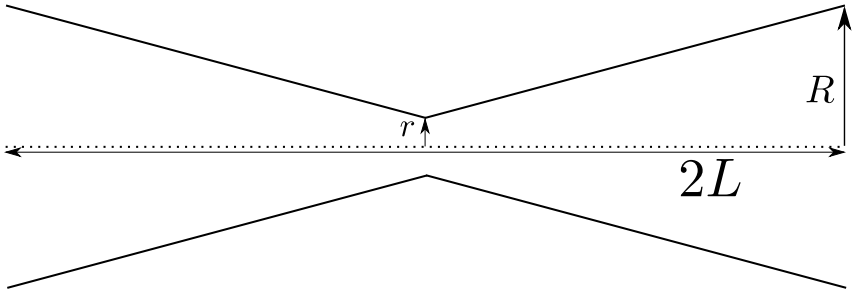

Figure 9.19: Double coned shape geometry of rod.

$$\mu_{WK} = \frac{M(40N + 32M)}{288\sqrt{3}LMN(2M + N)} = E\pi Rr^3 \frac{5L^2 + 3r^2}{24\sqrt{3}L^4(2L^2 + 3r^2)}. \tag{9.54}$$

The bulk modulus is

$$K_{H_2O} = E\pi Rr \frac{4L^4 + 2L^2r^2 + 3r^4}{36\sqrt{3}L^4(2L^2 + 3r^2)}. \tag{9.55}$$

An example using this geometry was found using steel double coned shaped rods with tetrahedral aluminum masses, shown in figure 9.20. Here we see a rather large range in frequency where only the purely longitudinal mode occurs in the band diagram. This design is capable of filling more space due to the rod geometry and exotic materials with extreme stiffness such as silicon carbide are not needed, making it easier to manufacture.

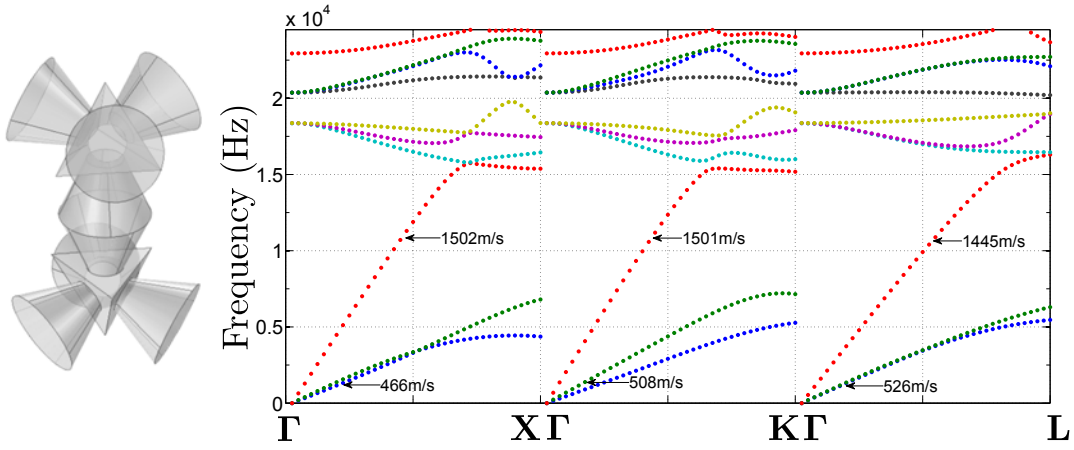

Figure 9.20: Double coned shaped example using steel rods and aluminum tetrahedral masses. Parameters are $L = 13\ mm$, $L/r = 1.8$, $R = r/2.5$, where R is the radius of the rod measured at the contact region with the tetrahedral mass.

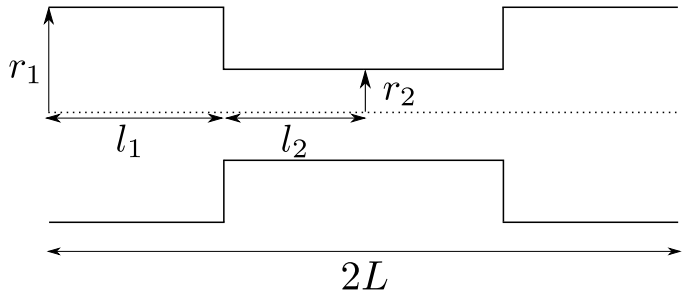

Figure 9.21: Two radii and length model, for possible reduction in shear modulus.

9.2.5 Two length and radii model

The geometry shown in figure 9.21 is considered here where there are two radii and lengths used to define the rod. The axial and bending compliances are

$$M = \int_0^{l_1} \frac{\mathrm{d}\,x}{E\pi r_1^2} + \int_{l_1}^{l_1+l_2} \frac{\mathrm{d}\,x}{E\pi r_2^2} = \frac{l_1}{E\pi r_1^2} + \frac{l_2}{E\pi r_2^2}, \tag{9.56}$$

$$N = \int_0^{l_1} \frac{x^2\,\mathrm{d}\,x}{E\pi r_1^4/4} + \int_{l_1}^{l_1+l_2} \frac{x^2\,\mathrm{d}\,x}{E\pi r_2^4/4} = \frac{4l_1^3}{3E\pi r_1^4} + \frac{4l_2}{3E\pi r_2^4}\left[3l_1^2 + 3l_1l_2 + l_2^2\right]. \tag{9.57}$$

Simplifying further gives

$$\begin{aligned} M &= M_0\left[1 + (\frac{r_1}{r_2})^2\frac{l_2}{l_1}\right], \\ N &= N_0\left[1 + (\frac{r_1}{r_2})^4\left[3\frac{l_2}{l_1} + 3(\frac{l_2}{l_1})^2 + (\frac{l_2}{l_1})^3\right]\right], \end{aligned} \tag{9.58}$$

where

$$M_0 = \frac{l_1}{E\pi r_1^2}, \quad \text{and} \quad N_0 = \frac{4l_1^3}{3E\pi r_1^4}. \tag{9.59}$$

The lamé moduli are rather complicated functions and are not reproduced here. What

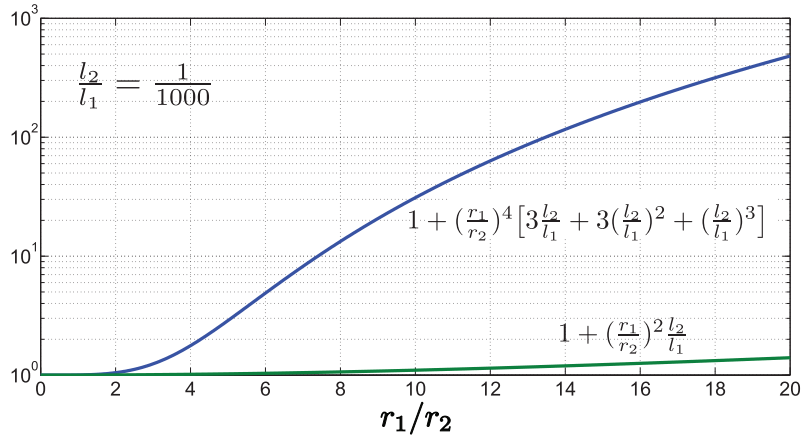

Figure 9.22: The effect on the axial and bending compliance by reducing the radius of a small piece of the midsection of the length is shown, using equation (9.58).

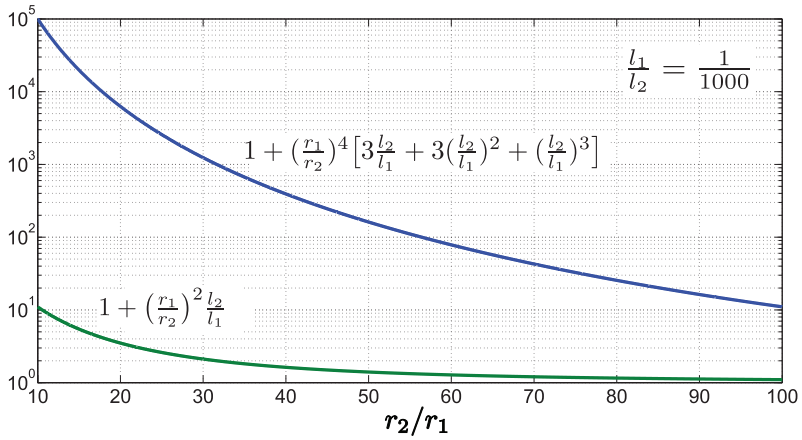

Figure 9.23: The effect on bending and axial compliance for reducing the radius of a small section near the junction, using equation (9.58).

is important are the studies shown in figures 9.22 and 9.23, where the parameters of figure 9.21 are used to change the bending and axial compliances of equation (9.58). It's seen that this model can affect the bending compliance much more than the axial by reducing a small length of the midsection of the rod. This will have the intended affect of lowering the effective shear modulus while maintaining most of the bulk modulus. Models using tungsten carbide rods with steel masses were constructed and studied using COMSOL located in figures 9.25 and 9.26. Again the rods are only in contact with the spherical mass at the rod base.

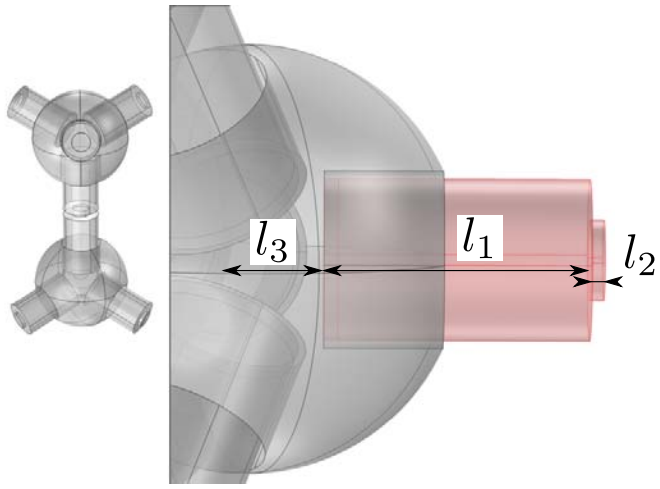

Figure 9.24: Geometry used for the two length and radii model, $L = l_1 + l_2 + l_3$, where l_3 begins at the junction center.

The approximate density in terms of design parameters is

$$\rho \approx \frac{9\pi\rho_{rod}(r_1^2 l_1 + r_2^2 l_2)}{16\sqrt{3}(l_1+l_2)^3} + \frac{9m}{64\sqrt{3}(l_1+l_2)^3}. \tag{9.60}$$

9.2.6 Tapered ends

The design considered here, shown in figure 9.27, consists of tapering the rod ends, this should have the effect of lowering the shear stiffness of the material. The radius is

$$r(x) = \begin{cases} \frac{r_2-r_1}{l_1}x + r_1, & 0 \le x \le l_1 \\ r_2, & x \ge l_1. \end{cases} \tag{9.61}$$

The axial and bending compliance are then

$$\begin{aligned} M &= \int_0^{l_1} \frac{\mathrm{d}\,x}{E\pi(\frac{r_2-r_1}{l_1}x + r_1)^2} + \int_{l_1}^{l_1+l_2} \frac{\mathrm{d}\,x}{E\pi r_2^2} = \frac{1}{E\pi r_2}\big[\frac{l_1}{r_1} + \frac{l_2}{r_2}\big], \\ N &= \int_0^{l_1} \frac{x^2\,\mathrm{d}\,x}{E\pi(\frac{r_2-r_1}{l_1}x + r_1)^4/4} + \int_{l_1}^{l_1+l_2} \frac{x^2\,\mathrm{d}\,x}{E\pi r_2^4/4} \\ &= \frac{4}{3E\pi r_2^3}\big[\frac{l_1^3}{r_1} + \frac{(l_1+l_2)^3 - l_1^3}{r_2}\big]. \end{aligned} \tag{9.62}$$

Using this design, COMSOL models were produced in figures 9.29 and 9.30 with design parameters located in figure 9.28. The best designs are those located in figures 9.20 and 9.30, both of which use machinable materials such as steel and aluminum. Further work must be done but clearly tapering the rod ends seems to be the most effective

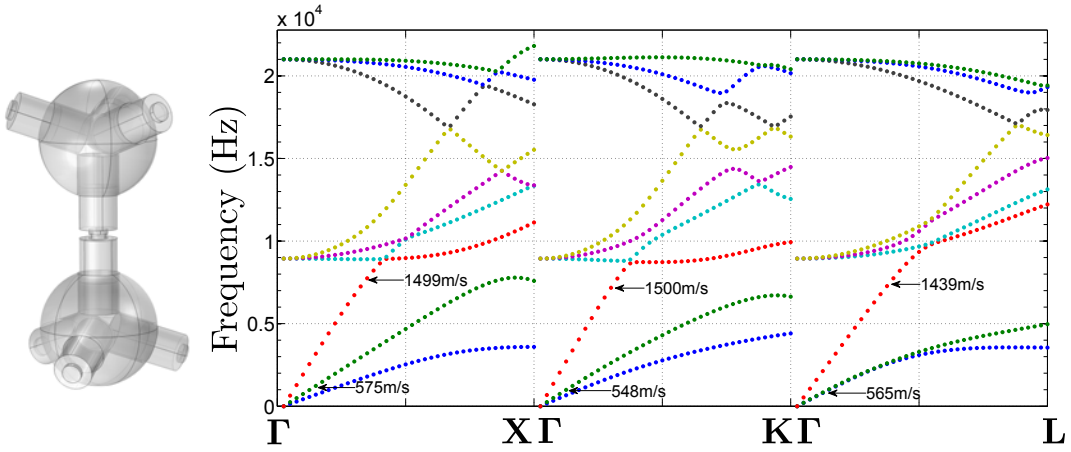

Figure 9.25: Two length and radii model with spherical masses. Tungsten carbide rods with steel spheres, effective density is 1000 kg/m^3. Parameters: $L = 13$ mm, $L/r_1 = 4.93$, $l_3 = L/6.1$, $r_2 = r_1/2$, $l_2 = L/20$, where l_1, l_2, and l_3 are shown in figure 9.24.

way of lowering the shear wave speed as compared to the other designs studied. In summary producing three dimensional metamaterials capable of mimicking the acoustic properties of water is a difficult task. A problematic hurdle here is that as we look into designs that seek to minimize shear stiffness we find the parameter $\alpha = L/r$ decreases which has the opposite effect. One solution could be a type of ball joint at the mass junctions, which would be able to sustain a hydrostatic loading but would deform rapidly due to a shear loading. Further work on producibility must be conducted however it is clear that designing a material capable of mimicking the acoustic properties of water is feasible. Next the cubic lattice is studied where matching to water is found along one direction.

9.3 Cubic example

Here the cubic lattice geometry shown in figure 9.31 is studied, it is noted that anisotropic behavior in the effective elasticity is to be expected. The goal here is to match the wave speed only in one direction while simultaneously matching density. This device will be water-like along three directions parallel to the rods in the unit cell. The Brillouin zone for the cubic lattice is shown in figure 9.32, where the points in the

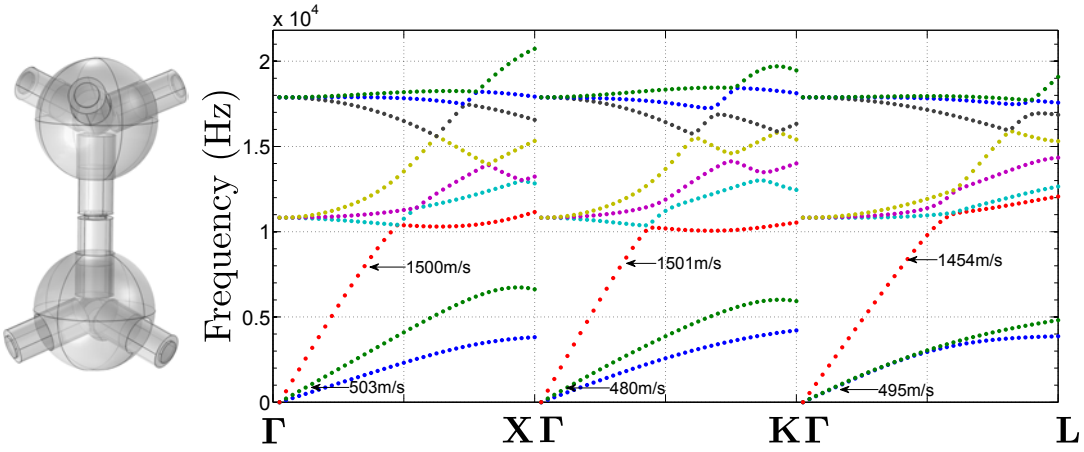

Figure 9.26: Two length and radii model with spherical masses. Tungsten carbide rods with steel spheres, effective density is 1000 kg/m^3. Parameters: $L = 13\ mm$, $L/r_1 = 5.34$, $l_3 = L/6.3$, $r_2 = r_1/1.5$, $l_2 = L/40$, where l_1, l_2, and l_3 are shown in figure 9.24.

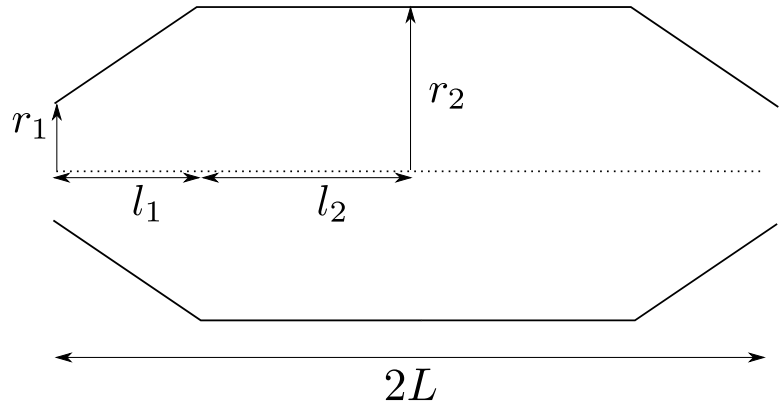

Figure 9.27: Rod geometry for tapered end design.

irreducible zone are defined by

$$\mathbf{\Gamma} = \frac{\pi}{L}\begin{bmatrix}0\\0\\0\end{bmatrix}, \quad \mathbf{X} = \frac{\pi}{L}\begin{bmatrix}0\\1\\0\end{bmatrix}, \quad \mathbf{M} = \frac{\pi}{L}\begin{bmatrix}1\\1\\0\end{bmatrix}, \quad \mathbf{R} = \frac{\pi}{L}\begin{bmatrix}1\\1\\1\end{bmatrix}. \tag{9.63}$$

An example using steel was created where the wave speed is matched to water along $\mathbf{\Gamma} - \mathbf{X}$, located in figure 9.33. Here there is full contact with the mass and the rods. Additionally the dispersion curves were generated at higher frequencies, shown in figure 9.34, where significant band gaps are present. This type of material could be used to filter undesired frequencies. The wave speeds calculated by COMSOL are checked using the Christoffel equation. The elasticity components of cubic materials are defined

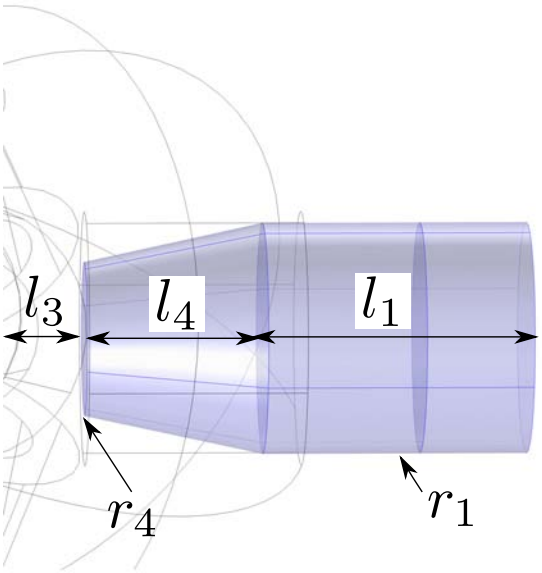

Figure 9.28: Geometry used for the tapered end model, $L = l_1 + l_4 + l_3$, where l_3 begins at the junction center. Radius r_1 is the larger radius of the rod which tapers to radius r_4 located at the contact zone of the rod with the mass junction.

by three parameters, κ, μ_1 and μ_2 [33]. This was derived earlier in equation (2.58), where the wave speeds were found using the wave vector directions used here. Equating the speeds this material has elastic properties $\kappa = 0.77\ GPa$, $\mu_1 = 0.026\ GPa$, and $\mu_2 = 1.11\ GPa$, which can be checked using (2.58) using $\rho = 1000\ kg/m^3$. In figure 9.33 water like behavior is seen in the $\mathbf{\Gamma} - \mathbf{X}$ branch. This is similar to what was seen in the previous section using the diamond lattice, however here this can only be accomplished in this one direction of the k path defined by the irreducible Brillouin zone. Since the $\mathbf{\Gamma} - \mathbf{X}$ direction in k space is equivalent to directions parallel to the rods the structure has water like response along three directions normal to the faces. This concludes the study of periodic lattice structures and the designing process of metamaterials here. The next chapter concludes the thesis where original contributions, current work and future work are discussed.

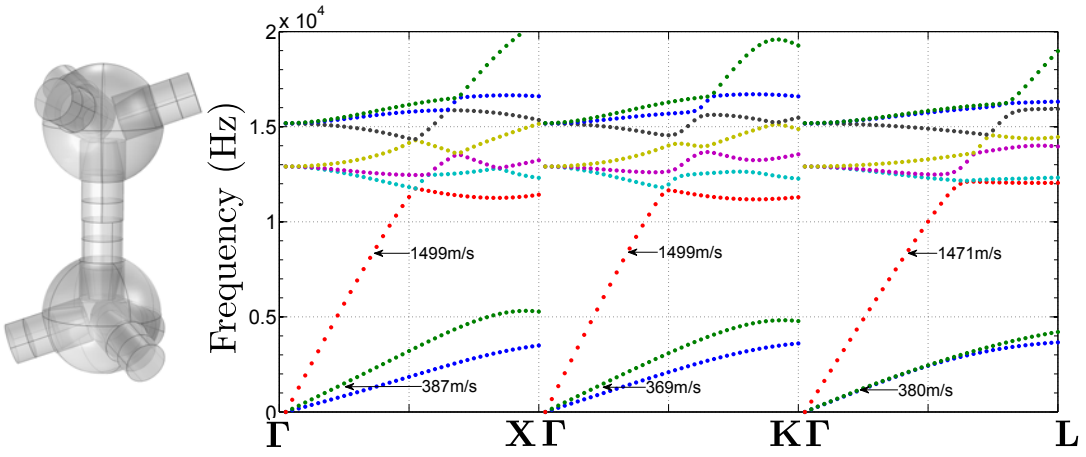

Figure 9.29: Tapered end geometry. Tungsten carbide rods with steel masses. Parameters: $L = 13\ mm$, $L/r_1 = 4.62$, $r_4 = r_1/1.5$, $l_3 = L/5.8$, $l_4 = L/3$. Dimension definitions shown in figure 9.28.

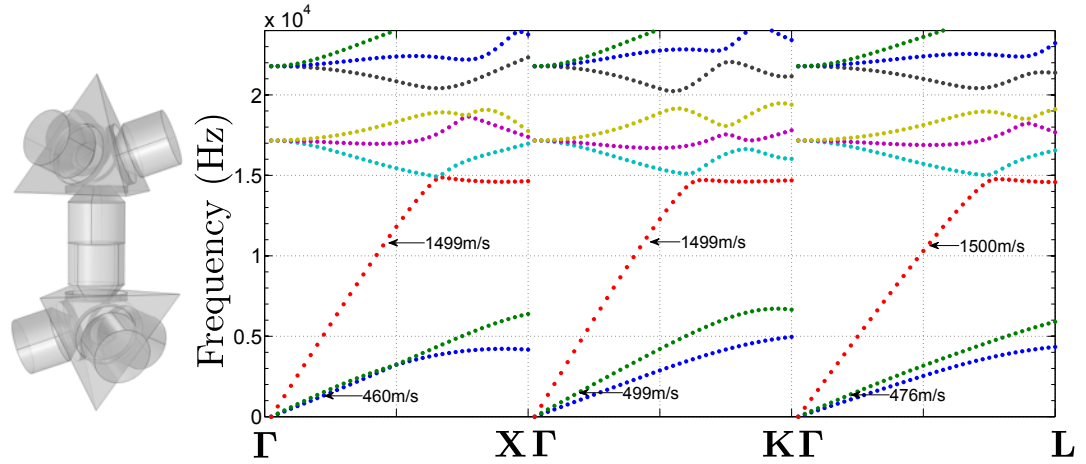

Figure 9.30: Tapered end geometry. All steel design. Parameters: $L = 13\ mm$, $L/r_1 = 2.80$, $r_4 = r_1/2$, $l_3 = L/3.5$, $l_4 = L/5$. Dimensions definitions shown in figure 9.28.

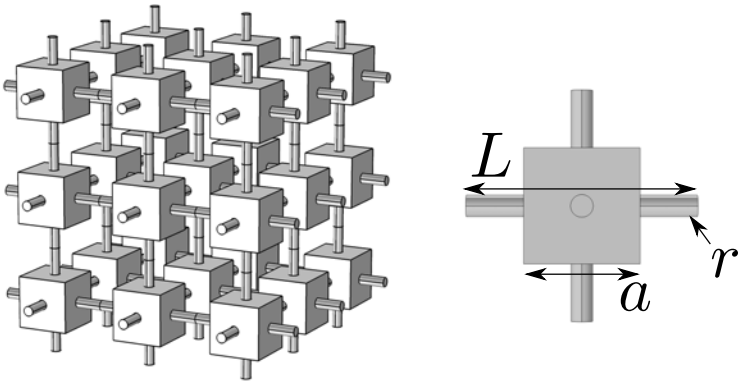

Figure 9.31: Cubic lattice design. Parameters are: L, the total length of the unit cell, a the length of one side of the cubic mass located at the joint, and r, the rod radius.

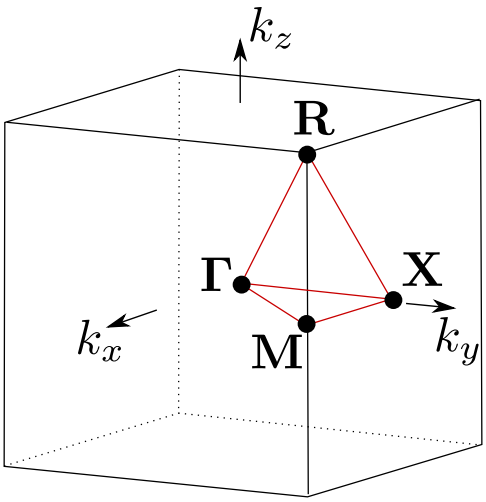

Figure 9.32: Brillouin zone of the cubic lattice [8]. Irreducible zone is enclosed by the points **Γ**, **M**, **X** and **R**, defined in equation (9.63).

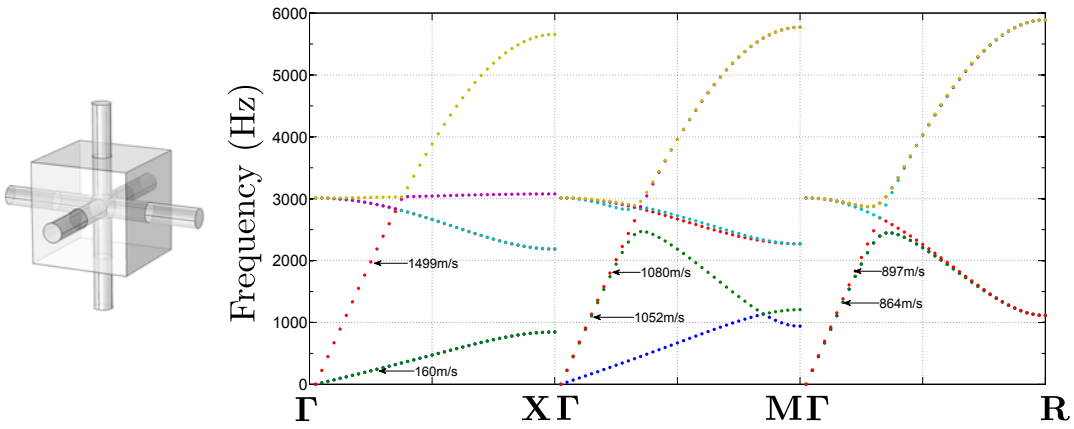

Figure 9.33: All steel design. Parameters: $L = 85.8\ mm$, $a = 42\ mm$, and $r = 4\ mm$. Dimension definitions shown in figure 9.31.

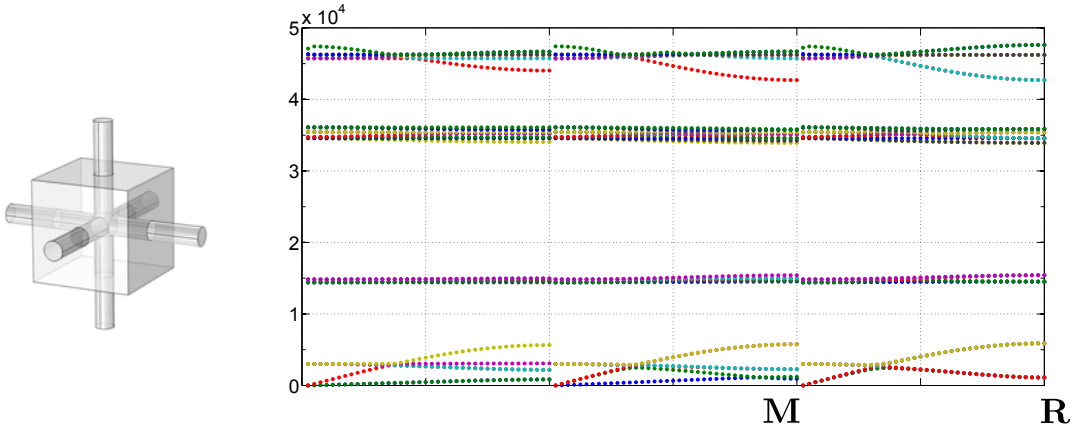

Figure 9.34: All steel design. Parameters: $L = 85.8\ mm$, $a = 42\ mm$, and $r = 4\ mm$. Effective density, $\rho = 1000\ kg/m^3$. Dimension definitions shown in figure 9.31.

Chapter 10

Conclusions and future work

The main objective of this thesis was to produce materials that mimic the acoustic properties of water. This was done by designing lattice type materials where elastic and density properties are found from analysis of a unit cell. A robust study was accomplished in which macroscopic material properties were found by static and dynamic methods and several designs were proposed and studied in both two and three dimensions. Before beginning such an analysis an exhaustive review was completed starting with general elastodynamic theory where acoustic and elastic waves were studied in chapter 2. Designed materials with periodic structure containing reflection planes were considered to achieve the desired goal, elastic material symmetries were reviewed as it becomes important to understand what components of the elasticity tensor should be considered when designing a new material. Chapter 2 ended with a review of the Christoffel equation which computes the group velocities for longitudinal and shear waves in elastic media. Understanding how to find wave speed behavior from a material's elastic and density properties became valuable as a check on the homogenization methods reviewed in chapters 6 and 7, where by using the static methods elastic moduli can be found and by the dynamic methods group velocities can be found.

In chapter 3 the standard global matrix method for scattering from a cylindrically layered elastic medium was developed. The medium could have at most elasticity described by transverse isotropy and the method was found to require the inversion of rather large matrices dependent on the number of layers considered. This is problematic, especially in the application of acoustic cloaking theory where material properties of the cloak are required to vary as a function of the radius. This problem was resolved by the integration method reviewed and developed in chapter 4, where the Stroh

formalism was used in conjunction with the matricant and impedance matrices offering a stable solution scheme. It was found that the method is able to quickly solve for a large number of layers with general anisotropy and was used in chapter 5 where acoustic cloaking theory was reviewed and examples were considered. It was shown that pentamode elasticity is required for devices that are created using transformation acoustics theory. This type of elasticity is so named due to the five zero valued eigenvalues of it's elasticity tensor. Additionally it was shown this special type of elasticity only allows for longitudinal waves to propagate as shear wave speeds are zero in such a medium. Examples of acoustic cloaks using pentamode elasticity were considered where some amount of shear modulus was added to the medium, this was done as any elastic material able to keep structure will require a certain amount of shear rigidity. The cloaking medium is able to tolerate some level of shear wave to be present and still be effective. This result makes it possible to consider designed elastic structures to serve as the cloaking medium.

As a first step towards producing pentamode type cloaks, the goal of acoustically simulating water was chosen. In order to do this periodic structures were considered and homogenization theories were reviewed to accurately design the material. Static homogenization methods are reviewed in chapter 6 where elasticity components of periodic media can be found by both analytical and finite element means. In chapter 7, Bloch-Floquet analysis is extensively reviewed using several different methods with new results in the application of Euler-Bernoulli beams. This offers dispersion curve analysis in which group velocities can be found and static elastic moduli can be backed out and compared against the results of the previous chapter.

Lastly, in chapters 8 and 9 Metal Water designs were considered and analyzed in two and three dimensions. In two dimensions it was found that by using the regular hexagonal lattice, simulating water like behavior is very possible and does not require the use of exotic materials. In three dimensions the diamond lattice was required for isotropic behavior, this is somewhat problematic as it is difficult to fill space in such a lattice and as a result much stiffer materials were found to be required. However, by analyzing several different types of strut geometries and mass junctions an example

was found where double coned steel rods with tetrahedral aluminum mass junctions was able to solve the problem offering a range of frequencies where only the longitudinal mode exists, refer to figure 9.20. The cubic lattice was studied last where matching to water occurs in three orthogonal directions. It was noticed that such a material has fairly large band gaps, noted in figure 9.34, and could be used as a filtering device.

10.1 Original contributions

The original work completed in this thesis is largely in chapters 8 and 9, where unit cell designs for Metal Water were found for two and three dimensional structures. In two dimensions, Metal Water I was developed and produced, a three dimensional version has not yet been produced. A cubic structure was also found in which acoustic matching to water occurs along three orthogonal directions. The application of static and dynamic homogenization theories has been used for other types of devices, especially in the use of Bloch-Floquet theory in developing dispersion curves. The analytical static homogenization theory of Kim and Al-Hassani [64] for which an estimate on elastic moduli was reviewed. It was further developed in section 8.1 where several different unit cells with various types of struts were considered. Other contributions include the stable integration method which combines the matricant and impedance matrices to solve for acoustic scattering from layered media, located in chapter 4 and first published in [41]. Also new is the development of Bloch-Floquet solutions for elastic honeycomb structures using Euler-Bernoulli beams, done in section 7.5.

10.2 Current and future work

Many methods were reviewed especially under the application of Bloch-Floquet theory in chapter 7. Only the new method of using Euler-Bernoulli beams was compared to finite element results. Comparison of the other methods where a study of how adding physics to the problem changes the dispersion curves can be done. For instance, in the mass spring model only longitudinal modes are captured, for the Euler-Bernoulli and Timoshenko beams both longitudinal and bending modes are captured. Current work,

in the process of being published, extends the use of Euler-Bernoulli beams into three dimensions where comparison to finite element results shows that torsional modes are not accounted for in the theory.

Other work currently being done is the design of a micro-structured elastic slab device which takes an incoming acoustic wave and speeds it up in a given direction without reflection. This type of device is being designed with the methods studied here and time domain simulations done in COMSOL show the effectiveness of the device. Another point not discussed in detail is the water-device boundary, in two dimensions it has been seen that by water filling the bordering edges of the device better acoustic conduction is seen in simulation. In the proposed three dimensional structures this type of boundary does not exist and the question of how to best couple the two mediums, fluid and elastic lattice, arises.

Currently two dimensional analysis can be done in COMSOL at Rutgers where things such as reflection transmission spectrum analysis and full scale simulations can be considered. In three dimensions there is a lack of computing power for full scale simulation, where the micro-structure lattice design cannot be present in the model. Instead by utilizing the static homogenization method, reviewed in chapter 6 for three dimensions, a solid medium with effective elastic and density properties can replace the lattice. This type of analysis works so long as the wavelengths considered are at least on the order of the unit cell size, the analysis would be limited as the homogenization limit of the structure would not be seen.

Possibly the greatest area for future work is in the general production of meta-material devices. In two dimensions the Metal Water I design was produced with waterjet machining, which has thickness limitations and can be costly. The proposed CMI designs, which are constructed by bonding corrugated sheets, has had problems in the bonding process but may have recently been resolved. Further development on anisotropic two dimensional designs for acoustic cloaks is currently in the process of being published. Three dimensional anisotropic designs has yet to be considered in the application of cloaking theory. The ultimate goal for future investigation is the creation of a multi-layered cloaking device and physical testing.

References

[1] B. Hassani. A direct method to derive the boundary conditions of the homogenization equation for symmetric cells. *Communications in Numerical Methods in Engineering*, 12:185–196, 1996.

[2] N. Kikuchi and M. P. Bendsoe. Generating optimal topologies in structural design using a homogenization method. *Computer Methods in Applied Mechanics and Engineering*, 71:197–224, 1988.

[3] P. I. Kattan. *MATLAB Guide to Finite Elements: An Interactive Approach*. Springer, 2008.

[4] Léon Brillouin. *Wave Propagation in Periodic Structures*. Dover Publications, Inc. NY, 1953.

[5] Martin Maldovan and Edwin L. Thomas. *Periodic Materials and Interference Lithography*. WILEY-VCH Verlag GmbH & Co. KGaA, Weinheim, 2008, ISBN: 978-3-527-31999-2.

[6] M. J. Leamy. Exact wave-based bloch analysis procedure for investigating wave propagation in two-dimensional periodic lattices. *Journal of Sound and Vibration*, 331:1580–1596, 2012.

[7] A. N. Norris. Mechanics of elastic networks. *Proceedings of the Royal Society A.*, 470(2172), 2014.

[8] W. Setyawan and S. Curtarolo. High-throughput electronic band structure calculations: challenges and tools. *arXiv*, 1004.2974v1, 2010.

[9] D. Schurig, J.B. Pendry, and D.R. Smith. Controlling electromagnetic fields. *Science*, 312:1780, 2006.

[10] A. Greenleaf, M. Lassas, and G. Uhlmann. Anisotropic conductivities that cannot be detected by EIT. *Physiological Measurement*, 24(2):413–419, May 2003.

[11] D. A. Roberts, S. A. Cummer, M. Rahm, D. Schurig and D. R. Smith. Design of electromagnetic cloaks and concentrators using form-invariant coordinate transformations of maxwells equations. *Photonics and Nanostructures - Fundamentals and Applications*, 6:87–95, 2008.

[12] D. Schurig, J. B. Pendry, M. Rahm, S. A. Cummer and D. R. Smith. Optical design of reflectionless complex media by finite embedded coordinate transformations. *Physical Review Letters*, 100:063903, 2008.

[13] S. A. Cummer and D. Schurig. One path to acoustic cloaking. *New Journal of Physics*, 9(3):45, 2007.

[14] B. J. Justice, S. A. Cummer, J. B. Pendry, A. F. Starr, D. Schurig, J. J. Mock and D. R. Smith. Metamaterial electromagnetic cloak at microwave frequencies. *Science*, 314:977–980, 2006.

[15] M. Briane, G. W. Milton and J. R. Willis. On cloaking for elasticity and physical equations with a transformation invariant form. *New Journal of Physics*, 8:248, 2006.

[16] J. R. Willis. The non-local influence of density variations in a composite. *International Journal of Solids and Structures*, 21:80517, 1985.

[17] D. Torrent and J. Sánchez-Dehesa. Acoustic cloaking in two dimensions: a feasible approach. *New Journal of Physics*, 10(6):063015, 2008.

[18] J. E. Boisvert, C. L. Scandrett and T. R. Howarth. Acoustic cloaking using layered pentamode materials. *The Journal of the Acoustical Society of America*, 127(5):2856–2864, 2010.

[19] A. N. Norris and A. J. Nagy. Acoustic metafluids made from three acoustic fluids. *The Journal of the Acoustical Society of America*, 128(4):1606–1616, 2010.

[20] A. N. Norris. Acoustic cloaking theory. *Proceedings of the Royal Society A*, 464:2411–2434, 2008.

[21] A. N. Norris. Acoustic cloaking. *Acoustics Today*, 11(1):38–46, 2015.

[22] G. W. Milton and A. V. Cherkaev. Which elasticity tensors are realizable? *Journal of Engineering Materials and Technology*, 117(4):483–493, 1995.

[23] A. N. Norris, N. H. Gokhale and J. L. Cipolla. Special transformations for pentamode acoustic cloaking. *The Journal of the Acoustical Society of America*, 132(4):2932–2941, 2012.

[24] N. Stenger, M. Thiel, M. Kadic, T. Bckmann and M. Wegener. On the practicability of pentamode mechanical metamaterials. *Applied Physics Letters*, 100, 2012.

[25] J. D. Smith and P. E. Verrier. The effect of shear on acoustic cloaking. *Proceedings of the Royal Society A*, 407(2132):2291–2309, 2011.

[26] M. Abramowitz and I. Stegun. *Handbook of Mathematical Functions with Formulas, Graphs, and Mathematical Tables.* Dover, New York, 1974.

[27] P. M. C. Morse and H. Feshbach. *Methods of Theoretical Physics.* McGraw-Hill, New York, 1953.

[28] A. E. H. Love. *A Treatise on the Mathematical Theory of Elasticity.* Cambridge University Press, 1906.

[29] Biswajit Banerjee. *An Introduction to Metamaterials and Waves in Composites.* CRC PRESS, 2011.

[30] Gilbert Strang. *Linear Algebra and Its Applications, 4th Edition.* Cengage Learning, 2006.

[31] Michael A. Slawinski. *Waves and Rays in Elastic Continua*. World Scientific Publishing Co. Pte. Ltd., 2010.

[32] M. Destrade and G. Saccomandi. *Linear Elastodynamics and Waves*. Eolss Publishers, Oxford, UK, 2012.

[33] L. J. Walpole. Fourth rank tensors of the thirty-two crystal classes: multiplication tables. *Proceedings of the Royal Society A*, A391:149–179, 1984.

[34] A. N. Norris. Poisson's ratio in cubic materials. *Proceedings of the Royal Society A*, 462:3385–3405, 2006.

[35] F. Honarvar and A. N. Sinclair. Acoustic wave scattering from transversely isotropic cylinders. *The Journal of the Acoustical Society of America*, 100:57–63, 1996.

[36] F. Léon, F. Lecroq, D. Décultot and G. Maze Scattering of an obliquely incident acoustic wave by an infinite hollow cylindrical shell. *The Journal of the Acoustical Society of America*, 91:1388–1397, 1992.

[37] V. T. Buchwald. Rayleigh waves in transversely isotropic media. *The Quarterly Journal of Mechanics and Applied Mathematics*, 14:293–317, 1961.

[38] P. Chadwick. Wave propagation in transversely isotropic elastic media i. homogeneous plane waves. *Proceedings of the Royal Society A*, A422:23–66, 1989.

[39] A. Rahman and F. Ahmad. Representation of the displacement in terms of scalar functions for use in transversely isotropic materials. *The Journal of the Acoustical Society of America*, 104(6):3675–3676, 1998.

[40] A. N. Norris and A. L. Shuvalov. Wave impedance matrices for cylindrically anisotropic radially inhomogeneous elastic materials. *The Quarterly Journal of Mechanics and Applied Mathematics*, 63:1–35, 2010.

[41] A. N. Norris, A. J. Nagy and F. A. Amirkulova. Stable methods to solve the impedance matrix for radially inhomogeneous cylindrically anisotropic structures. *Journal of Sound and Vibration*, 332(10):2520–2531, 2013.

[42] A. L. Shuvalov. A sextic formalism for three-dimensional elastodynamics of cylindrically anisotropic radially inhomogeneous materials. *Proceedings of the Royal Society A*, 459(2035):1611–1639, 2003.

[43] T. C. T. Ting. Pressuring, shearing, torsion and extension of a circular tube or bar of cylindrically anisotropic material. *Proceedings of the Royal Society A*, 452(1954):2397–2421, November 1996.

[44] M. C. Pease. *Methods of Matrix Algebra*. Academic Press, New York, 1965.

[45] J. Schiff and S. Shnider. A natural approach to the numerical integration of riccati differential equations. *SIAM Journal on Numerical Analysis*, 36(5):1392–1413, 1999.

[46] R. Bellman and G. M. Wing. An Introduction to Invariant Imbedding. *Society for Industrial and Applied Mathematics*, 1987.

[47] J. P Berrut and L. N. Trefethen. Barycentric lagrange interpolation. *SIAM Review*, 46(3):501–517, 2004.

[48] W. Magnus. On the exponential solution of differential equations for a linear operator. *Communications on Pure and Applied Mathematics*, 7(4):649–673, 1954.

[49] A. Iserles and S. P. Norsett. On the solution of linear differential equations in lie groups. *Philosophical Transactions: Mathematical, Physical and Engineering Sciences*, 357(1754):983–1019, 1999.

[50] Y. Y. Lu. A fourth-order magnus scheme for helmholtz equation. *Journal of Computational and Applied Mathematics*, 173(2):247–258, 2005.

[51] V. K. Varadan L. Flax and V. V. Varadan. Scattering of an obliquely incident acoustic wave by an infinite cylinder. *The Journal of the Acoustical Society of America*, 68:1832–1835, 1980.

[52] U. Leonhardt. Optical conformal mapping. *Science*, 312(5781):1777–1780, June 2006.

[53] J. B. Pendry, D. Schurig, and D. R. Smith. Controlling electromagnetic fields. *Science*, 312(5781):1780–1782, June 2006.

[54] M. Lassas A. Greenleaf, Y. Kurylev and G. Uhlmann. Cloaking devices, electromagnetic wormholes, and transformation optics. *SIAM Review*, 51 (1):3–33, 2009.

[55] K. M. Moore D.C. Calvo G.J. Orris C. N. Layman, T. P. Martin. Designing acoustic transformation devices using fluid homogenization of an elastic substructure. *Applied Physics Letters*, 99:163503, 2011.

[56] L. Wu and L. Chen. Acoustic planar hyperlens via transformation acoustics. *Journal of Physics D: Applied Physics*, 44:125402, 2011.

[57] R. V. Craster and S. Guenneau. *Acoustic Metamaterials*. Springer, 2013.

[58] S. A. Cummer and D. Schurig. One path to acoustic cloaking. *New Journal of Physics*, 9(3):45+, March 2007.

[59] H. Chen and C. T. Chan. Acoustic cloaking in three dimensions using acoustic metamaterials. *Applied Physics Letters*, 91(18):183518+, 2007.

[60] L-W Cai and J. Sánchez-Dehesa. Analysis of CummerSchurig acoustic cloaking. *New Journal of Physics*, 9(12):450+, December 2007.

[61] S. A. Cummer, B. I. Popa, D. Schurig, D. R. Smith, J. Pendry, M. Rahm, and A. Starr. Scattering theory derivation of a 3D acoustic cloaking shell. *Physics Review Letters*, 100(2):024301+, 2008.

[62] Lorna J. Gibson and Michael F. Ashby. *Cellular Solids. Structure and properties-Second edition*. Cambridge University Press, 1997.

[63] J. B. Park E. A. Friis, R. S. Lakes. Negative poisson's ratio polymeric and metallic foams. *Journal of Materials Science*, 23:4406–4414, 1988.

[64] S.T.S. Al-Hassani H.S. Kim. A morphological elastic model of general hexagonal columnar structures. *International Journal of Mechanical Sciences*, 43:1027–1060, 2001.

[65] W. E. Warren and A. M. Kraynik. The linear elastic properties of open-cell foams. *Journal of Applied Mechanics*, 55:341–346, 1988.

[66] A. P. Boresi and R. J. Schmidt. *Advanced Mechanics of Materials*. Wiley, 1993.

[67] Yu Wang and Alberto M. Cuitino. Three-dimensional nonlinear open-cell foams with large deformations. *Journal of the Mechanics and Physics of Solids*, 48 (2000):961–988, 1999.

[68] J. M. Guedes and N. Kikuchi. Preprocessing and postprocessing for materials based on the homogenization method with adaptive finite element methods. *Computer Methods in Applied Mechanics and Engineering*, 83:143–198, 1990.

[69] E. Hinton B. Hassani. A review of homogenization and topology optimization i–homogenization theory for media with periodic structure. *Computers and Structures*, 69:707–717, 1998.

[70] E. Hinton B. Hassani. A review of homogenization and topology optimization ii-analytical and numerical solution of homogenization equations. *Computers and Structures*, 69:719–738, 1998.

[71] E. Hinton and B. Hassani. A review of homogenization and topology optimization iii– topology optimization using optimality criteria. *Computers and Structures*, 69:739–756, 1998.

[72] Ellis H. Dill. *The Finite Element Method for the Mechanics of Solids with ANSYS Applications*. CRC Press, 2011.

[73] O.C. Zienkiewicz and R.L. Taylor. *The finite element method 4th ed, vol. 1*. McGraw-Hill, London, 1989.

[74] P. G. Martinsson and A. B. Movchan. Vibrations of lattice structures and phononic band gaps. *The Quarterly Journal of Mechanics and Applied Mathematics*, 56(1):45–64, 2002.

[75] J. Woodhouse A. S. Phani and N. A. Fleck. Wave propagation in two-dimensional periodic lattices. *The Journal of the Acoustical Society of America*, 119(4), 2006.

[76] Steven H. Simon. *The Oxford Solid State Basics*. Oxford University Press, 2013.

[77] Robert J Marks II. *Handbook of Fourier Analysis & Its Applications*. Oxford University Press, 2009.

[78] W. J. Bottega. *Engineering Vibrations*. CRC Press Taylor & Francis Group, New York, 2006.

[79] G. R. Cowper. The shear coefficient in timoshenko's beam theory. *Journal of Applied Mechanics*, 33:335–340, 1966.

[80] M.L. Accorsi L.S. Beale. Power flow in two- and three-dimensional frame structures. *Journal of Sound and Vibration*, 185(4):685–702, 1995.

[81] B. Kang C.A. Tan. Wave reflection and transmission in an axially strained, rotating timoshenko shaft. *Journal of Sound and Vibration*, 213(3):483–510, 1998.

[82] C. Mei and B. R. Mace. Wave reflection and transmission in timoshenko beams and wave analysis of timoshenko beam structures. *Journal of Vibration and Acoustics*, 127(4):382–394, 2004.

[83] Y. W. Kwon and H. Bang. *The Finite Element Method Using Matlab second edition*. CRC Press, New York, 2000.

[84] W. E. Warren and A. M. Kraynik. The linear elastic response of two-dimensional spatially periodic cellular materials. *Mechanics of Materials*, 6:27–37, 1987.

[85] H. S. Kim and S. T. S. Al-Hassani. Effective elastic constants of two-dimensional cellular materials with deep and thick cell walls. *International Journal of Mechanical Sciences*, 45(12):1999–2016, 2003.

[86] J. Vasseur, B. Dubus, A. N. Norris, A. Hladky-Hennion, and C. Cronne. Negative index phononic crystals made of metal based microstructure. In *Proceedings of the ASME 2012 International Mechanical Engineering Congress and Exposition Track 13-2 Symposium on Phononic Crystals and Acoustic Metamaterials November 9-15, 2012, Houston, Texas, USA*, 2012.

[87] G. Haw, C. Croenne, L. Haumesser, A. C. Hladky-Hennion, J. O. Vasseur and A. N. Norris. Negative refraction of acoustic waves using a foam-like metallic structure. *Applied Physics Letters*, 102:144103, 2013.

[88] A. N. Norris and A. J. Nagy. Metal water: A metamaterial for acoustic cloaking. In *Proceedings of Phononics, Santa Fe, New Mexico, USA*, May 29-June 2 2011, pp. 112113.

[89] Roman Solecki and R. Jay Conant. *Advanced Mechanics of Materials*. Oxford University Press, 2003.

[90] Donald R. Askeland and Pradeep P. Phulé. *The Science & Engineering of Materials*. Thomson, 2006.